

University of Alberta  
Department of Civil &  
Environmental Engineering



Structural Engineering Report No.290

## **Welding of Light Gauge Infill Panels for Steel Plate Shear Walls**

by  
David Andrew Hunter Neilson  
Gilbert Y. Grondin  
and  
Robert G. Driver

September, 2010.

# **Welding of light gauge infill panels for steel plate shear walls**

by

David Andrew Hunter Neilson  
Gilbert Y. Grondin  
and  
Robert G. Driver

Structural Engineering Report 290

Department of Civil and Environmental Engineering  
University of Alberta, Edmonton, Alberta

September, 2010.

## **Abstract**

Ductile steel plate shear walls are an established lateral load resisting system. Past research indicates that cold-rolled infill panels less than 1 mm in thickness present one solution to an overstrength problem arising from selecting an infill panel thickness based on ease of welding and handling. This research program examines several possible welding procedures and joint geometry to connect the thin infill panel to the thick boundary elements.

Primary welding parameters include short-circuiting gas metal arc welding process, electrode and shielding gas selection, heat input, and use of a chill strip. Four configurations of the infill panel-to-boundary element joint and two configurations of a lap splice joint between two sheets of thin steel in the infill panel were tested in monotonic tension and cyclic tension-compression. A quasi-static cyclic test of a single-storey moment resisting frame steel plate shear wall validated the use of one welding procedure and joint geometry.

## **Acknowledgements**

This report forms the basis for the MSc thesis of the senior author.

The authors would like to thank Collins Industries Ltd. for their donation of materials and labour for the construction of the moment frame for the steel plate shear wall test specimen. Special thanks to Dean Anderson, P.Eng., for managing this work.

Financial support in the form of scholarships to the senior author was received from the Natural Sciences and Engineering Research Council of Canada (NSERC) CGS M Scholarship, the Canadian Institute of Steel Construction G.L. Kulak Scholarship for Steel Structures Research, and the Cohos-Evamy Graduate Scholarship.

Financial support for the experimental work presented in this report was made possible through funding from the Natural Sciences and Engineering Research Council to the second author.

Technical contributions to this work deserve acknowledgement. Thanks to Sean Watt (welding and physical test setup), Greg Miller (instrumentation), Clark Bicknell (welding), and Michael Frost (physical test setup assistance).

## Table of Contents

Chapter 1: Introduction .....	1
1.1 Unstiffened Thin Infill Panel Steel Plate Shear Walls.....	1
1.2 Problem and Objectives of this Research Program .....	2
1.3 Research Program Outline .....	3
Chapter 2: Steel Plate Shear Walls With Light Gauge Infill Panels–Review of the Literature .....	5
2.1 Introduction .....	5
2.2 Caccese <i>et al.</i> (1993): Experimental Study of Thin Steel-Plate Shear Walls Under Cyclic Load.....	5
2.3 Schumacher <i>et al.</i> (1999): Connection of Infill Panels in Steel Plate Shear Walls .....	8
2.4 Berman and Bruneau (2005): Experimental Investigation of Light-Gauge Steel Plate Shear Walls .....	11
2.5 Kharrazi, M.H. (2005): Rational Method for Analysis and Design of Steel Plate Walls .....	15
2.6 Summary and Conclusions .....	18
Chapter 3: Weld Process Design .....	20
3.1 Fabrication Environment.....	20
3.2 Joint Geometry.....	22
3.3 Materials .....	25
3.4 Heat Input .....	26
3.5 Weld Process Selection .....	27
3.6 Electrode .....	30
3.7 Shielding Gas.....	31
3.8 Drawbacks of Short Circuit GMAW .....	32
3.9 Typical Problems Related to Welding of Carbon Steel .....	32
3.9.1 Lamellar Tearing.....	32
3.9.2 Porosity in the Weld.....	33
3.9.3 Solidification Cracking.....	33
3.9.4 Hydrogen-Assisted Cracking .....	34
3.9.5 Work-Hardened Materials and the Heat Affected Zone.....	36
3.9.6 Residual Stresses and Distortion.....	37
3.10 WPS Qualification Requirements.....	39

Chapter 4: Weld Procedure Development.....	40
4.1 Introduction .....	40
4.2 Experimental Program .....	40
4.3 Ancillary Materials Tests .....	40
4.4 Trial Welds and Welding Parameter Development .....	41
4.4.1 Test Parameters .....	42
4.4.2 Welding Equipment .....	44
4.4.3 Trial Weld Test Procedure.....	48
4.5 Results of Visual Inspection of Trial Welds .....	49
4.6 Mechanical Testing of Lap Joint Configurations .....	56
4.6.1 Welded Connection Configurations.....	56
4.6.2 Test Specimen Design .....	58
4.6.3 Quasi-static Tension Tests.....	59
4.6.4 Cyclic Tests .....	60
Chapter 5: Results and Discussion of the Weld Procedure Development	65
5.1 Introduction .....	65
5.2 Ancillary Materials Tests .....	65
5.3 Quasi – Static Tension Tests.....	66
5.4 Cyclic Tests .....	77
5.4.1 Data Interpretation .....	77
5.4.2 Infill Panel-to-Fish Plate Connection.....	77
5.4.3 Infill Panel Splice .....	88
5.5 Wedge Push-Out Test of Weld #2.....	93
5.6 Summary and Conclusions .....	96
Chapter 6: Steel Plate Shear Wall Test Design	97
6.1 Objectives.....	97
6.2 Specimen Design .....	97
6.2.1 Infill Panel-to-Fish Plate Connection Detail .....	100
6.2.2 Strip Model.....	100
6.3 Specimen Fabrication.....	107
6.3.1 Moment Frame Fabrication .....	107
6.3.2 Infill Panel Installation.....	108
6.3.3 Infill Panel Installation – Evaluation.....	110

6.4 Instrumentation and Specimen Preparation .....	119
6.5 Loading Protocol .....	121
Chapter 7: Results and Discussion of the Steel Plate Shear Wall Test.....	124
7.1 Introduction .....	124
7.2 Global Behaviour and Failure Mode .....	124
7.2.1 Initial Load to Failure .....	125
7.2.2 Failure Mode .....	136
7.2.3 Post-Failure Loading.....	137
7.2.4 Infill Panel Performance.....	140
7.3 Infill Panel-to-Fish Plate Connection Behaviour .....	140
7.3.1 Corner Detail .....	142
7.3.2 Infill Splice at Infill Panel-to-Fish Plate Connection Detail.....	145
Chapter 8: Summary and Conclusions .....	146
8.1 Summary .....	146
8.2 Conclusions .....	147
8.3 Recommendations for Future Work .....	149
List of References.....	150
Appendix A: Materials Data .....	155
Appendix B: Weld Process Development, Supplementary Data .....	178
Appendix C: SPSW Test Specimen Design Calculations .....	188
Appendix D: SPSW Fabrication and Test Setup Drawings.....	204
Appendix E: Steel Plate Shear Wall Test, Supplementary Data .....	221

## List of Abbreviations

AISC	American Institute of Steel Construction
ASTM	American Society for Testing and Materials
AWS	American Welding Society
CE	Carbon Equivalent
CISC	Canadian Institute of Steel Construction
CSA	Canadian Standards Association
CVN	Charpy V – Notch
CWB	Canadian Welding Bureau
FCAW	Flux Cored Arc Welding
GMAW	Gas Metal Arc Welding
GMAW-P	Pulsed Gas Metal Arc Welding
GMAW-SC	Short-Circuiting Gas Metal Arc Welding
GTAW	Gas Tungsten Arc Welding
GTAW-P	Pulsed Gas Tungsten Arc Welding
HAC	Hydrogen Assisted Cracking
HAZ	Heat Affected Zone
HCS	Hot Cracking Susceptibility
NDT	Non-Destructive Testing
SLRS	Seismic Load Resisting System
SMAW	Shielded Metal Arc Welding
SPSW	Steel Plate Shear Wall
WPS	Welding Procedure Specification



## List of Symbols

$A_c$	Area of column ( $\text{mm}^2$ )
$E$	Voltage of welding power source (Volts), or modulus of elasticity (MPa)
$F_y$	Yield stress (MPa)
$F_u$	Ultimate stress (MPa)
$h_s$	Height of storey
$I$	Current of welding power source (Amps), or moment of inertia ( $\text{mm}^4$ )
$j$	Load step in SPSW test protocol (integer)
$K_e$	Elastic stiffness of the load versus storey displacement curve measured as a straight – line fit drawn between (0,0) and ( $0.75Q_y, \delta^*$ ) (kN/mm)
$n_j$	Number of repetitions at load step “j” (integer)
$M$	Moment (kN•m)
$M_p$	Plastic moment (kN•m)
$M_{pc}$	Column plastic moment (kN•m)
$N$	$5 \leq N \leq$ Loading step at which maximum load is less than 85% of peak load for the SPSW test (integer)
$P$	Axial load (kN)
$P_y$	Axial load that results in gross yield of the cross section (kN)
$Q$	Base shear of the SPSW specimen (kN)
$Q_y$	Estimate of the base shear causing yield of the SPSW specimen based on static pushover analysis results of a strip model (kN)
$q$	Heat input per unit length (kJ/mm)
$v$	Weld travel speed (mm/s)
$T_L$	Temperature in liquid weld metal at boundary with solid base metal
$T_x$	Temperature at outer boundary of HAZ
$Z$	Plastic modulus ( $\text{mm}^3$ )

$\delta$	Lateral storey displacement of the SPSW specimen (mm)
$\delta^*$	Lateral storey displacement of the SPSW specimen, measured during cyclic testing, required to mobilize $0.75Q_y$ (mm)
$\delta_j$	Maximum lateral storey displacement of the SPSW specimen at step "j" (mm)
$\delta_y$	Lateral storey displacement of the SPSW specimen corresponding to yield (mm)
$\varepsilon_{rupture}$	Rupture strain (mm/mm)
$\Delta_e$	Elastic axial deformation
$\Delta_I$	Inelastic axial deformation
$\Delta_y$	Yield axial deformation
$\eta$	Heat source efficiency (fraction, where "1" = 100% efficient)
$\theta$	Rotation (radians)

## Chapter 1: Introduction

### 1.1 Unstiffened Thin Infill Panel Steel Plate Shear Walls

Ductile steel plate shear walls (SPSW) are a well established form of lateral load resisting system for steel frame structures. The system can be compared to a plate girder stood on end with transverse stiffeners, with the flanges of the plate girder corresponding to the columns of the SPSW and the transverse stiffeners as the inter-storey beams. An installed SPSW panel is shown in Figure 1-1 below. The steel plate connected to the beams and columns is referred to as an infill panel and the beams and columns are sometimes referred to collectively as boundary elements.

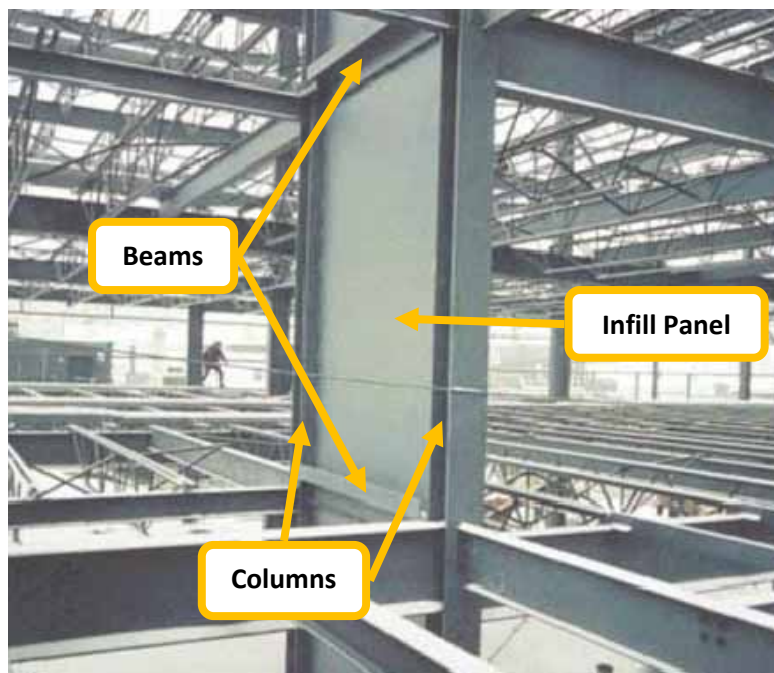


**Figure 1-1: Steel Plate Shear Wall in a High-Rise Building Frame  
(adapted from Martin, 2007)**

The system provides high lateral stiffness under service wind loads, and high energy absorption during extreme load events such as earthquakes. There are two primary elements of the SPSW that contribute to the energy dissipation under seismic loading. First, if the boundary elements are rigidly connected, the plastic hinges that form when large lateral displacement is applied to the frame dissipate energy. Second, when a large lateral displacement is applied the infill panel buckles in the direction of principal compressive stresses and a tension field forms in the direction of principal tensile stress, as demonstrated by Basler and Thurlimann (1961) in plate girder tests and illustrated in Figure 1-2. Tensile yielding of the infill panel is the principal energy dissipating mechanism of the system. The system exhibits high redundancy; as the infill panel accumulates damage under cyclic load, the tension field is able to find load paths

through undamaged portions of the plate. Due to this relatively high energy absorption and redundancy relative to conventional steel bracing systems, ductile steel plate shear walls are accorded the highest ductility rating of any seismic lateral load resisting system by the National Building Code of Canada (NRCC, 2005).

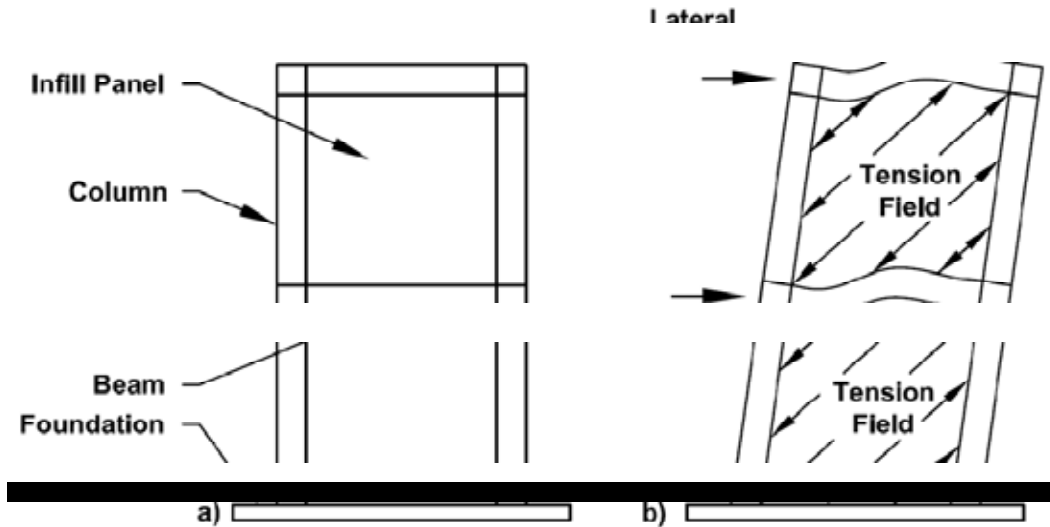


**Figure 1-2: Thin Steel Plate Shear Wall Structural Concept; a) Unloaded, b) Under Load**

Since the early work of Kulak and collaborators at the University of Alberta in the 1980s, global interest in the use of the unstiffened steel plate shear wall system has grown. Additional research programs conducted in Canada, the United States, the Middle East and Asia have vastly expanded on the original body of knowledge. Numerous analytical and experimental studies confirm that unstiffened SPSWs that take advantage of the post-buckling strength of a thin infill plate are effective seismic load resisting systems (SLRS) (Timler and Kulak, 1983; Tromposch and Kulak, 1987; Caccese *et al.*, 1993; Rezai, 1999; Lubell *et al.*, 2000, and others). A review of classical SPSW research is available in AISC Design Guide 20: Steel Plate Shear Walls (AISC, 2005).

The unstiffened thin infill panel steel plate shear wall system has several advantages over traditional reinforced concrete shear walls. First, the lower mass reduces the demand on the gravity load system and foundation. Second, and more importantly, an increase in total structural stiffness when compared with a moment-frame structure is realized, but without the significant increase in mass, and thus seismic demand, of concrete shear walls (Sabouri-Ghomi *et al.*, 2005). This increase in seismic resistance without increasing seismic demand makes this system very attractive for seismic rehabilitation of existing steel-frame structures (Caccese *et al.*, 1993; Berman and Bruneau, 2005). Timler (1998) showed that use of the SPSW system in steel framed high-rise structures can result in moderate cost savings over traditional concrete core structures.

## 1.2 Problem and Objectives of this Research Program

It has been found that for low rise structures and for the upper stories of high rise structures that the infill plate thickness required for the design loads is less than 1 mm

(Berman and Bruneau, 2005). However, handling and welding concerns dictate a thickness of infill plate that is much larger than required. According to the capacity design philosophy of modern design standards, the energy-dissipating infill plate must buckle and deform plastically while boundary elements are sufficiently stiff to anchor the inward forces of the tension field without experiencing excessive pull-in (AISC, 2005). Thus, if the SPSW design calls for a 1 mm infill panel, but a steel fabricator requires a 4 mm infill plate to facilitate handling and welding, columns and beams surrounding the infill plate must be strengthened in order to ensure the full yield of the infill panel does not cause excessive pull-in of boundary members. In addition, the increased forces required to yield a thicker infill panel and larger boundary members will require significant reinforcing of the entire lateral load path, which may result in significant increases in project cost.

Two obvious potential solutions to this problem exist. One option is to use a plate sufficiently thick for handling and welding, and somehow weaken it such that it yields well before the boundary elements. Research programs have investigated the use of low yield steels (Nakashima, 1995; Vian and Bruneau, 2004; Sheng-Jin and Chyuan, 2008), or perforations in the infill panel, which can take the form of either a single hole (Roberts and Sabouri-Ghomi, 1992), a series of vertical slits (Hitaka and Matsui, 2003), a series of circular perforations (Vian and Bruneau, 2005), or quarter-circle corner cut-outs (Vian and Bruneau, 2005).

The second option is to use a very thin infill panel, such as cold-rolled steel sheet, and address the handling and welding concerns. Some quasi-static tests of shear walls with thin cold-rolled steel sheet infill panels have produced excellent energy-dissipating behaviour (Caccese *et al.*, 1993; Berman and Bruneau, 2005; Kharrazi, 2005).

Unfortunately, the welding procedure for connecting thin infill panels to relatively thick boundary members has yet to be documented in any detail. Since the infill panel is the major energy dissipating element of the SPSW system, the connection of this plate to boundary elements can be considered critical, and merits careful attention. Identification and mitigation of difficulties associated with welding thin sheet to thick plate, and practical fabrication considerations are required before thin cold rolled steel plate can be used reliably in steel plate shear walls.

The goals of this research program are to:

- 1) Review the use of thin cold-rolled infill panels in SPSW and evaluate a welding procedure and joint geometry for connecting the such an infill panel to boundary members;
- 2) Validate this connection detail and its impact on global SPSW behaviour by cyclic testing of a large-scale SPSW specimen.

### **1.3 Research Program Outline**

The research program is divided into several distinct stages, separated into the following chapters in this document.

Chapter 2 presents a review of past research on SPSW with thin, cold-rolled infill panels, with a focus on the performance of the connection of the infill panel to boundary elements.

Chapter 3 focuses on aspects of welding a thin cold-rolled infill panel to a thicker mild steel boundary element, as well as welding a splice between two sheets of thin cold-rolled steel, which may be required to build an infill panel sufficiently large to fit a realistically sized bay in a steel-framed building.

Chapter 4 describes the design of small-scale tests for several promising variations of the infill panel-to-boundary element connection and infill panel splice connection. Both the welding procedure adopted for the test program and testing procedure for small scale specimens are described in detail. The results and discussion of the tests on these small-scale specimens are presented in Chapter 5.

Chapter 6 details the design, and test protocol, of a single-storey SPSW specimen constructed with the infill panel-to-boundary element and infill panel splice joints chosen in Chapter 5. A strip model of the specimen is defined, including material properties and plastic hinge definitions, and the predictions of the model are discussed. The fabrication of the specimen, and connection of the infill panel to the boundary members, is documented in images and descriptions. Last, instrumentation for the test and a cyclic loading protocol based on seismic testing standard ATC-24 (ATC, 1992) are presented.

Chapter 7 includes the results and discussion of the steel plate shear wall test. Visual observations, photographs, plots of base shear versus storey sway and energy, and strain gauge results describe the performance of the specimen. The global behaviour of the specimen, failure mode, and performance of the infill panel-to-boundary element connection are discussed.

Summary, conclusions and recommendations for future work are presented in Chapter 8.

## Chapter 2: Steel Plate Shear Walls With Light Gauge Infill Panels– Review of the Literature

### 2.1 Introduction

Numerous researchers have reviewed in detail the classical research on the unstiffened infill panel steel plate shear wall system. For consistency with the principal objectives of the current research project, this literature review focuses on steel plate shear wall experimental research with thin-gauge cold-rolled steel infill panels, and research into the connection detail of the infill panel to the boundary members. For a general overview of steel plate shear wall research, refer to AISC Design Guide 20: Steel Plate Shear Walls (AISC, 2005).

### 2.2 Caccese *et al.* (1993): Experimental Study of Thin Steel-Plate Shear Walls Under Cyclic Load

Caccese *et al.* (1993) tested one rigid frame and five unstiffened infill panel steel plate shear walls under cyclic lateral load. All test specimens were three-storeys tall and were built at 1:4 scale. Infill panel thicknesses were 22 gauge (0.76 mm) (two specimens), 14 gauge (1.90 mm) (two specimens), and 12 gauge (2.66 mm) (one specimen). Both simple and rigid beam-to-column connections were tested. All specimens had identical beam and column member sizes and centerline geometry.

The connection of all of the infill panels to the boundary elements of the frame were continuously welded to the flanges of the beams and columns in the plane of their webs. No specific details of weld procedure are provided, nor is a diagram of the connection geometry presented.

Each wall was loaded with an actuator at the top storey only. Out-of-plane movement was prevented by bracing at each storey. No gravity loads were applied to the columns. Loading consisted of three quasi-static load cycles at a top storey drift of 2% followed by a monotonic push to the limit of the actuator stroke.

The hysteresis behaviours of Specimens F0 (moment resisting frame only), S22 (simply supported beam-to-column connections, 22 gauge infill panel), and M22 (moment resisting beam-to-column connections, 22 gauge infill panel) are shown in Figure 2-1, Figure 2-2, and Figure 2-3, respectively. A photograph of Specimen M22 at maximum drift is shown in Figure 2-4; the out-of-plane buckling of the infill panel and tension field action are clearly apparent.

Both SPSWs (Specimens S22 and M22) show clear performance enhancements over the base-case moment frame (Specimen F0). The increased initial slope of the load versus displacement curves reflects the dramatic increase in initial stiffness, nine times that of the moment frame in the case of Specimen M22. The significantly larger area enclosed by the SPSW hysteresis loops reflects the high degree of energy absorption when compared with the moment frame alone. The total pushover force of steel plate shear wall M22 was 2.8 times larger than that of the moment frame, and the post-yield force was twice the force at initial yield, highlighting the significant post-yield energy absorption potential of the steel plate shear wall system.

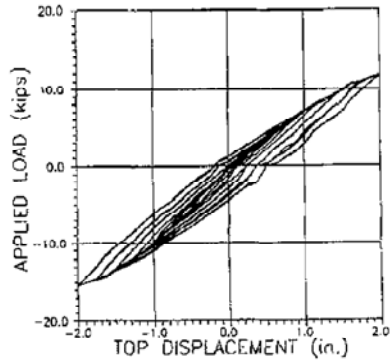


Figure 2-1: Hysteresis of Specimen F0  
(Caccese *et al.*, 1993)

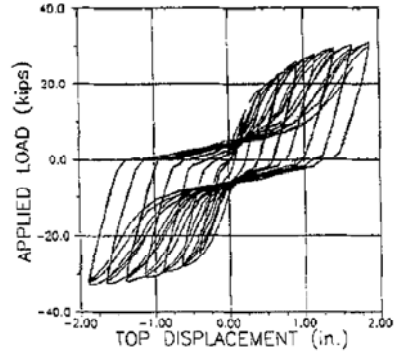


Figure 2-2: Hysteresis of Specimen S22  
(Caccese *et al.*, 1993)

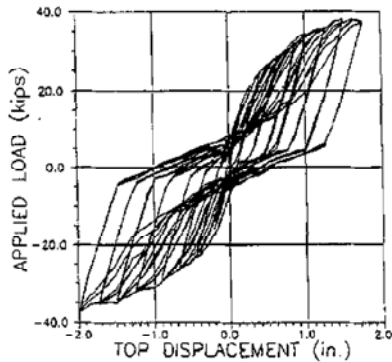


Figure 2-3: Hysteresis of Specimen M22  
(Caccese *et al.*, 1993)

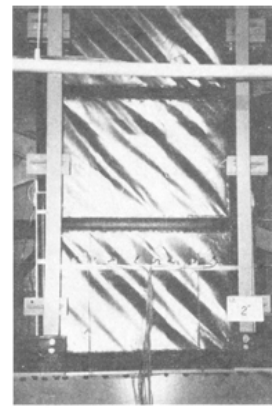


Figure 2-4: Specimen M22 at Maximum Drift  
(Caccese *et al.*, 1993)

The authors of this study concluded that the addition of a thin plate to a moment frame results in significant increases of initial stiffness, load-carrying capacity and energy absorption potential. They separate failure into two categories. When the infill panel is slender enough, inelastic behaviour and energy dissipation commence with infill panel yielding, and ultimate strength is governed by column plastic hinging. Relatively thick infill panels cause the failure mode to be dominated by column instability, and when this failure mode governs, thickening of the infill panel results in only negligible increases in system strength. The authors conclude that slender plates, where energy absorption is dominated by plate yielding, are the more promising system.

Experimental load versus displacement envelopes comparing the rigid (“M” – series) and shear (“S” – series) beam-to-column connected specimens are shown in Figure 2-5. Overall, the influence of the connection type is relatively minor. The authors postulate that the additional rigidity the continuously welded infill panel brings to the region near the beam-to-column connection enables a “shear” beam-to-column connection to resist significant rotation. For the most slender plate (22 gauge), the type of beam-to-column connection has the most relative influence. In the case of the 14 gauge thick infill panel specimens, the result of the shear connection (S14) achieving a higher peak load than the moment connection (M14) is unexpected. The authors believe this is a result of



specimen M14 having a slightly lower actual infill panel yield strength, and a premature failure of one of specimen M14's column base welds at 0.5 inches of top displacement.

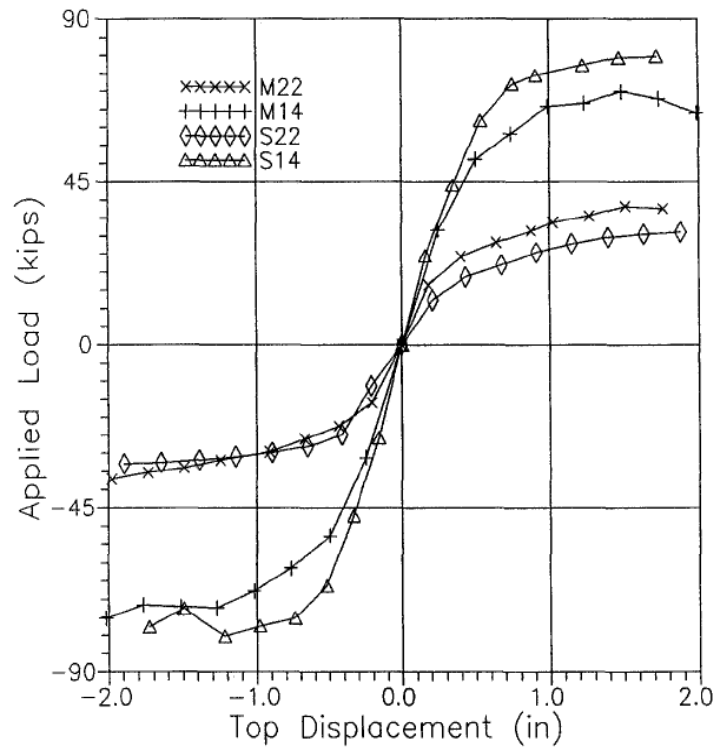


**Figure 2-5: Load versus Displacement Envelopes Comparing M-Series Specimens to S-Series Specimens (Caccese *et al.*, 1993)**

### 2.3 Schumacher *et al.* (1999): Connection of Infill Panels in Steel Plate Shear Walls

Due to the high reversing strains experienced at the corners of the infill panel-to-fish plate connection as a SPSW sways under cyclic loading, the corner detail bears investigation. The corner detail was tested using a setup developed by Rabinovitch and Cheng (1993) for testing corner gusset plates under cyclic loading. The setup consisted of a rigidly connected length of beam and column, with 6.0 mm thick fish plates connected by a two-sided fillet weld lap joint to a portion of 4.8 mm thick infill panel. To join the fish plates at the corner, Driver *et al.* (1997) had provided a strap plate for continuity between the fish plates after testing its behaviour in a test of the corner detail. This detail was felt to be unnecessary and needed further investigation.

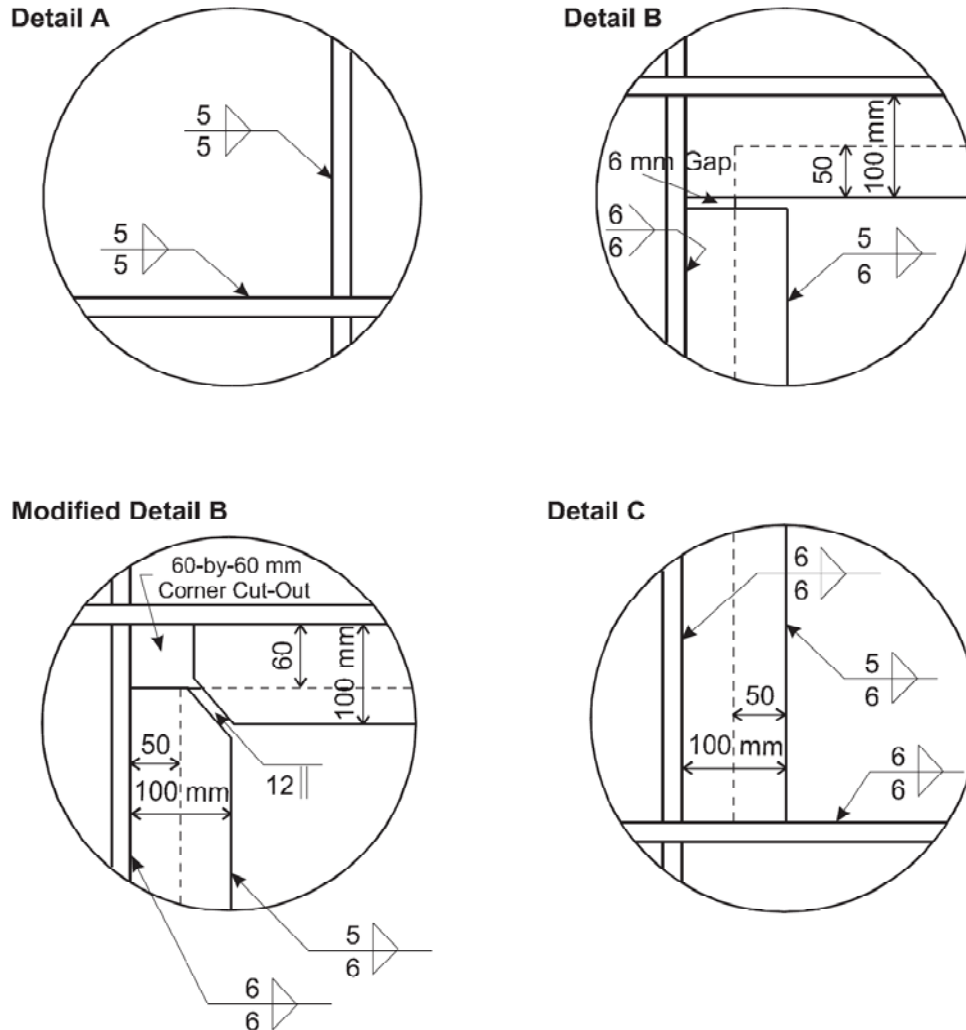


Figure 2-6: Corner detail in test setup (Schumacher *et al.* (1999))

Schumacher *et al.* (1999) conducted a series of quasi-static cyclic tests on four additional corner details, described below and shown schematically in Figure 2-7:

- 1) Detail A: infill panel welded directly to the boundary members with fillet welds;

- 2) Detail B: fish plates welded to the beam and column, and infill panel welded in a lap splice;
- 3) Modified detail B: as Detail B, but with a corner cut out in an attempt to minimize high stresses;
- 4) Detail C: fish plate welded to only one boundary member and infill panel welded directly to the adjacent boundary member, then lapped and welded to the fish plate.



**Figure 2-7: Four corner connection details investigated by Schumacher *et al.* (1999)**

Lap splices to the fish plates were fillet welded on both sides in all cases. The infill panel thickness was 4.8 mm and the fish plates were 6.0 mm thick. The material was CSA G40.21 grade 300W structural steel plate.

Detail A (infill panel welded directly to boundary elements) showed no weld tearing, but failed through the beam-to-column connection. The details using fish plates experienced varying levels of weld tearing in a localized area close to the corner. Interestingly,

modified Detail B suffered similar tearing damage to the original Detail B, despite efforts to rearrange the geometry to reduce local peak stress.

As a measure of the success of the different details, energy dissipation for each detail at each loading level is presented in Figure 2-8. The energy dissipation is comparable for all four details.

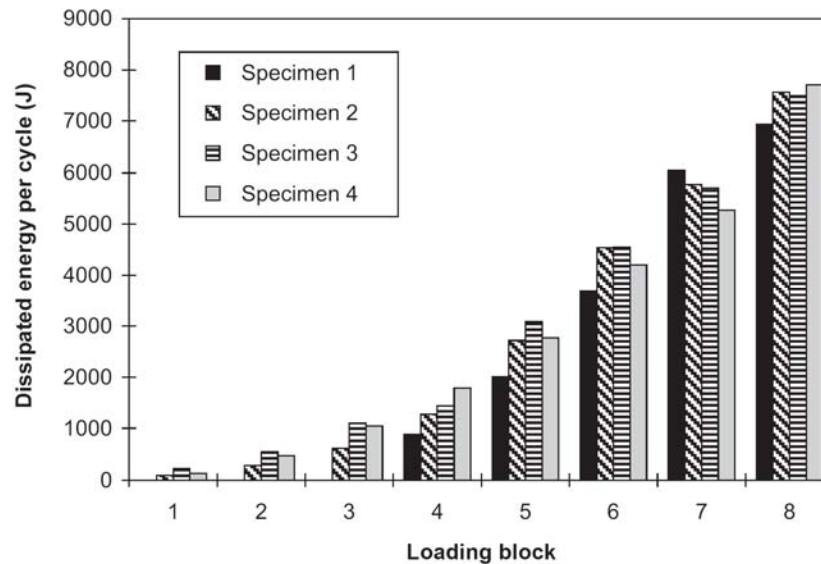


**Figure 2-8: Measured energy dissipated per loading cycle (Schumacher *et al.*, 1999)**

The authors concluded that the presence of localized tearing does not affect the energy dissipation capacity of the infill panel.

Past experimental work by Timler and Kulak (1983) demonstrated that the maximum load occurred when a weld tear began at the fish plate to infill panel corner connection of their SPSW specimen. Schumacher *et al.* (1999) postulate that the presence of a groove weld, as opposed to the 6 mm gap shown in Detail B of Figure 2-7, may be liable for this tear initiation. Similarly in full shear wall tests by Tromposch and Kulak (1987) and Driver *et al.* (1997), corner tears initiated at welds of a strap plate connecting two adjacent fish plates. Schumacher *et al.* (1999) recommend that a gap similar to that shown in Detail B be used in practice to achieve the superior performance shown in this test series.

## 2.4 Berman and Bruneau (2005): Experimental Investigation of Light-Gauge Steel Plate Shear Walls

Berman and Bruneau (2005) conducted a test program to examine light gauge steel plate shear walls as a seismic rehabilitation option for a fictitious hospital equipped with an existing moment-frame SLRS. The addition of the infill panel to the existing frames increased the initial stiffness and ultimate capacity of the SLRS, without adding significant mass. Since seismic demand is a function of mass, in general terms a good seismic rehabilitation significantly increases ductility, and cyclic robustness with a minimal increase in mass.

Three single-storey specimens, two with 20 gauge flat infill panels and one with a 22 gauge corrugated infill panel, were subjected to cyclic quasi-static loading using the setup shown in Figure 2-9. The infill material was ASTM A1008 CS (cold-rolled commercial grade steel sheet). The infill panel thickness was full-scale, while the frame geometry was approximately half-scale due to testing equipment limitations. Beams were simply connected to columns using double angle shear connections. The boundary members were designed to remain elastic throughout infill panel buckling and plastification.

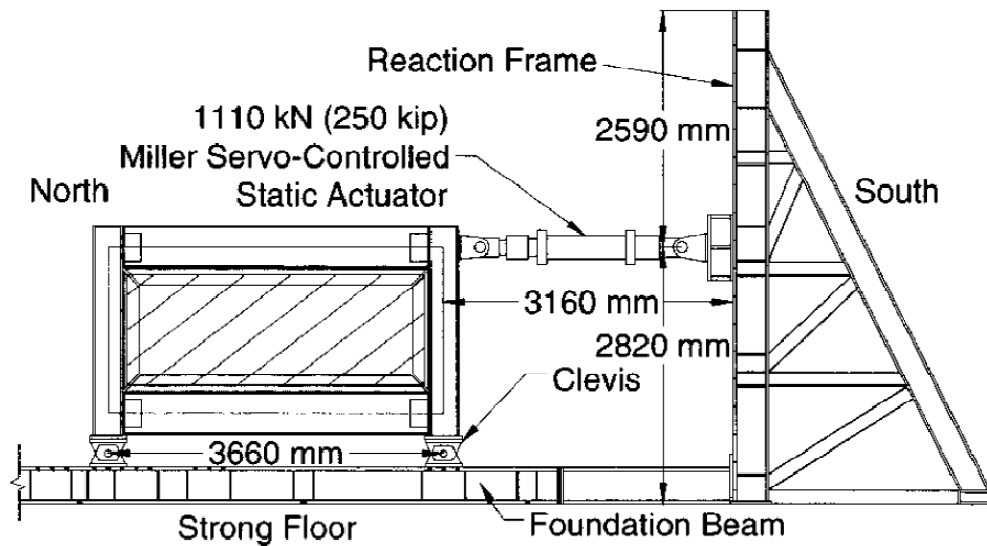


Figure 2-9: Pushover Test Setup (Berman and Bruneau, 2005)

Infill panel-to-boundary element connection details are shown in Figure 2-10. Specimen C1 (corrugated infill panel) and Specimen F1 (flat infill panel) were connected to boundary elements by industrial strength epoxy. Specimen F2 was reported to be “fully welded”; the detail appears to show a continuous fillet weld on one side of the lap joint. As seen in Figure 2-11, the joint geometry of the corner infill panel-to-boundary member connections appears to consist of an angled gap between adjacent outstanding legs of angles which are connected to the boundary elements. Specimens F1 and F2 had infill panels composed of a single plate, while Specimen C1 had an infill panel built up of four corrugated steel sheets riveted together by 1.6mm diameter steel pop rivets spaced at 100mm on center.

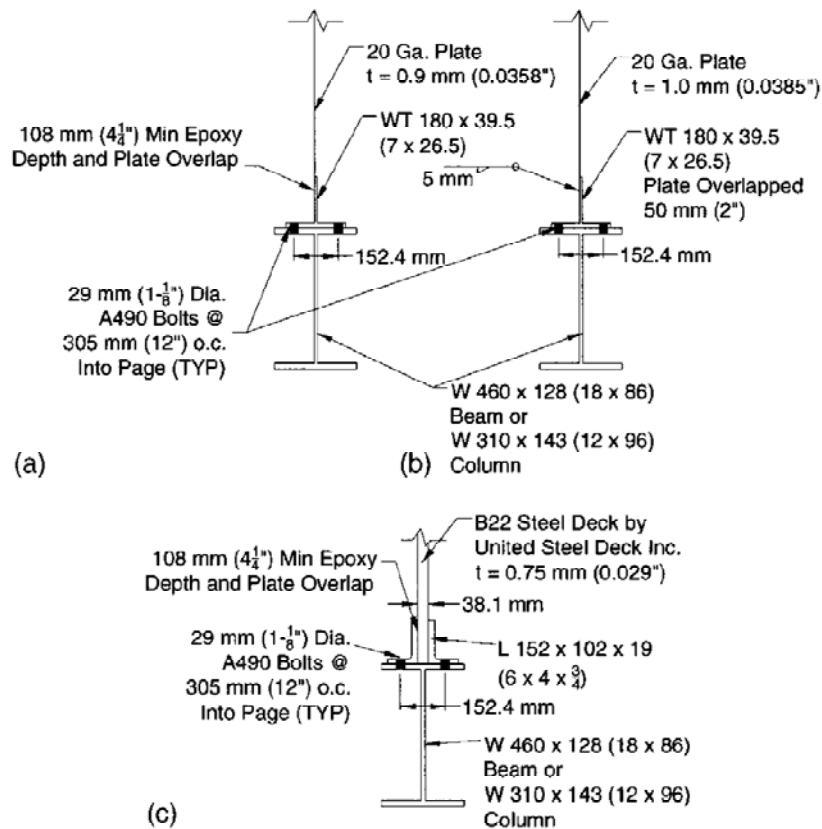


Figure 2-10: Infill Panel-to-Boundary Frame Connections (a) Specimen F1; (b) Specimen F2; (c) Specimen C1 (Berman and Bruneau, 2005)

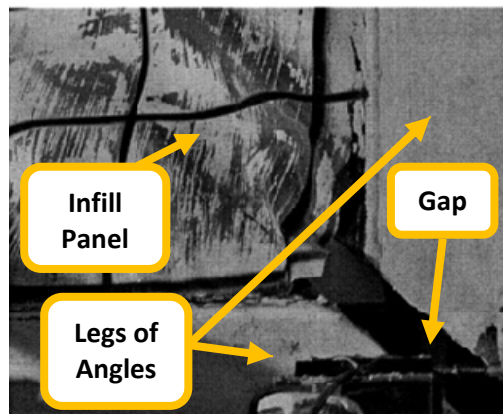


Figure 2-11: Corner Detail of Specimen F2 (adapted from Berman and Bruneau, 2005)

Specimen C1 was connected to the boundary elements by a lap joint between the outstanding leg of an angle bolted to the flange of the boundary members. Corrugations were oriented at 45 degrees to the horizontal, such that the tension field would develop roughly parallel to the corrugations.

Specimen C1 was tested to examine whether significant energy absorption would be observed in excursions when the compression field was oriented parallel to the corrugations, which have an increased stiffness and resistance to buckling relative to a flat infill panel. The additional strength provided by compression of the corrugations was not observed after initial buckling. At approximately 1.4% drift, rapid degradation of strength was observed. This is attributed to fractures at locations of repeated local buckling in the corrugated infill panel. Hysteretic behaviour was characterized by high peak load and energy absorption in excursions where the tension field formed parallel to the infill panel corrugations, and small peak load and energy absorption in excursions where a compression field formed parallel to the corrugations. Thus, the hysteresis profile appears lopsided. It is for this reason that when using corrugated infill panels, two panels with corrugations angled in opposite directions (at  $90^\circ$  to each other) must be used.

Specimen F1 experienced a premature failure at only 0.25% drift due to poor epoxy coverage in the lap joint. However, a similar epoxy lap joint detail was used in Specimen C1, and the joint appeared to perform in a satisfactory manner.

As shown in Figure 2-12, Specimen F2 exhibited excellent hysteretic behaviour. It showed the greatest energy absorption of all three specimens, and had the highest initial stiffness and highest ductility. Good agreement was reached with a static pushover curve produced from a simple strip model based on the work of Thorburn *et al.* (1983).

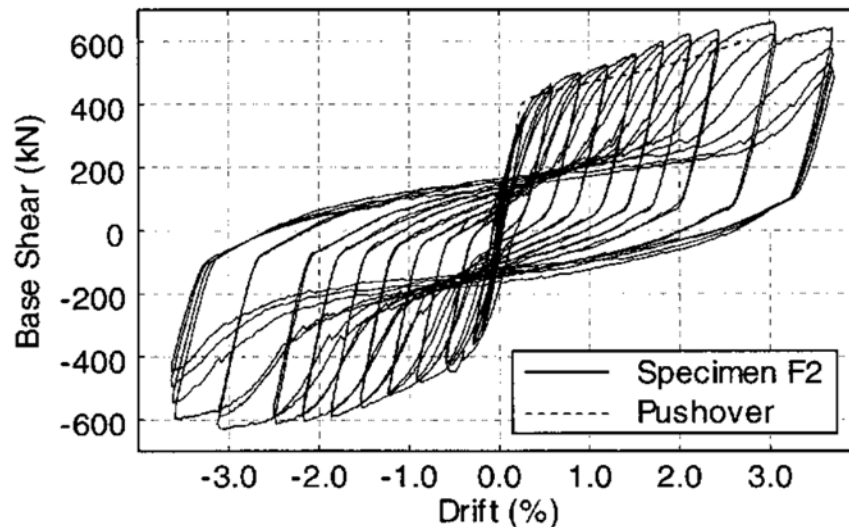


**Figure 2-12: Hysteresis Results and Strip Model Pushover Curve Prediction for Specimen F2 (Berman and Bruneau, 2005)**

Failure was in the form of tearing of the infill material adjacent to the welded connection at a corner, as shown progressively in Figure 2-13. Although tearing began to show early in the test, significant strength loss did not occur until 3.7% drift, or  $12 \delta_y$ ,

where  $\delta_y$  is the storey displacement corresponding to the initiation of infill panel yielding.

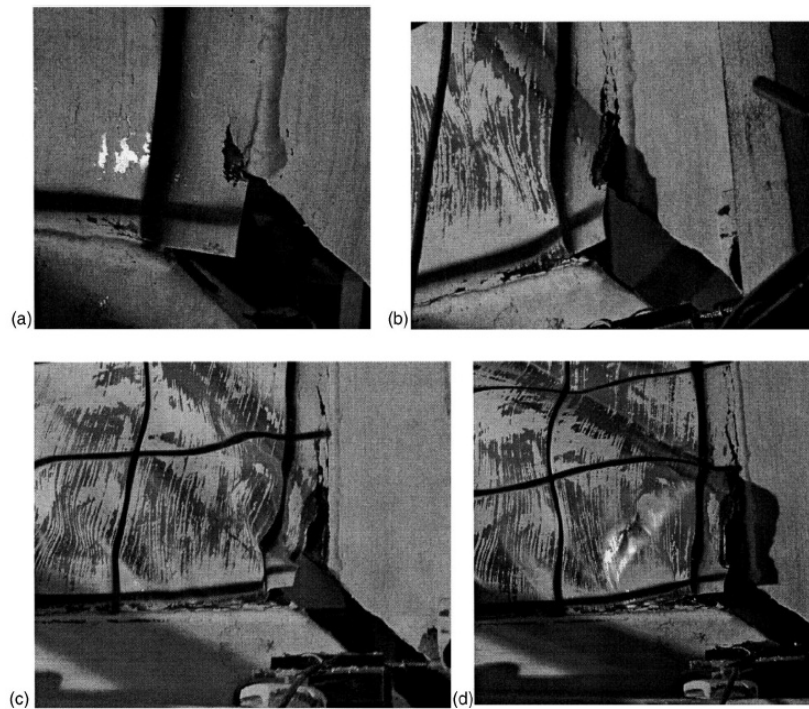


**Figure 2-13: Fracture Propagation – Lower South Corner of Specimen F2, a) 0.90% drift; b) 1.82% drift; c) 2.44% drift; d) 3.07% drift (Berman and Bruneau, 2005)**

Of the three specimens tested, Specimen F2 clearly shows the most promise. The flat plate is more appealing than corrugated plate, since it can be implemented in a single bay, whereas the corrugated infill requires two bays with corrugations angled at  $90^\circ$  to one another. The lap splice detail for the flat plate is also easier to fabricate than the double-angle connection used for the corrugated infill panel, as shown in Figure 2-10. Last, a welded connection appears more desirable to implement than an epoxy connection, as variable levels of epoxy coverage resulted in a poor infill panel-to-boundary member connection in the case of Specimen F1, whereas the welded connection of Specimen F2 performed well.



## 2.5 Kharrazi, M.H. (2005): Rational Method for Analysis and Design of Steel Plate Walls

As a portion of his PhD research developing a method for analysis and design of steel plate walls, Kharrazi conducted both quasi-static and dynamic tests of single storey SPSW specimens.

For quasi-static testing, two single-storey ductile steel plate walls (DSPW-1 and DSPW-2) and one moment resisting frame (SF-1), identical to the frames in the ductile steel plate walls, were tested. Columns were HSS and beams W-shapes. Infill panel material was 22 gauge cold-rolled steel sheet. The side elevation of the specimens is shown in Figure 2-14. DSPW-1 and DSPW-2 had infill panel yield strengths of 200 MPa and 150 MPa, respectively.

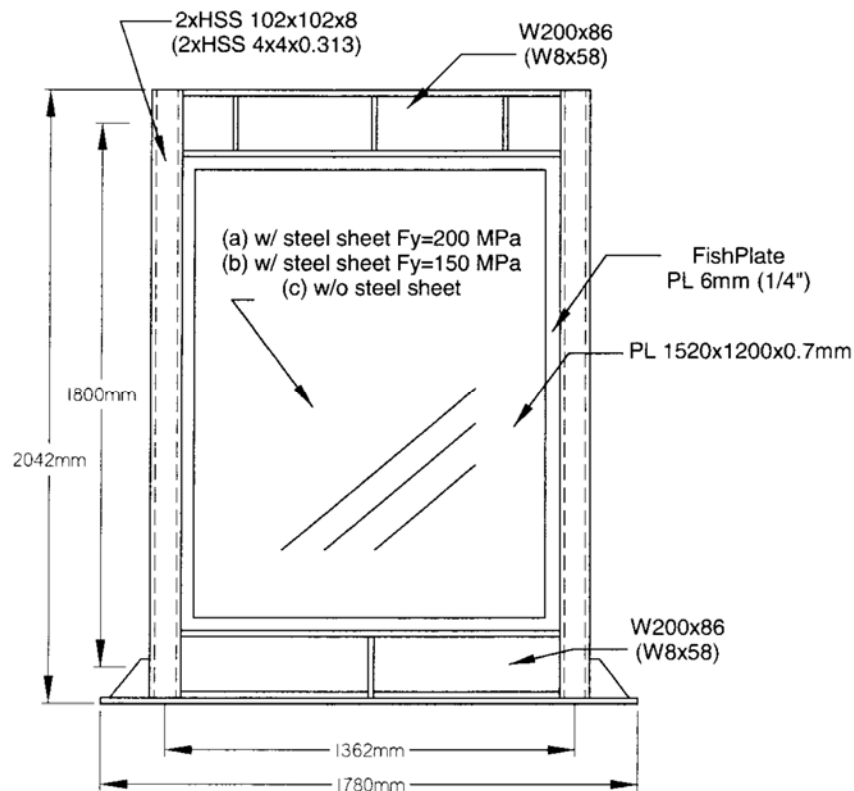
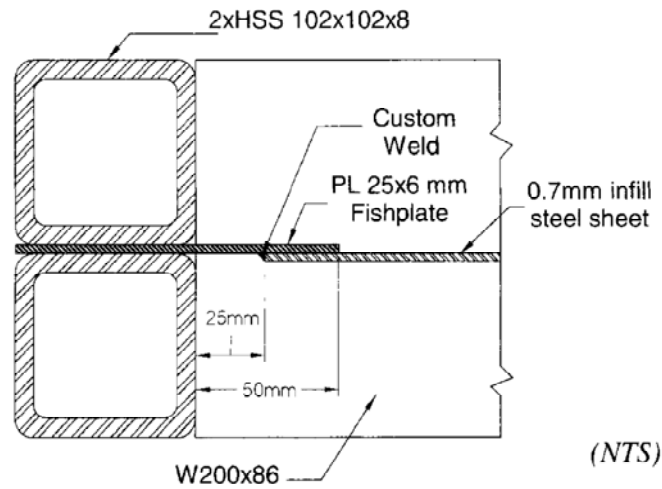


Figure 2-14: Dimensions of the Single Storey Test Specimens (a) DSPW-1, (b) DSPW-2, and (c) SF-1 (Kharrazi, 2005)

The fish plate connection detail of the infill panel to the boundary members is shown in Figure 2-15. No description of the weld is provided beyond the term “custom weld”.



**Figure 2-15: Fish Plate Connection Detail (Kharrazi, 2005)**

Testing consisted of three successive cycles of equal magnitude at incremental amounts of storey drift, increased until excessive damage was observed and load carrying capacity deteriorated significantly.

Following the formation of plastic hinges at the top and bottom of the columns around 4.0% drift, Specimen DSPW-1 exhibited fracture along the weld lines between the fish plate and the steel panel at a nominal drift of 5.8%. At a drift of 7.5%, a fracture in one of the beam-to-column connections was observed. Immediately afterwards, the weld between the steel plate and the fish plate of the north column failed suddenly along 60% of its length. This increased to 80% of the length over the next half-cycle, followed by complete separation of the infill panel from the fish plate, as well as complete rupture of the beam-to-column connection.

Despite the sudden nature of this failure, it occurred at  $14\delta_y$ , a very ductile value and comparable to the  $12\delta_y$  attained by Berman and Bruneau’s Specimen F2.

DPSW-2 performed in a similar manner to DPSW-1; however, the infill panel-to-fish plate connection weld tearing was quite premature. During the last cycle at a storey drift of 2.0%, a short tear had formed at the top-right of the infill panel to weld connection. At a storey drift of 4.0%, this crack had extended to approximately 400 mm, and additional cracks formed at the weld at other corners of the infill panel. During the second cycle at 6.0% drift, weld tears propagated rapidly the full length of the vertical edge of the infill panel at the left column, and during the following cycle this tear propagated the full length of the top beam.

The load versus displacement diagrams for DPSW-1, DPSW-2, and SF-1, shown in Figure 2-16, illustrate the energy dissipation and overall performance of the three test specimens. As expected, significant energy absorption occurs only after inelastic behaviour is observed. In later cycles, as damage accrues in the infill panel-to-boundary

element connection, the energy dissipating capacity of the SPSW specimens approaches that of the moment frame alone. These conclusions are also reflected in Figure 2-17, which compares the energy absorption of the three specimens in each loading cycle.

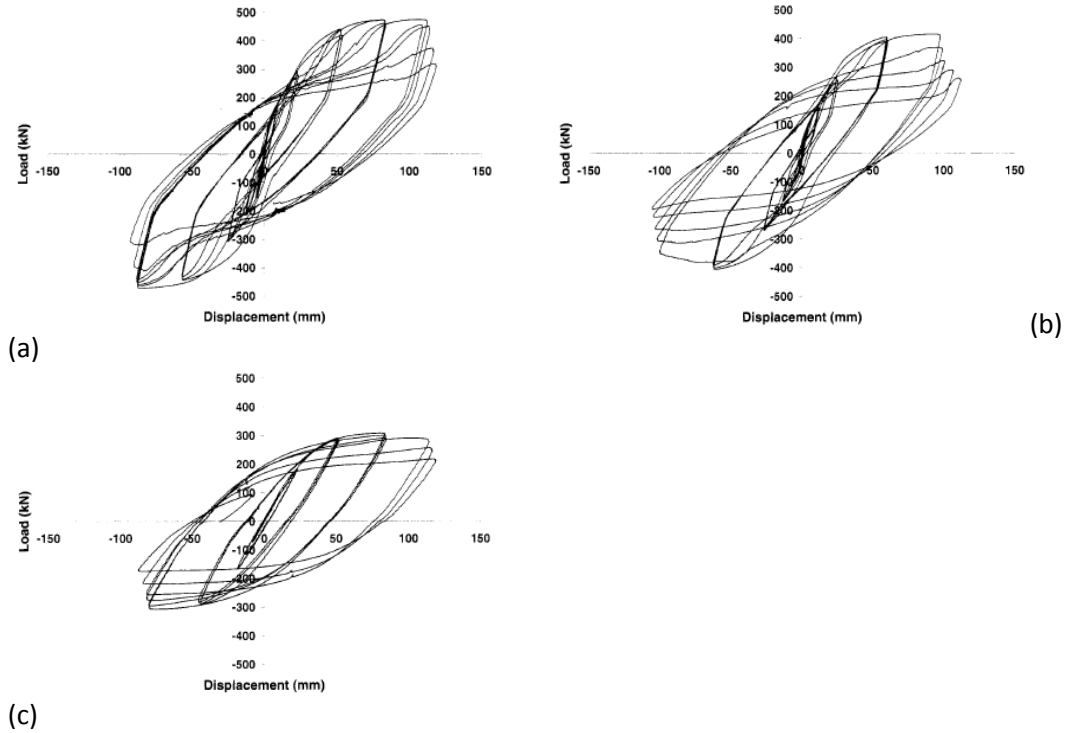


Figure 2-16: Hysteresis Results for Quasi - Static Testing of (a) DSPW-1, (b) DSPW-2, and (c) SF-1 (Kharrazi, 2005)

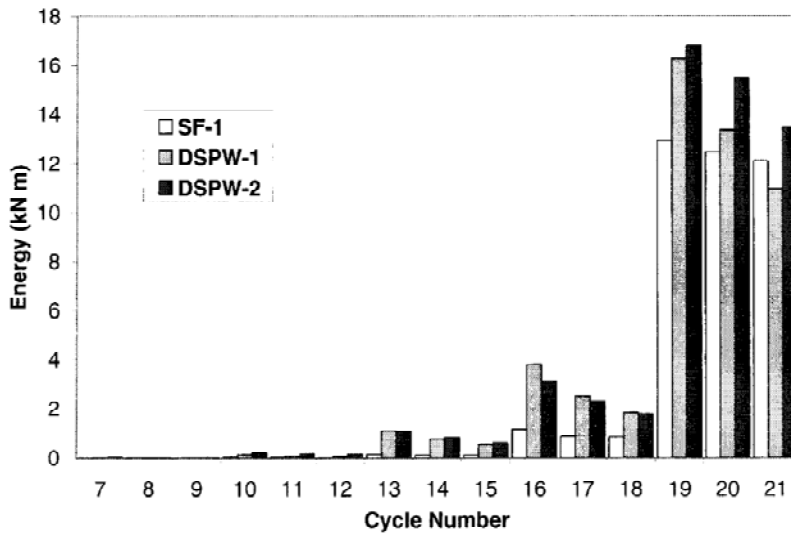


Figure 2-17: Hysteretic Energy Dissipation for SF-1, DSPW-1, and DSPW-2 (Kharrazi, 2005)

Kharrazi (2005) also tested a third steel plate shear wall, DSPW-3, designed identical to DSPW-1, and rigid frame SF-2, designed identical to SF-1, dynamically on the shake table at the University of British Columbia. The capacity of the frame was large enough that the shake table could barely take these two specimens past the range of elastic response. As there is no mention of welding or weld damage during testing, these specimens are not discussed further.

## **2.6 Summary and Conclusions**

Three test programs of SPSWs having cold-rolled infill panels and one test program of infill panel to boundary member connection details are reviewed. The performance of the welded connections from the SPSW tests is summarized in Table 2-1.

Damage from stress concentrations at weld corners is expected; however, the overall load-carrying capacity is largely unaffected when certain experimentally verified details are used (Schumacher *et al.*, 1999). It is logical that ultimate failure of the system may occur due to propagation of weld fractures at corners. However, the weld should be expected to provide the system with the integrity to produce stable hysteresis through a reasonable deformation before ultimate failure. Premature weld failure negatively impacts post-buckling stiffness and energy dissipation capacity of the SPSW system.

In none of the SPSW experimental programs was the welding procedure discussed in any detail; there was no mention of the welding process used, type of shielding, electrode, heat input, or other details. Moreover, weld performance varied considerably over the range of tests reported in the literature. In a real-world design scenario for a seismic fracture-critical weld, a detailed welding procedure specification (WPS) is required prior to fabrication.

**Table 2-1: Summary of Infill Panel-to-Boundary Element Connections and Performance in Past Thin Cold-Rolled Infill Panel SPSW Research**

Test Program	Infill Panel to Boundary Element Connection	Weld Performance at Infill Panel to Boundary Element Connection
Cacesse <i>et al.</i> (1993)	<p>Infill panel is “continuously welded to the beams and columns in the plane of their webs”. No additional weld geometry or weld procedure details provided.</p> <p>Infill Panel Thicknesses: 22, 14, and 12 gauge</p>	<p>Stable, ductile hysteresis curves observed. No reports of premature weld failure.</p>
Berman and Bruneau (2005)	<p>Infill panel fillet welded to the outstanding stem of a WT section bolted to the flange of boundary elements (see Figure 2-10b). No details provided regarding welding procedure.</p> <p>Infill Panel Thickness: 20 gauge (flat)</p>	<p>Stable, ductile hysteresis observed. Ultimate failure, at satisfactory storey drift, is characterized as a fracture in the infill panel to boundary element weld propagating from the corners of the panel.</p>
Kharrazi (2005)	<p>Infill panel lap welded to a fish plate connected to boundary elements. Figure 2-15 appears to show the infill panel welded to the fish plate only on one side of the lap. No description of welding procedure beyond the words “custom weld” is provided.</p> <p>Infill Panel Thickness: 22 gauge</p>	<p>Early weld tearing contributed to reduced post-yielding stiffness of the system. The hysteretic performance of DSPW-2 (Figure 2-16b), where more severe early weld tearing occurred than in specimen DSPW-1, resembles more closely the hysteretic performance of rigid frame specimen F0 (Figure 2-16c).</p>

## Chapter 3: Weld Process Design

### 3.1 Fabrication Environment

Two possible fabrication scenarios exist. In modular construction, the SPSW panel is assembled completely at a fabrication facility in a controlled environment, transported to the construction site and erected as a panel. In the second, either during new construction or retrofitting of an existing steel frame structure, the frame exists in the final position with beams horizontal and columns vertical. The infill panel is lifted into the vertical position and held in place so that welding can be performed. This presents a field fabrication scenario as follows:

- 1) Welding in all positions (flat, vertical, horizontal, and overhead) may be required;
- 2) Welding equipment must be portable;
- 3) Manual welding (no robotics) will be required;
- 4) Welders must be familiar with the equipment;
- 5) Welding may be subject to outdoor conditions (moisture, wind, etc.).

Though data are not readily available for the structural steel fabrication industry, Figure 3-1 and Figure 3-2 report recent survey data for weld processes used in the pipeline and pressure vessel industry in Alberta. Yarmuch (2008) suggests that as the pipeline industry modernizes, high-efficiency wire-feed welding processes such as gas metal arc welding (GMAW) and flux cored arc welding (FCAW) will increase in popularity in comparison with less efficient shielded metal arc welding (SMAW), the currently dominant process. Modern portable wire feeder equipment renders GMAW and FCAW increasingly appealing for field applications (Yarmuch, 2008). It is considered likely by the author that the structural steel fabrication industry is experiencing a similar transition.

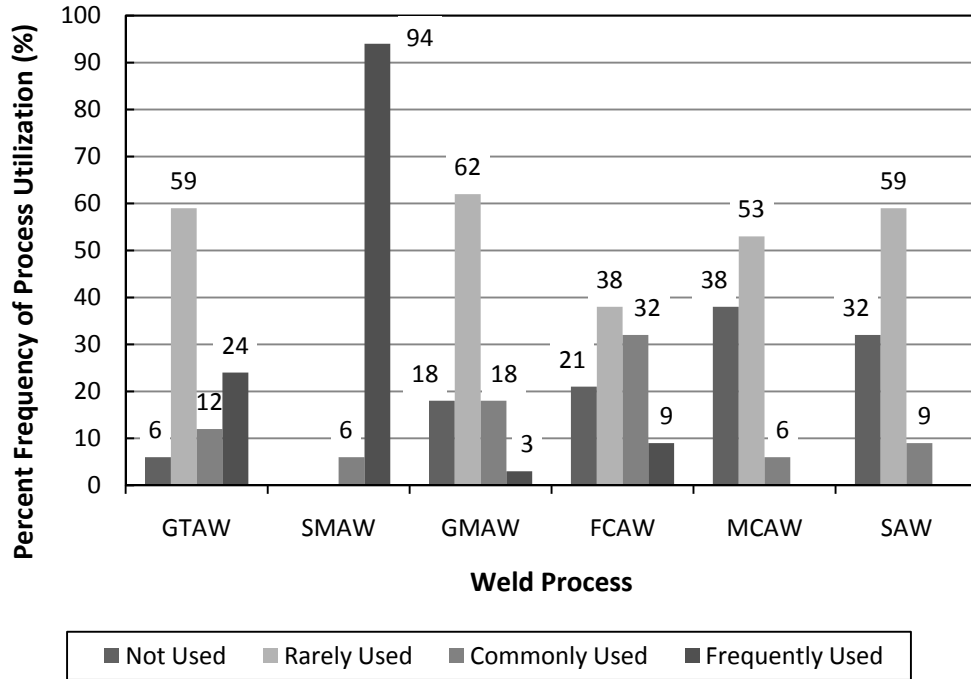


**Figure 3-1: Processes Used for Field Erection (Pipeline Industry) in Alberta (adapted from Yarmuch, 2008)**

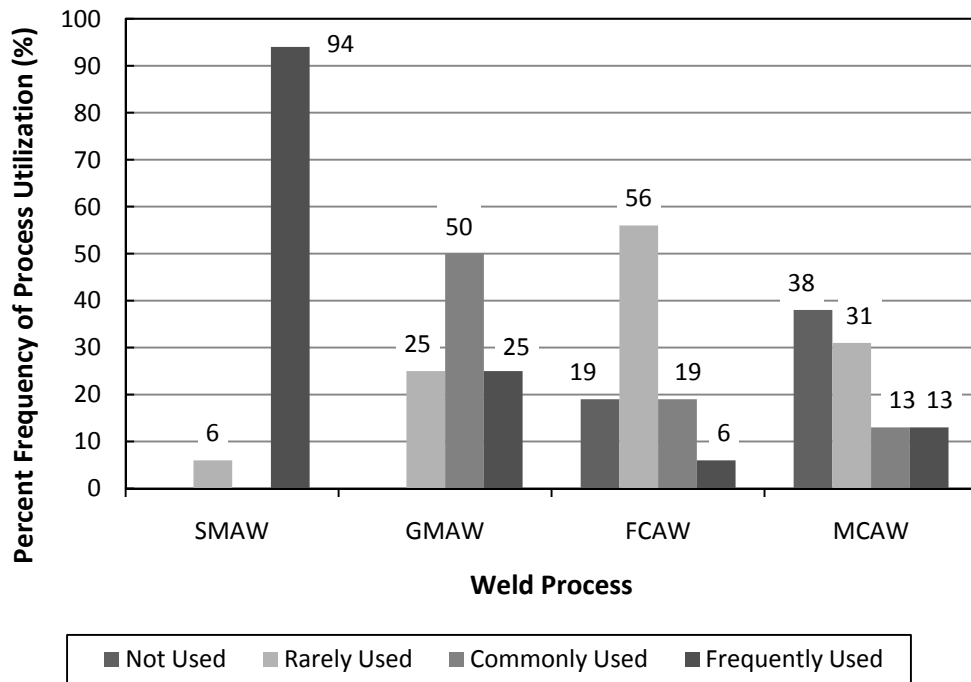


**Figure 3-2: Utilization of Manual vs. Wire - Feed Processes for Pressure Piping (Fabricators Only) in Alberta (adapted from Yarmuch, 2008)**

The infill panel will be made of cold rolled sheet steel. The roll width will depend on what is locally available; for example, at the time of this test program, rolls having width 1219mm (4') are available. This dimension is significantly smaller than a typical bay width or height; thus, several lengths of sheet steel must be connected to form one panel sized correctly for the bay, and this panel will be lifted into place. Also, in a retrofit situation where an infill panel is being added to an existing frame, it may not be practical to transport a large prefabricated infill panel to the frame, but rather to transport several smaller plates and assemble the infill panel as near to the installation location as possible.

Since the panel width or height to thickness ratio is very high (in the order of 3300 for a 20 gauge steel sheet spanning a 3050mm high storey), it will buckle when lifted. Magnets are not a practical solution for handling these thin sheets since the magnetic field generated will interfere with welding. Suction, either through suction cups or high powered vacuum suction devices for heavy loads, is commonly used to lift sheet metal (Cort, 2008), however it is unlikely that structural steel fabricators and erectors who are accustomed to working with thicker steel sections are equipped for suction lifting. Most likely some form of temporary stiffening will be required, for example, the infill panel could be clamped to a plate of similar dimension that will not buckle when lifted, and that stiffening plate could be removed after tack welds temporarily secure the infill panel to the frame.

An additional alternative is to connect the infill panel to a light frame in the flat position, then tilt-up this module and weld the light frame to the boundary members of the SPSW. This alternative is discussed further in Chapter 8, Section 8.3 Recommendations for Future Work.

For simplicity, in this test program the infill panel is connected while the SPSW is laid down in the flat position, which simulates new construction.

### **3.2 Joint Geometry**

Two joints are required; one to connect the thin infill panel to the thicker fish plates, and one to merge several lengths of sheet steel into an infill panel sufficiently large to occupy an entire bay. As discussed in Chapter 2, a lap joint between the infill panel and fish plates attached to the boundary members is more favourable for fit-up than welding the infill panel directly to the boundary members. Similarly, a lap joint is appropriate for splicing together lengths of steel sheet to form the infill panel.

Under seismic loading structural components can be subjected to low cycle fatigue, a cracking phenomenon taking place under a small number of load cycles. At the infill panel-to-fish plate joint, welds will be loaded in both longitudinal and transverse directions. Fracture of the weld could typically start at a weld flaw and propagate perpendicular to the applied tensile stresses (Fisher *et al.*, 1997). Cracks initiate at



geometric stress raisers such as weld undercut, lack of fusion, highly reinforced toes, porosity, inclusions, microcracks, and brittle intermetallic inclusions (Kou, 2003; Fisher *et al.*, 1997). Typical crack locations in fillet welds include root cracks, toe cracks, and underbead cracks. These sources of weld cracking are illustrated in Figure 3-3.

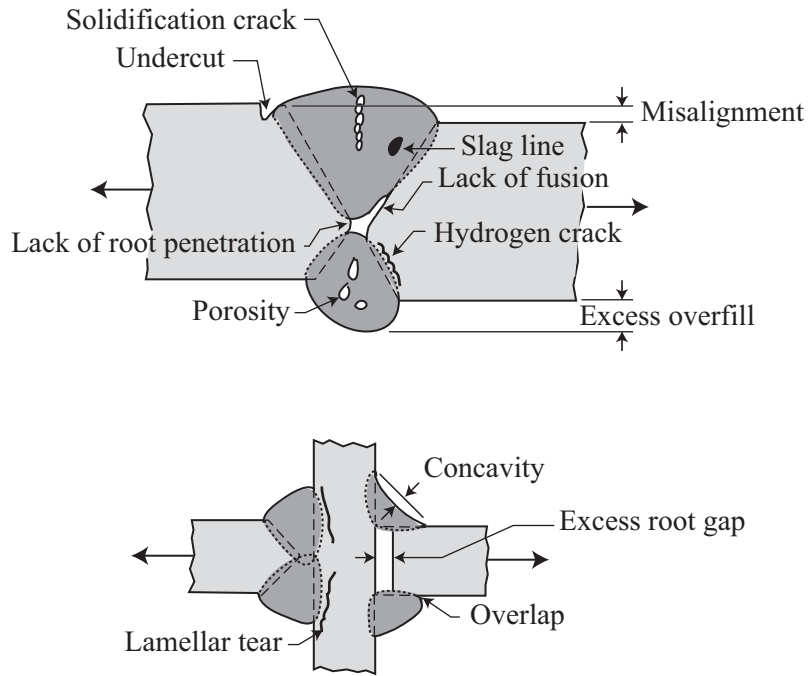


**Figure 3-3: Weld Flaws**

For cyclically loaded structures Clause 12.4.7.1 of CSA W59 (CSA, 2003) states that the “minimum overlap of parts in load-carrying lap joints shall be five times the thickness of the thinner part joined and not less than 25mm. Unless lateral deflection of the parts is prevented, they shall be connected by two transverse lines of fillet welds, or by longitudinal fillet welds in edges or in slots”. Since the SPSW infill plate is expected to buckle out-of-plane under load, two transverse lines of fillet welds at the lap joint are expected to meet the intent of this requirement. An overlap length of 50mm should be sufficient to allow for clamping the parts together during welding. Further, Clause 12.4.14 stipulates that intermittent fillet welds are prohibited for cyclically loaded structures (barring certain exemptions), therefore these welds must be continuous. Good performance of continuously welded lap joints between infill plate and fish plate under cyclic loading was demonstrated through experimental work by Schumacher *et al.* (1999) discussed in Chapter 2.

The proposed geometry of the infill panel-to-fish plate weld and the infill panel splice weld are shown in Figure 3-4. The 6 mm fish plate thickness specified is the smallest thickness that is readily available and easily fillet welded to beam and column boundary elements. A 20 gauge thickness of fish plate material is a similar thickness to those tested in previous SPSW tests discussed in Chapter 2. The labels “Weld #1”, “Weld #2”

and “Weld #3” refer to the three different heat dispersion characteristics of each weld location, discussed in Section 3.4.

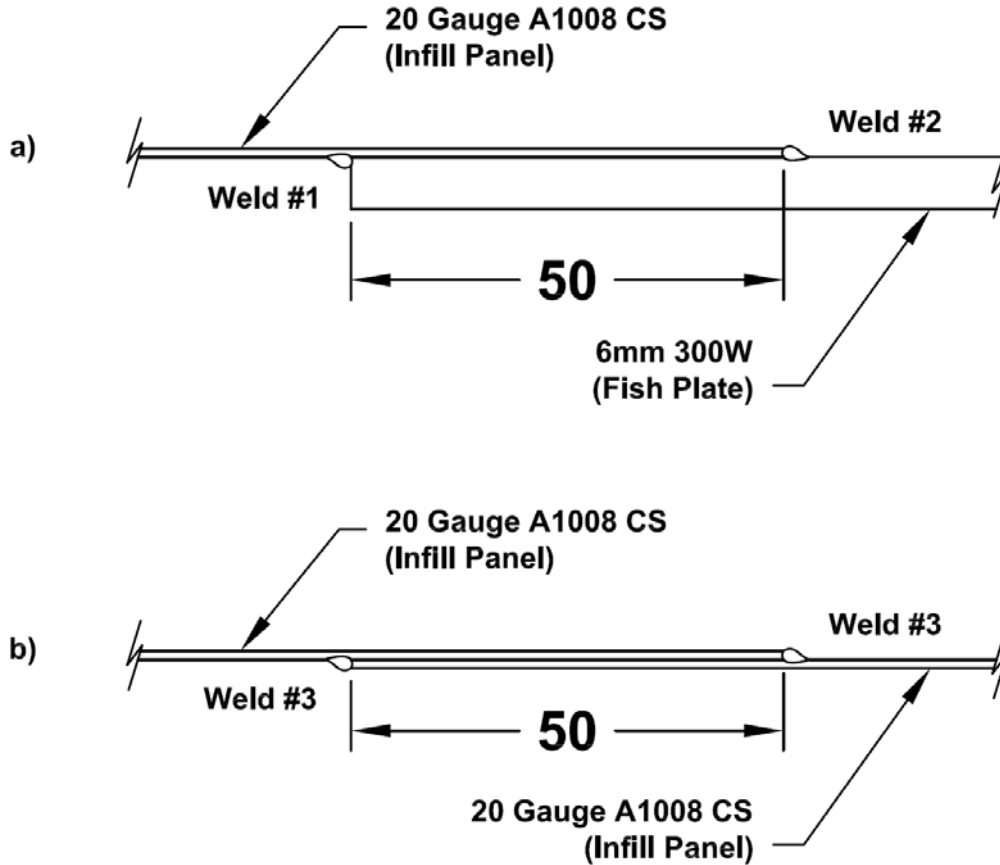


**Figure 3-4: Cross-Sections of Lap Joints, a) Infill Panel-to-Fish Plate, and b) Infill Panel Splice**

The reason for the required two lines of weld is the eccentricity of the load path through the joint. If a single transverse weld is used, and no additional out-of-plane restraint is provided at the joint, under direct tensile load the joint may rotate and prying action will open the joint (Miller, 2001). This opening notch is a stress raiser that can initiate unstable crack propagation at the root of the weld.

In the case of the proposed 20 gauge infill panel connection to a fish plate, the proposed fish plate is much stiffer than the infill panel and will not rotate significantly as the infill plate buckles. The out-of-plane rotation of the infill panel will cause an opening effect at the weld root when only one transverse weld is provided, as shown in Figure 3-5.

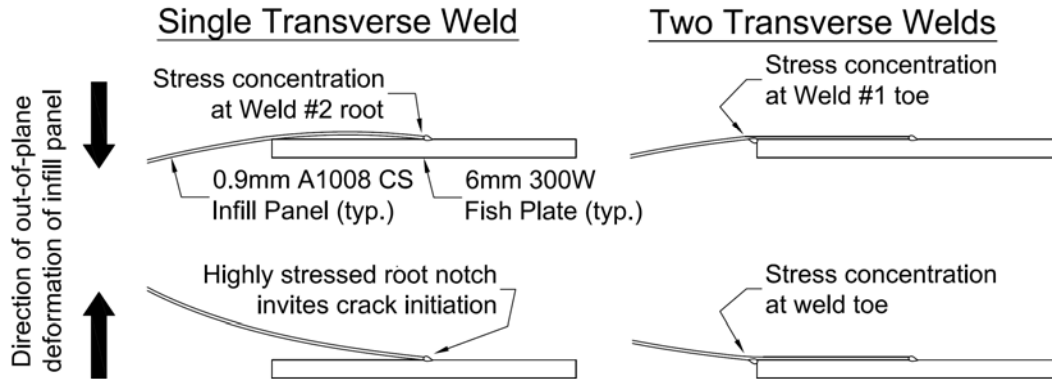


**Figure 3-5: Qualitative Impact of Infill Panel Buckling on Fillet Weld Stresses at Infill Panel-to-Fish Plate Connection, for Two Joint Geometries**

Berman and Bruneau (2005) and Kharazzi (2005) used only a single weld, as shown in the “Single Transverse Weld” in Figure 3-5. This welded joint configuration is intended to simulate a rehabilitation situation where weld access to the joint is only available from one side, such as an exterior frame in a building where cladding restricts access. However, this connection geometry may negatively impact the overall performance of the system.

In order to investigate whether a significant difference in performance can be expected between these two details, testing to compare a single transverse weld to a double transverse weld lap joint is required.

### 3.3 Materials

As shown in Figure 3-4, the fish plates are made of CSA G40.21 300W steel, and the infill panel is ASTM A1008 CS Type A cold-rolled steel. In the case of the fish plates, 300W steel is the most commonly available structural steel plate and has higher nominal yield strength than the infill panel. In the case of the infill panel material, the designation CS stands for Commercial Steel, and Type A is one of three sub-designations of Commercial Steel (Types A, B, and C), which differ primarily by their chemical composition. All three designations are weldable (ASTM, 2008). Though mechanical properties are not specified for steels designated CS, the probable yield strength is typically between 140 to 275 MPa (ASTM, 2008).

In a steel plate shear wall design scenario, the design engineer would specify A1008 SS, where SS denotes Structural Steel, and a grade denoting the desired yield strength. For instance, A1008 SS Grade 33 would be guaranteed by the supplier to have a minimum yield strength of 230MPa (33 ksi). Both A1008 CS and SS steels are cold-rolled and have similar mechanical properties and chemistries; the main difference being that CS steels have no guaranteed mechanical properties. ASTM A1008 CS was used in this program since it was readily available from local sheet steel suppliers, whereas none had any type SS sheet steel in stock. Given that the properties of A1008 type SS and type CS

material are essentially identical, the use of type CS material was considered a valid substitute for investigating the procedures for welding the infill panel. Berman and Bruneau (2005) appear to have reached a similar conclusion, as they also used A1008 CS steel for the infill panels in their research program.

### 3.4 Heat Input

It is clear from the literature that heat input is the most critical welding parameter when welding thin sheet to thick plate. Kou (2003) points out that the thicker a component is, the faster it dissipates heat, and thus the faster its cooling rate. In mild steels, fast cooling rates are known to produce brittle martensitic micro-structures (Kou, 2003). Mohler (1983) indicates that heat input must be high enough to ensure proper fusion to the thick metal, yet low enough to prevent burn-through of the thin metal.

Excess heat input can cause weakening of the heat affected zone (Section 3.9.5), can increase the probability of solidification cracking (Section 3.9.3), and can increase the magnitude of residual stresses and distortion (Section 3.9.6).

For arc welding, Kou (2003) indicates that heat input per unit length of weld can be calculated as shown in Equation 3.1.

$$[3.1] \quad q = \eta \frac{EI}{v}$$

where  $q$  = heat input per unit length [kJ/mm]

$\eta$  = heat source efficiency [fraction, where 1 = 100% efficient]

$E$  = voltage of power source [Volts]

$I$  = current of power source [Amps]

$v$  = weld travel speed [mm/s]

Heat source efficiency is a fractional measure of the energy that actually reaches the workpiece after heat losses, and depends on the welding process. For GMAW, the efficiency is typically  $80\% \pm 10\%$  (Kou, 2003). The calculation of “nominal” heat input per unit length of weld is the same as shown for equation 3.1, but omitting the heat source efficiency term.

Since heat input per unit length varies inversely with weld speed, increasing the speed of welding can reduce heat input. However, it is very difficult for manual arc welding to maintain a constant travel speed. Also, faster welding reduces the width of the weld pool and may result in improper fusion for narrow welds (Blodgett, 2007b). In developing a welding procedure, care must be taken to keep the welding speed manageable for the welding technique (manual or automatic) used.

It is important to differentiate between the three different heat dispersion conditions at the weld locations, shown in Figure 3-4. Weld #1 requires a balance between sufficient heat to fuse with the 6mm steel plate, and low enough heat to prevent burn-through of the thin sheet. Weld #2 poses less risk of burn-through, however too little heat input may result in a lack of weld fusion due to the relatively large heat sink formed by the 6mm steel plate for the small weld size. Weld #3 risks burn-through since the thin sheet steel is so thin.

### 3.5 Weld Process Selection

For lap joints composed of a sheet less than or equal to 1mm thick and a thick member, Houldcroft (1990) suggests that several different processes are appropriate. These are brazing and soldering, diffusion bonding, electron beam or laser beam welding, and ultrasonic welding. If the thin sheet is between 1mm and 2mm in thickness, SMAW, GMAW, and gas tungsten arc welding (GTAW) are also deemed acceptable, though Houldcroft indicates preheat is required for all arc welding except pulsed GTAW (GTAW-P), presumably due to its low heat input.

Though capable of providing satisfactory welds, processes other than SMAW, FCAW, GMAW, and GTAW are used infrequently by steel fabricators (AISC, 2006) and will not be considered in this research. Nonetheless, it should be noted that laser beam welding and hybrid laser-gas metal arc welding technologies are being successfully applied, often with the aid of robotics, for low heat input welding in the automotive, aeronautic, and ship building industries (Kou, 2003; Kelly *et al.*, 2006).

SMAW and FCAW can be eliminated as potential welding processes for welding thin plates to thick plates. Neither process is regarded as a low heat input process. Furthermore, SMAW is inefficient relative to wire-feed processes, and the consumable flux does not provide the same quality of shielding as a gas directed under pressure towards the weld pool. FCAW requires substantial heat in order to vaporize the solid flux “core” inside the electrode which provides shielding (Kou, 2003).

Numerous sources confirm that GTAW or GTAW-P are two of the best arc welding options for welding thin sheets (Mohler, 1983; Brace and Brook, 2002; Kou, 2003). However, though they can produce very high quality welds, GTAW is known to require a high operator skill level, is prone to relatively slow production speeds, and is relatively expensive (Kou, 2003; Lancaster, 1992).

GMAW may provide a sufficiently robust weld requiring less operator skill than GTAW, at greater production speed, and lower cost (Kou, 2003; Lancaster, 1992). This reduction in operator skill is mainly due to the so-called “self-regulating arc” phenomenon present in GMAW. As the operator varies the distance of the electrode from the workpiece, the power supply compensates for the change in arc voltage by changing the current. If the electrode is brought too close to the workpiece, the arc length and arc voltage are

reduced, and the power supply compensates by increasing current which increases the melting rate of the electrode and prevents stubbing. If the electrode is raised away from the workpiece, the arc length and arc voltage increase, and the power supply compensates by reducing the current, slowing the melting rate of the electrode so the wire feeder can bring it closer to the workpiece before melting (Kou, 2003, Lancaster, 1992). Recent literature suggests that GMAW employing spray-pulsed (GMAW-P) or short-circuit (GMAW-SC) waveforms is being used with increasingly thin sections, in the range of 20 or 22 gauge sheet steel (Brace and Brook, 2002; Kou, 2003; Lancaster, 1992).

GMAW joins metals by heating them with an arc between a continuously fed solid metal filler wire and the base metal. A schematic of the process is shown in Figure 3-6. Shielding from impurities is provided by gases directed towards the weld region. The consumable electrode and shielding gas are provided through a “gun”, hand-held in the case of manual arc welding (Kou, 2003).

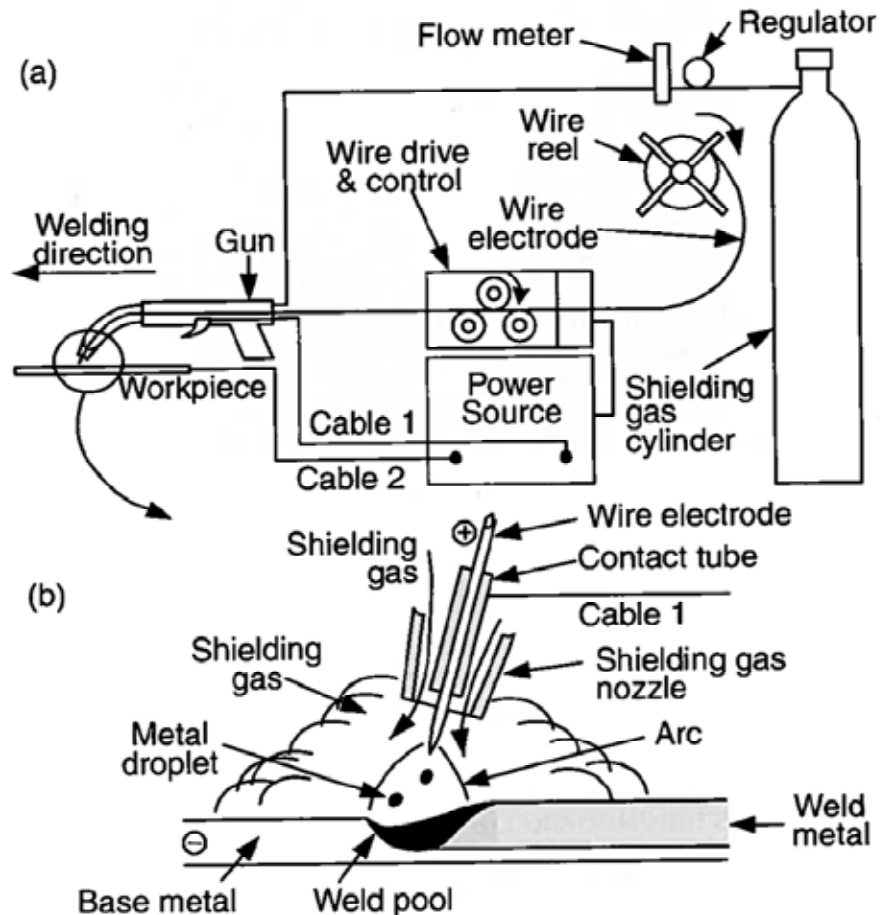
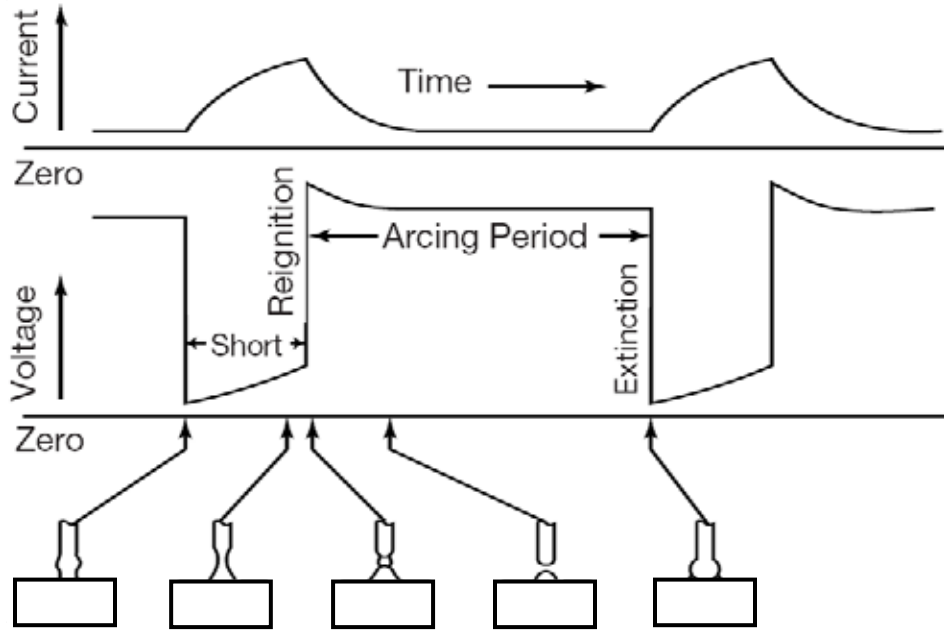


Figure 3-6: Schematic of GMAW Process, a) Overall, b) Welding Area Enlarged (Kou, 2003)

In pulsed GMAW, the current output changes (“pulses”) between a peak value and a lower value at a rapid rate. The peak current surges to above the value required for spray transfer, and then drops to a background level so that at each pulse a drop of metal is transferred across the arc. The background current is sufficient to maintain the arc, but not enough to create a drop of metal (AISC, 2006). Drops are deposited at between 100 and 400 Hz, resulting in an efficient deposition process with a relatively low average current. Welding can occur in all positions (AISC, 2006). The main drawback of GMAW-P is the additional cost associated with more sophisticated welding equipment when compared with other GMAW metal deposition modes.

The weld metal transfer mechanism of GMAW-SC is such that a drop of molten electrode at the tip of the electrode wire contacts the base metal, temporarily extinguishing the arc. This causes a short circuit which raises the electrode temperature, causing the molten drop to be deposited against the workpiece, breaking away from the solid electrode wire, and the arc re-initiates (AISC, 2006). The process occurs at between 20 and 200 Hz. The lowest range of welding currents and smallest diameter electrodes can be used, and due to the fast-freezing characteristics of the weld, welding can occur in all positions (CSA, 2003). For GMAW, this is the preferred transfer mode for very thin sheets due to its low heat input (AISC, 2006; Mohler, 1983; Brace and Brook, 2002; Kou, 2003; Lancaster, 1992; CSA, 2003).

For GMAW-SC, direct current electrode positive (DCEP) polarity is generally used since it minimizes the amount of heat transferred to the workpiece when compared to DCEN or AC, and positively charged gas ions bombard and deoxidize the workpiece surface (Kou, 2003; Lancaster, 1992). The frequency of short circuiting is generally between 20 and 250 Hz (Lancaster, 1992). Currents between 50 and 225 amps maintain the arc (AISC, 2006), while the current may rise to 320 to 370 amps during the short-circuiting (Green, 2004). An example of a short-circuit waveform is shown in Figure 3-7. The voltage and current are plotted against time, and small figures show the corresponding physical process of weld metal being deposited to the workpiece.



**Figure 3-7: Schematic of Short - Circuit Waveform for GMAW  
(adapted from AWS, 1976)**

One important benefit of the modern short-circuit process is so-called “one-knob control”. This ensures that the operator can adjust one welding parameter, and the other parameters are automatically adjusted by the software to ensure no negative impact on the welding process (Lancaster, 1992; Yarmuch, 2008). For example, if wire-feed rate is changed, the current is automatically adjusted to help maintain a stable arc.

### 3.6 Electrode

The choice of electrode is based principally on the required strength and toughness of the finished weld, and electrode availability. An ER70S-6 electrode appears appropriate for the combination of plate thicknesses and material grades to be welded. The solid electrode is readily available in small diameters appropriate for welding thin sheet, is prequalified under relevant welding standards for GMAW of steel sheet (AWS D1.3, 2008; AWS A5.18, 2005), and is especially suited for sheet metal applications (AWS A5.18 Appendix A, 2005). The 480 MPa (70 ksi) ultimate strength of the electrode exceeds that of both metals being welded. The minimum ultimate strength of the 300W steel plate is 450 MPa (65 ksi), and while no ultimate strength is specified for the A1008 CS sheet steel, its yield strength is expected to be between 140 and 275 MPa (ASTM A1008, 2008), which is relatively low. Last, the electrode has a specified Charpy V-Notch (CVN) toughness of 27J at  $-30^{\circ}\text{C}$ , satisfying the minimum CVN toughness of fracture critical welds under AWS D1.8: Structural Welding Code – Seismic Supplement (2005), which is 27J at  $-20^{\circ}\text{C}$ .



### 3.7 Shielding Gas

Gas mixtures for thin steel sheet welding typically consist of either 100% argon (Ar), 100% CO<sub>2</sub>, a balance of Ar and CO<sub>2</sub> (typically in the range of 75%Ar-25% CO<sub>2</sub>), a balance of Ar and small amount of O<sub>2</sub>, or a tri – mix of Ar, CO<sub>2</sub>, and O<sub>2</sub> (Lancaster, 1992). An optimization between cost, arc properties, and finished weld quality is sought. The effectiveness of shielding gas depends on its composition, the composition of the weld metal, the gas flow rate, cross – wind conditions, and weld orientation.

For low – heat input welding, argon is a good choice since it is inert and thus introduces no impurities to the weld metal, has low ionization potential which reduces the energy required for arc initiation, is relatively cheap, and has a high density and thus good resistance to cross - drafts (Kou, 2003). Brace and Brook (2002) also indicate that high Ar mixes reduce weld spatter. Drawbacks of 100% Ar shielding include potential problems with weld pool edge wetting, undercut, and arc wandering (Lancaster, 1992).

CO<sub>2</sub> gas is the cheapest of all shielding gases to produce, and has an even lower ionization potential than argon, improving arc initiation and maintaining good arc energy (Kou, 2003). Arc energy is important to ensure a consistent bead profile, good weld penetration, and minimize undercut (Green, 2004; Kou, 2003). Drawbacks of 100% CO<sub>2</sub> shielding include the possibility of excessive spatter, and potential porosity and oxidation since CO<sub>2</sub> decomposes into carbon (C) and oxygen (O) in the heat of the arc (Kou, 2003).

In order to keep the process developed for welding thin infill panels in this experimental program as simple to adopt as possible, only common mixtures of shielding gas are considered. 25%CO<sub>2</sub> – 75%Ar or pure CO<sub>2</sub> mixes were first considered. The ER70S – 6 electrode is qualified for both shielding gases (AWS A5.18, 2005). It contains high concentrations of manganese (Mn) and silicon (Si), which are strong deoxidizers. Possible excess spatter can be resolved by increasing the Ar content. If undercut or wetting problems that cannot be rectified by changing heat input are observed the CO<sub>2</sub> content can be increased. Inspection of weld samples ensures CO<sub>2</sub> use does not result in excess weld porosity.

Gas flow rate must be sufficient to ensure good protection of the weld metal, however, excessively high flow rates can affect the shape of the weld pool and weld bead (Kou, 2003). Since Ar is heavier than air, during overhead welding particular care must be taken to ensure sufficient gas flow rate to maintain a good shield. Flow rates for short circuiting GMAW with CO<sub>2</sub> or mixed shielding gases are in the range of 25 to 30 cubic feet per hour (Nadzam, 2006).

CSA - W59 Clause 5.5.4.3 states that GMAW welding must not be performed in the presence of a cross – draft or wind unless the weld region is sheltered such that the

effective wind speed is less than 8 kph (CSA, 2003). This may be a consideration in the SPSW system if the thin gauge infill panel is installed in the field.

### **3.8 Drawbacks of Short Circuit GMAW**

Spatter can be a problem in short circuiting, since a small explosion occurs which vaporizes the weld metal and deposits it when the short-circuit occurs. Aside from using an Ar – based shielding gas, this can be minimized by reducing the current that flows immediately prior to the rupture of the “bridge” (i.e., weld metal stuck to the base metal). This is typically achieved by employing a waveform that ensures the short circuit and arc re-ignition occur when the current is lowest, as shown in Figure 3-7 (Lancaster, 1992). This requires an electronically controlled inverter power source (Lancaster, 1992). The “one drop per pulse” rule of thumb is believed to minimize the amount of oscillation, and thus spatter, of the weld pool (Lancaster, 1992).

The main drawback of GMAW – SC is that, due to the low heat input associated with this process, it can suffer from a lack of sidewall fusion in thicker sections (AISC, 2006; Lancaster, 1992). Lancaster (1992) recommends limiting use of this process to plates thinner than 18mm. This potential fusion problem is also why CSA W59 does not prequalify GMAW – SC welding, though it is permitted when satisfactory qualification tests have been performed to validate a welding procedure (CSA, 2003).

### **3.9 Typical Problems Related to Welding of Carbon Steel**

The following sub-sections list typical problems encountered when welding carbon steels, and strategies employed for their mitigation for the infill panel welds discussed in this research program.

#### **3.9.1 Lamellar Tearing**

Lamellar tearing can occur when weld shrinkage strains cause tensile load perpendicular to planes of weakness in the base metal. These planes of weakness are caused by inclusions flattened into long strings between layers of strong material, roughly parallel to the rolling direction of the steel. Under tensile load perpendicular to the rolling direction of the steel, fracture following the planes of weakness appears, typically in or just outside the heat affected zone (HAZ) (AISC, 2006; Kou, 2003). The HAZ is the region adjacent to the weld which does not melt but whose properties change as a result of temperature change during welding.

Lamellar tearing is not expected to be an issue in the lap joints in Figure 3-4. The shrinkage strains imposed by the small weld bead are negligible, and when tensile load from the tension field in the infill panel passes through the joint, it travels parallel to the rolling direction of the plates, not perpendicular.

### 3.9.2 Porosity in the Weld

Porosity refers to gas inclusions that are trapped by the solidifying weld metal. These inclusions represent stress raisers and can serve as initiation sites for cracking, reducing the toughness of the weld metal (Kou, 2003).

When welding carbon steels, oxygen (O), nitrogen (N), and hydrogen (H) gases are the main concerns. All can form inclusions when provided in excess of the quantities that are soluble in the weld metal. GMAW is one of the “cleanest” welding processes, since the gas shielding effectively protects the weld from O, N, and H in the air (Kou, 2003). Additional sources of O and H include moisture on poorly maintained electrodes, and poorly cleaned base metal surfaces.

As discussed in section 3.7, in GMAW the greatest potential for porosity is from oxygen or carbon monoxide inclusions produced from the breakdown of CO<sub>2</sub> shielding gas in the heat of the arc. However, the ER70S – 6 electrode has high concentrations of deoxidizing elements, 1.40% to 1.85% Mn and 0.80% to 1.15% Si (AWS A5.18, 2005), to prevent porosity formation. Thus, it is qualified for use with 100% CO<sub>2</sub> shielding gas (AWS A5.18, 2005).

### 3.9.3 Solidification Cracking

Solidification cracking, also known as hot cracking, occurs during the final stages of solidification when residual tensile stresses between adjacent solidified grains exceed the capacity of the partially molten weld metal (Kou, 2003). During this “terminal stage” of solidification, the remaining liquid weld metal is located between the grain boundaries, which causes a weakening of the grain boundaries. This is exacerbated by the presence of high quantities of low – melting point elements, particularly sulphur (S). Stresses arising from solidification shrinkage and thermal contraction as the weld cools cause a crack to form at the weakened grain boundaries (Kou, 2003).

Ensuring a high weld metal Mn : S ratio is typically the solidification cracking control used for low – carbon steels. Note that the maximum permissible carbon content for 300W steel is 0.22% (CSA, 2004). Kou (2003) indicates that for steels with carbon contents between 0.2 and 0.3% control of the Mn:S ratio ceases to be an effective means of controlling solidification cracking. Instead, reducing the weld filler metal carbon content is more effective, presumably to reduce the probability of forming a brittle martensitic structure prone to cracking. The carbon content of the ER70S-6 electrode is between 0.06% and 0.15% (AWS A5.18, 2005), which should dilute the carbon content of the weld metal and reduce the solidification cracking risk.

Patchett (2003) provides an equation to gauge the hot cracking susceptibility (*HCS*) of weld metal, based on the percent chemical composition of the filler metal. A value greater than 4 indicates a potential problem.

$$[3.2] \quad HCS = \frac{\%C * (\%S + \%P + \frac{\%Si}{25} + \frac{\%Ni}{100})}{3 * \%Mn + \%Cr + \%Mo + \%V} * 10^3$$

Taking the worst-case allowable compositions of the ER70S-6 electrode (AWS A5.18, 2005), a value of 3.84 is obtained. Therefore, hot cracking is not expected to be a problem for this electrode.

### 3.9.4 Hydrogen-Assisted Cracking

Hydrogen-assisted cracking (HAC), also known as cold cracking, is a well known problem in carbon steels. AWS D1.3 Clause 1.5.2.1 states that measures must be taken to prevent underbead cracking, which Kou (2003) and AISC (2006) identify as a type of hydrogen cracking that occurs in the weld metal or the heat affected zone (HAZ) parallel to the fusion boundary.

AISC (2006), Kou (2003), and Patchett (2003) identify several factors that must be present for hydrogen cracking to occur:

- 1) *Significant hydrogen must be present in the weld metal.* The presence of hydrogen can be a result of moisture (water) or hydrocarbons (oil) on an improperly cleaned work surface, moisture on improperly stored electrodes, hydrogen from certain fluxes (e.g. SMAW cellulosic flux), or poor atmospheric shielding.

Atomic hydrogen at ambient temperatures is soluble to roughly 6ppm in ferrite (Patchett, 2003). Thus less than 5ppm is regarded as “very low hydrogen content”, while anything higher than 20ppm is regarded as “high hydrogen content” (Patchett, 2003). CSA W59 assigns the most favourable hydrogen level to electrodes with less than 5mL of hydrogen per 100g of deposited weld metal when measured with standard techniques discussed in CSA W59 Clause P4.2. CSA W59 explicitly states that the use of GMAW with clean, solid wires can be assumed to meet this requirement without testing, presumably because the GMAW process has excellent atmospheric shielding and no flux is used (CSA, 2003). Use of this process and ensuring the workpiece is free of oil and moisture prior to welding are the main HAC prevention strategy implemented in this work.

- 2) *Tensile residual stresses at the weld.* Tensile residual stresses approaching the yield strength of the base material are always present in welded assemblies (AISC, 2006). Though various processes such as shot peening, arc oscillation or vibration, and pre- or post-weld heat treatment can reduce residual tensile stresses, these processes are not necessarily readily available or cost-effective in a field construction environment.

- 3) *Susceptible microstructure*, such as the brittle martensite phase in carbon steels. Martensite formation is likely in the infill plate-to-fish plate weld considering the fast cooling rates associated with welding small volumes of weld metal to the relatively thick fish plates.

A scalar number known as carbon equivalent (CE) is an accepted method of gauging the likelihood of undesirable microstructures to form in the HAZ. CSA W59 (CSA, 2003) uses equation 3.3, below, to calculate carbon equivalent. Patchett (2003) cautions that this equation should only be used for steels with a carbon content greater than 0.15%, and AISC (2006) indicates it should only be used for steels with carbon contents between 0.18% and 0.30%. The maximum carbon content of 300W steel is 0.22% (CSA, 2004), so this formula is appropriate.

$$[3.3] \quad CE = \%C + \frac{(\%Mn + \%Si)}{6} + \frac{(\%Cr + \%Mo + \%V)}{5} + \frac{(\%Ni + \%Cu)}{15}$$

Taking the worst-case allowable chemical composition for 300W steel, a CE of 0.56 is obtained. This steel is highly susceptible to forming an undesirable microstructure; it is a so-called “Zone III” steel on the Graville diagram labeled Figure P1 in CSA W59 Appendix P. CSA W59 (2003) indicates that for such steels, strict control of hydrogen levels, is the most effective method of mitigating hydrogen cracking (CSA, 2003). Hydrogen levels are discussed in point 1), above.

- 4) *Low temperatures (between – 100°C and 200°C)*. Since structural steel is typically at ambient temperature, this condition is unavoidable.
- 5) *Time*. Hydrogen cracking is a delayed process, possibly due to time required for diffusible hydrogen to migrate through steel and reach concentrations high enough to cause cracking. It has been suggested this time may be between 16 and 72 hours. For this reason, in certain highly susceptible steels, codes require non-destructive inspection to be delayed 48 hours (AWS D1.1, 2008; AISC, 2006).

Though heat treatments are not preferred since they reduce production speed and increase cost, they are effective mitigation methods for hydrogen cracking. Preheat removes excess moisture on the base metal, reducing available hydrogen, and also slows the cooling rate, reducing the likelihood of martensite formation. Post-heat consists of heating the steel to between 400 and 450°F immediately after welding (i.e. before it cools to room temperature) and holding this temperature for an hour per inch of base material thickness (AISC, 2006). The higher temperature increases hydrogen mobility and allows it to migrate away from the weld region.

Clause 5.7 of CSA W59 indicates that for steels approved by CAN/CSA G40.21 where the thickest part joined is less than 20 mm thick, no preheat is required. Furthermore, based on the worst-case steel chemistries allowed for the fish plate and infill plate steels, the

procedures of CSA – W59 Appendix P : Guideline and Commentary on Alternate Methods of Determining Preheat indicate that no preheat is required (CSA, 2003).

### 3.9.5 Work-Hardened Materials and the Heat Affected Zone

Cold-rolled materials are plastically deformed by mechanical means, generating dislocations in the microstructure. These dislocations act to prevent further plastic deformation in the metal, and as a result the strength and hardness of the metal increase, while the ductility of the metal decreases (Callister, 2003).

In the heat-affected zone (HAZ), the strain energy stored by the work-hardening process provides driving force for the nucleation of new, soft, grains that have not been strain – hardened. Following recrystallization, depending on the magnitude and duration of the welding temperatures, the HAZ grains will grow in an attempt to reduce the total grain boundary surface area (Kou, 2003).

Since grain boundaries are obstacles to dislocation movement, grain growth reduces strength, toughness, and hardness (Kou, 2003; Callister, 2003). This is illustrated in Figure 3-8. Point 1 is adjacent to the liquid weld metal, whereas Point 3 is at the outside edge of the HAZ. Points 1 and 2 are heated significantly by the liquid weld metal, and suffer a significant loss of strength due to recrystallization and grain growth. The rate and extent of both recrystallization and grain growth increase with temperature and with time, thus a low – heat input process is preferred to reduce HAZ weakening.

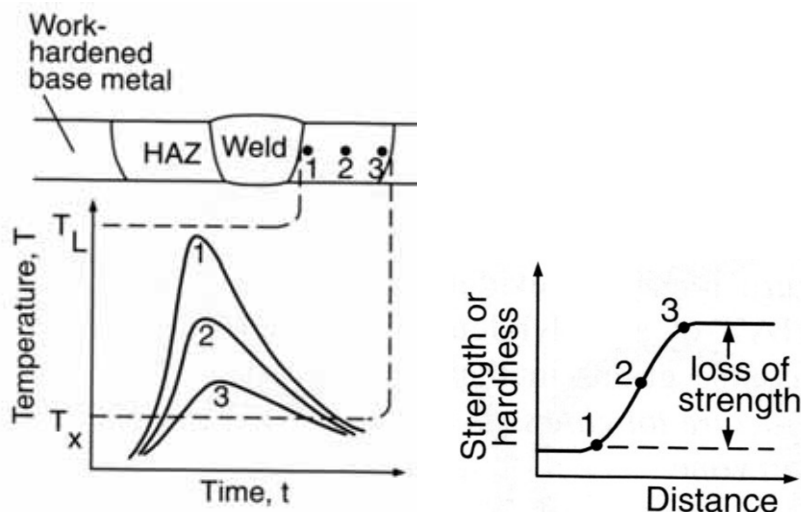


**Figure 3-8: Softening of Work-Hardened Material Caused by Welding (Kou, 2003)**

For welds as small as those required for a 20 gauge thick steel plate, it is difficult to predict the impact of heat on the HAZ, and whether it will have a significant impact on overall connection behaviour. With regards to the SPSW lap joint being studied, small –

scale mechanical testing of different joint designs will provide some experimental evidence of weld soundness.

### 3.9.6 Residual Stresses and Distortion

Residual stresses are internal stresses that result from differential cooling in various regions of the parts being welded. The metal at and near the weld undergoes a cycle of heating and cooling, while the material outside the HAZ undergoes no heating and cooling and thus no expansion and contraction. A combination of thermal shrinkage and solidification shrinkage resulting from phase changes as the liquid weld metal cools provide the volume change which gives rise to residual stresses (Kou, 2003). The material outside the heated zone restrains the weld and HAZ material, resulting in tensile stresses being generated at the weld, and compressive stresses away from the weld.

Both the tensile residual stresses and compressive residual stresses have an impact on the performance of the weld and the surrounding structure. Tensile stresses are large, on the order of the yield strength of the weld metal (AISC, 2006), and they can initiate or propagate cracks in the weld material or HAZ (Kou, 2003). Compressive residual stresses away from the weld can exceed the compressive strength of the connected part, and cause it to distort (Kou, 2003; Bhide *et al.*, 2006).

Distortion is either in – plane or out – of – plane. In – plane distortion is caused by longitudinal, transverse, or rotational shrinkage of the weld metal (see Figure 3-9). Out – of – plane distortion includes so – called angular (Kou, 2003), bowing, or buckling distortions (Bhide *et al.*, 2006; Kou, 2003; Ikeagu, 2007; Kelly *et al.*, 2006). Distortion can result in fit – up problems between structural components, which may reduce structural integrity and increase fabrication costs (Bhide *et al.*, 2006).

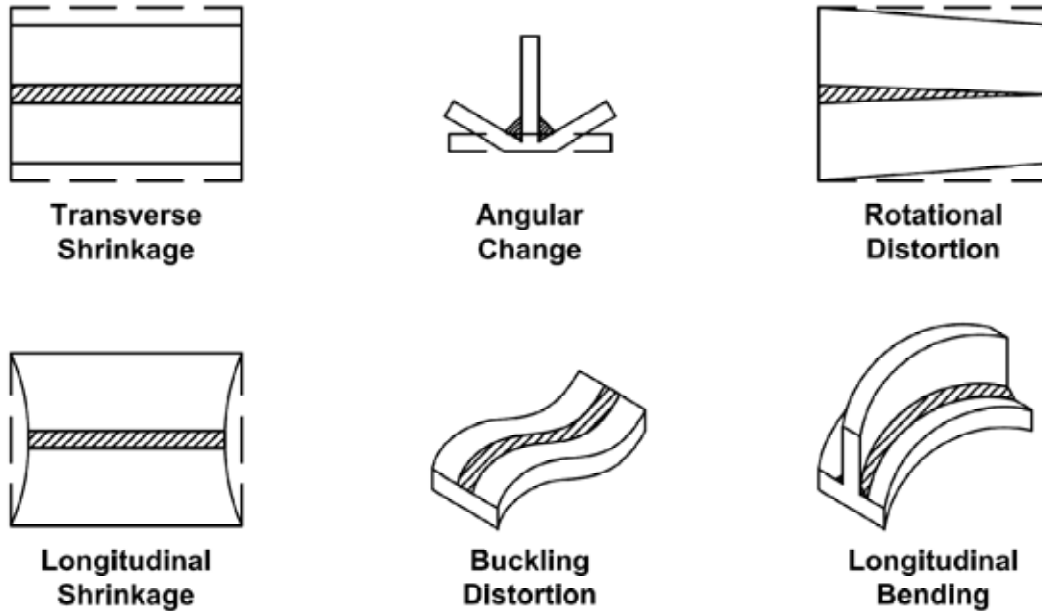


**Figure 3-9: Types of Welding Distortion (adapted from Masuchi, 1980)**

Buckling distortion is the most common type of distortion in thin plate structures (Bhide *et al.*, 2006), due to the low buckling resistance of thin sections. Angular distortion is also a distinct possibility in the lap joints being developed in this program. Assume Weld #2 is completed prior to Weld #1 (Figure 3-4). As weld metal at Weld #2 shrinks during cooling, the fit – up gap at Weld #1 will grow due to angular distortion, as shown in Figure 3-10. Clamping will be required to minimize the fit-up gap.

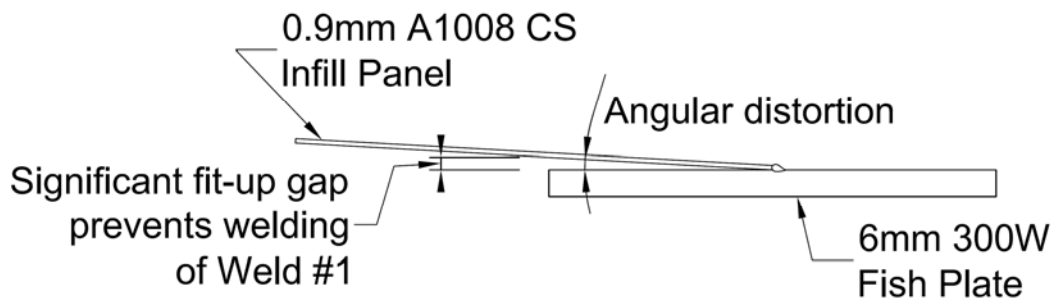


**Figure 3-10: Potential Angular Distortion Problem in Infill Panel-to-Fish Plate Joint**

Common strategies for reducing welding-induced distortions include minimizing weld metal volume, using a welding sequence that minimizes distortion, and reducing the heat input to the weldment (Bhide *et al.*, 2006; Kou, 2003; Blodgett, 2007 (a,b,c)). Blodgett (2007c) emphasizes that overwelding is particularly a problem with thin sections, since keeping weld size small is difficult and thin sections are flexible and distort easily. Excessively reinforced welds (e.g. very convex fillet welds) also increase distortion (Blodgett, 2007c).



In the lap joints under investigation, mechanical clamps and “stitch welding” will be employed to ensure tolerable fit – up. Note that clamp access to the infill panel-to-fish plate joint may be restricted in certain SPSW construction scenarios, such as where large columns are present, or when SPSWs occupy adjacent bays.

The so – called “stitch – welding” technique consists of tack welding intermittently around the entire circumference of a part to hold it in place. The operator then performs a series of passes around the circumference, making intermittent welds at a set spacing each time, until the final weld is continuous.

So long as the distortion does not cause the plates to separate such that welding is not possible, some initial warping of the infill panel in the SPSW is acceptable. Tension field action is the primary lateral load resisting mechanism of the system, and the tensile strength should not be affected by initial imperfections. Distortion – induced infill panel buckling may slightly reduce the initial stiffness of the SPSW when compared to an idealized model that does not contain initial imperfections.

### **3.10 WPS Qualification Requirements**

The majority of welding standards, such as AWS D1.3, D1.1, and CSA W59, outline certain prequalified joint geometries and welding procedures. Unfortunately the infill panel-to-fish plate and infill panel splice lap joints are not prequalified since the thickness of the thin sheet is less than 18 gauge, and the welding procedure is short-circuiting GMAW (AWS, 2008a; AWS, 2008b; CSA, 2003). A welding procedure requiring qualification must be developed.

Visual inspection and two successful bend tests, as described in AWS D1.3 Clause 4.6.2.2, are required for each welding procedure specification (WPS). The WPS is only valid for a unique combination, within certain tolerances, of variables such as electrode composition, strength, diameter, melting rate, amperage, wire feed speed, polarity, steel plate thickness, weld position, weld direction (“up” or “down” for vertical welding only), shielding gas composition, shielding gas flow rate, metal transfer mode (e.g. pulse, spray, globular, short-circuit), or the removal of a backing bar.

It should be noted that AWS D1.3 allows the use of a fillet weld in a sheet-to-sheet lap joint to qualify a sheet-to-supporting structural member connection (AWS D1.3, 2008). The sheet-to-sheet connection does not have the same fast cooling problem associated with the thick portion of the sheet-to-structural member connection. Other concerns, such as HAC, will vary in severity depending on the thickness of the thick sheet. Engineering judgment suggests that separate tests be conducted on both thin-to-thick and thin-to-thin joints, particularly for crucial load transfer connections such as the one investigated in this research program.

## Chapter 4: Weld Procedure Development

### 4.1 Introduction

The goal of the experimental program is to develop welding parameters and a joint geometry suitable for welding a very thin infill panel to a significantly thicker boundary element such as a fish plate in a steel plate shear wall. In addition, since thin sheet steel is typically cut from rolls that have a limited width, it is necessary to overlap two or more sheets to cover the area bounded by the boundary elements of an infill panel. Consequently, a procedure for joining two lengths of sheet steel will also be validated.

### 4.2 Experimental Program

In order to meet the objectives listed above, the experimental program is divided into three phases:

- 1) Ancillary tension tests of representative material samples in order to determine accurate material properties.
- 2) A justifiable comparison of trial welds to support the selection of a particular welding procedure. This comparison is based on weldability and visual assessment of weld quality.
- 3) Mechanical testing of the selected welding procedure, including quasi-static strength tests for a measure of weld quality, and cyclic tests to simulate the action of the infill panel buckling on the weld. Different configurations of the connection under investigation are tested.

The results of these tests will be used to select the connection configuration for the large-scale steel plate shear wall specimen, discussed in Chapter 6.

### 4.3 Ancillary Materials Tests

Representative samples of material from all stages of the experimental program are tested. Tension tests conforming to ASTM A370 (ASTM, 2001) for “sheet” specimens (< 19 mm thick) are conducted on coupons water-jet cut from samples of the following three materials:

- 1) 20 gauge ASTM A1008 CS steel sheet selected for the infill panel;
- 2) 6mm thick grade 300W plate used to simulate the fish plate. When connected in a T-joint to the bottom of the boundary members, the 6mm 300W plate is referred to as a “fish plate”;
- 3) Grade 350W W200x31 flange and web material, used for beams and columns in the large-scale steel plate shear wall specimen.

All tension coupons are cut to the geometry shown in Figure 4-1.

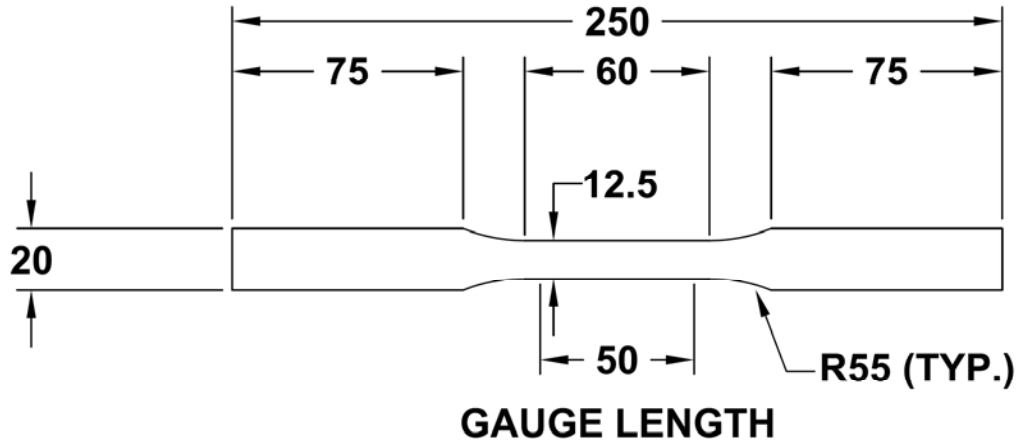


Figure 4-1: Tension Coupon Geometry

#### 4.4 Trial Welds and Welding Parameter Development

Trial weld specimens consist of the lap joints between two 150 mm X 150 mm steel plates shown in Figure 3-4. The infill panel-to-boundary member connection overlaps a 20 gauge A1008 CS steel sheet with a 6 mm thick 300W steel plate. The splice in the infill panel consists of two 20 gauge A1008 CS steel sheets. For ease of repeatability, all welding for these trials is conducted in the flat position.

The weld procedures developed with small specimens were tested on 610 mm x 610 mm specimens where distortion control is more difficult. The specimen design for these so-called “distortion specimens” is shown in Figure 4-2. These specimens consist of 610 mm x 610 mm 20 gauge sheet welded to 6 mm fish plates on four sides using the lap splice shown in Figure 3-4a. Corner details have a 5 mm gap identical to the detail used for the corners of the infill panel connection to the steel plate shear wall specimen (see Figure 6-2).

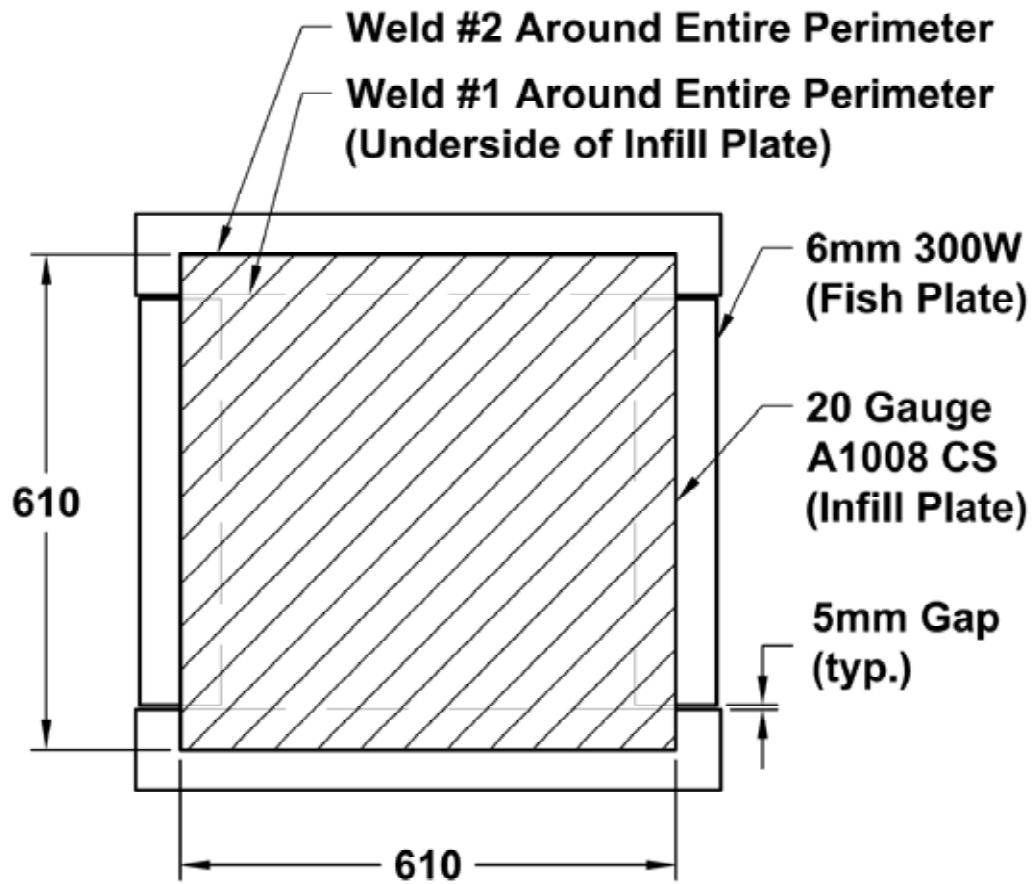


Figure 4-2: Typical Distortion Specimen

#### 4.4.1 Test Parameters

The test parameters are broken into two categories. The fixed parameters are listed in Table 4-1, and the parameters that are varied are listed in Table 4-2, along with a brief discussion of the rationale for each selection or variance.

**Table 4-1 : Welding Procedure Parameters - Fixed Parameters**

<b>Parameter</b>	<b>Discussion</b>
Process	GMAW-SC for low heat input
Current & Polarity	Direct Current Electrode Positive (DCEP) for low heat input.
Welding Position	For ease of repetition, all welds in this series are made in the flat position. Note that a horizontal position weld appears appropriate; however, due to the small thickness of the 20 gauge infill panel material, the welder does not need to tilt the electrode towards the joint as with a lap joint between two thicker pieces of material. A position similar to a flat bead-on-plate weld can be used.
Clamping Arrangement	The clamping is performed in a manner which provides sufficient restraint without interfering with welding, and the same clamping arrangement is used for every test specimen.
Surface Preparation	Uniform for all specimens. Consists of removing mill scale from the grade 300W plate by wire brushing, and removing oil from the A1008 CS sheet steel with an acetone-based cleaner.
Electrode Composition	ER70S-6. This selection is discussed in Chapter 3.
Welding Hand Motion	Directly affects weld pool and solidified weld geometry, strength, etc. The weld is too small for a weaving hand motion; a straight bead will be pulled or pushed.
Electrode Diameter (d)	The smallest electrode available, with diameter 0.6mm (0.023"), is the only diameter tested since minimizing the size of the weld helps minimize distortion, and this diameter will already produce larger than necessary weld volume.

**Table 4-2: Welding Procedure Parameters - Varied Parameters**

Parameter	Discussion
Voltage (E)	The higher the voltage, the higher the heat input per unit length.
Wire Feed Speed (WFS)	The current is automatically adjusted with changes to wire feed speed. This is known as “one-knob control”. Current directly affects heat input per unit length.
Weld Speed (v)	The faster the speed, the lower the heat input per unit length.
Heat Input Per Unit Length (q)	Heat sensing equipment is not available. Thus, nominal theoretical heat input per unit length is calculated from Equation 3.1
Chill Strip	A chill strip, in this case a piece of spare 6 mm thick 300W steel, placed behind the sheet steel acts as a heat sink and reduces the probability of burn-through. Trial specimens with and without a chill strip are evaluated.
Shielding Gas	75Ar-25CO <sub>2</sub> or 100CO <sub>2</sub> (discussed in Chapter 3).
Welding Equipment	A spool gun wire feeder or a suitcase wire feeder  (Power source is constant. See Section 4.4.2).

#### 4.4.2 Welding Equipment

A typical gas metal arc welding system requires four main components: a power source, a method of feeding the electrode, shielding gas, and a gun where power, electrode, and gas meet and contact is made with the weldment (Kou, 2003). Two wire-feed equipment options, referred to as Setup #1 and Setup #2, are tested in this research program. Both setups utilize the same power source, the Miller XMT 350 CC/CV, and the same gas cylinder. The differences are found in the wire-feed method and the gun.

Setup #1 utilizes a spool-gun style wire feed system, where a small spool of electrode is mounted directly to the gun, as shown in Figure 4-3.

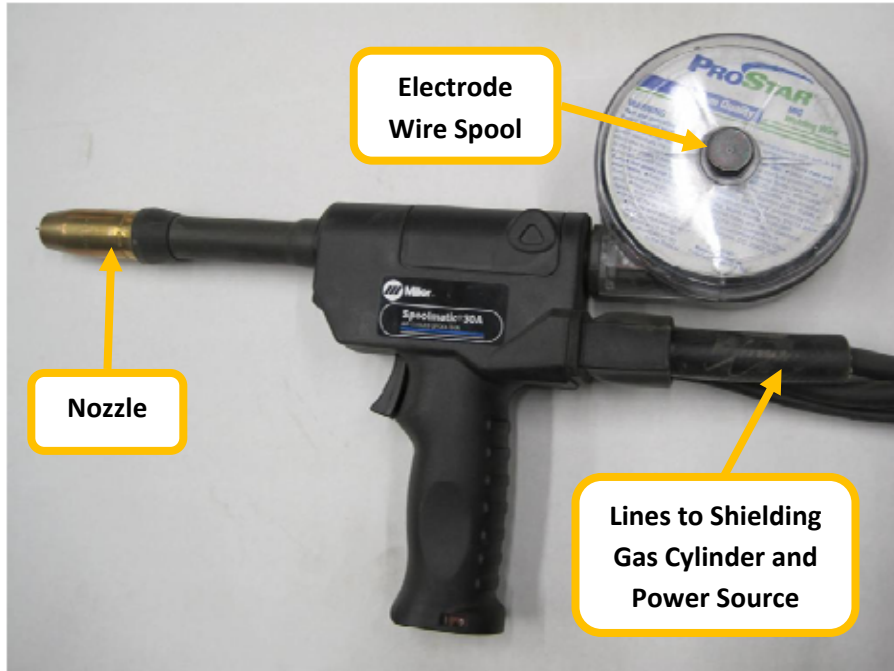


**Figure 4-3 : Spool Gun of Setup #1**

Setup #2 consists of a typical heavy-duty suitcase-style wire feed system used on structural steel projects, but modified to accommodate small wire diameters. The Miller Suitcase X-Treme 12VS Wire Feed System is a typical example of a wire-feed unit used for large diameter flux-cored wires (Anon., 2010b). The system is “voltage sensing”, meaning the wire feeder adjusts its speed to maintain the voltage set on the power source (Anon., 2010a). The modifications required to accommodate a very small electrode include changing the gas nozzle, contact tips, inlet wire guide, and drive roll to accommodate small wire. Setup #2 is shown in Figure 4-4, while the open suitcase is shown in Figure 4-5.

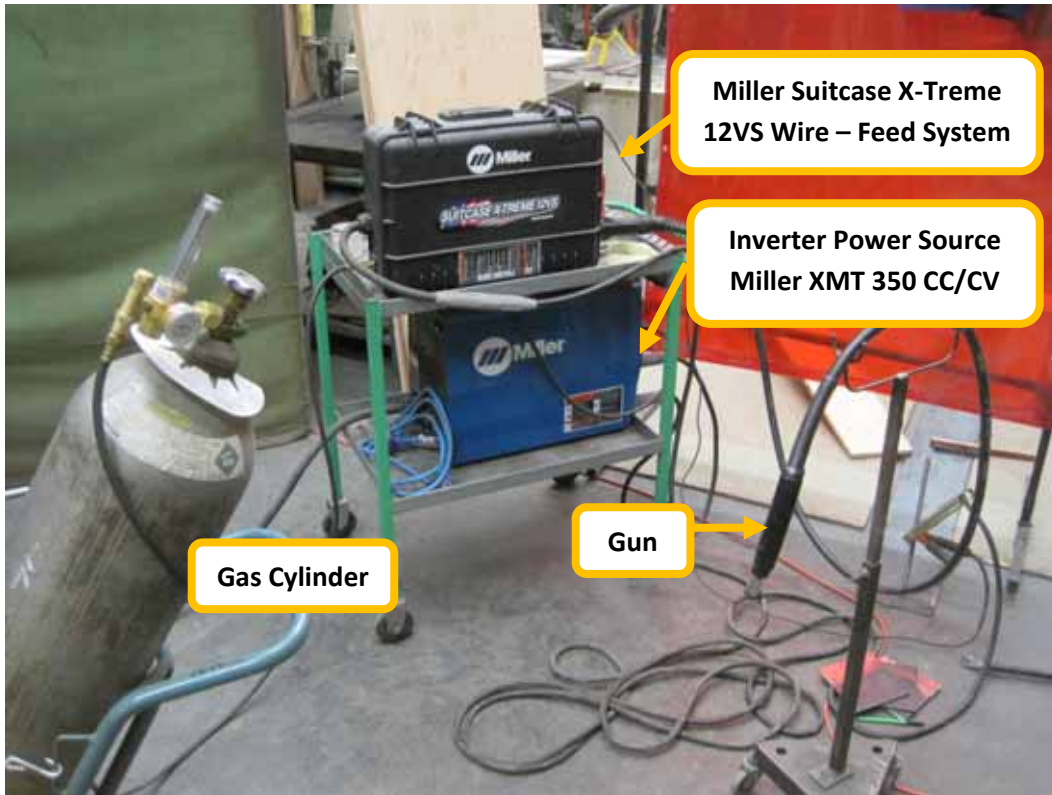


Figure 4-4: Welding Setup #2

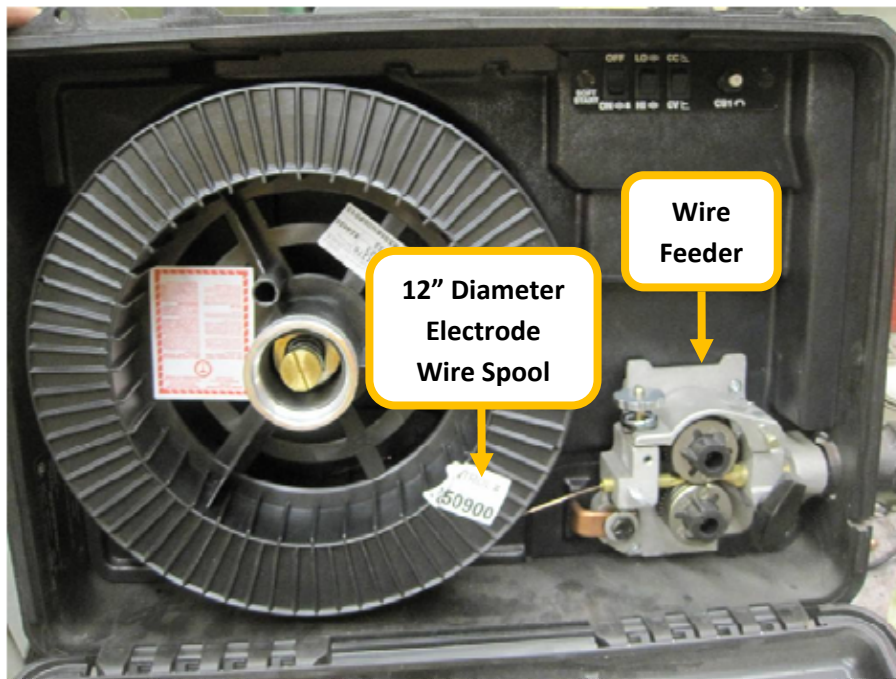


Figure 4-5: Interior of the Miller Suitcase X-Treme 12VS Wire-Feed System



One interesting feature of the Suitcase X-Treme 12VS Wire Feed System is the so-called “soft start” option. This setting gives the arc more time to initiate by slowing the initial wire feed speed to 20% of the set WFS, whereas without “soft start” the initial WFS is 50% of the set WFS. This is designed to prevent stubbing in large diameter electrodes during arc initiation (Anon., 2010b). A comparison of the two welding setups is shown in Table 4-3. They both have advantages and drawbacks; the ease of welding of the two systems during testing will determine which is preferred for use in this program.

**Table 4-3 : Comparison of Two Different Welding Equipment Setups**

Setup	Advantages	Disadvantages
#1 (Spool Gun)	<ul style="list-style-type: none"> <li>• Self-contained spool; welding can take place far from the power source, since the wire feed length is independent of the distance away from the power source.</li> <li>• Spool gun is inexpensive. If switching between typical push-feed GMAW and a specific application where small-diameter wire is required, changing to a spool gun is quick and time efficient (Harris, 2010). This may apply where the only small-diameter welding required on a SPSW job is the infill panel-to-fish plate weld.</li> </ul>	<ul style="list-style-type: none"> <li>• Gun + spool is heavier than a conventional gun without spool mount. Hand-motions are more cumbersome, and weldment access is more difficult.</li> <li>• For large volumes of electrode, small spools are not cost effective when compared with larger spools of wire (Harris, 2010).</li> <li>• Wire feed speed is set on an arbitrary scale from 1 (slowest) to 10 (fastest) by a dial on the handle of the gun, as opposed to a uniform measure such as “inches per minute”. This renders adopting a particular wire feed speed difficult.</li> </ul>
#2 (Suitcase Wire-Feed)	<ul style="list-style-type: none"> <li>• No cumbersome spool mount on the gun; superior ease of handling relative to Setup #1.</li> <li>• Cost economies when large volumes of electrode are required relative to Setup #1.</li> </ul>	<ul style="list-style-type: none"> <li>• Somewhat more complex adaptation than Setup #1; require a conventional suitcase wire-feed system with new gas nozzle, contact tips, inlet wire guide, and drive roll to accommodate small electrode wire.</li> </ul>

### 4.4.3 Trial Weld Test Procedure

The test procedure for specimens consisting of 150 mm x 150 mm plates is summarized below. The larger “distortion specimens” are tested using a similar procedure. No clear test matrix is defined. A reasonable number of trials are conducted, until a satisfactory result is obtained.

- 1) The weld surfaces of two plates being joined are prepared for welding. Oil on 20 gauge steel sheet is removed by scrubbing with an acetone-based solvent. Mill scale on the 6 mm thick 300W steel plate is ground off with a wire brush electric grinder. Cleaning takes place shortly before welding.
- 2) Plates are clamped together with a 50 mm lap width. Clamps apply pressure to the center of the lap in the joint, while not obstructing the welding area.

Two marks 100 mm apart delineating the “test region” are inscribed on the specimen using chalk. The time it takes for the welder to pass through this region is measured with a stopwatch. In the event that intermittent welds between tack welds are conducted, the corresponding distance between tack welds is measured. Time and distance are recorded to measure the welding speed. The fillet welds are performed in the flat position. The welds may be continuous or intermittent and they may include tack welds. Successive trials alter the varied parameters of Table 4-2 based on judgment until a visually acceptable weld is performed.

- 3) The recorded parameters include voltage (E), current (I), wire feed speed (WFS), and weld pass speed ( $v$ ). Observations may include:
  - a. welder’s remarks on ease of welding/ arc or weld pool characteristics
  - b. heat effects and distortion
  - c. weld cross – section consistency and shape
  - d. surface defects, such as porosity or undercut
- 4) Photos of areas of interest, including overall weld geometry and cross – section geometry, are taken as required.

### 4.5 Results of Visual Inspection of Trial Welds

At the conclusion of numerous tests, a procedure was obtained to produce a weld with no visually detectable undercut, porosity, or lack of fusion. Twenty-three specimens consisting of 150 mm x 150 mm plates, and two large “distortion” specimens were welded. For simplicity, and because they appeared to be operating near the lowest heat possible for this equipment, the same weld parameters are adopted for Weld #1, Weld #2, and Weld #3 (whose locations are shown in Figure 3–4). Table 4-4 summarizes the final settings determined for the welding procedure. An extensive table detailing observations and parameters for each specimen is available in Appendix B.

**Table 4-4: Weld Process Settings Selected from Visual Inspection of Weld Trials**

<b>Parameter</b>	<b>Setting</b>
Weld Process	Short-Circuiting Gas Metal Arc Welding (GMAW-SC)
Equipment	Suitcase wire-feed system with the “soft start” option turned to the “off” position
Electrode	ER70S-6, 0.023” Diameter
Current and Polarity	DCEP
Position	Flat
Hand Motion	Straight push or pull, but not weaving. The arc is directed towards the thicker material at the joint, to minimize the heat transferred to the thin sheet.
Voltage	19.5 V
Wire Feed Speed	5.08 m/min (200 ipm)
Weld Pass Speed	Good results are achieved with speeds around 5 mm/s.
Current	Self-adjusting since one-knob control adjusts the wire feed speed. Typical currents on this welding equipment for these conditions are in the range of 50 – 60 A.
Process	<p>Prepare 6 mm thick 300W plate by grinding to remove mill-scale in the weld region. Prepare 20 gauge steel sheet by removing dust and oil with an acetone-based cleaner.</p> <p>Install clamps as required to restrain the thin steel sheet from distorting during welding. Starting at the midpoint of each edge and finishing at the corners, tack weld the entire plate perimeter at a maximum spacing of 75 mm. If both Weld #1 and Weld #2 are used, tack Weld #2 is executed first, and then the thin sheet is flattened and tack weld along weld line #1 is executed. “Stitch weld” by fillet welding every second length between tacks around the entire perimeter to reduce distortion. Once every second weld is complete, circle the perimeter again welding in the remaining gaps. Start and stop welds at the tack weld locations; do not run the fillet weld continuously over the tacks welds.</p>

Figure 4-6 shows a plan view of a typical trial specimen for the infill panel-to-fish plate connection. Trial specimens for the infill panel splice are similar, except both plates are A1008 0.9 mm thick.

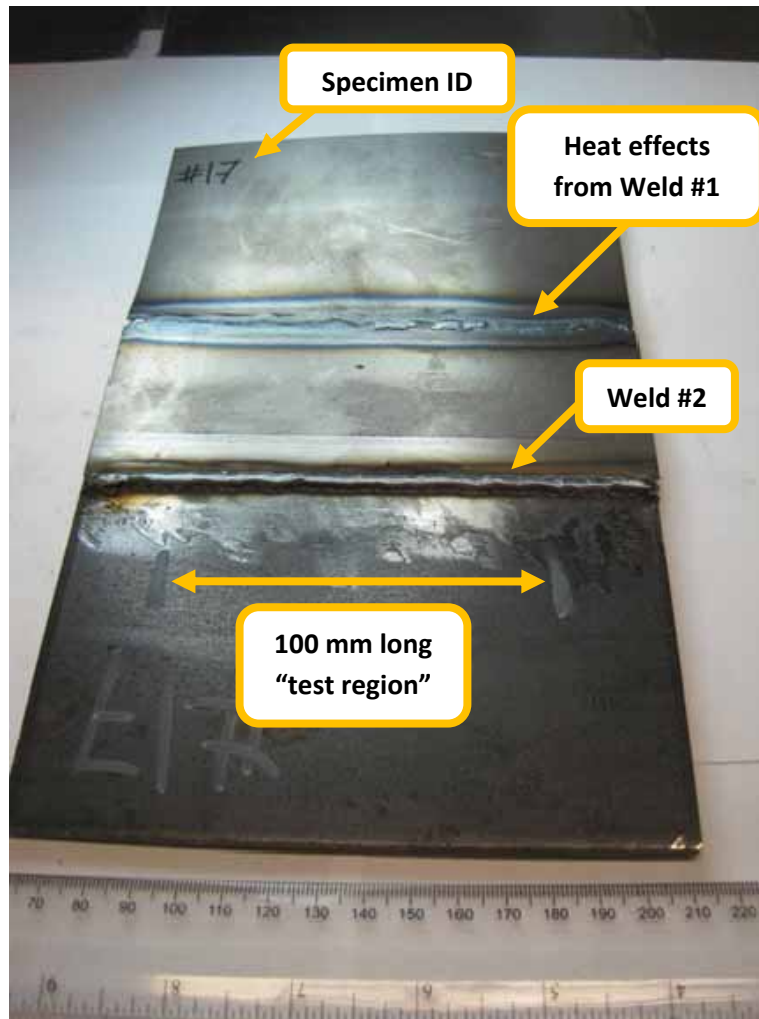


**Figure 4-6: Plan View of a Typical Weld Trial Specimen**

Figure 4-7, Figure 4-8, and Figure 4-9 show exposed cross-sections of Weld #1, Weld #2, and Weld #3, respectively. All three welds have a sufficiently large throat to force failure in the thin infill plate. All three welds show some degree of weld metal penetration into the base material for complete fusion, though this is difficult to see in these images.

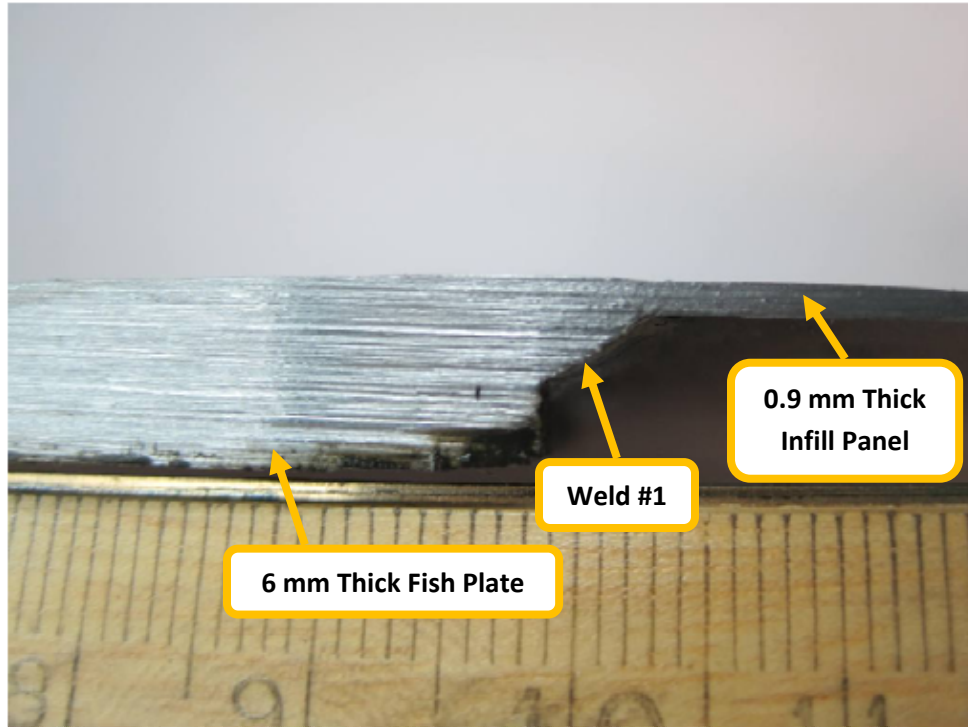


Figure 4-7: Cross-Section Showing Weld #1

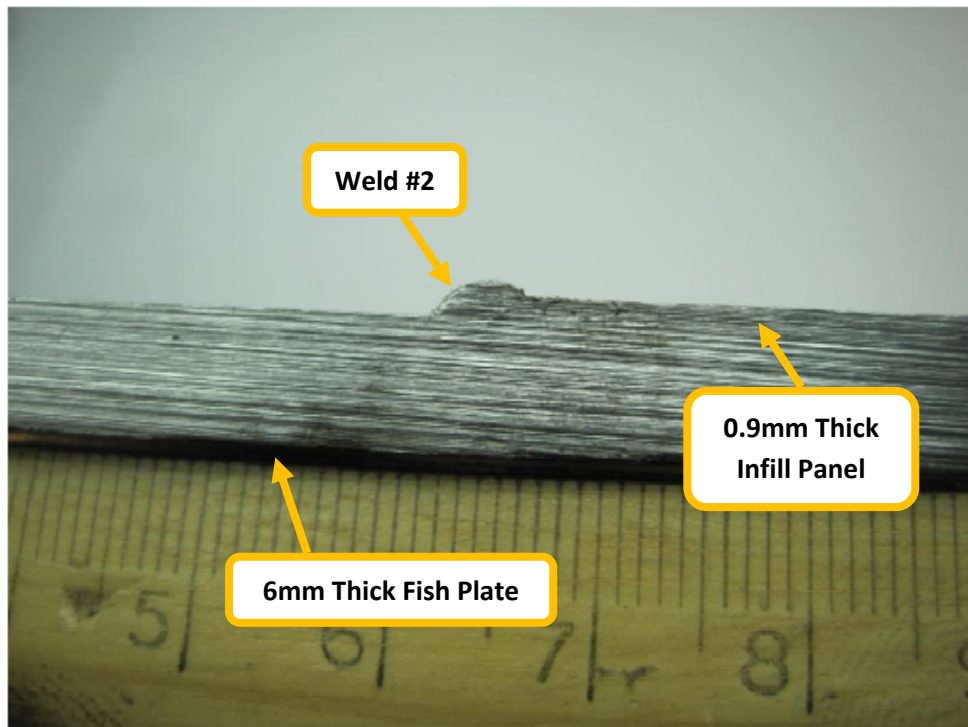
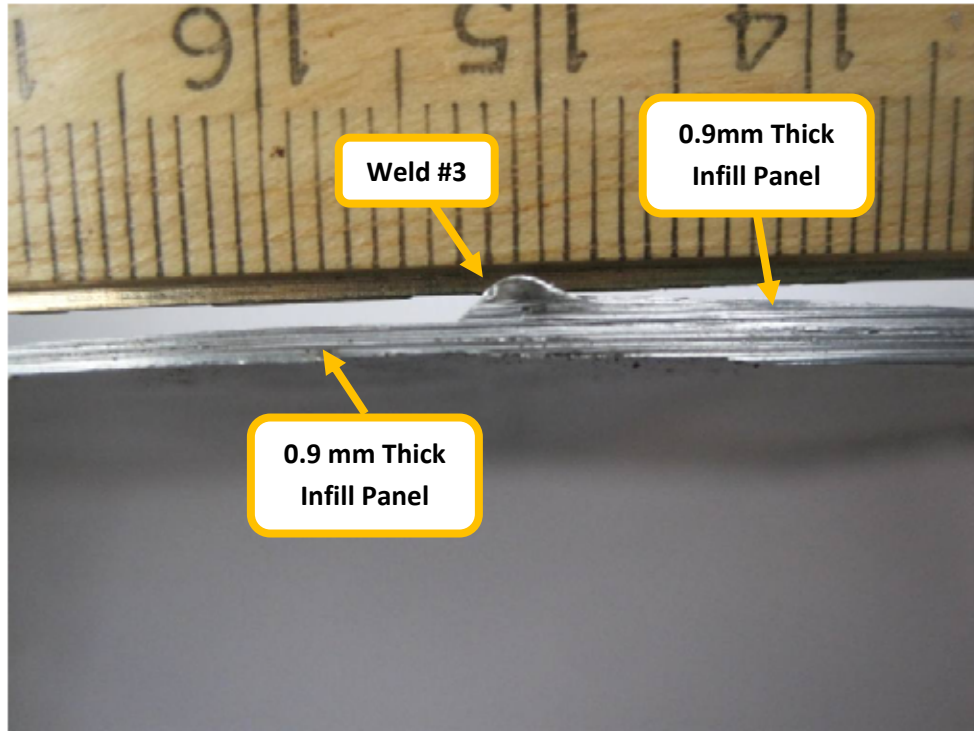


Figure 4-8: Cross-Section Showing Weld #2



**Figure 4-9: Cross-Section of Weld #3**

Figure 4-10 and Figure 4-11 show the difference between Weld #1, where no chill strip is used during welding, and when a chill strip is used, respectively. The damage from burn-through is certainly higher when a chill strip is not used. Both Weld #1 and Weld #3 required a chill strip to achieve the least burn-through (the geometry of Weld #2 precludes the use of a chill strip).

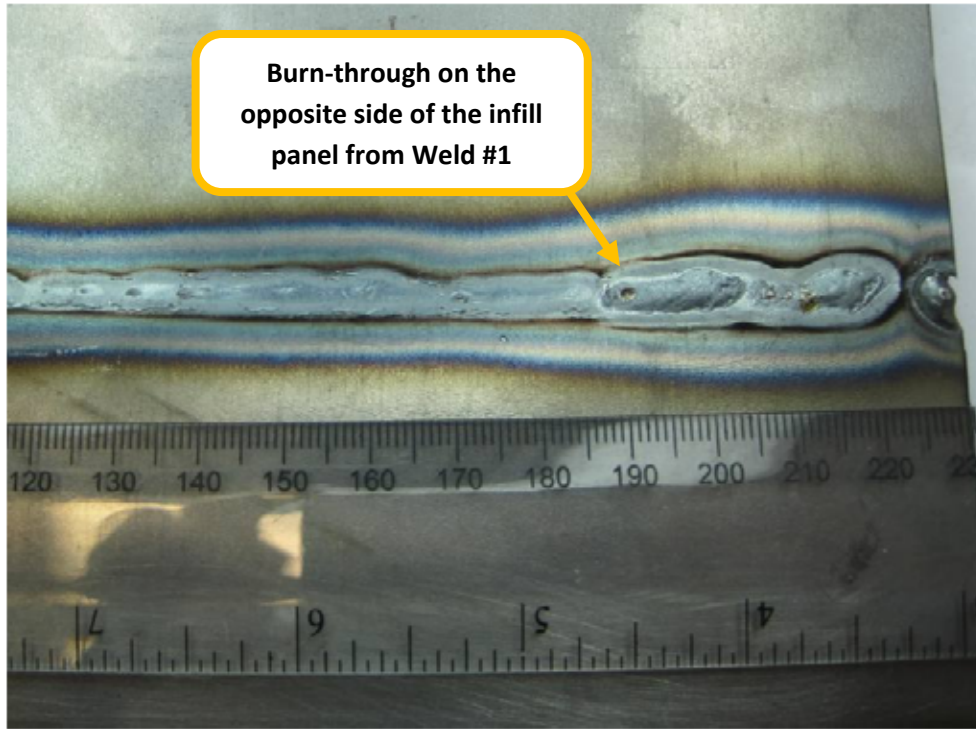


Figure 4-10: Infill Panel Opposite Weld #1, No Chill Strip Used During Welding

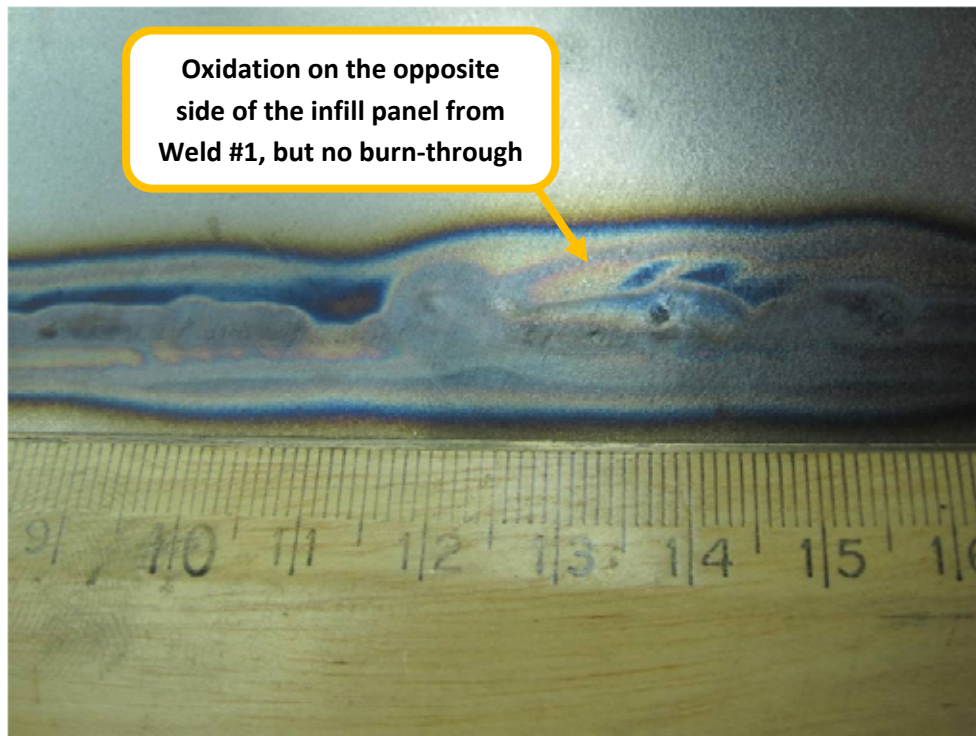
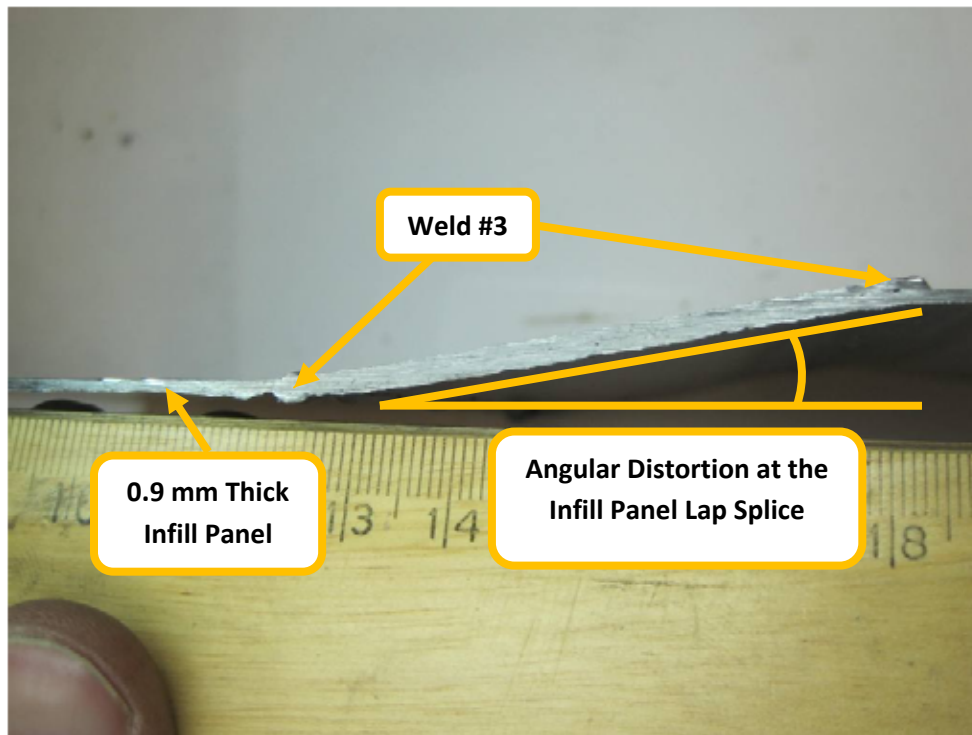


Figure 4-11: Infill Panel Opposite Weld #1, Chill Strip Used During Welding

Similarly, in the case of the infill panel splice, Weld #3 experiences higher angular distortion. Tack welds are required to prevent significant fit-up problems when splicing together two thin sheets. Poorly controlled heat input can open a gap between the two plates that cannot be welded; if the gap becomes too large, the welder must reduce his or her speed to deposit extra weld metal to fill it, and the dramatic increase in heat input inevitably burns through the thin sheet. Even when a chill strip is used, as shown in Figure 4-12, some degree of distortion is inevitable. However, the reduction in burn-through damage validates the use of a chill strip for this weld.



**Figure 4-12: Angular Distortion at the Infill Panel Lap Splice, Chill Strip Used**

The tests of the so-called distortion specimens, one of which is shown in Figure 4-13, yielded two key insights. First, low heat settings and clamping do not prevent distortion from affecting fit-up of Weld #1 and Weld #2. Tack welds at a spacing of no greater than 75 mm are required. Second, either backstepping or stitch welding are a viable method of filling the gaps between the tack welds.



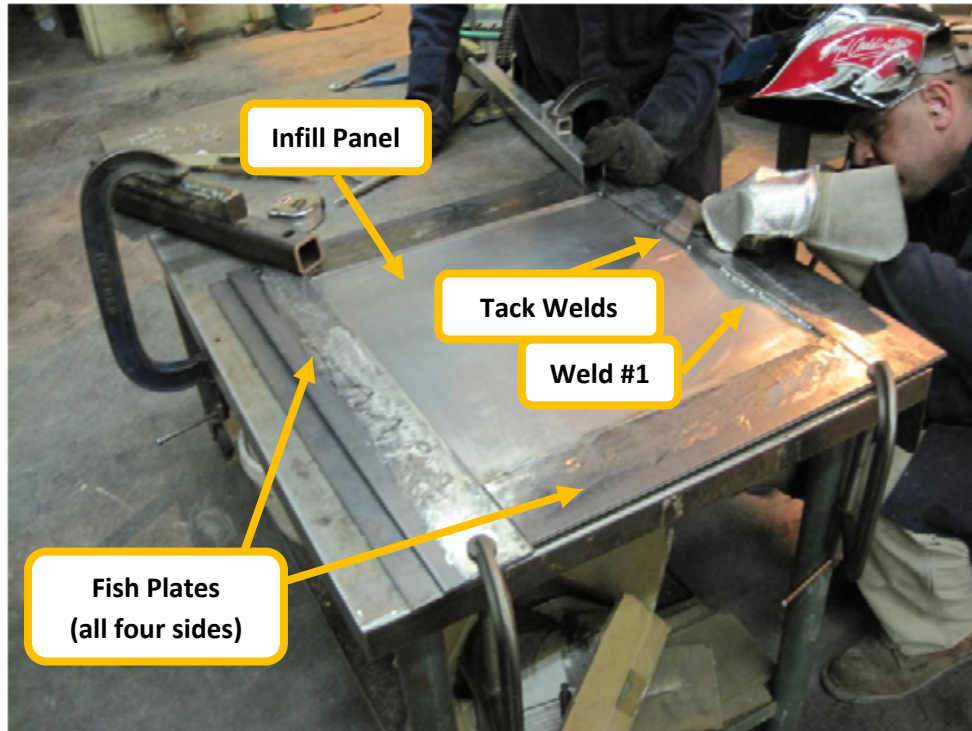


Figure 4-13: Plan View of a Distortion Specimen during Welding

#### 4.6 Mechanical Testing of Lap Joint Configurations

This series of mechanical tests compares the performance of different configurations of the welded joints at both the infill panel-to-boundary member connection, and at the infill panel splice. Mechanical tests are broken into two categories. First, quasi-static tension tests are conducted on the proposed joints to determine whether the weld can develop the full capacity of the infill panel. Second, cyclic tests are conducted to assess the resistance of the proposed joints to cyclic out-of-plane deformation of the infill panel.

The tests are conducted in a MTS 1000 universal testing machine equipped with hydraulic grips, and having a maximum load capacity of 1000 kN and an actuator range of 150 mm.

##### 4.6.1 Welded Connection Configurations

Based on judgment and the results of the visual inspection weld tests (see Chapter 5), four possible configurations of welds for the thin infill panel-to-fish plate connection and two configurations for the infill panel splice are tested. The configuration details are described below in Table 4-5.

Each specimen is labelled " $T_x - C_y - z$ ", where " $T_x - C_y$ " is one of the joint configurations presented in Table 4-5, and " $z$ " is a number from one to six. Six specimens of each configuration allow for three repetitions of each of the quasi-static and cyclic tests, for each of six joint configurations, yielding a total of 36 tests.

**Table 4-5: Connection Configurations**

Configuration	Welds Present at the Joint Tested	Is a Chill Strip Used?	Is There a Tack Weld at the Mid-Width of the Joint?
T2-C1	Weld #2	No; not required for Weld #2	Yes
T2-C2	Weld #2	No; not required for Weld #2	No
T2-C3	Welds #1 & #2	Yes; at Weld #1	Yes
T2-C4	Welds #1 & #2	No	Yes
T3-C1	Weld #3 at both sides of the lap joint	Yes; at Weld #3	Yes
T3-C2	Weld #3 at both sides of the lap joint	No	Yes

Configurations T2-C1 and T2-C2 have the advantage of only requiring one weld. This requires access to only one side of the joint, which may be a construction advantage. The weld does not require the use of a chill strip; such a backing plate could be very cumbersome to install, particularly in a retrofit scenario if welding is required in vertical and horizontal positions. Last, tack welds are preferred for distortion control and fit-up of the infill panel, but they introduce weld discontinuities that may serve as sites for fracture initiation. Comparing T2-C1 and T2-C2 configurations will indicate whether tack welds have a detrimental effect on system performance.

Configurations T2-C3 and T2-C4 require two welds. However, the “effective” weld is Weld #1; that is, the volume of weld metal is such that a material failure in the thin sheet at Weld #1 is the likely failure mode, and Weld #2 is not likely providing additional strength to the joint. Weld #1 has the possible geometric advantage that cyclic out-of-plane buckling of the infill panel causes high stresses at the toe of this weld, compared with a cyclic opening and closing of the root of Weld #2 in configurations T2-C1 and T2-C2 (see Figure 3–5). A comparison between T2-C1 and T2-C3 may indicate whether using one weld or two welds influences the joint performance.

As discussed in section 4.5, when a chill strip was present during welding, the burn-through damage to the infill panel steel appears less serious than when it is not present. A comparison between the T2-C3 series and the T2-C4 series should indicate whether an improved visual appearance significantly improves mechanical performance.

The final two configurations investigate this same phenomenon for the infill panel splice. A comparison between T3-C1 and T3-C2 may indicate whether the strength loss from not using a chill strip is significant or not.

### 4.6.2 Test Specimen Design

Two classes of specimen are required; one for the infill panel-to-fish plate connection (joint configurations starting with “T2”), and one for the infill panel lap splice (joint configurations starting in “T3”).

Specimens were designed to be simple and repeatable, so that several different welding configurations could be investigated economically. The test specimens are loaded transverse to the weld axis. Though this loading does not replicate the true conditions of a SPSW infill panel, where the weld is subjected to a combination of transverse tension and longitudinal shear, it still enables comparison between weld configurations.

For tests of the infill-to-fish plate connection, each specimen consists of two identical connections as shown in Figure 4-14, spanned by the infill panel steel sheet. A relatively long span of A1008 steel was selected in order to ensure the weld configuration could tolerate large plastic deformations in the thin sheet.

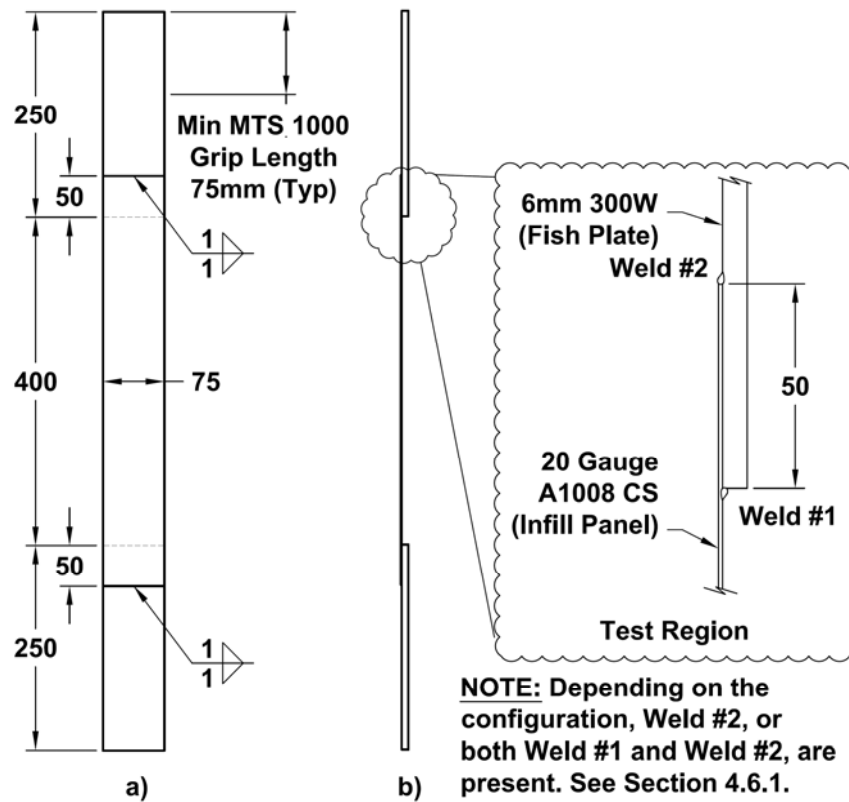


**Figure 4-14: Infill Panel-to-Fish Plate Connection, Test Specimen Geometry**  
a) Front View, b) Side View

For the infill panel splice connections, specimens are similar to the T2 series except the tested region is the lap splice at the center of the span, as shown in Figure 4-15. The

specimen width is narrowest at the infill panel splice to force the highest stresses to occur at this location.

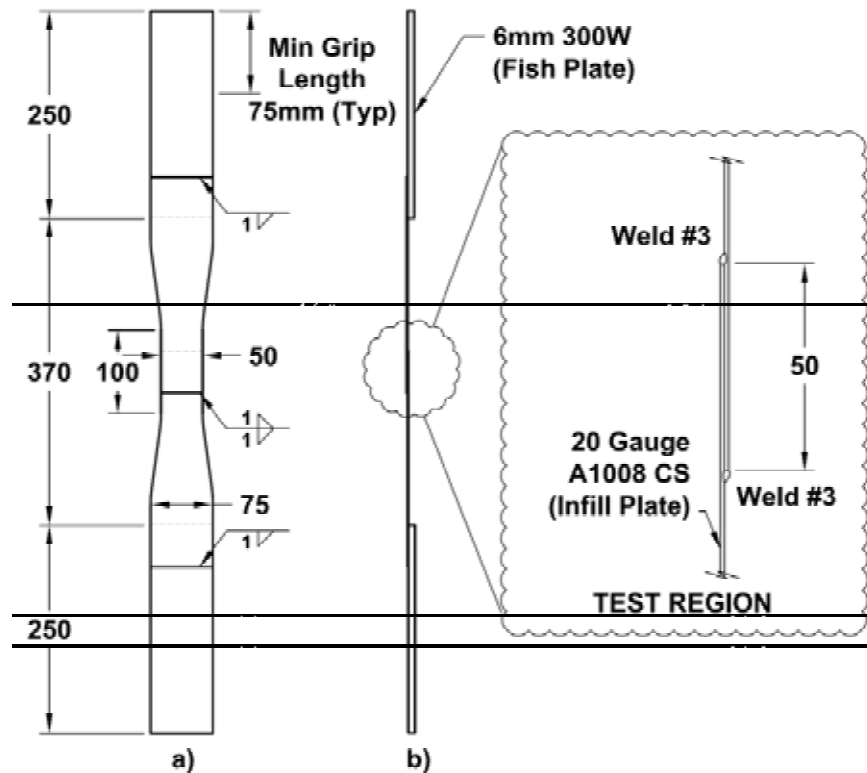


**Figure 4-15: Infill Panel Splice Connection, Test Specimen Geometry**  
a) Front View, b) Side View

It is known that the start and end of a weld segment are likely to be of poorer quality than the remainder of the weld. In order to prevent start and stop effects, a minimum of 25 mm of material is removed by water – jet cutting from the outside edges of all specimens. The original specimens for the T2 and T3 – Series are 125 mm wide. Figure 4-14 and Figure 4-15 show the specimen configuration as tested.

### 4.6.3 Quasi-static Tension Tests

#### 4.6.3.1 Test Design and Instrumentation

Due to the very small size of the welds, instrumenting the weld itself is difficult. Stress-strain results for the specimens, combined with observations of the failure mode, provide sufficient information to compare the performance of different joint configurations.

Specimen cross-section dimensions and gauge lengths are measured prior to testing, and engineering stress versus strain curves are produced for comparison of results. Load data are recorded from the testing machine load cell. The elongation is measured over

the full length of the infill panel material using a cable extensometer. In the case of the infill panel-to-fish plate configurations (the T2 series specimens), the gauge length corresponds to the full length of infill panel material. However, in the case of the infill panel splice specimens (the T3 series specimens) the gauge length was taken as only the length of the reduced portion having a single sheet thickness. Since the total reduced portion, not including the tapered region, is 100 mm long (Figure 4-15), this value less the 50 mm lap length leaves a 50 mm length with a single sheet thickness. This was taken as the gauge length to calculate the strain.

It should be noted that the measured elongation is the sum of elastic elongations in the widest portion of the steel sheet, and some elastic and inelastic deformations in the tapered section and the reduced portion. Since the cable extensometer is measuring strains over this entire region (a 470 mm length), but the gauge length is taken as the 50 mm where the majority of the deformation occurs, the results for the T3 series of joints are expected to produce unrealistically high strain values.

#### 4.6.3.2 Loading Protocol

Failure is expected at a relatively low load (10 to 20 kN), assuming the full tensile capacity of the infill panel steel is reached. Load is applied in displacement control only. A relatively low loading rate is used until a clear peak load plateau is reached, then to speed up the test, a significantly higher loading rate is used to complete the test. Based on some trial specimens, the loading rates summarized in Table 4-6 were adopted.

**Table 4-6: Load Rates for Quasi – Static Tension Tests of Various Joint Configurations**

Infill Panel-to-Fish Plate Joints Configurations T2-CX (X=1, 2, 3, or 4)		Infill Panel Splice Configurations T3-CX (X=1 or 2)	
Displacement [mm]	Rate [mm/min]	Displacement [mm]	Rate [mm/min]
0 -> 5	0.5	0 -> 2	0.5
5 -> Failure	10	2 -> Failure	5

#### 4.6.4 Cyclic Tests

##### 4.6.4.1 Test Design and Instrumentation

The results of the monotonic tension tests (see section 5.3) suggest that a more harsh loading condition should be placed on the joint to assess the performance of the different joint configurations. Reducing the gauge length of the test region from the quasi-static test range of roughly 300 mm to something significantly shorter, and subjecting the test region to more severe out-of-plane deformations over this short gauge length will impose a more severe loading condition on the weld. The gauge length was therefore shortened by clamping 6 mm steel plates, referred to as a clamping

plates, to either side of the thin sheet, as shown in Figure 4-16 through Figure 4-18. The length of the specimen covered by the clamping plates is essentially rigid since the 6 mm thick plates are several times stiffer than the 20 gauge infill panel material in the test region. The resulting gauge length is 25 mm for all specimens. During cyclic tension-compression loading the thin sheet buckles out-of-plane, opening the root of the single weld of the test specimen configurations T2-C1 and T2-C2 (Figure 4-16), and working the toe of the welds in test specimen configurations T2-C3 and T2-C4 (Figure 4-17), and T3-C1 and T3-C2 (Figure 4-18).

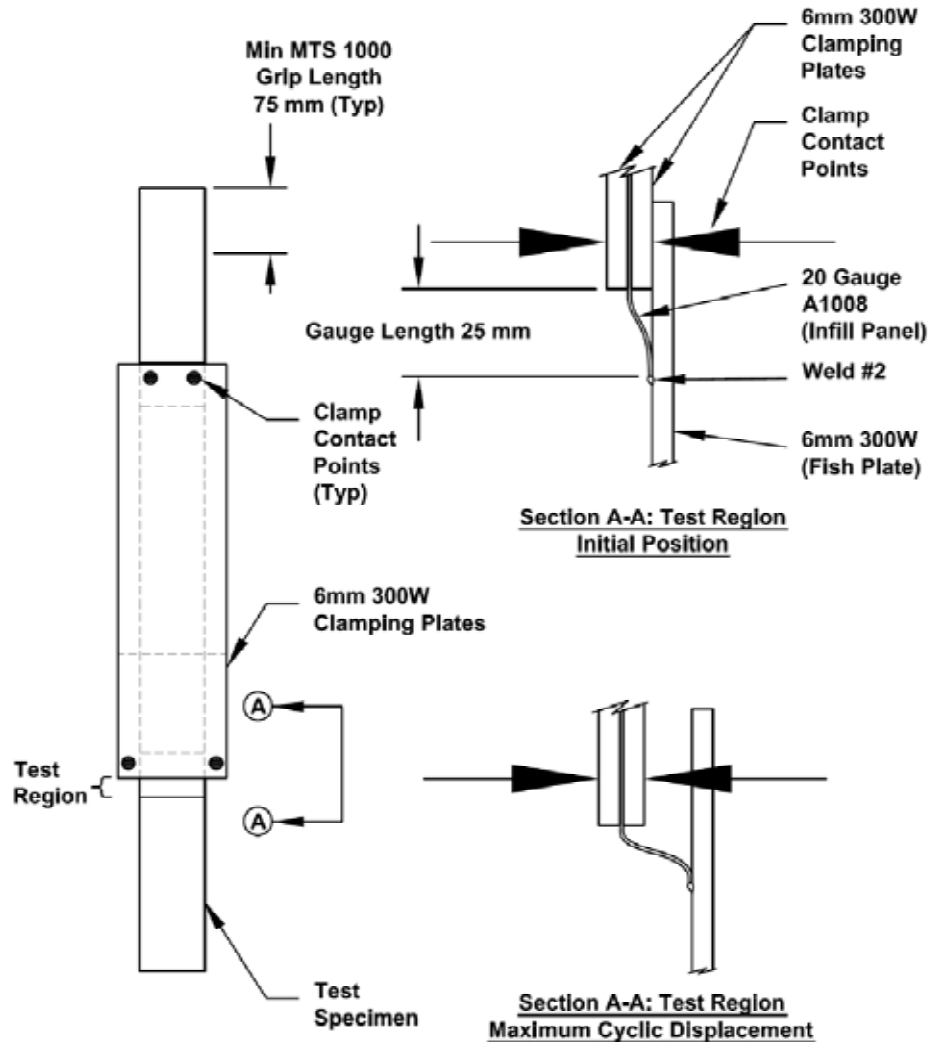


**Figure 4-16: Cyclic Test Supplementary Clamping Plates and Anticipated Test Region Behaviour, T2-C1 and T2-C2 Joint Configurations**

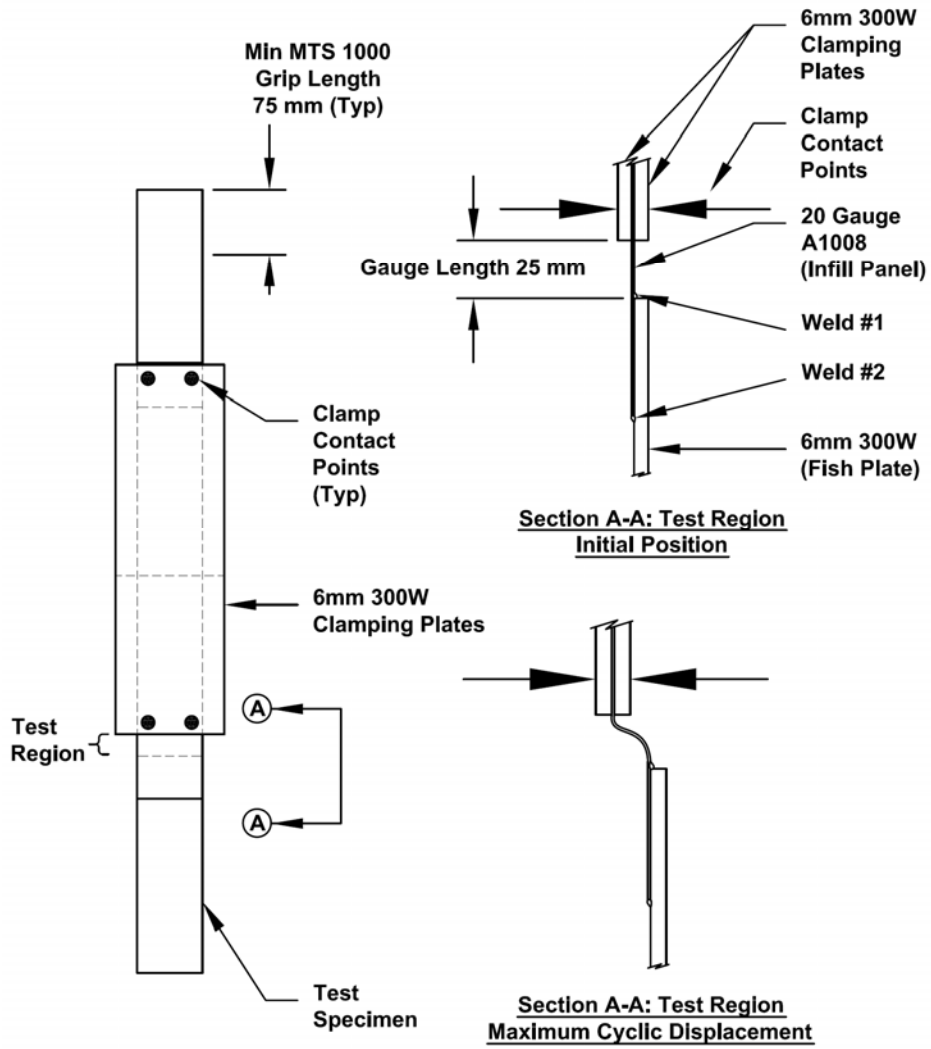
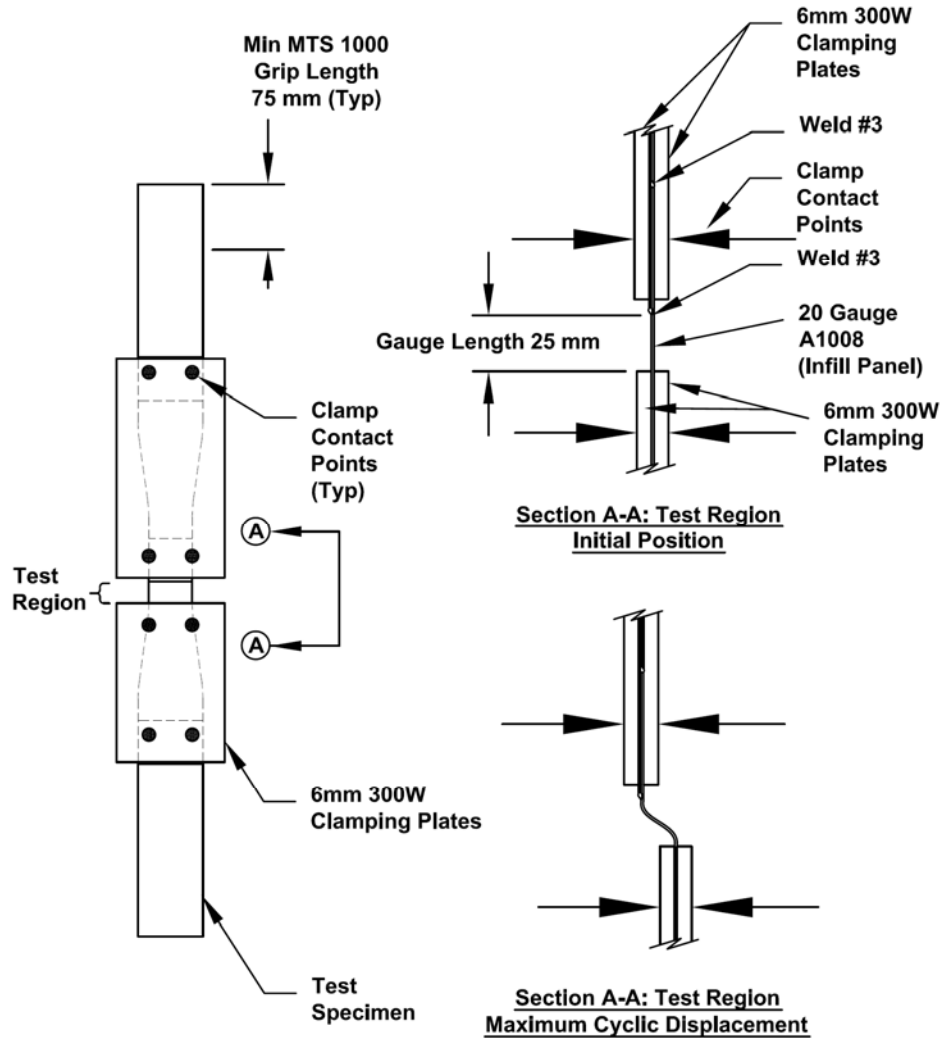


Figure 4-17: Cyclic Test Supplementary Clamping Plates and Anticipated Test Region Behaviour, T2-C3 and T2-C4 Joint Configurations



**Figure 4-18: Cyclic Test Supplementary Clamping Plates and Anticipated Test Region Behaviour, T3-C1 and T3-C2 Joint Configurations**

#### 4.6.4.2 Loading Protocol

The tests are conducted under displacement control. The test specimens are subjected to sufficient displacement to cause a severe out-of-plane angular change of  $40^\circ$  at the welds. The specimen is cycled through this angular change 30 times at a displacement rate of 0.5 mm/min, a number of cycles similar to the number of load reversals expected during a severe earthquake, and then pulled in tension at a rate of 10 mm/min until failure.

#### 4.6.4.3 Failure Mode of Mechanical Tests

A desirable failure mode for these test specimens would be failure in the base material prior to failure in the welded joint. Failure of transverse fillet welds in light gauge steel is predominantly by tearing in the base metal, as opposed to weld shear failure (Pekoz and McGuire (1981), AISI and CSA (2002)). Pekoz and McGuire (1981) associate this mainly



to the relatively large throat geometry of sheet metal fillet welds; the vertical weld leg is customarily at least as thick as the sheet metal, and the horizontal weld leg size is often two to three times the sheet metal thickness.

#### **4.6.4.4 Wedge Push-Out Tests of Weld #2**

As discussed in Chapter 5, during the quasi-static testing, only one specimen failed at the welded connection: specimen T2-C2-3. However, of the specimens with only one weld at the joint, the T2-C2 specimens were expected to perform better or the same as the T2-C1 specimens, as they had no tack weld at their midpoint. In order to investigate whether the poor fusion shown in this test is a recurring phenomenon, and whether it is a result of poor welding parameters or poor electrode coverage at the joint, a series of wedge push-out tests on several of these welds is conducted.

Since all other quasi-static test specimens failed far from the weld, the weld region of these already-tested specimens is undamaged. One joint from each of the T2-C1 specimens, and one joint from the two T2-C2 specimens that failed in the base material are tested.

The test setup consists of a wedge held in the upper grips of the testing machine applying a downward compression force to the root of the weld, as the welded joint is held in the lower grips of the testing machine. The wedge was fabricated from a piece of 6 mm grade 300W steel plate and has an angle of roughly  $45^\circ$ , which applies a prying force to the weld and tends to lift it from the fish plate material and expose the fusion area, as shown in Figure 4-19.

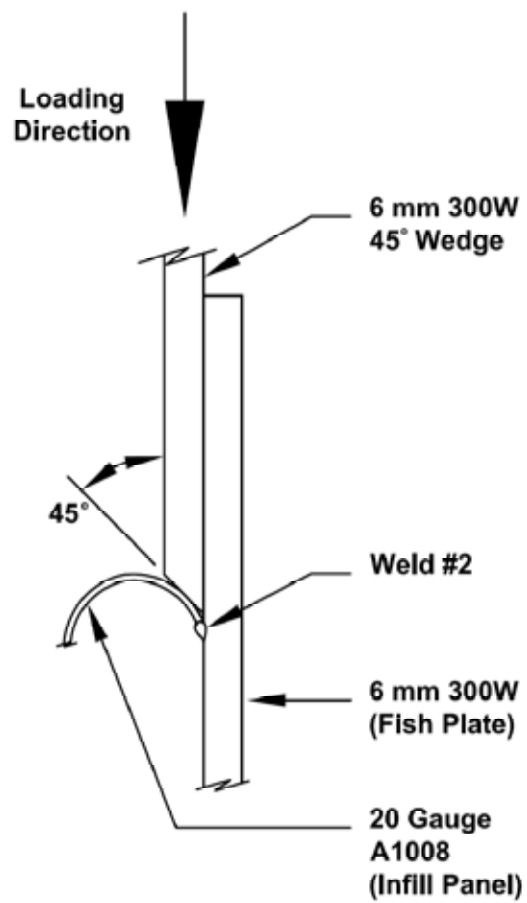


Figure 4-19: Side View of Wedge Push-Out Test of Weld #2

## **Chapter 5: Results and Discussion of the Weld Procedure Development**

### **5.1 Introduction**

The weld procedure development yielded generally encouraging results. Tension coupon tests confirmed the actual properties of the materials in the test program. Quasi-static and cyclic tension and compression tests confirmed that all welded joints performed well, as failure in all cases but one was a tensile material failure far from the weld location. Supplementary wedge push-out tests were conducted to investigate the single case of failure of weld #2 at its fusion face with the 6 mm fish plate material, and demonstrated that failure of this particular specimen resulted from a reduced effective weld throat.

### **5.2 Ancillary Materials Tests**

The stress vs. strain behaviour from the tension coupons was as expected. The grade 300W and 350W steels show a distinct yield plateau before strain hardening, while the cold-rolled A1008 steel showed a yield radius prior to a long plateau at the ultimate strength. All three steels are very ductile, showing an average rupture strain of 0.39, 0.30, and 0.46 for 350W, 300W, and A1008 steel coupons, respectively.

Unfortunately, many of the static points collected during the tests were found to be unreliable due to erroneous settings in the data collection system and questionable static point behaviour during testing. Thus, judgment was required when selecting a stress-strain response for modeling the steel behaviour. Further discussion of these issues, detailed stress vs. strain plots for each of the coupons, and dimensions of the material coupons are available in Appendix A.

Table 5-1 explains the labelling system for the coupons. Table 5-2 provides a summary of results before the discovery of the unreliability of the static stress values. Only dynamic values are displayed since the static values were not used in the calculations.

Table 5-3 shows results for four additional coupons of infill panel material tested at the slowest displacement rate possible, 0.1 mm/min, since it was not possible to take reliable static points.

**Table 5-1: Labelling Scheme for Tension Coupons**

Label	Description
A	6 mm, Grade 300W steel plate used for weld procedure development. So-called “thick” portion of “thin-to-thick” specimens.
B	Grade A1008 CS Type A, 20 gauge sheet steel used for the infill panel and the “thin” portion of “thin-to-thick” and “thin-to-thin” specimens.
C	Grade 350W, W200x31 used for the SPSW test specimen moment frame. Suffix “-F” for pieces cut from the flange, and “-W” for pieces cut from the web.

### 5.3 Quasi – Static Tension Tests

For both the infill panel-to-fish plate connection, and the infill panel splice, in every case but one, the specimens reached the ultimate capacity of the A1008 infill panel material. Following inelastic stretching and necking, failure took the form of a tensile fracture away from the weld as shown in Figure 5-1 and Figure 5-2. The weld region showed no damage.

Specimen T2-C2-3, unlike all other specimens, failed prematurely due to a lack of fusion of the infill panel-to-fish plate weld. The failure, shown in Figure 5-3, began at the left edge of the specimen and propagated suddenly towards the right. The exposed surface of the 6 mm fish plate following weld tear-off shows a relatively small fusion area towards the extreme left of the weld, which widens progressively until the weld is arrested at the right of the specimen.

It is believed that the primary cause of this failure was poor weld coverage, meaning the effective area of weld metal deposited towards the left of the joint was not sufficient to mobilize the full tensile capacity of the strip of infill panel tested. One drawback of this joint is that it is physically difficult to see the edge where the thin infill panel rests against the fish plate during welding, and the deposited weld metal is quite small. Small deviations in hand movement can easily affect the weld coverage. The weld cross-section is still two-to-three times thicker than the 0.9 mm infill plate, but if the effective throat of this weld is not sufficient at the joint of the plates, the joint is susceptible to premature fracture.

The severity of this issue is investigated further in the wedge push-out tests of weld #2 presented in Section 5.5.

Figure 5-4 through Figure 5-9 show the stress versus strain response for the quasi-static tests. The premature failure of specimen T2-C2-3 is clearly evident by the sudden drop of capacity seen in Figure 5-5.

**Table 5-2: Summary of Tension Coupon Test Results**

VARIABLE	E [MPa]	F <sub>y</sub> dynamic [MPa]	F <sub>u</sub> dynamic [MPa]	ε <sub>rupture</sub> [mm/mm]	
DEFORMATION RATE [mm/s]	0.30	5.00	5.00	5.00	
COUPON	A1	201,000	334	500	0.31
	A2	209,000	325	489	0.33
	A3	211,000	328	493	0.34
	A4	213,000	342	508	0.28
	A5	215,000	343	509	0.25
	A6	N/A	345	511	0.26
	CF-1	217,000	356	455	N/A
	CF-2	213,000	356	460	N/A
	CF-3	206,000	352	460	0.40
	CF-4	211,000	353	458	0.40
	CW-1	210,000	369	465	0.38
	CW-2	206,000	375	466	0.39
	B1	261,000	158	278	0.50
	B2	239,000	154	278	0.45
	B3	229,000	155	279	0.46
	B4	295,000	139	278	0.48
B5	212,000	144	283	0.46	
B6	230,000	143	278	0.45	

**NOTE**

~~N/A = no points captured by the data collection unit, or gauge reading could not be measured after rupture~~

**Table 5-3: Summary of Tension Coupon Results, Supplementary Tests**

VARIABLE	E [MPa]	F <sub>y</sub> slow load [MPa]	F <sub>u</sub> slow load [MPa]	F <sub>u</sub> dynamic [MPa]	ε <sub>rupture</sub> [mm/mm]	
DEFORMATION RATE [mm/s]	SLOW [0.10]	SLOW [0.10]	SLOW [0.10]	DYNAMIC [5.00]	DYNAMIC [5.00]	
COUPON	B7	221,000	168	288	N/A*	0.45
	B8	225,000	173	303	312	0.48
	B9	274,000	175	294	306	0.41
	B10	212,000	176	296	306	0.43

**NOTE**

N/A\* = Specimen B7 loaded entirely to failure at the "slow" rate of 0.1mm/s

When reviewing the plots of Figure 5-8 and Figure 5-9, it should be noted that inelastic behaviour in the tapered portion of the specimens is not captured by the 50 mm gauge length used for calculating strains (this was discussed in Section 4.6.3.1). Thus, the strain magnitude appears unrealistically large. Nonetheless, since the specimens have identical geometries and are loaded identically, comparisons can be drawn between the T3-C1 and T3-C2 configurations.

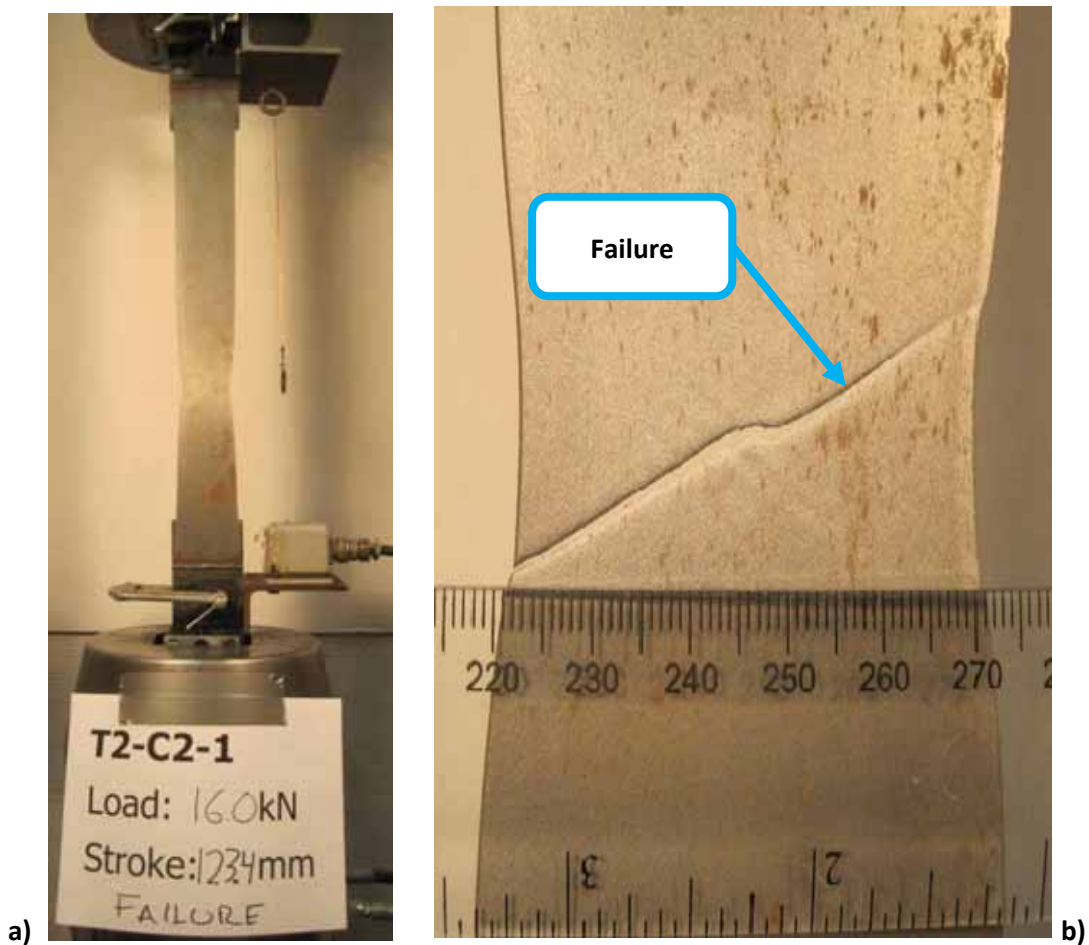


**Figure 5-1: Typical T2 - Series Quasi – Static Tension Tests at Failure  
a) Specimen in Test Frame, b) Failure Region**

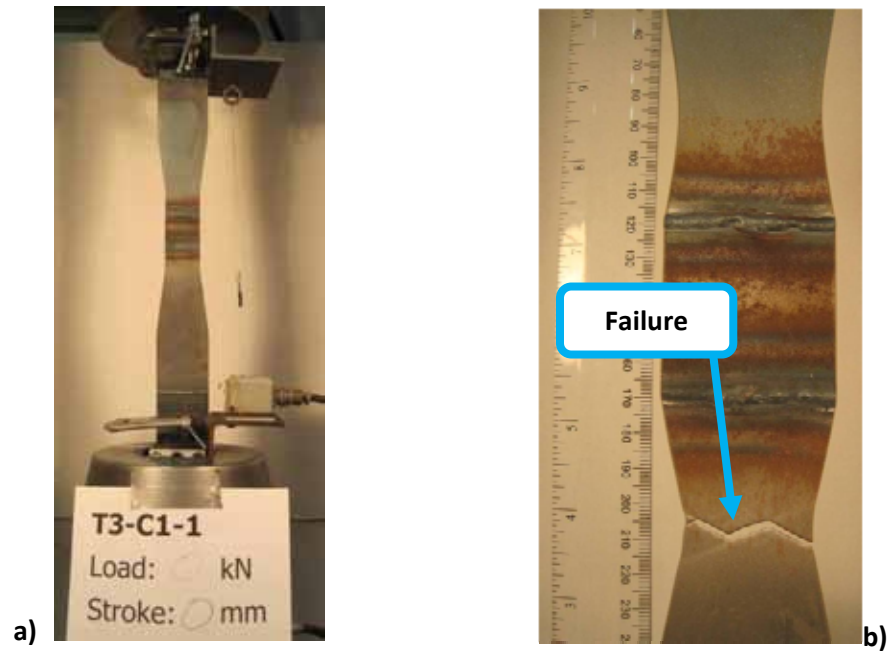


**Figure 5-2: Typical T3 - Series Quasi – Static Tension Test**  
 a) Specimen in Frame at Zero Load, b) Failure Region

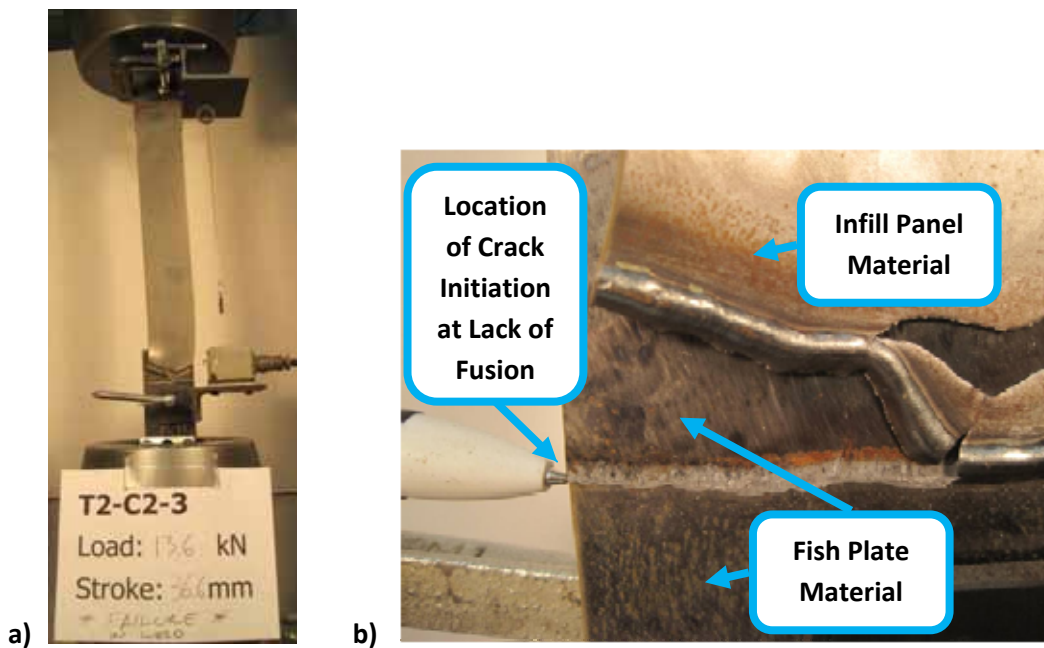


**Figure 5-3: Specimen T2-C2-3, Undesirable Failure at Fusion Line Between Weld Metal and 6 mm Fish Plate Material, a) Specimen in Test Frame, b) Failure Region**

Though all weld processes performed well, selection of the preferred welding procedure would have been easier if greater differences in performance had been observed. If the

failure in specimen T2-C2-3 is considered an anomaly, there is really no quantifiable difference between the performance of the various joint configurations under these loading conditions.

Since the specimens for the cyclic testing are identical to the specimens used in the quasi-static tests, it is recommended that for cyclic tests modifications be made to the test setup and loading rate to increase the severity of the loading condition on the welded joint.



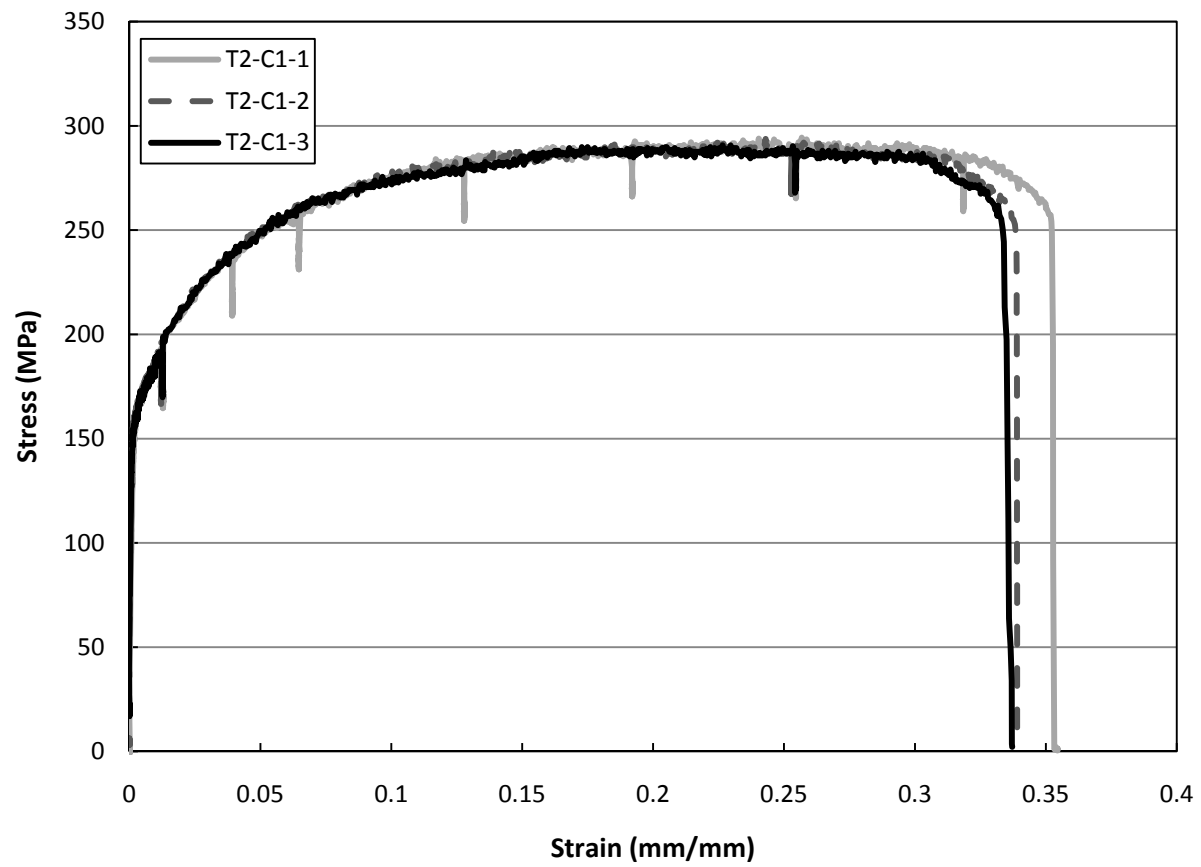


Figure 5-4: Monotonic Weld Test Configuration T2-C1; Weld #2 Only, Tack Weld at Midpoint

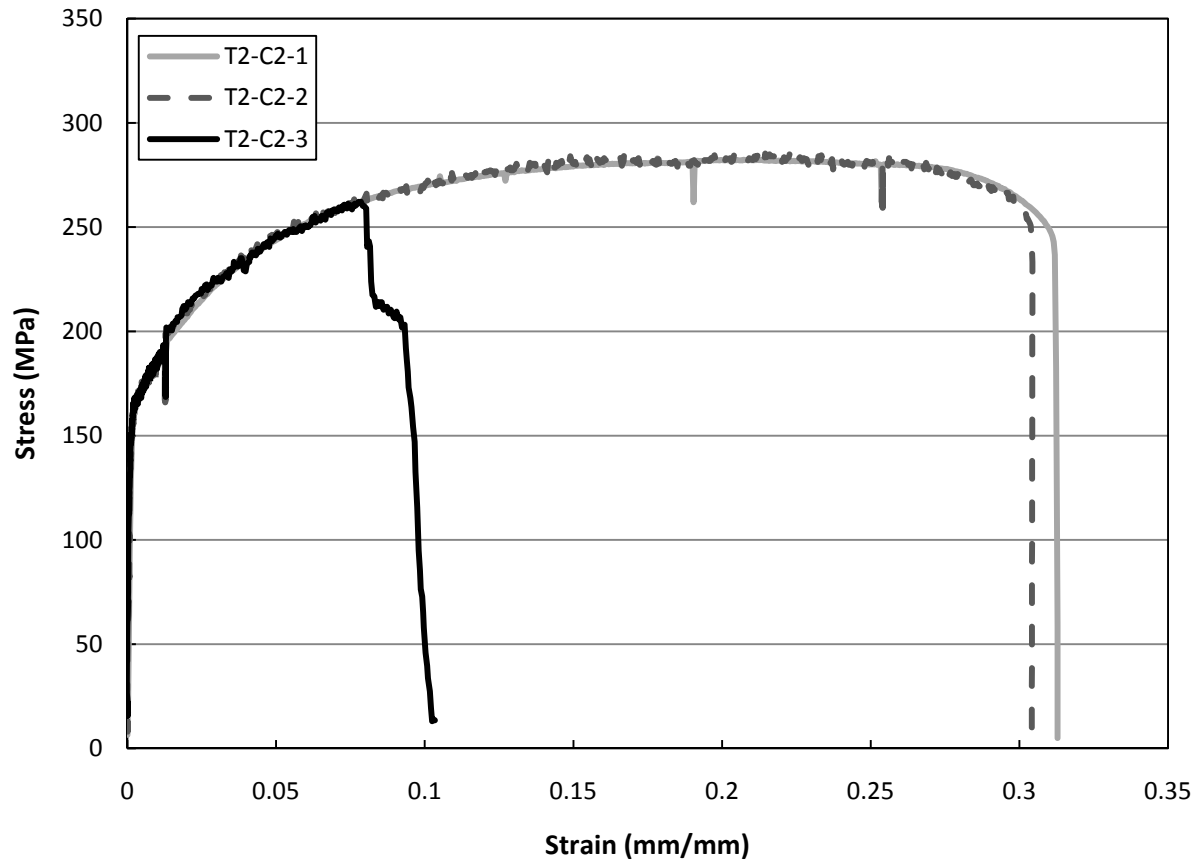


Figure 5-5: Monotonic Weld Test Series Configuration T2-C2; Weld #2 Only

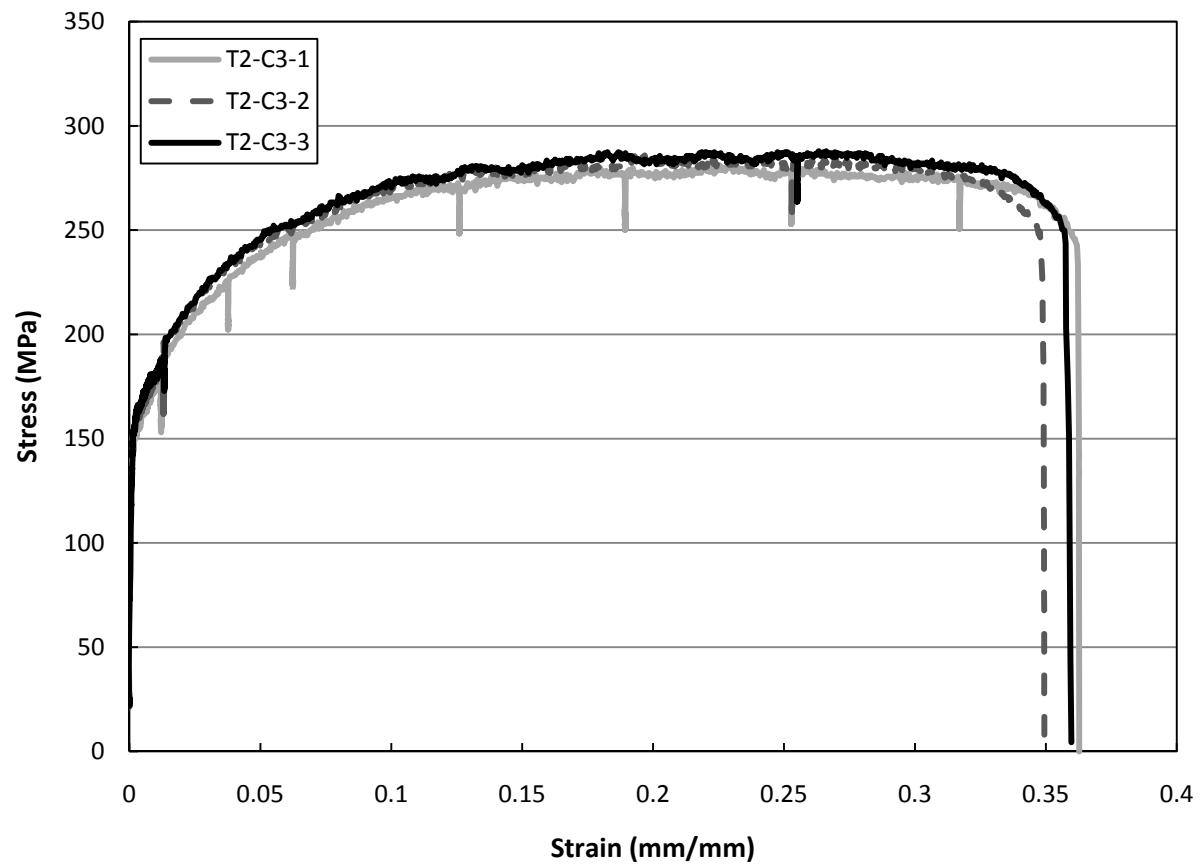


Figure 5-6: Monotonic Weld Test Series Configuration T2-C3; Weld #1 and Weld #2, With Chill Strip

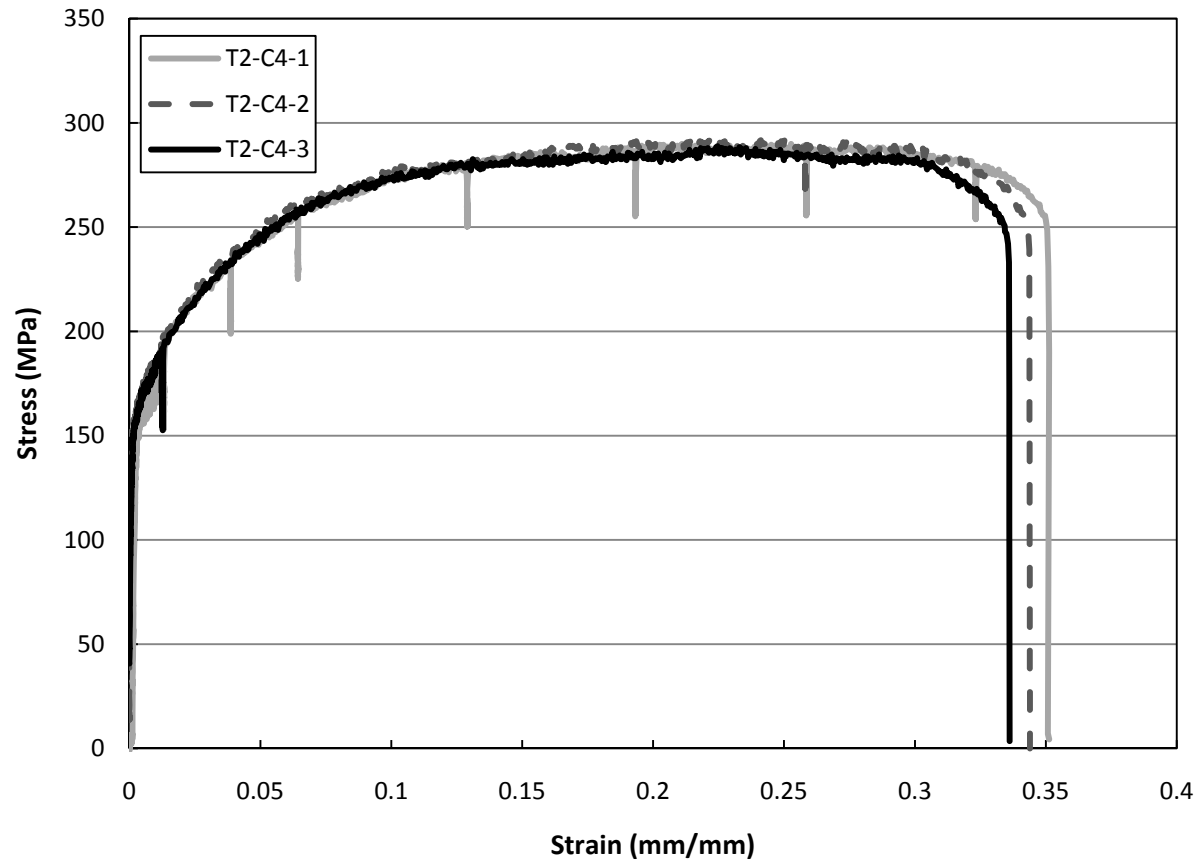


Figure 5-7: Monotonic Weld Test Series Configuration T2-C4; Weld #1 and Weld #2, Without Chill Strip

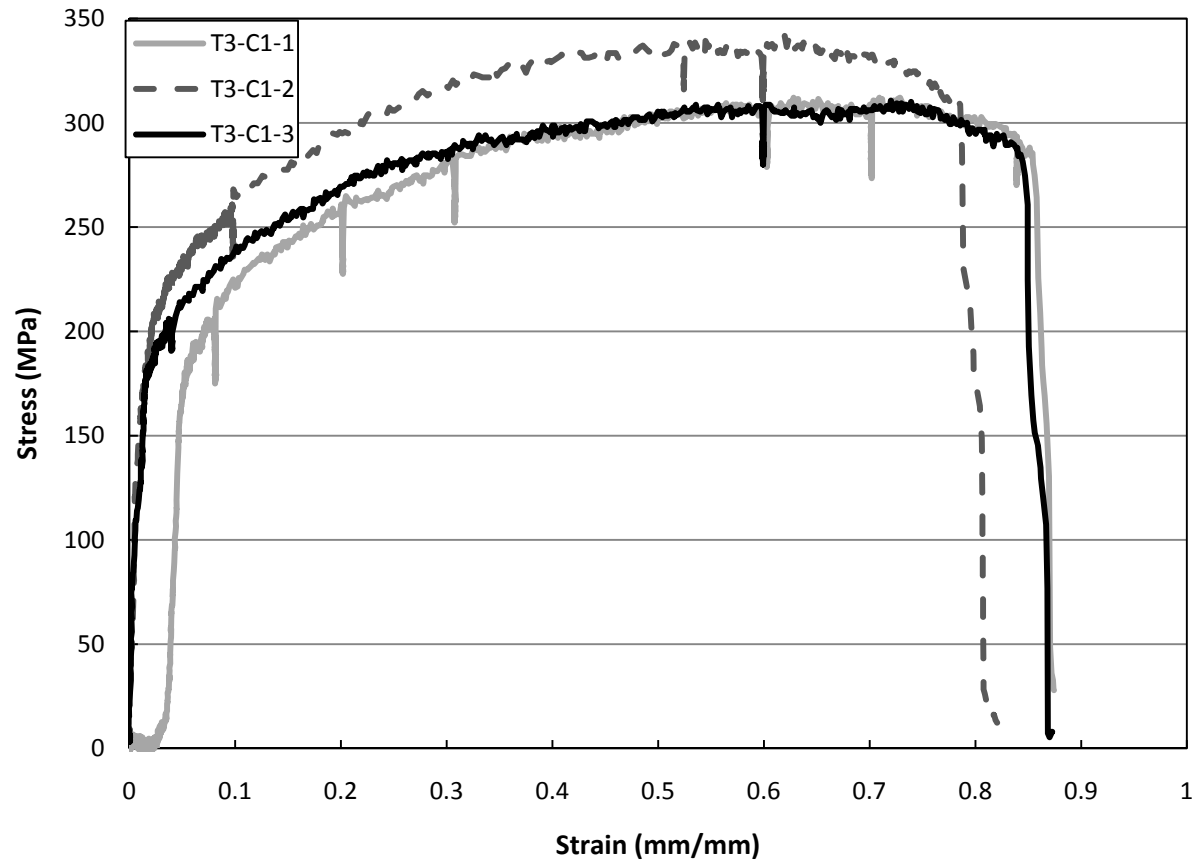


Figure 5-8: Monotonic Weld Test Configuration T3-C1; Weld #3 (Both Edges), With Chill Strip

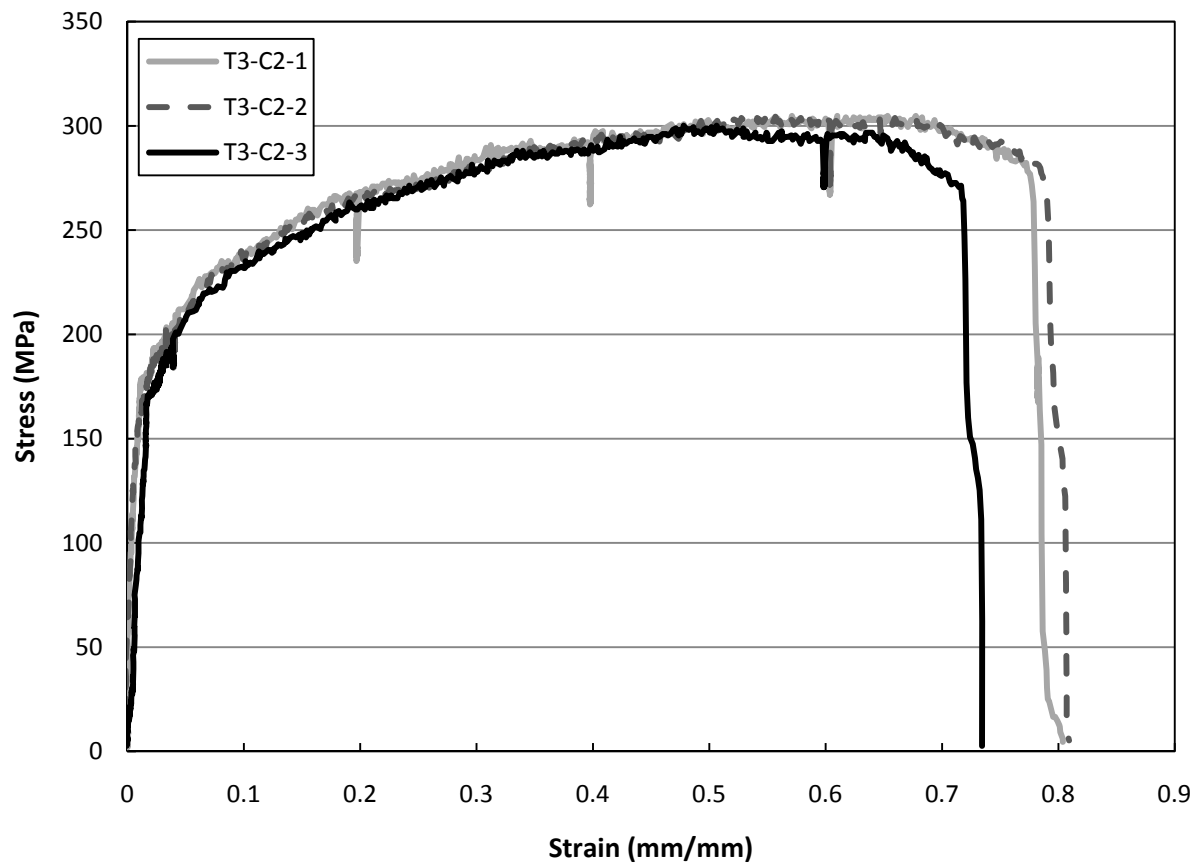


Figure 5-9: Monotonic Weld Test Configuration T3-C2; Weld #3 (Both Sides), Without Chill Strip

## 5.4 Cyclic Tests

### 5.4.1 Data Interpretation

Due to the large out-of-plane deformation during the compression portion of each cycle (see Figure 4-16 to Figure 4-18), it was not possible to instrument the test region. Thus strains are calculated as the relative displacement of the fish plates at either end of the specimens divided by the nominal gauge length of 25 mm. Also, during the inelastic phase some slippage of the infill panel material through the clamping plates occurred. Thus, caution should be used when interpreting the strain results beyond the elastic range in the plots of Figure 5-18 to Figure 5-21, Figure 5-25, and Figure 5-26.

During the initial 30 displacement-controlled cycles, two types of behaviour are noted from the stress versus strain plots of Figure 5-18 to Figure 5-21, and Figure 5-25 and Figure 5-26. During the first cycle the compression stiffness and the peak compression load are substantially higher than in the subsequent cycles. This behaviour is similar to tension-only bracing in a building; the first instance of buckling in compression introduces an imperfection, which causes buckling to initiate earlier in subsequent cycles (Bruneau *et al.*, 1998). The other aspect of the behaviour relates to the large variation in gross magnitude of loading imparted during the end of the tension half-cycle. This is due to the high stiffness of the material; since loading is in displacement control, small changes in the imposed strain result in large changes in stress magnitude.

Due to the variations in load history of each specimen, only general conclusions are drawn, based mainly on the failure mode, and the load at failure.

### 5.4.2 Infill Panel-to-Fish Plate Connection

In all cases, the failure occurred as a fracture in the base material far (at least 25 mm) from the weld location. In some cases the full tensile capacity of the base material was reached, while in others the cumulative damage to the base material during the 30 cycles of angular deformation resulted in an earlier failure.

The testing configuration for the T2-C1 and T2-C2 specimens is shown in Figure 5-10 (which corresponds to the design sketch in Figure 4-16), while side views of the test region during testing are shown in Figure 5-11 and Figure 5-12. The overall test setups for T2-C3 and T2-C4 specimens are similar, except the test region spans from the edge of weld #1 to the edge of the clamping plates, as seen in Figure 5-15 through Figure 5-17 (and corresponding to the design sketch in Figure 4-17).

An examination of Figure 5-11, Figure 5-12, Figure 5-15, and Figure 5-16 illustrates that although the angular distortion range sustained by the infill panel material during the 30 load cycles was of similar magnitude for all specimens, the absolute angle from the original position of the infill panel was different, due to the different geometry of the single-weld specimens (T2-C1 and T2-C2) compared with the two-weld connection

specimens (T2-C3 and T2-C4). The infill panel material of the two-weld specimens only experienced a maximum angle of  $40^\circ$  (Figure 5-15 to Figure 5-16), while the infill panel material of the single-weld specimens experienced a maximum angle of roughly  $70^\circ$  (Figure 5-12). This increased angular deformation resulted in high local bending at the sharp edge of the clamping plate, causing failure at a load less than the ultimate strength of the material. A comparison of the two failure modes observed in single weld specimens is shown in Figure 5-13 and Figure 5-14.



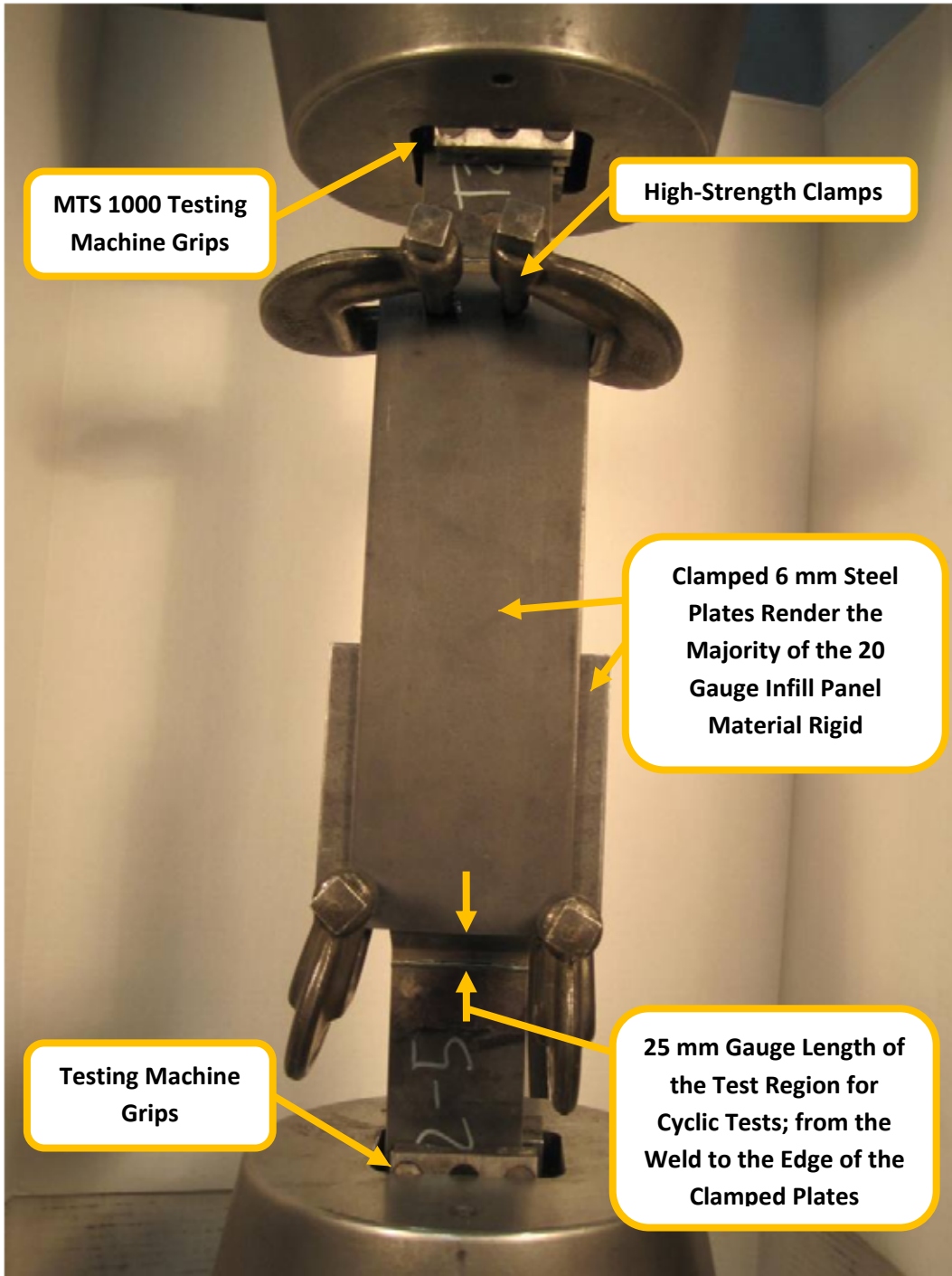


Figure 5-10: T2-C1 or T2-C2 Configuration; Overall View of Cyclic Test Setup

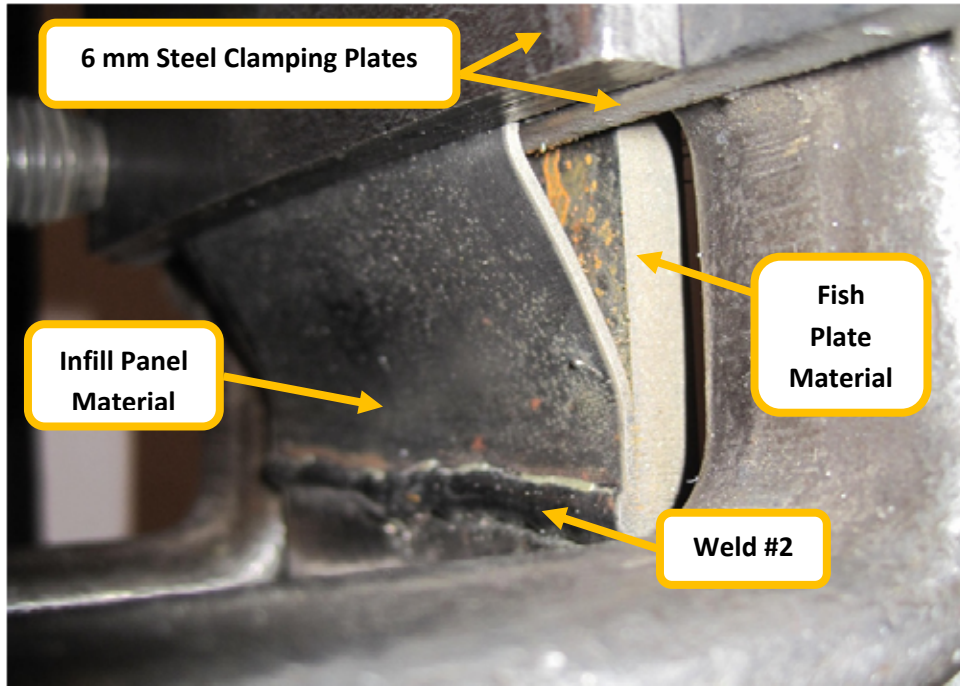


Figure 5-11: T2-C1 and T2-C2 Configurations, Minimum Angular Deformation in Cycle

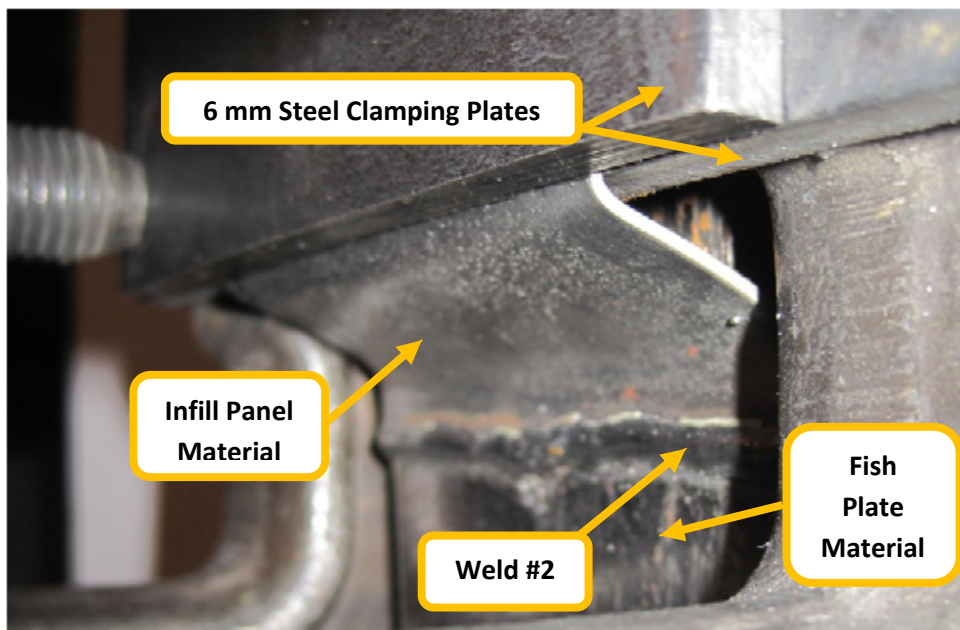


Figure 5-12: T2-C1 and T2-C2 Configurations; Maximum Angular Deformation in Cycle

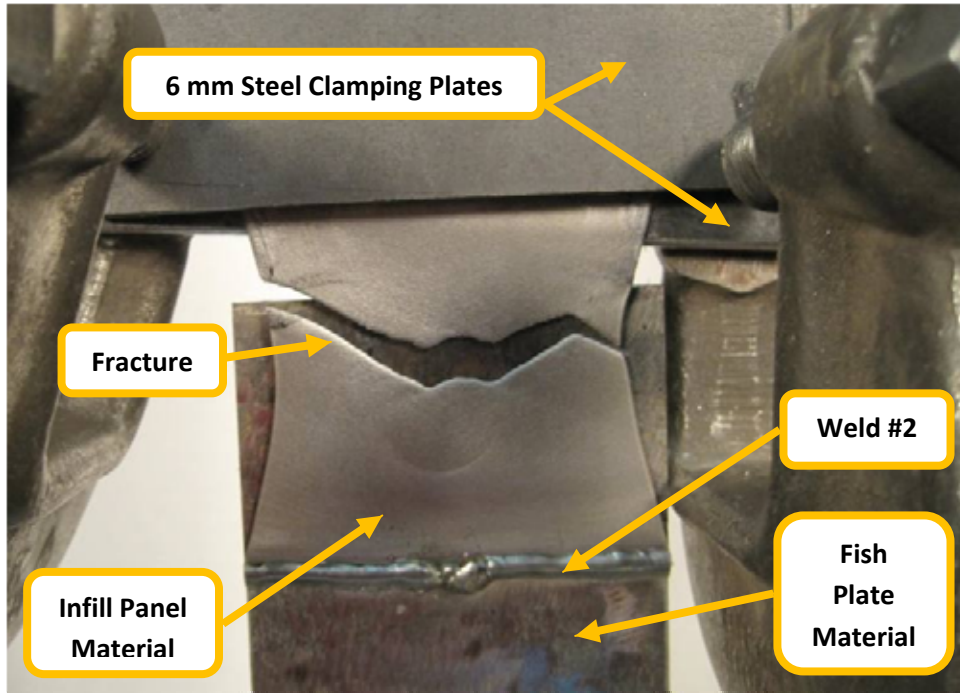


Figure 5-13: T2-C1 and T2-C2 Configurations; Tension Coupon-Style Failure Where Material Capacity is Reached

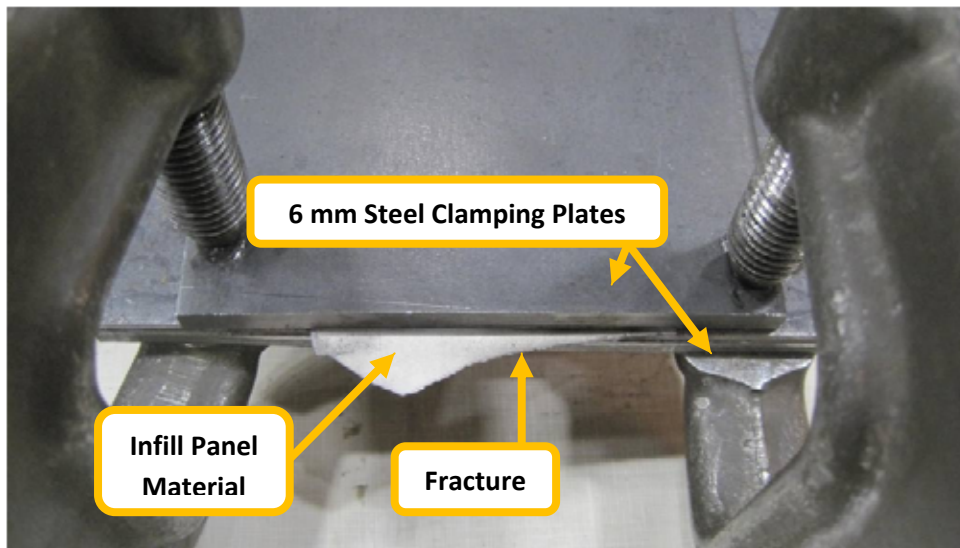


Figure 5-14: T2-C1 and T2-C2 Configurations; Early Failure at Clamped Edge of Steel Sheet

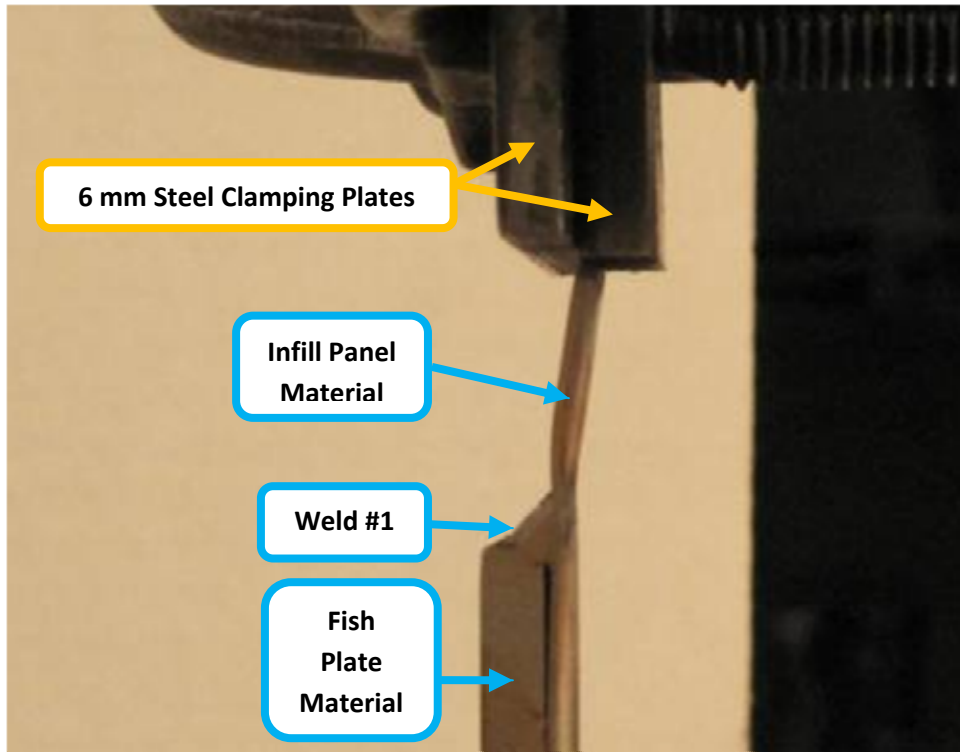


Figure 5-15: T2-C3 and T2-C4 Configurations; Minimum Angular Deformation in Cycle

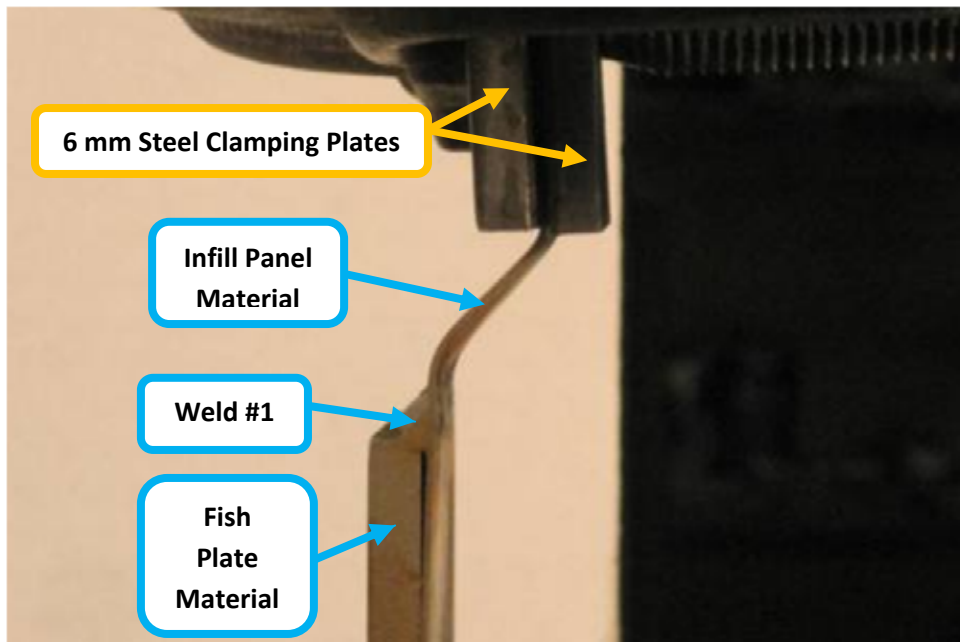
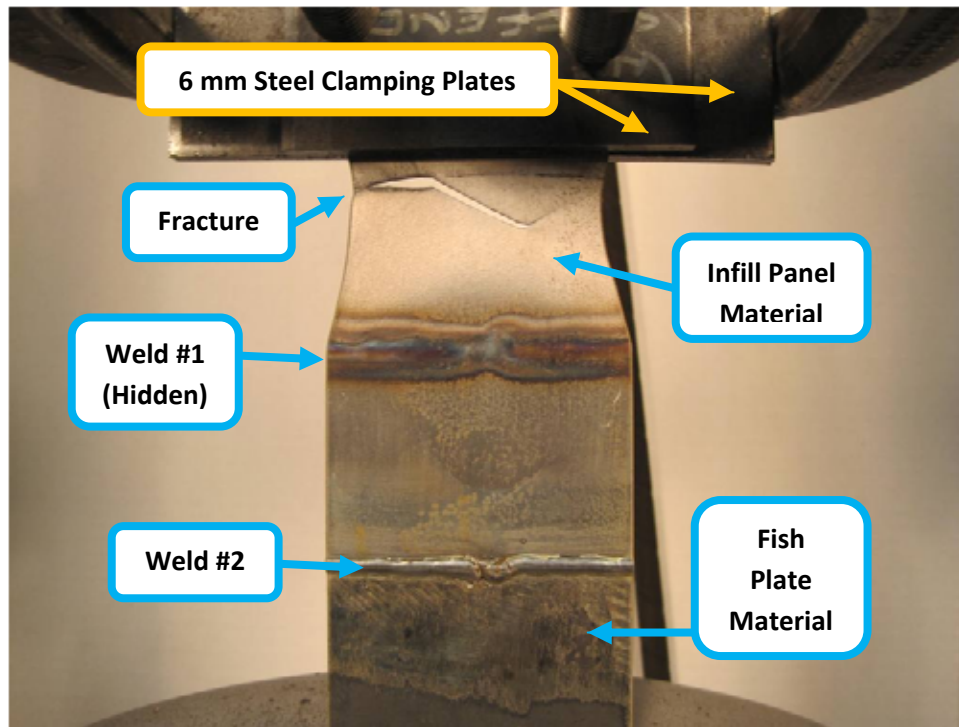


Figure 5-16: T2-C3 and T2-C4 Configurations; Maximum Angular Deformation in Cycle



**Figure 5-17: T2-C3 and T2-C4 Configurations; Typical Failure**

When comparing the overall results of single weld specimens (Figure 5-18 and Figure 5-19) with two-weld specimens (Figure 5-20 and Figure 5-21), the two-weld specimens appear to show greater ductility. However, as discussed above, two-weld specimens are not subjected to the same degree of angular deformation as single-weld specimens, and their failure mode is akin to a tensile fracture in the infill plate (Figure 5-17).

The key point is that, regardless of the failure mode in the infill panel material, failure takes place far from the welded joint (at least 25 mm in the tested specimens), and the weld region is not the weak point for either two-weld or single-weld specimens. It does not appear as if exposing the root of weld #2 or the toe of weld #1 to cycles of angular displacement has any impact on the failure mode.

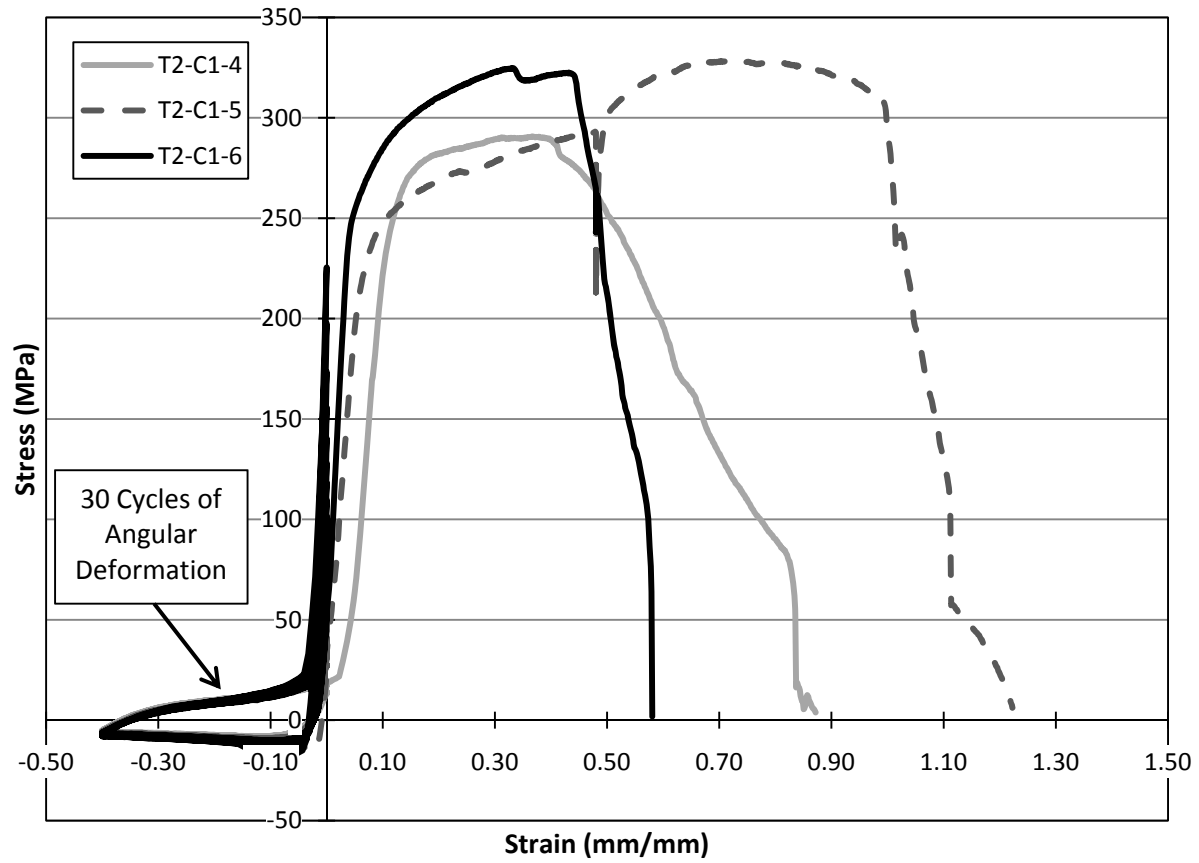


Figure 5-18: Cyclic Weld Test Configuration T2-C1; Weld #2 Only, Tack Weld at Midpoint

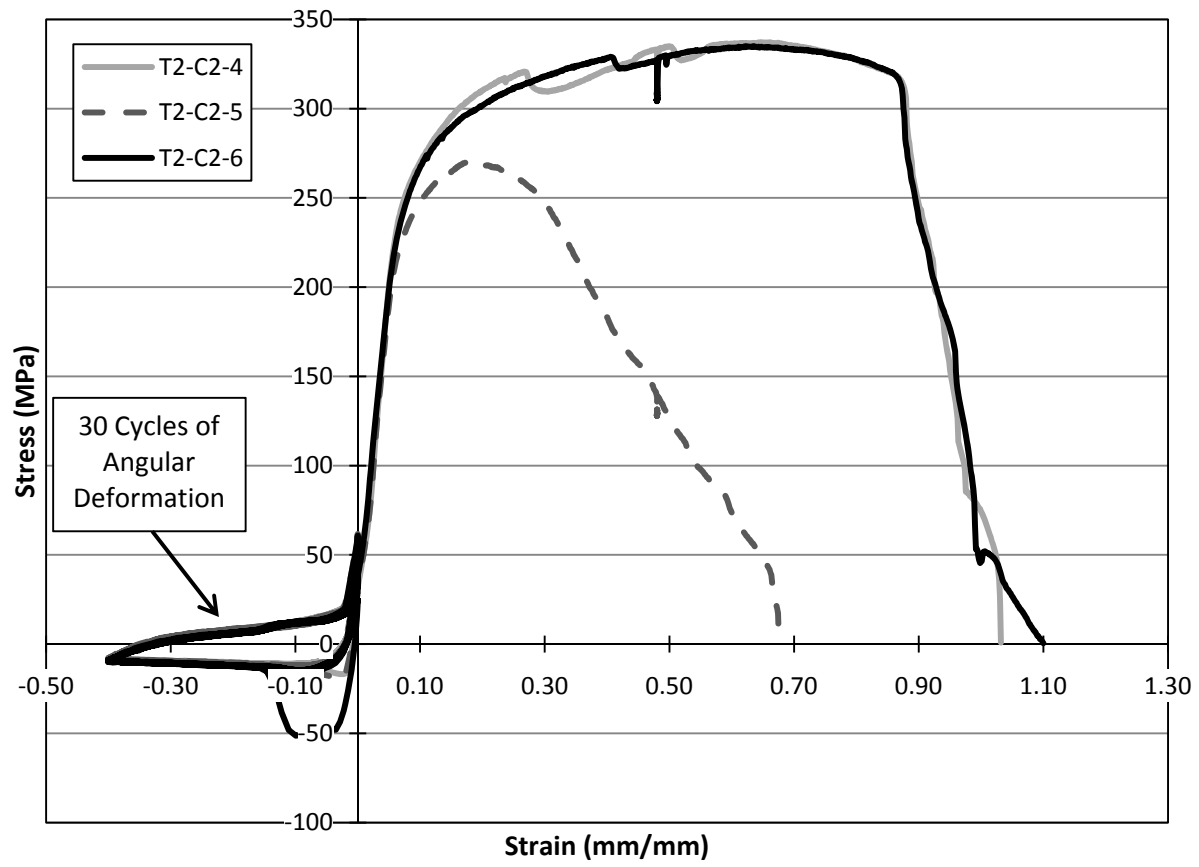


Figure 5-19: Cyclic Weld Test Configuration T2-C2; Weld #2 Only

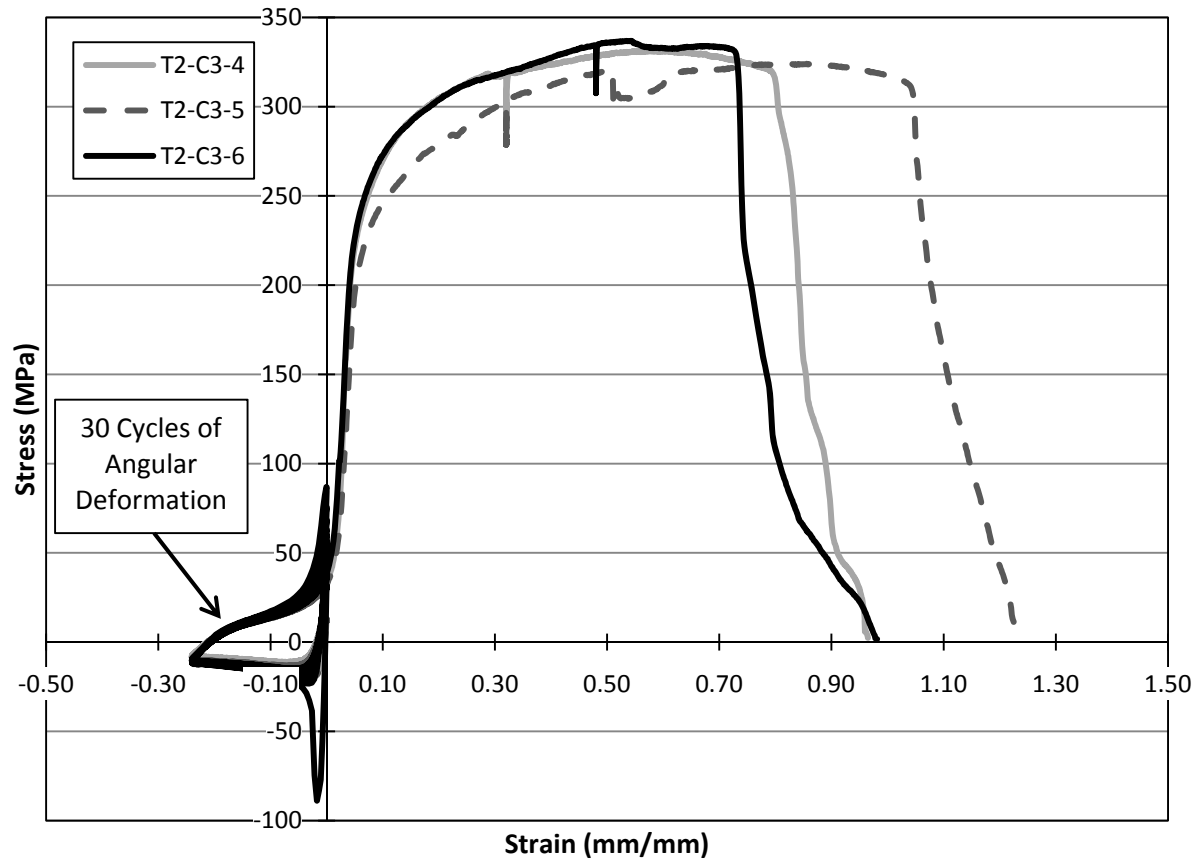


Figure 5-20: Cyclic Weld Test Configuration T2-C3; Weld #1 and Weld #2, With Chill Strip



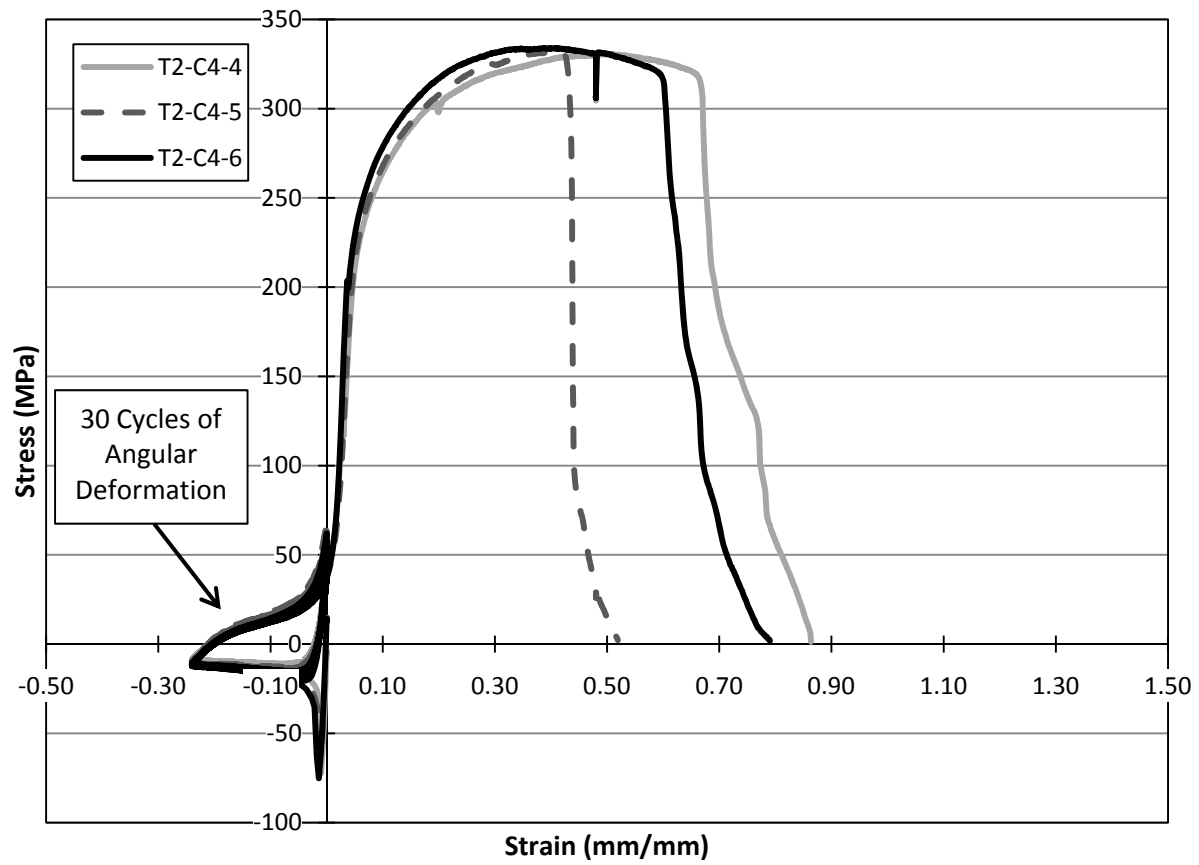


Figure 5-21: Cyclic Weld Test Configuration T2-C4; Weld #1 and Weld #2, Without Chill Strip

### 5.4.3 Infill Panel Splice

The cyclic tests of the infill panel splice indicated that joints welded with (T3-C1) or without (T3-C2) a chill strip fail away from the weld in the infill panel material. However, due to the small stiffness of the infill panel splice, unintentionally high angular rotation was imposed on the infill panel material, as shown in Figure 5-23. The result was a premature low cycle fatigue failure in the base metal at regions of cyclic kinking, as shown in Figure 5-24. In the case of specimen T3-C1-4, failure occurred at less than 10% of the tensile strength of the infill panel material following the 30 cycles of displacement (Figure 5-25). Note that failure took place in the heat affected zone, but it is believed that the kinking was the main factor affecting the location of rupture. Specimen T3-C2-4, which was welded without a chill strip at weld #1 (refer to Figure 3-4) and thus should demonstrate greater HAZ strength reduction, appears to perform better than specimen T3-C1-4 (Figure 5-26 and Figure 5-25, respectively). Thus, excessive kinking, as opposed to heat affects, appear to be the cause of these early failures.

All efforts to prevent excessive kinking while maintaining the axial deformation of the infill panel material failed. In view of the fact that this test was not yielding any useful information regarding the weld performance, testing was stopped after specimens T3-C1-1 and T3-C2-1.

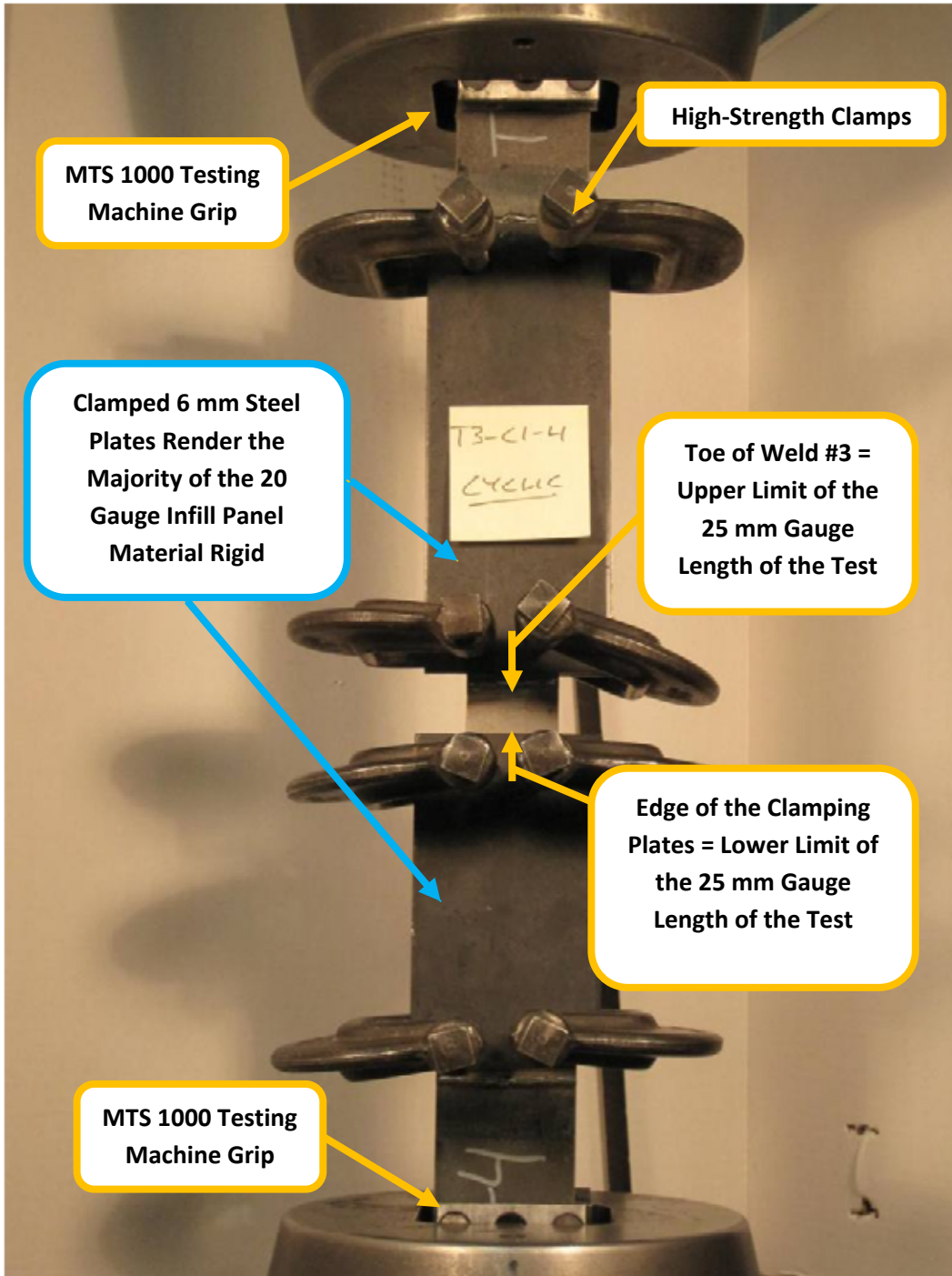


Figure 5-22: T3-C1 or T3-C2 Configurations; Overall View of Specimen

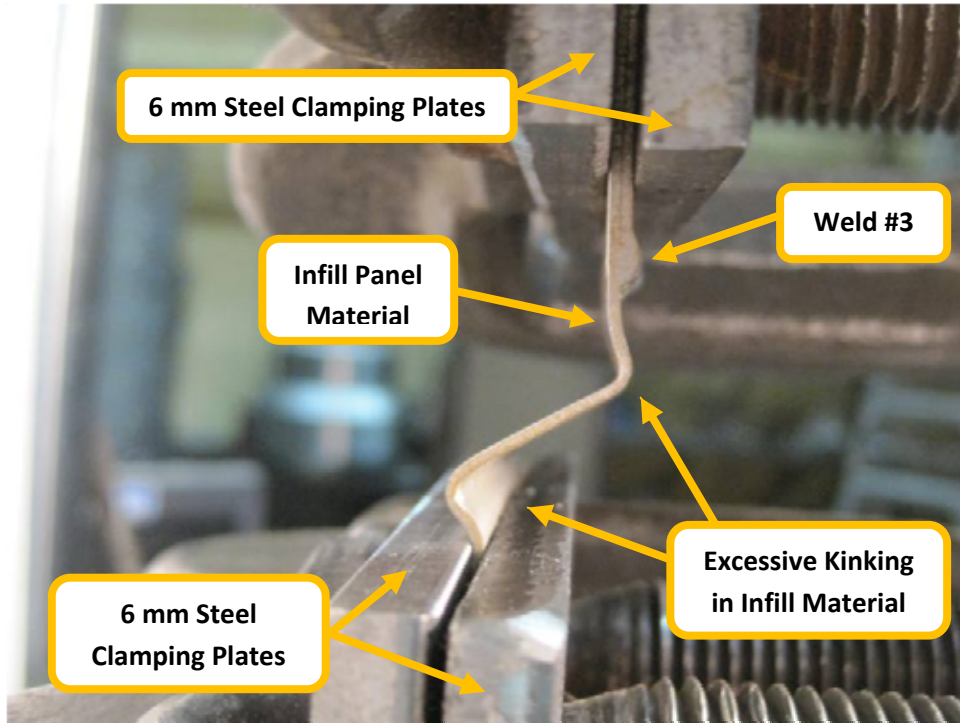


Figure 5-23: T3-C1 or T3-C2 Configurations; Severe Angular Change During Cycling

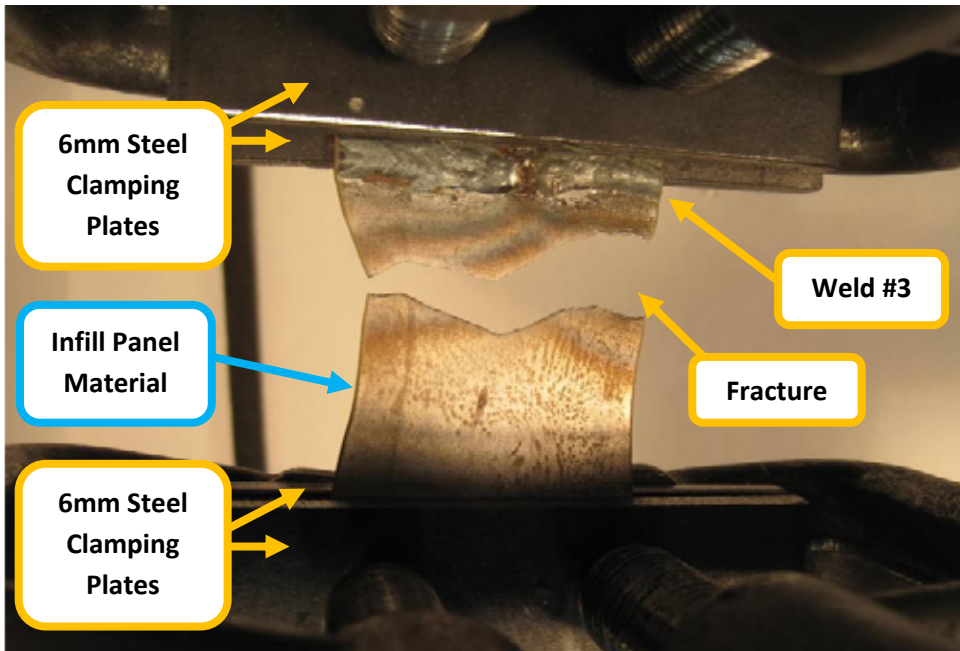


Figure 5-24: T3-C1 or T3-C2 Configurations; Typical Failure at Low Load, Initiating in Region of Severe Angular Change During Cycling

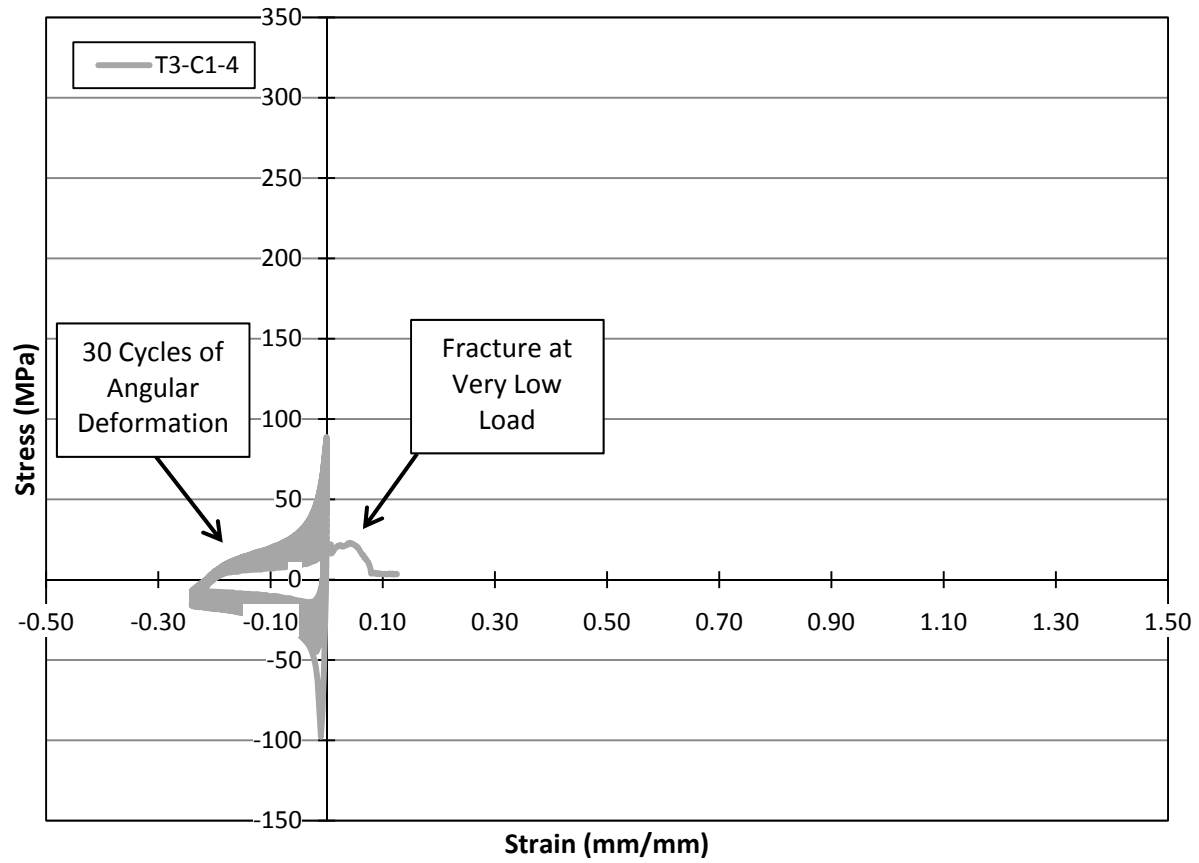


Figure 5-25: Cyclic Weld Test Configuration T3-C1; Weld #3 (Both Sides), With Chill Strip

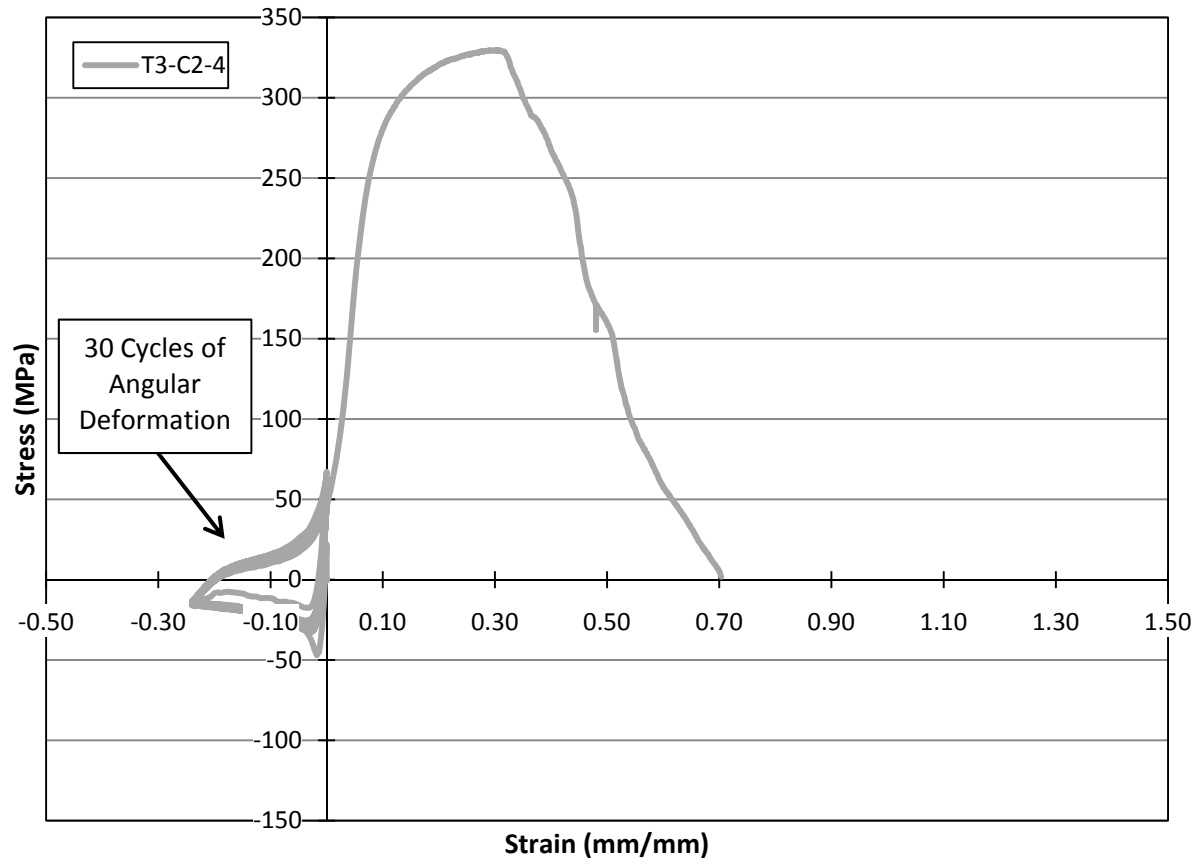
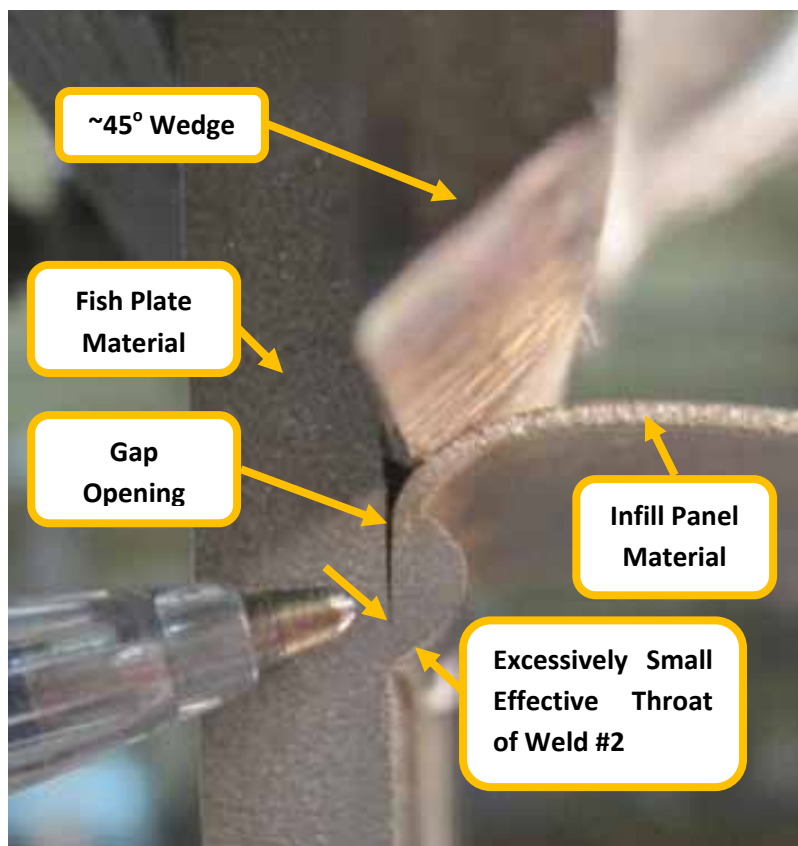


Figure 5-26: Cyclic Weld Test Configuration T3-C2; Weld #3 (Both Sides), Without Chill Strip

### 5.5 Wedge Push-Out Test of Weld #2

The five wedge push-out tests revealed a weld coverage problem. As shown in Figure 5-27 and in the load-displacement curves presented in Figure 5-29, for specimens T2-C1-2 and T2-C1-3 the weld sheared off at relatively low loads. This was clearly a result of poor weld coverage at the joint of the infill panel material and the fish plate material, resulting in a very short weld throat. As shown in Figure 5-29, if the weld covers the edge of the infill panel material and only a small portion of the weld is touching the fish plate, a very short weld throat results and the weld strength is severely reduced. It is impossible to assess visually the geometry of the effective throat of a finished weld without cutting a section from the finished workpiece.



**Figure 5-27: T2-C1-3-Bottom, Load = 12 kN, Crack Opening Due to Poor Weld Coverage**

In comparison, the three remaining joints tested could not be failed by the wedge. As load was applied, the 6mm thick fish plate began bending and the wedge slipped off of the small weld. No gap opened between the infill panel and fish plate materials; fusion appeared very thorough, as shown in Figure 5-28.

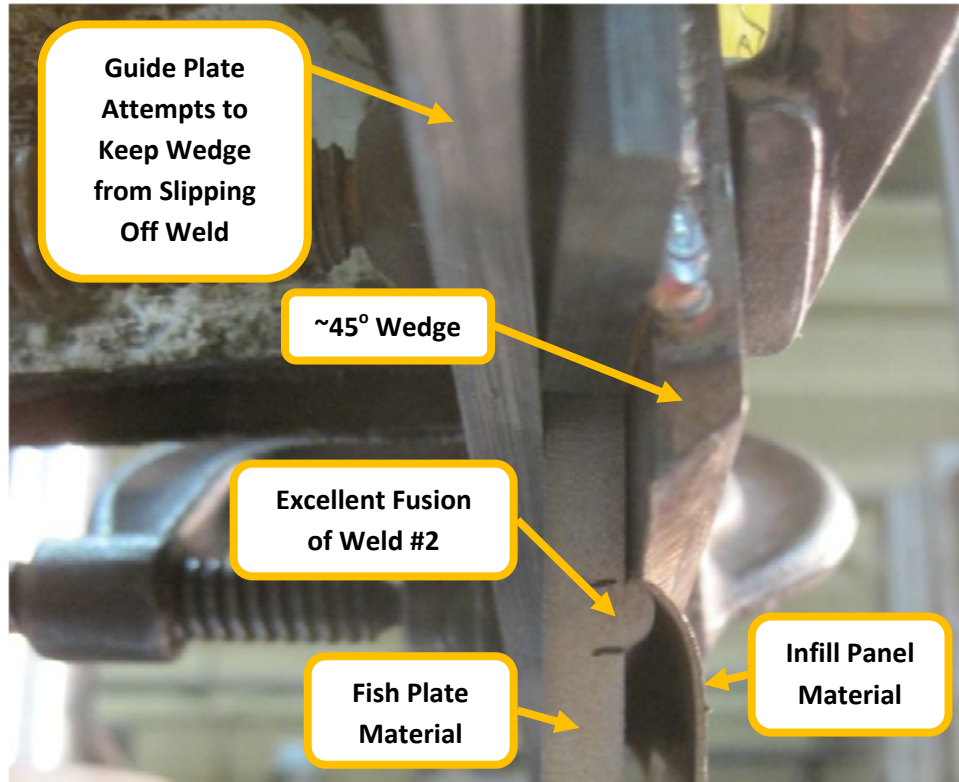


**Figure 5-28: T2-C2-1-Bottom, Load = 40 kN, Excellent Weld Fusion**

These tests indicate that the early failure in the tension test of T2-C2-3 resulted from the poor weld coverage, not poorly selected weld parameters. Assuming the attentiveness and skill of the structural engineering lab welding technician was typical, or better than expected in an industrial fabrication setting, it can be assumed that this type of variable weld coverage is inherent in manually welding with such a small electrode. However, the author believes that perfect weld coverage is not necessary to develop the full potential of the SPSW system, as the weld is significantly stronger than the base material, and the inherent redundancy of the SPSW system to redistribute load once deterioration begins should enable the tension field to anchor at an adjoining well-fused weld region.



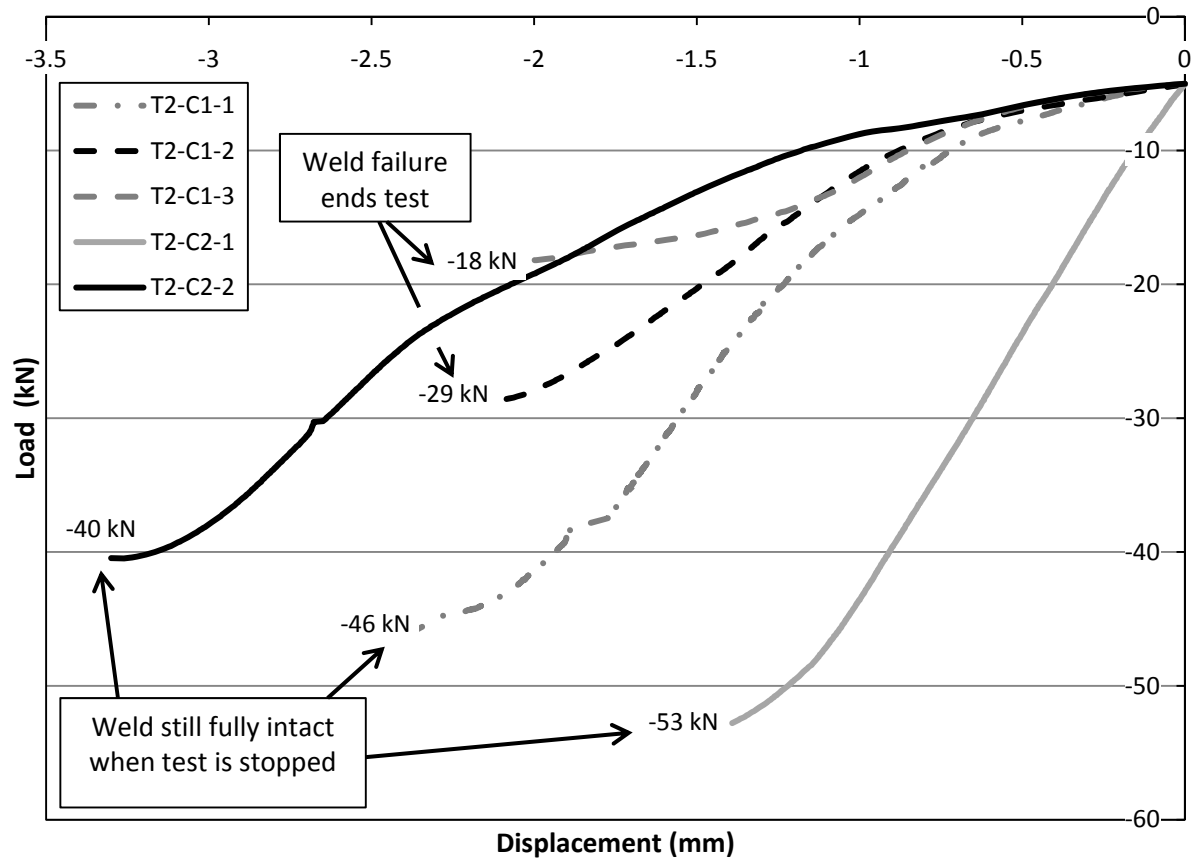


Figure 5-29: Transverse Wedge Push-Out Test of Weld #2

## 5.6 Summary and Conclusions

Six joint configurations are tested in quasi-static tension, and cyclic tension and compression. Failure in all cases except one took place in the infill panel material far from the weld, which shows potentially good behaviour of these joints in a SPSW system. The test program is unable to detect significant strength differences between the six different weld configurations; though welds that do not employ a chill strip are visually inferior, they still performed well under load.

A series of wedge push-out tests of the weld #2 configuration is conducted to investigate whether the weld parameters or a reduced weld throat are to blame for the premature failure of quasi-static test specimen T2-C2-3. Welding parameters are not to blame; the difficulty of manual welding with such a small electrode and against such a thin plate makes the joint difficult to see, which results in the occasional areas of poor weld coverage. However, only in one case out of all 32 tests conducted did this result in a premature failure. It is expected that the significant overstrength of the weld electrode relative to the base metals, and the inherent redundancy of the SPSW system more than offset the impact of occasional regions of poor weld coverage.

Because of the good performance of all the joints tested, the selection of the weld configuration for the large SPSW test must be based principally on ease of fabrication, while maintaining quality. In the case of the infill panel-to-fish plate splice, the use of a chill strip significantly complicates fabrication, since it must somehow be clamped to remain flush against infill panel during welding. This may be required when the frame is already in the upright position. Weld #2 on the fish plate and along the edge of the infill panel does not pose any risk of burn-through, and the redundancy of the SPSW system is expected to prevent occasional areas of poor fusion from resulting in catastrophic failure. Thus configuration T2-C1, consisting of weld #2 and tack welds at a maximum spacing of 75 mm, is selected for the infill panel-to-fish plate joint.

In the case of the infill panel splice, the fabrication condition is such that the weld is executed in the flat position, and using a steel surface as a chill strip is not nearly as difficult. Due to the relative ease of mitigating the burn-through risk, configuration T3-C1 consisting of a lap splice with tack welds at 75 mm spacing, and weld #3 on both edges of the lap splice joint, is selected for the large SPSW test specimen.

## Chapter 6: Steel Plate Shear Wall Test Design

### 6.1 Objectives

One of the primary objectives of this research program was to investigate the behaviour under cyclic lateral displacements of a large scale steel plate shear wall with a thin infill plate welded using the procedures developed in this research program. The level of performance was gauged by:

- 1) Ductility in the global behaviour, characterized by the ability of the infill panel and boundary elements to sustain load while dissipating a large amount of energy over the number of repetitions at specific storey drifts.
- 2) The nature of the failure mode and the resistance of the infill panel-to-boundary element connection. A welded joint that would be reliable and allow the infill panel and frame to develop their full potential was sought.

### 6.2 Specimen Design

The test specimen was designed with the goal of subjecting the infill panel-to-boundary element connection to large forces from the yielding infill panel. Thus, the sizing of beams and columns does not reflect a design scenario governed by design loads. Rather, very small boundary elements were selected to provide a minimal contribution to the lateral stiffness and resistance of the system. They must be sufficiently stiff to develop the tension field in the infill panel, to avoid a buckling failure, and they must be sufficiently stocky to preclude local buckling before plastic hinges develop and contribute several cycles of energy dissipation.

The design details were based on the requirements of CAN/CSA S16 – 01(CSA, 2001) for Type D (Ductile) plate walls. At the time of this design, CAN/CSA S16 – 01 was the governing standard, however, some clause changes now shown in CAN/CSA S16 – 09 (CSA, 2009) were anticipated and incorporated into the design. The beam-to-column connections were fully rigid moment connections, and detailed with guidance from CISC Moment Connections for Seismic Applications (CISC, 2008). Some small design deviations from these guidelines due to the differences between the quasi-static loading applied in this test, and the dynamic loading applied in an actual earthquake should be noted. For economy, stiffeners are welded with fillet welds, as opposed to full penetration welds. Also, since the sizing of the beams, columns, and infill panel was not based on design loads, clauses of CAN/CSA S16 – 01 pertaining to design loads are not relevant. In summary, the design is based on capacity design principals, bracing for frame and member ductility, and detailing for local ductility. Detailed calculations are presented in Appendix C.

For convenience, the specimen geometry was designed to fit the lateral load testing frame used by Deng *et al.* (2008). The specimen consisted of a single-storey MRF of centerline height 1900 mm and width 2440 mm, with 6 mm thick and 100 mm wide

steel plates, called “fish plates”, welded with fillet welds to the inside of the beam, columns, and baseplate. The thin infill panel was connected to the fish plates using the lap joint and weld discussed in Chapter 5. The columns were rigidly connected to a 3240 mm by 800 mm by 76 mm baseplate bolted to the strong floor of the I.F. Morrison Structural Engineering Lab using pre-tensioned anchor rods. Horizontal load was applied at the centerline of the top storey beam using two hydraulic jacks mounted to a stiff steel reaction wall. Watt bracing restricted out-of-plane movement at either end of the frame without restraining in-plane movements. An elevation view of the specimen in the test setup is shown in Figure 6-1. Detailed drawings are presented in Appendix D.

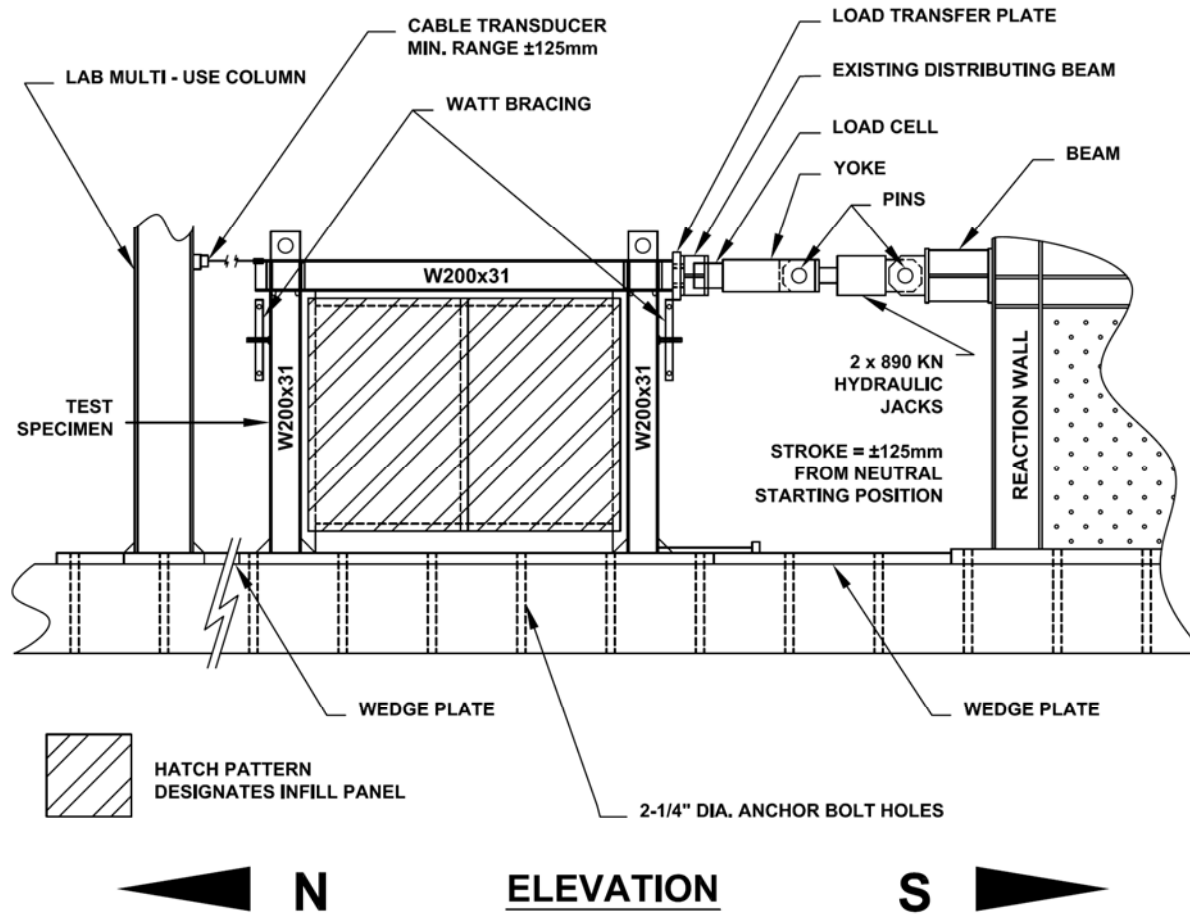


Figure 6-1: SPSW Test Setup – Elevation

### 6.2.1 Infill Panel-to-Fish Plate Connection Detail

As concluded in Chapter 5, the infill panel-to-fish plate connection took the form of a lap splice with a fillet weld on one side only. Two regions of this connection are of particular interest; the corners, which are locations of high restraint and high stress, and the connection of the infill panel to the fish plates at the location of infill panel splice, due to the discontinuity of the splice weld and the increased stiffness of the infill panel at the splice. These locations and details are shown in Figure 6-2.

The corners were designed with a 5mm gap between the horizontal and vertical fish plates, which is one of the details recommended by Schumacher *et al.* (1999) following an experimental study of infill panel-to-fish plate corner connections (see Chapter 2).

The configuration of the infill panel-to-fish plate connection at the location of the infill panel splice is less well established. It was found during small-scale testing that welding the lap splice causes distortion in the infill panel, and a clamping force is necessary to ensure the edge of the infill panel is flat against the fish plate for welding. Since the weld bead can be two-to-three times the thickness of the infill panel, extending the lap splice weld all the way to the end of the splice edge would prevent the infill panel from fitting flush against the fish plate for welding (Figure 6-2). This short interruption in the continuity of the infill panel weld is not expected to impact the anchorage of the tension field.

### 6.2.2 Strip Model

In order to predict the specimen behaviour, a simple strip model (Thorburn *et al.*, 1983) was constructed using SAP2000 software version 12. A static pushover analysis was conducted by applying incremental displacement to the top storey, in order to predict the storey shear versus storey sway envelope, determine the maximum lateral force required for the test, and approximate the significant yield load,  $Q_y$  (ATC, 1992). An elevation view of the model is depicted in Figure 6-3.

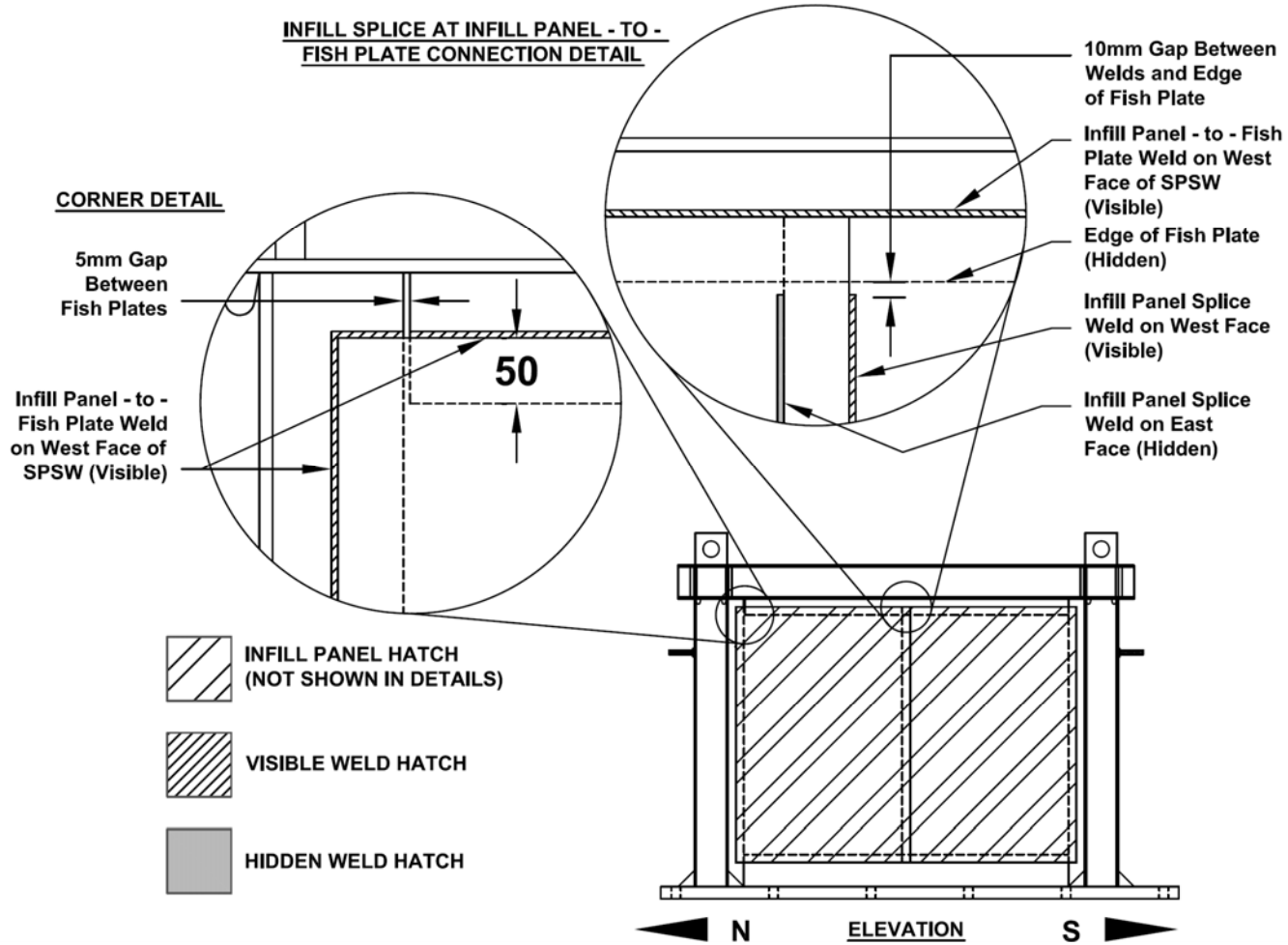


Figure 6-2: Particular Details for Infill Panel Welds

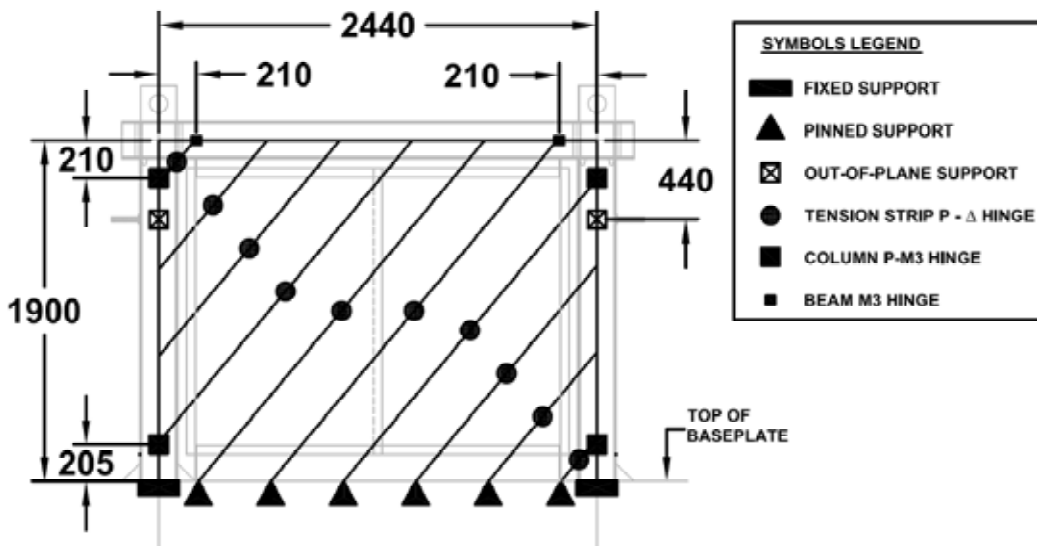


Figure 6-3: Strip Model Representation of SPSW Specimen

The model dimensions followed the centerlines of the test specimen; columns were 1900 mm high and the beam was 2440 mm long. Beams and columns were modeled as built-up frame elements consisting of W200x31 sections with a 6 x 100 mm fish plate. Beam-to-column connections were fully rigid, and considered infinitely stiff over a length of the frame element equal to the distance from the centerline of the connection to the edge of the joint panel zone. Full out-of-plane restraint was provided at roughly 2/3 of the column height where a Watt bracing was connected to the test specimen. The infill panel was divided into tension strips, which are pin-ended tension-only frame members. A total of 10 strips were used, which is the minimum recommended for adequate discretization (Thorburn *et al.*, 1983). In accordance with the findings of Shiskin *et al.* (2005), the model prediction is sufficiently accurate when the angle of the tension strips is taken approximately at 40° from the vertical. The baseplate anchored to the strong floor was considered infinitely stiff and was represented by pinned end reactions for tension strips and fixed end reactions for columns.

### 6.2.2.1 Material Properties Used In Model

Engineering judgement was required in selecting material properties from the results of the tension tests, as some questions arose regarding the validity of the static stress values obtained from testing. It is the author's judgment that the dynamic material properties, though they may somewhat over-predict the material performance, are a closer approximation than the so-called "static" values that appear inconsistent and unrealistically low (see Appendix A for further discussion). The average dynamic values of  $F_y$  and  $F_u$  were used for the grade 350W W200x31 boundary element material. As no measured material properties were available for the 300W fish plate material in the specimen, nominal values for grade 300W steel were used. A stress-strain profile based



on the lower bound of tension coupons B7 to B10 is implemented for the A1008 infill panel tension strips, as shown in Figure 6-4. Straight lines between five discrete points approximate the yield radius and yield plateau of the cold-rolled material. The principal engineering stress-strain material properties used in the model are summarized in Table 6-1.

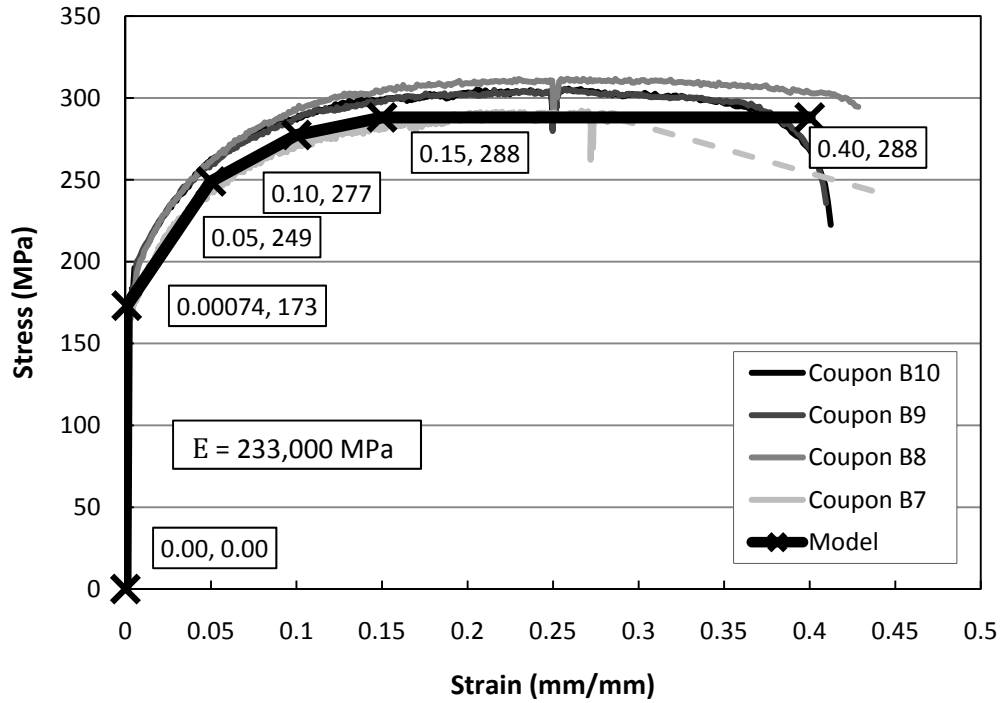


Figure 6-4: Stress-Strain Model Adopted for A1008 Material

Table 6-1: Material Properties Adopted for Strip Model

Material	E (MPa)	$F_y$ (MPa)	$F_u$ (MPa)
350W (W200x31 Boundary Elements)	210,000	360	461
300W (Fish Plates)	200,000	300	450
A1008 (Infill Panel Tension Strips)	233,000	173	288

**6.2.2.2 Hinges**

In this analysis, the panel zones formed by the intersection of the beam and columns were considered completely rigid. Beam plastic hinges were located at half of the beam depth from the face of the panel zone. Column plastic hinges were located at half of the column depth from the face of the panel zone, and at half of the column depth above the stiffeners at the base of the column. Hinge locations are shown in Figure 6-3.

Shiskin *et al.* (2005) found that simple bilinear elastic-plastic hinges provide a reasonable, if slightly underestimated peak load when compared with more complex hinges that include strain hardening.

Three hinge definitions were used. Beam hinges consider only bending behaviour, as this is the dominant mode (Shiskin *et al.*, 2005). The rigid-plastic “M3” hinge, where “3” represents bending about the strong axis, is defined in Figure 6-5. The plastic moment,  $M_p$ , was calculated based on the built-up section including the W200x31 member and attached fish plate. It should be noted that in reality local buckling may prevent the fish plate, which is not stocky enough to be a Class 2 section, from contributing fully to the plastic moment; thus, the actual maximum hinge moment will be between the plastic moment for the W200x31 section alone and the plastic moment for a section which includes the W200x31 boundary element and attached fish plate. The addition of the fish plate to the model hinge definition increases the hinge plastic moment by 20%.

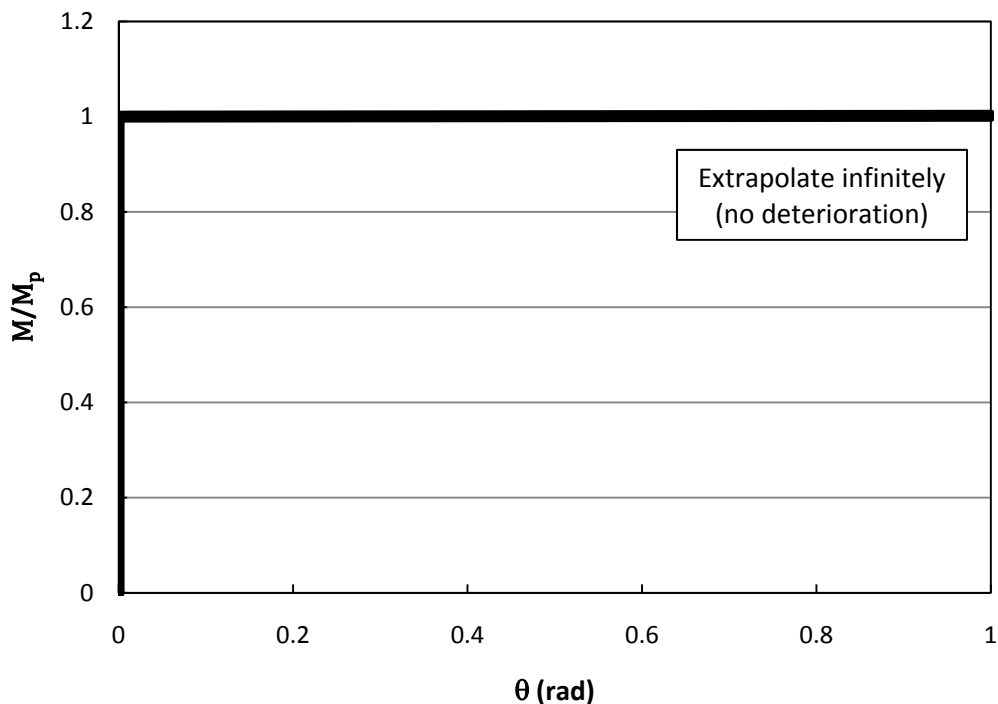


**Figure 6-5: Beam M3 Hinge Definition**

Interacting axial load-bending, or P-M3 hinges, were used for columns. The rigid-plastic moment behaviour shown in Figure 6-5 above captures bending behaviour. Axial deformation is the sum of two components. Elastic axial deformation,  $\Delta_e$ , was calculated based on elastic strains and the member length. Axial behaviour following yield,  $\Delta_I$ , was considered perfectly plastic, as illustrated in Figure 6-6. The axial and bending models were related by the FEMA 356 (2000) interaction equation shown in

[6.1], which is identical to the interaction equation adopted in CSA-S16-01 for bending of Class 1 or 2 I-shape members about the strong axis (CSA, 2001).

$$[6.1] \quad M_{pc} = 1.18ZF_y \left( 1 - \frac{P}{A_c F_y} \right) \leq ZF_y$$

For tension strips, the hinge can be placed at any location along the strip; in this model hinges were located at the midpoint of the strips. Since the A1008 CS infill panel material has a large ratio of ultimate strength to yield strength ( $F_u/F_y \cong 1.66$ ), an axial load vs. inelastic displacement hinge definition simulating the material model of Figure 6-4 was used, as shown in Figure 6-7.

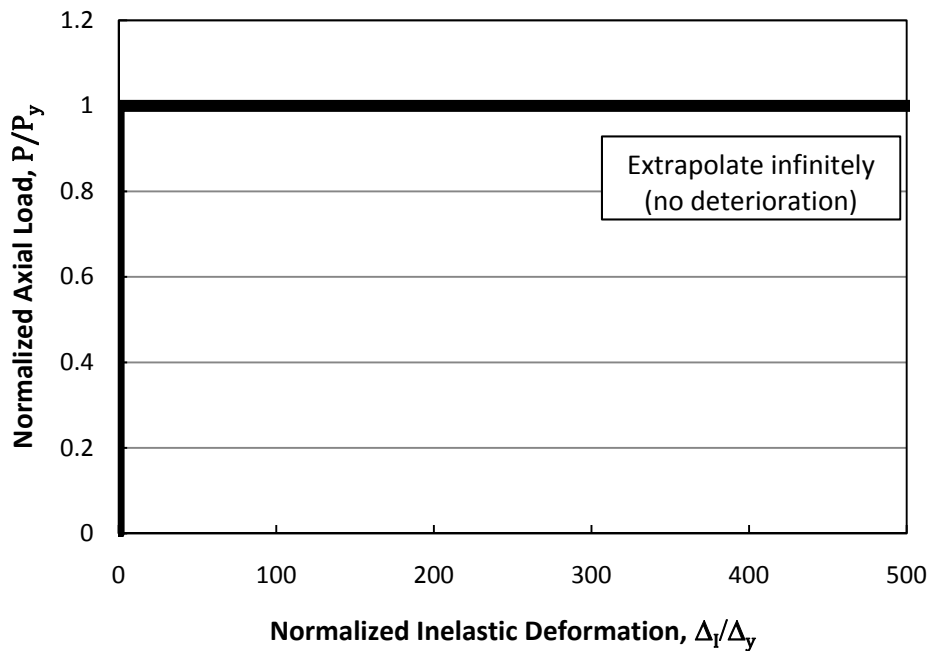
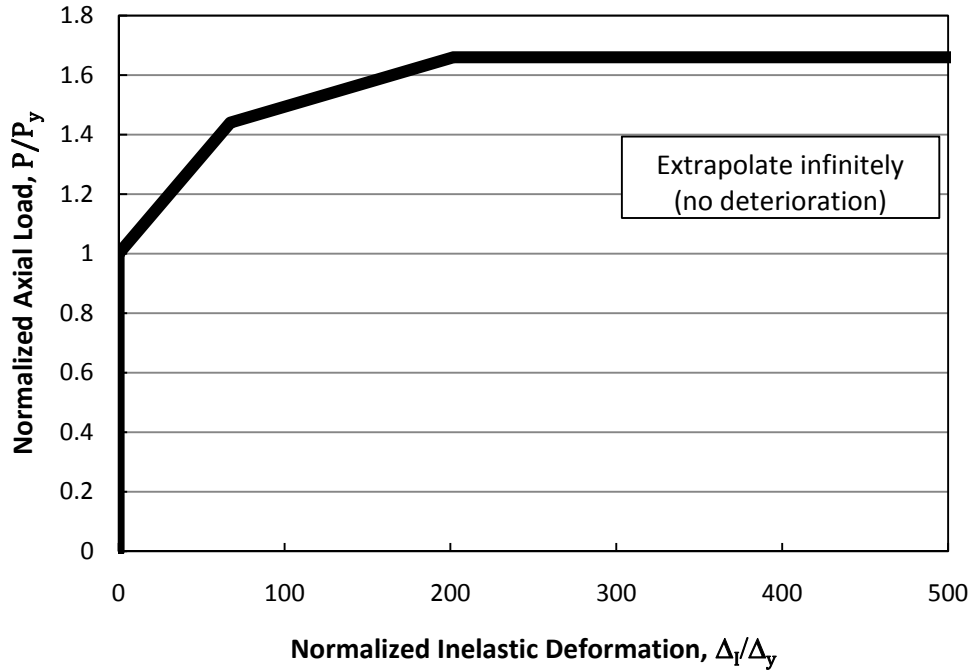


Figure 6-6: Load-Deformation Axial Behaviour of P-M3 Column Hinges



**Figure 6-7: Load - Displacement Hinge Model for Infill Panel Tension Strips**

### 6.2.2.3 Pushover Curve

The static pushover curve for the SPSW specimen is shown in Figure 6-8. The small reduction in stiffness at a load of 251 kN occurs due to the majority of the infill panel plastic hinges reaching their point of first yield. The significant softening that begins at 541 kN is a result of several hinges forming in the boundary members. Based on the region of the curve where significant softening takes place, the anticipated “significant yield” force,  $Q_y$ , is taken as 550 kN, as shown in Figure 6-8. This value is required for testing as discussed in Section 6.5, which describes the loading protocol.

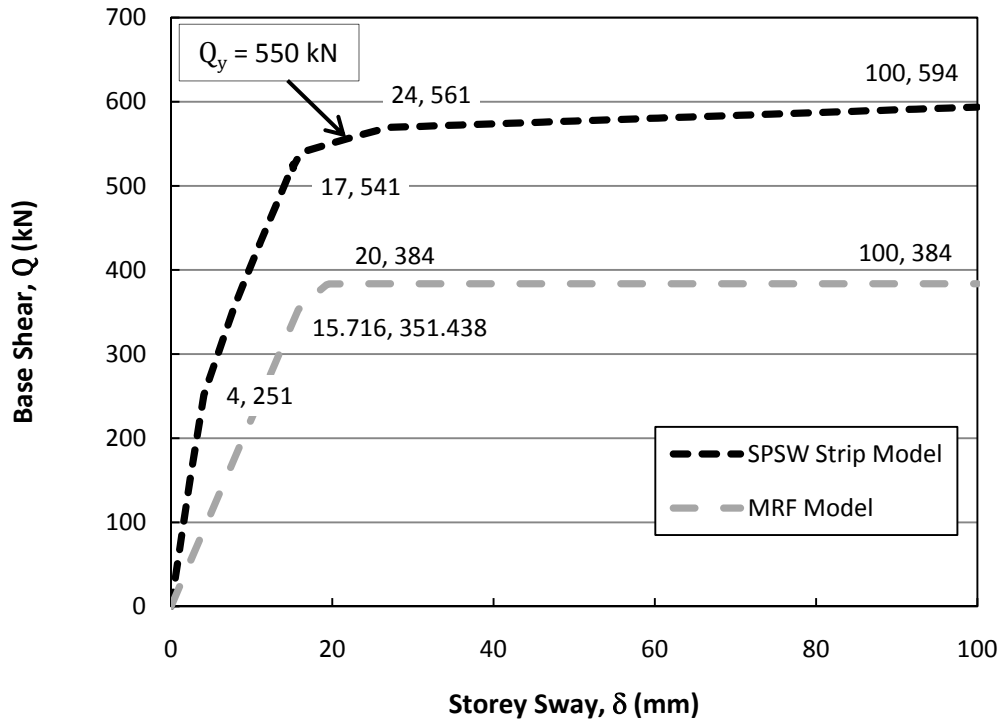


**Figure 6-8: Strip Model Pushover Curve**

The static pushover curve for the moment resisting frame (MRF) without the infill panel is also plotted in Figure 6-8. As expected, the addition of the infill panel to the MRF results in a significant increase in elastic stiffness (initially 280%) and ultimate load capacity (48% at a storey sway of 24 mm). The substantial reduction of the SPSW stiffness near 4 mm storey sway is a result of the relatively early onset of yielding in the infill panel. Note that the stiffness of the SPSW past 4 mm is nearly identical to the stiffness of the MRF alone (less than 3% difference), since all of the tension strips had yielded and their axial hinge definitions contribute a significantly reduced post-yield stiffness (less than 1% of the elastic stiffness). The slightly positive slope seen following the point of significant yielding,  $Q_y$ , when compared with the MRF is a result of the slight post-yield stiffness in the axial load-displacement hinge definition for the tension strips, which is the only hinge definition in this model that is not elastic-plastic.

### 6.3 Specimen Fabrication

The specimen was fabricated in two phases. First, the moment resisting frame and base plate assembly were shop-fabricated by a local steel fabricator. Second, the infill panel was assembled and welded into the frame at the I.F. Morrison Structures Lab.

#### 6.3.1 Moment Frame Fabrication

Construction of the moment frame was typical, with the exception of the column-to-base plate connections. These are T joints where uplift forces in the columns create tension in the through-thickness direction of the thick steel base plate. This tensile load

accelerates the formation of plastic hinges in the columns, since no gravity loads are applied in this test. Due to the high loads, there was a chance that lamellar tearing would occur in the base plate, resulting in an undesirable premature failure. In an effort to prevent this, base stiffeners were provided to distribute the tensile force over a larger area, reducing the tensile stress in the through-thickness direction of the base plate. Also, preheat was applied to the base plate prior to welding to reduce the cooling rate and minimize the formation of brittle martensitic phases in the heat affected zone of the welds. An ultrasonic non-destructive test performed on the column-to-base plate welds did not detect any deficiencies.

### **6.3.2 Infill Panel Installation**

The installation procedure for the infill panel was directly related to the selection of weld geometry and process from earlier phases of this test program. From the results of the small-scale testing, configuration T3-C2 was selected for the infill panel splice, and configuration T2-C1 was selected for the infill panel-to-fish plate connection.

The following procedure was followed:

- 1) Two 20 gauge, 1090 mm x 1595 mm, A1008 CS sheets were sheared. When overlapped on the long edge by 50 mm, these sheets formed a panel 1595 mm x 2130 mm. The sheets were sandwiched between two 12 mm sheets of plywood, with a 12 mm thick steel plate under the joint to act as a “chill strip” for welding. The plywood protected the thin infill panel from damage as the welding technician worked on top of it to access the weld area. Steel weights were applied to the lap joint to reduce distortion. A cross-section of the setup is shown in Figure 6-9.

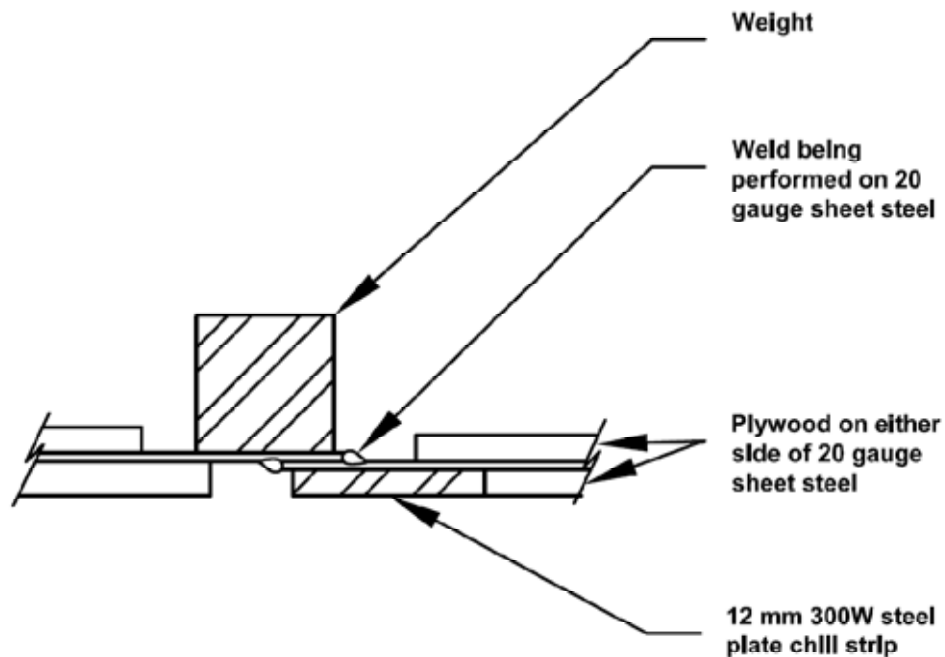


**Figure 6-9: Cross-Section of Infill Panel Splice Welding Setup**

- 2) Beginning at the midpoint of the joint, tack welds were placed at 50 mm spacing on alternating sides of the midpoint, working towards the outside edge of the panels. No welds were placed in the final 60 mm at either end in order to accommodate the infill splice at the infill panel-to-fish plate connection detail shown in Figure 6-2. The clamping weight and top layer of plywood were removed, and the panel flipped over. The steel chill strip was aligned under the unwelded side of the joint, and the steel weights and plywood repositioned as in Figure 6-9. The same procedure was used to tack weld the opposite side of the joint.
- 3) Beginning at the centre of the joint, the sheet was “stitch” welded by fillet welding a 50 mm length between two adjacent tack welds, then skipping the following 50 mm interval and welding the next interval. Once every second interval was welded, the infill panel was flipped over and the same welding procedure was used on the opposite side of the joint.
- 4) The remaining intervals were then welded until a continuous weld was achieved on both sides of the joint, always ensuring the chill strip and weight positions of Figure 6-9 were followed.
- 5) The moment frame was tipped from the upright position  $90^\circ$  and set on wood blocking such that the beams and columns were parallel to the floor. A sheet of plywood which fitted the full dimension of the bay bounded by the fish plates was shimmed on blocks to the same elevation as the upper face of the fish plates. The infill panel was laid on this plywood into its final position, with a 50 mm lap length onto the bounding fish plates. Mechanical clamping was provided at the lap joint to

ensure the thin sheet, which will have distorted during the welding of the infill panel splice, was flat against the fish plates.

- 6) The infill panel was tack welded to the fish plates at a spacing of 50 mm, starting at the midpoint of an edge side of the infill panel. Once roughly half of this length was secured by tack welds, the welding technician switched to the opposite edge of the infill panel and tack welded the centermost half of its length. Each of the two remaining sides of the infill panel were tack welded in a similar manner. The remainder of the infill panel was then tack welded to the fish plates, finishing by tack welding the corners. Tack welds were placed to either side of the 5 mm gap between fish plates at each of the corners.
- 7) A procedure similar to the lap joint welding procedure was followed for welding the intervals between tack welds. Starting at the midpoint of one edge, each second interval between tack welds is fillet welded. Once roughly half of the length of one edge is complete, the welding technician switched to the opposite infill panel edge and stitch welded half of the length at the centre, and did likewise with remaining edges of the infill panel. Stitch welding was continued, working towards the corners of the infill panel, until all four corners were welded. The remaining intervals were then welded (order is less important since significant restraint is present now) until a continuous weld was achieved.

### **6.3.3 Infill Panel Installation – Evaluation**

Connection of the infill panel to the boundary elements proceeded relatively smoothly according to the procedure outlined in Section 6.3.2. Figure 6-10 to Figure 6-21 show key stages of the assembly.

The welding of the infill panel splice, depicted in Figure 6-10, was particularly challenging. The scale of the sheets was much larger than those used in small-scale trials, and the restraint force provided by the 50 lb weights was insufficient to prevent distortion. These welding induced distortions caused portions of the plate to lift away from the chill-strip, and increased the likelihood of burn-through. Approximately 400 mm above the bottom edge of the infill panel, full burn-through of the infill panel splice occurred. The hole was repaired by plug welding, as shown in Figure 6-11.





**Figure 6-10: Welding Infill Panel Lap Splice Joining Two 20 Gauge A1008 CS Steel Sheets**

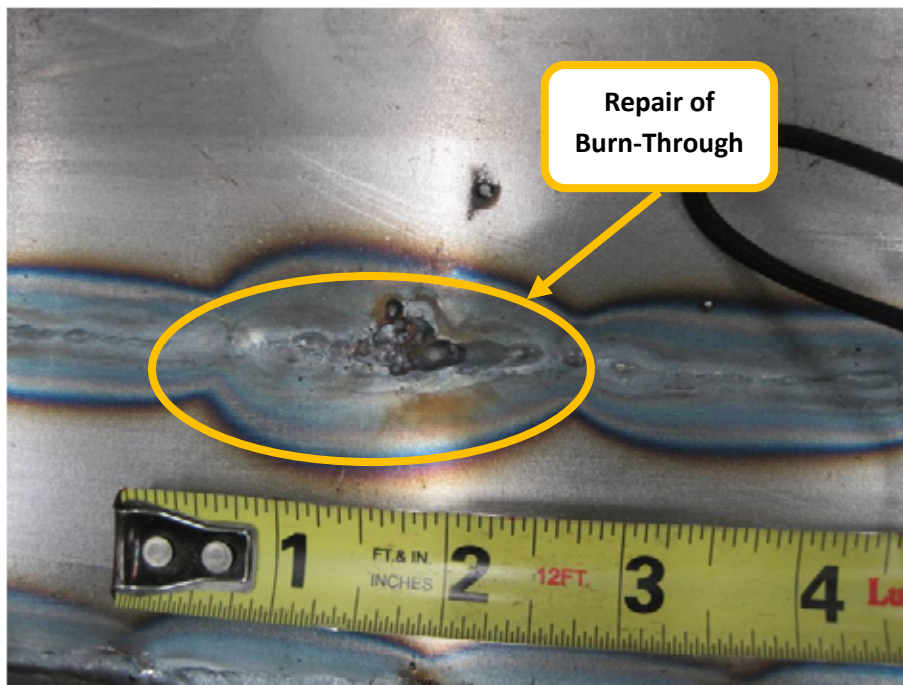


**Figure 6-11: Burn-Through Repair of Infill Panel Splice**

The frame is shown prior to the addition of the infill panel in Figure 6-12. The angular distortion of the finished infill panels (Figure 6-13) necessitated clamping of the infill panel to the fish plates as shown in Figure 6-14. Once tack welding was complete, the clamps could be removed. Tack welding, stitch welding, and the completed corner detail are depicted in Figure 6-15 through Figure 6-17, respectively.

At the conclusion of the assembly all welds were visually satisfactory. However, in addition to the burn-through previously discussed, the weld quality was likely inferior at some locations. At the north top corner, a roughly 25 mm length of weld adjacent to the gap between fish plates contained numerous starts and stops due to stubbing of the electrode as the welding technician sought a comfortable welding position. Near the infill panel-to-fish plate connection where the infill panel lap splice doubles the thickness of material to be welded, some pitting occurred (Figure 6-18) and a second pass was required to fill the voids. Figure 6-19 shows the completed infill panel-to-fish plate connection at the infill panel lap splice location.

Figure 6-20 shows the frame being tilted upright in a controlled manner by a hoist system. Figure 6-21 shows the finished SPSW anchored to the strong floor and prepared for testing.



**Figure 6-12: Rigid Frame Laid Down Flat for Infill Panel Installation**

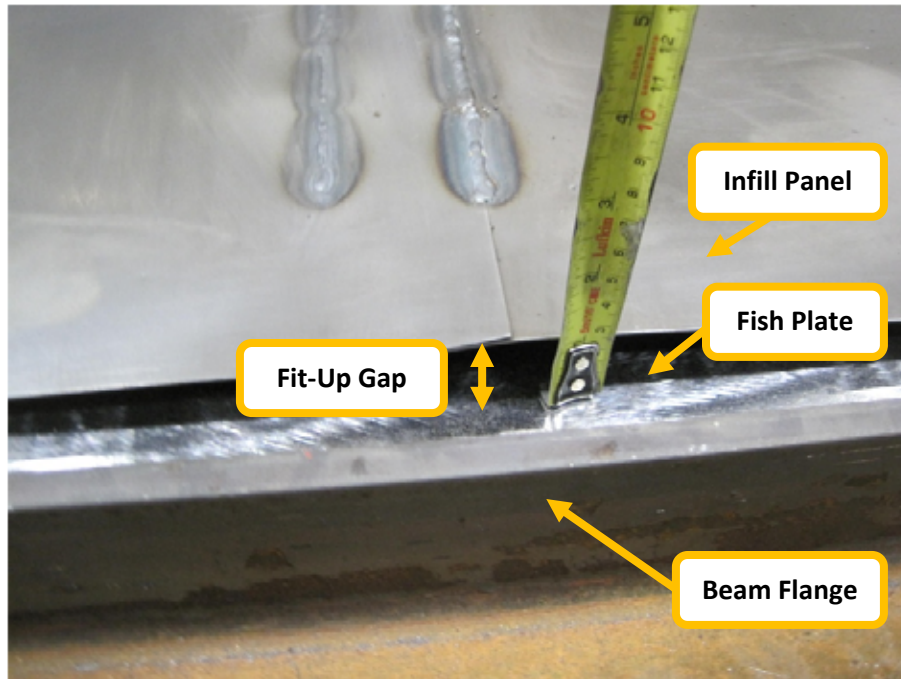


Figure 6-13: Gap Between 20 Gauge Infill Panel and Fish Plate Before Clamping

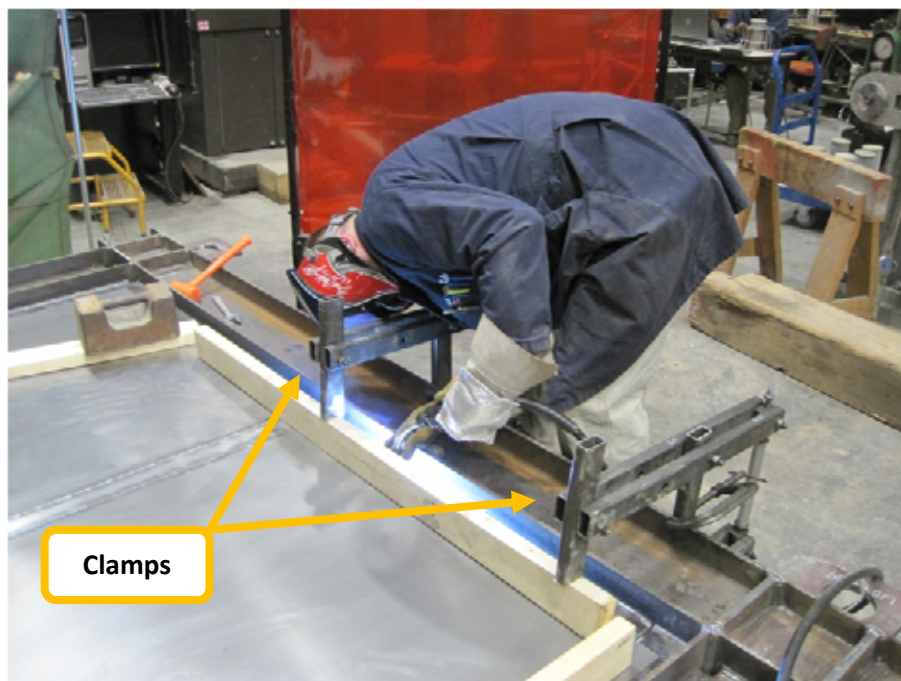


Figure 6-14: Clamping Force Holds Infill Panel-to-Fish Plate Joint During Tack Welding

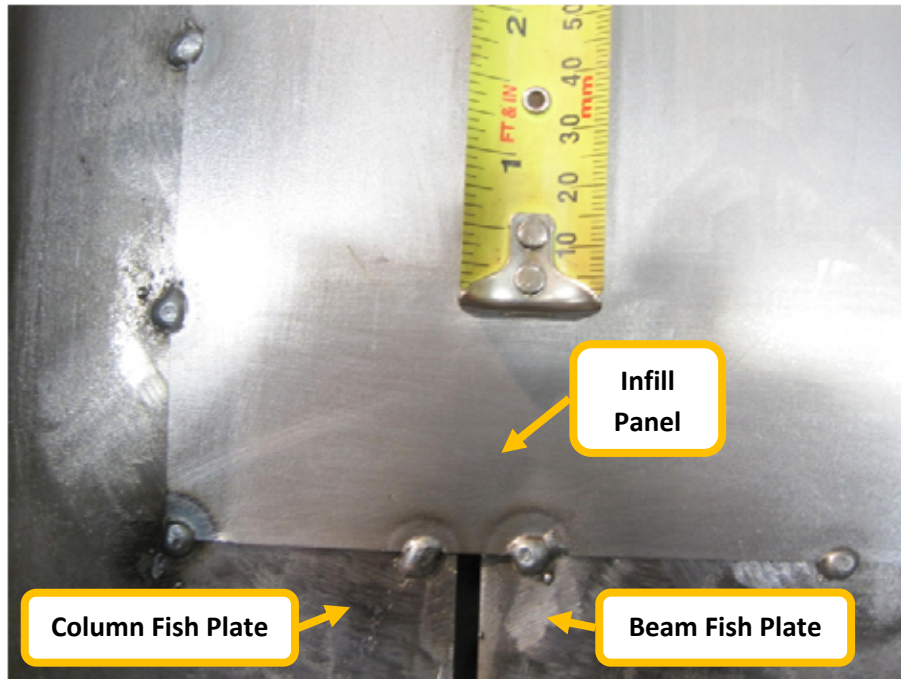


Figure 6-15: Tack Welds at Typical Corner Detail

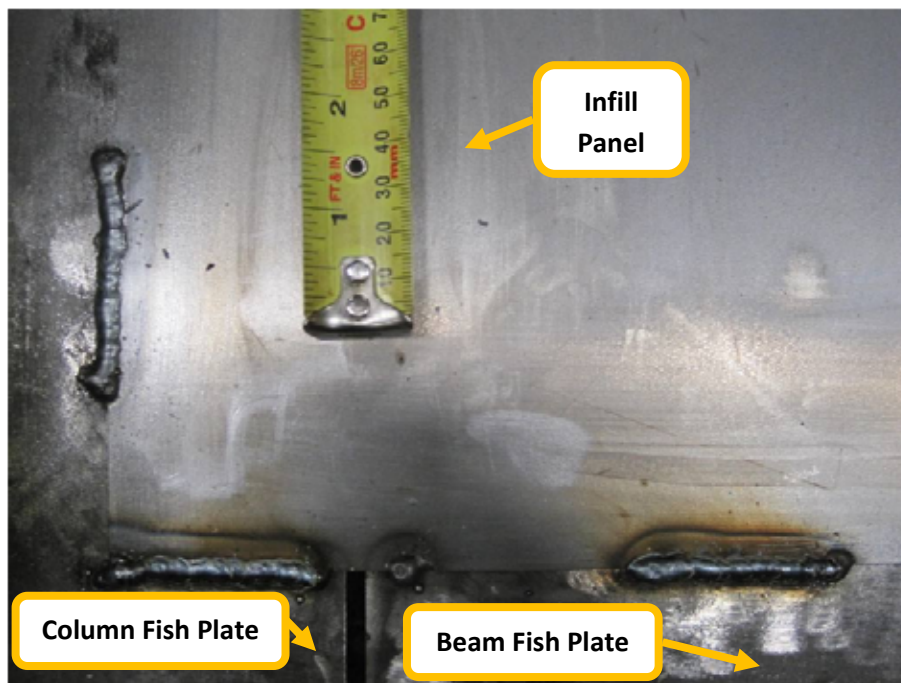


Figure 6-16: Typical Corner Detail Following the First Cycle of Stitch Welding

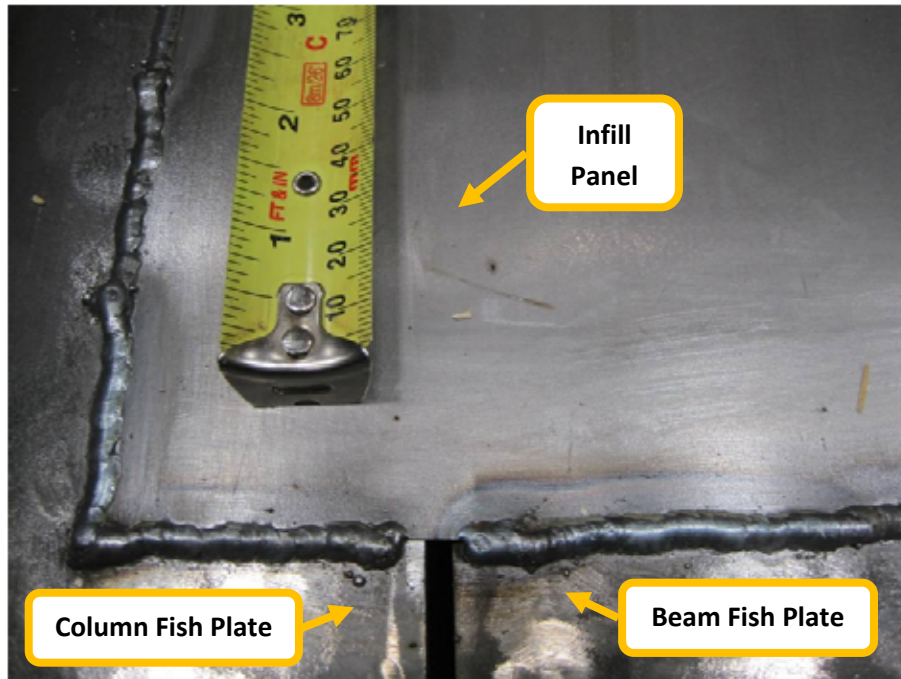


Figure 6-17: Finished Corner Detail Following the Second Circuit of Stitch Welding

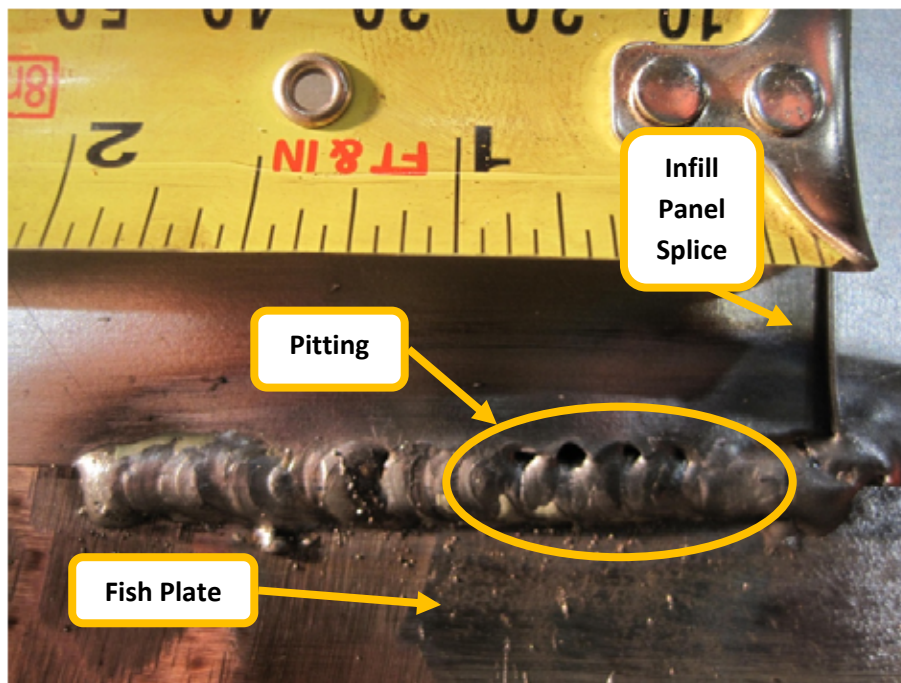
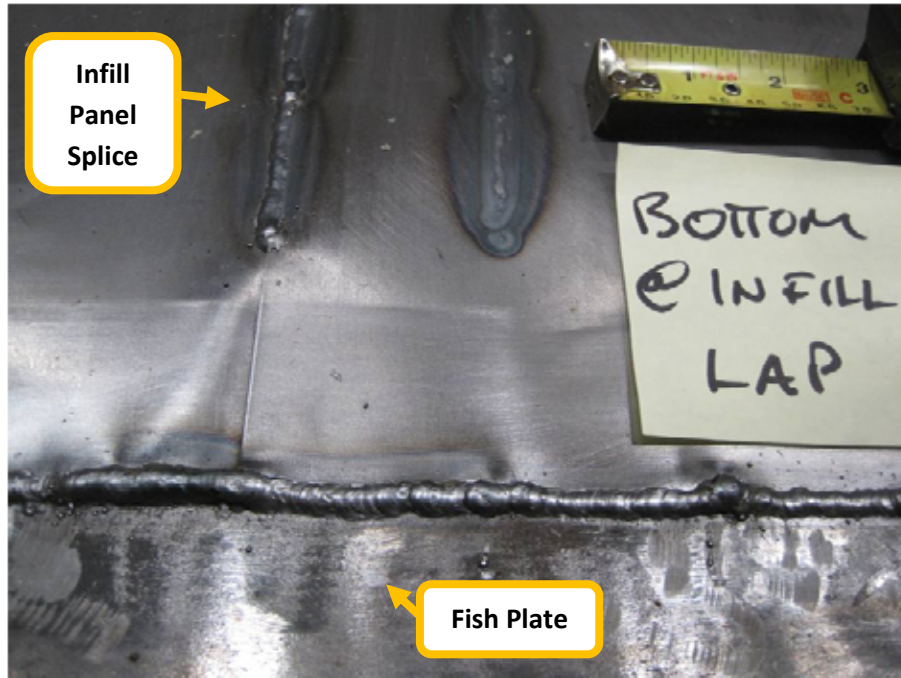


Figure 6-18: Pitting in Infill Panel-to-Fish Plate Weld Left of the Bottom of the Infill Panel Lap Splice



**Figure 6-19: Final Configuration of the Infill Panel-to-Fish Plate Connection at the Infill Panel Splice Location**

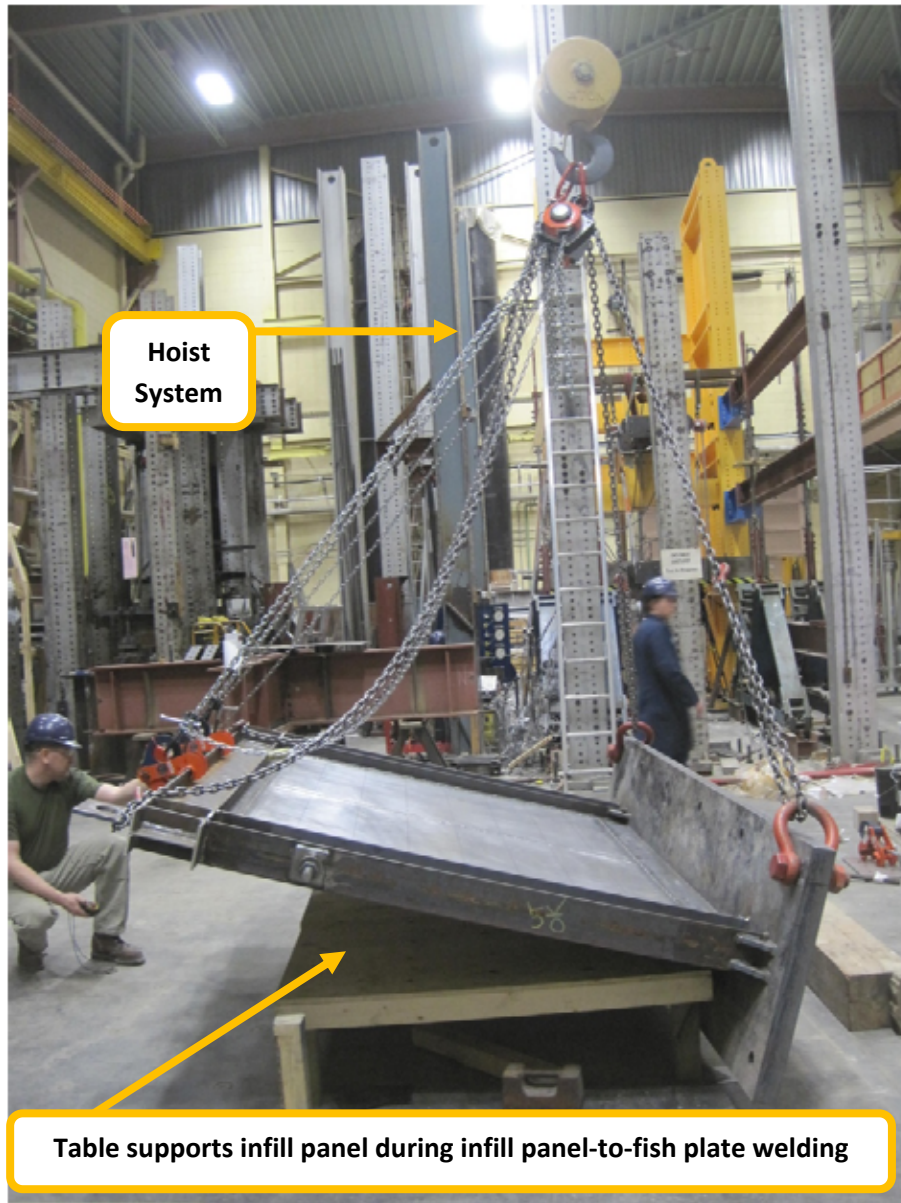


Figure 6-20: Hoist - Controlled Tilt-Up of SPSW Specimen

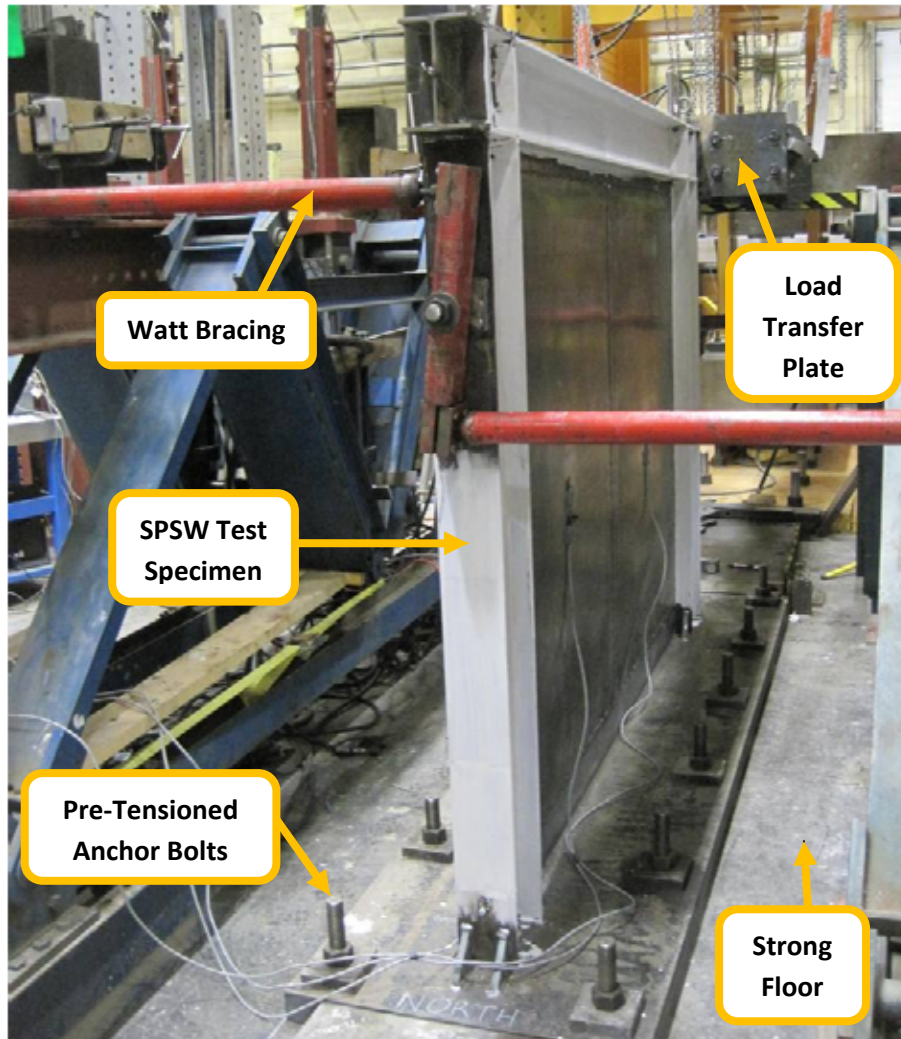


Figure 6-21: SPSW Specimen in Testing Frame, Prior to Load Application



#### **6.4 Instrumentation and Specimen Preparation**

An elevation drawing of the instrumented specimen is shown in Figure 6-22. The primary metrics of the global performance of the SPSW are gained from a plot of base shear versus storey sway. These metrics were collected by a load cell at the hydraulic jacks and a cable transducer at the north beam-to-column connection. Four strain gauges mounted to the infill panel monitored the infill panel strains and the angle of the tension field. Whitewash on boundary members helped detect the start of yielding in the boundary members. Since the infill panel-to-boundary element weld was so small and difficult to instrument, careful visual inspection of damage at this weld correlated against other metrics for the specimen were used to assess the general performance of the infill plate to fish plate welds. Cable transducers were used to monitor out-of-plane displacements of the wall and slippage of the base plate against the strong floor.

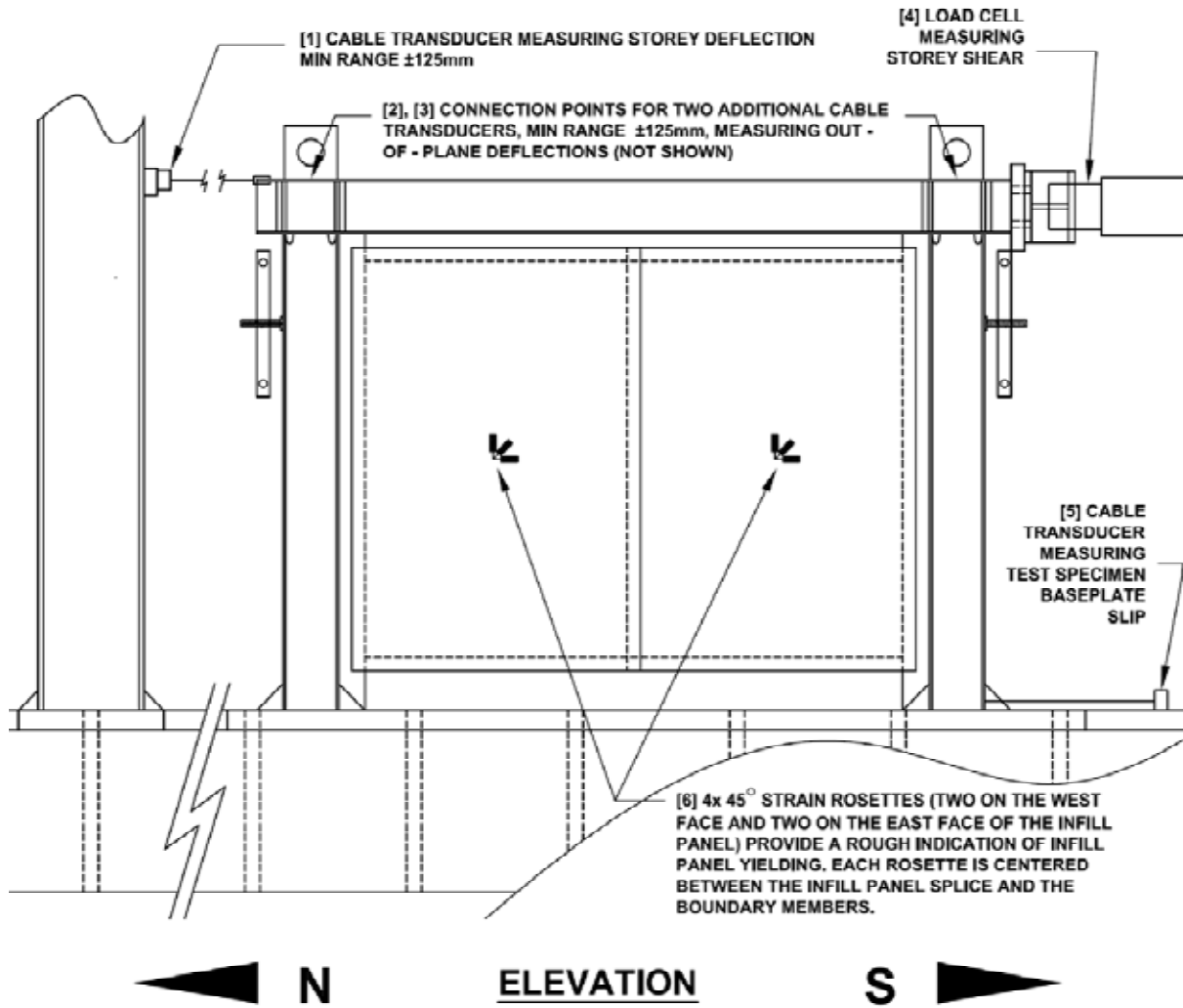


Figure 6-22: SPSW Specimen Instrumentation

## 6.5 Loading Protocol

Load was applied by controlling hydraulic pressure to the jacks shown in Figure 6-1. The flow of hydraulic fluid was controlled using a manually operated valve system. Real-time channel output for storey sway and base shear plotted by the data acquisition system enabled the operator to follow the established loading protocol.

Loading followed the recommendations of ATC 24: Guidelines for Cyclic Seismic Testing of Components of Steel Structures (ATC, 1992) for single-specimen tests. The loading history adapted for this test is shown in Figure 6-23, and explained in Table 6-2. The loading history is based on the anticipated substantial yield force,  $Q_y$ , and yield displacement,  $\delta_y$ . The deformation measured during the test required to mobilize  $0.75Q_y$  is known as  $\delta^*$ . Once  $\delta^*$  was determined during the first six cycles of loading,  $\delta_y$  was determined using equation [6.2], which assumes the line drawn from (0,0) to  $(\delta^*, 0.75Q_y)$  on the base shear versus storey sway curve can be extrapolated to find  $(\delta_y, Q_y)$ .

$$[6.2] \quad \delta_y = 1.33 * \delta^*$$

Each cycle consists of equal magnitude displacements in the north and south directions (symmetric cycling). According to ATC (1992), the first six cycles should be below the anticipated yield point, a minimum of three of the elastic range cycles should be at magnitude  $0.75Q_y$ , and the increment in peak storey sway per load step should be equal to the yield displacement,  $\delta_y$ , unless a different value is reasoned to be more appropriate.

Through to and including a maximum storey sway of  $3\delta_y$ , three loading cycles were applied at each deformation step. The maximum displacement was increased by an additional  $\delta_y$  for each successive load step, and the load cycles were repeated only twice once the storey drift exceeded  $3\delta_y$ . ATC (1992) indicates that the test should be concluded once a significant drop in load carrying capacity is observed. A 15% drop in load carrying capacity was the limit used in this work. The SPSW test of Driver *et al.* (1997) was terminated at the same limit.

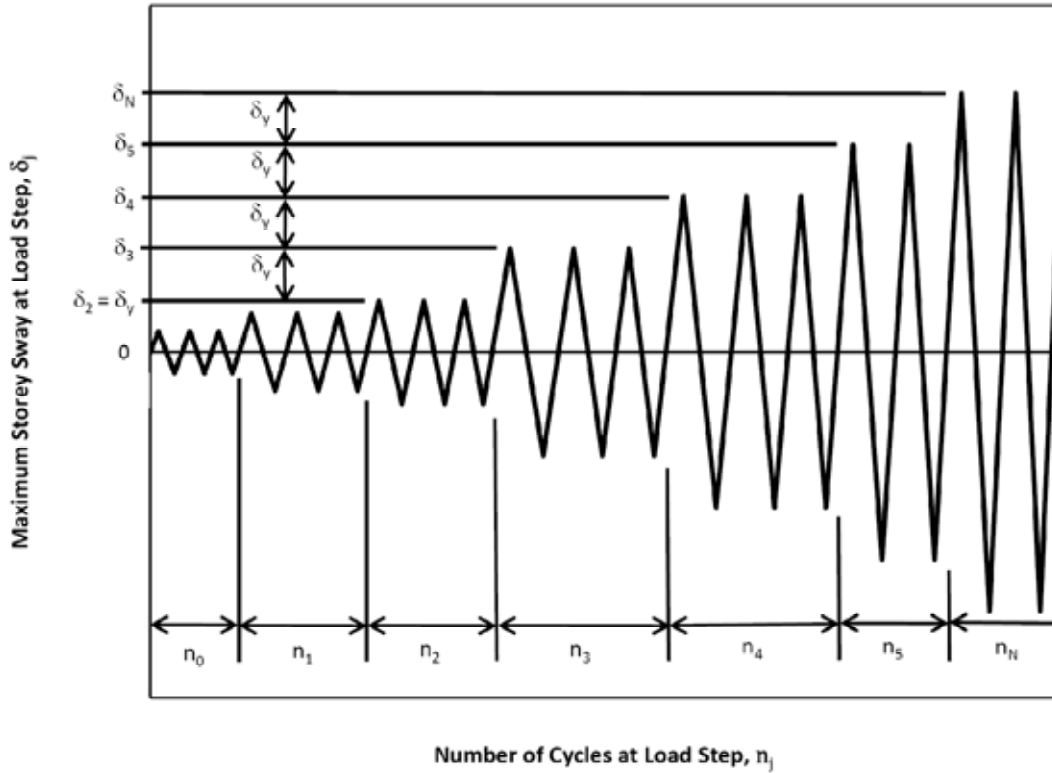


Figure 6-23: Design Deformation History for SPSW Test (adapted from ATC, 1992)

Table 6-2: Load Protocol for Quasi-Static Cyclic Testing of SPSW Specimen

Load Step, $j$	Peak Storey Sway at Load Step, $\delta_j$	Number of Cycles, $n_j$	Cycle No.	Comments
0	$\delta$ corresponding to 220kN ( $0.4Q_y$ )	3	1 – 3	<ul style="list-style-type: none"> <li>• Verify data acquisition</li> <li>• Elastic Range</li> </ul>
1	$\delta$ corresponding to 413kN ( $0.75Q_y$ )	3	4 – 6	<ul style="list-style-type: none"> <li>• Elastic Range</li> </ul>
Determine yield displacement $\delta_y$ based on ATC – 24 guidelines				
2	$\delta_y$	3	7 – 9	<ul style="list-style-type: none"> <li>• Yield</li> </ul>
3	$2\delta_y$	3	10 – 12	<ul style="list-style-type: none"> <li>• Plastic deformation</li> </ul>
4	$3\delta_y$	3	13 – 15	<ul style="list-style-type: none"> <li>• Plastic deformation</li> </ul>
5	$4\delta_y$	2	16 – 17	<ul style="list-style-type: none"> <li>• Plastic deformation</li> </ul>
N	$N\delta_y$	2	18 +	<ul style="list-style-type: none"> <li>• Plastic deformation</li> <li>• Continue increasing peak displacement per cycle until a significant loss of capacity occurs.</li> </ul>

## Chapter 7: Results and Discussion of the Steel Plate Shear Wall Test

### Test

#### 7.1 Introduction

The SPSW test specimen performed generally as expected. No substantial damage to either the infill panel splice welds or the infill panel-to-fish plate welds was observed at any point during the test. The ultimate load of 630 kN achieved at cycle 16<sup>-1</sup>, at a storey sway of  $4.5 \delta_y$ , is 1.08 times the strip model envelope load of 583 kN corresponding to this displacement. A gradual reduction in peak load was observed up to cycle 17<sup>-</sup>, at which point a fracture through the north flange at the base of the north column was noted. Unfortunately, excessive out-of-plane deflection and rotation at the south beam-to-column connection limited the number of further northward excursions. During a final southward excursion to the limit of the hydraulic jack stroke, at  $9 \delta_y$ , the system achieved a maximum load of 86% of the peak load reached during the test and the test was stopped. The infill panel remained fully connected to the boundary members throughout the test, and no significant signs of distress appeared at the infill panel-to-fish plate connection or at the infill panel splice, despite large plastic deformations in the infill panel.

#### 7.2 Global Behaviour and Failure Mode

In general, the global physical and hysteretic behaviour of the specimen was as desired; hysteresis was stable and failure took the form of a column fracture and not a premature infill panel-to-fish plate weld failure. The tension field in the infill panel, shown in Figure 7-1 for a measured storey sway of 65.8 mm ( $4.5 \delta_y$ ), was visually obvious as early as the first excursion. A summary of maximum storey displacement and load, and visual observations, is shown in Table 7-1. The overall hysteretic behaviour is described by the plot of base shear versus storey sway shown in Figure 7-2, which depicts the entire history of the test. As shown, the base shear versus storey sway envelope is well predicted by the strip model. Table 7-1 describes each excursion in terms of load step magnitude as a factor of  $\delta_y$ , maximum load and maximum stroke, drift ratio ( $\delta_y/h_s$ , where  $h_s$  is the height of the storey), and lists significant visual observations noted during the test. Overall, symmetric loading to the north and south resulted in reasonably symmetric hysteresis loops, as expected of a symmetric specimen.

---

<sup>1</sup> When referring to cycles of loading, the cycle number followed by a "+" indicates the half-cycle from the neutral position to the maximum northward excursion of storey sway and back to the neutral position. Conversely, the cycle number followed by a "-" indicates the half-cycle from the neutral position to the maximum southward excursion and back to the neutral position.

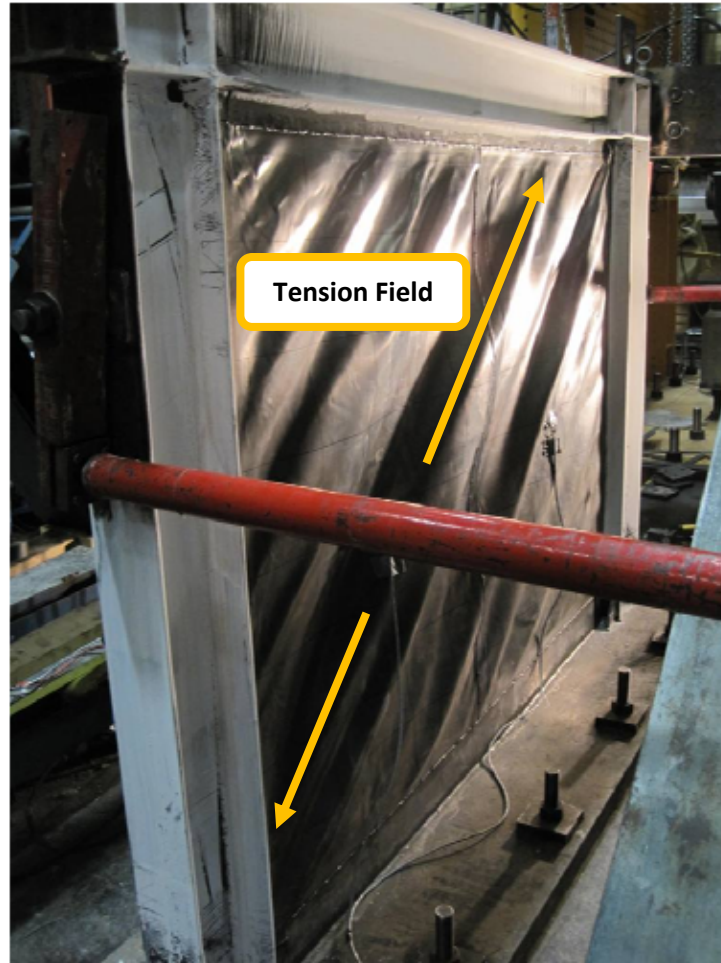


Figure 7-1: Overall Specimen at Time of North Column Fracture, Cycle 17-

### 7.2.1 Initial Load to Failure

Cycles 1 to 9 and  $\delta_y$  are shown in Figure 7-3 ( $\delta_y$  is determined according to the procedure outlined in Section 6.5). During the first three load cycles (at a peak shear of 220 kN in each direction), the plate wall displayed strictly elastic behaviour and a stiffness of roughly 85 kN/mm. The infill panel was observed to buckle elastically during the very first excursion. As predicted by a kink in the shear versus deflection curve obtained from the strip model near a load of 250 kN, and demonstrated by the reduction in stiffness and increased hysteresis loop size during load cycles 4 to 9, some softening in the infill panel and possibly of the boundary frame occurred relatively early. This is due primarily to the relatively low yield strength of the A1008 infill panel steel. As shown in Table 7-2, strain gauges placed on the infill panel recorded strains approaching the yield strain as early as in the first cycle, and by cycle 4+ all four strain rosettes reported a peak cycle tensile principal strain exceeding the yield strain of  $743 \times 10^{-6}$  mm/mm. It should be noted that a direct comparison between principal

stresses in the infill panel and yield stress results from uniaxial tension coupons was deemed appropriate since the principal compressive stresses in the infill panel are negligible and tension field behaviour can be considered essentially uniaxial. As shown in Figure 7-2, the computed  $\delta_y$  of 14.5 mm appears to match well with the onset of significant softening of the measured base shear versus storey sway response.

As expected, storey sways greater than  $\delta_y$  are characterized by significant inelastic deformation in the SPSW. This is physically reflected by permanent elongation of the infill panel present when the frame is returned to the neutral position (storey sway of zero), as well as increased whitewash flaking at plastic hinges in boundary elements.

As the base shear versus storey sway plot is in units of force versus displacement, the area enclosed by the hysteresis loops is equivalent to the energy dissipated by the system. The significant increase in inelastic energy dissipation as storey sway is increased from  $\delta_y$  to  $2\delta_y$ , and in further load steps, is quantitatively evident in Figure 7-4.

“Pinching” of the hysteresis loops results from the decreased stiffness in the load reversal region when the tension field changes orientation (Driver *et al.*, 1997). The inelastic stretching of the infill panel introduced by the first cycle at a given storey sway must be overcome during successive cycles at that same magnitude of displacement before the tension field can fully develop. The phenomenon is shown on a hysteresis plot for cycles 13 to 15 in Figure 7-5, and is obvious in the steady decline of energy absorbed in successive cycles at each load step in Figure 7-4.

It should be noted that cycles 16 and 17 were designed for a maximum excursion of  $4\delta_y$ , but an operator error in the first excursion of cycle 16+ resulted in a peak deformation of  $4.5\delta_y$ . For consistency, this larger deformation was applied to the remainder of cycle 16 and to cycle 17.

Table 7-1: Test Observations

Cycle	Peak Storey Sway at Load Step	Max Load (kN)	Measured Max Stroke (mm)	Measured Drift Ratio (%)	Observations
1	$\delta$ matching $0.4Q_y$	214	2.8	0.1%	• Infill plate buckles during the first cycle.
-1		-220	-3.6	-0.2%	
2		218	2.5	0.1%	
-2		-220	-3.7	-0.2%	
3		221	2.6	0.1%	
-3		-217	-3.8	-0.2%	
4	$\delta$ matching $0.75Q_y$	408	11.6	0.6%	<ul style="list-style-type: none"> <li>• Significant buckling in infill panel; tension field is obvious.</li> <li>• Whitewash flaking begins in flange of north column at base.</li> <li>• The infill panel - to - fish plate weld has a small tear (approx. 5mm long) adjacent to the 5mm gap between the fish plates. This initiated due to significant out - of - lane buckling of the infill plate across the 5mm gap.</li> <li>• Weld tearing at North - top corner of infill panel due to compression buckling of infill panel across 5mm gap. Weld is debonded from fish plate over a 5mm length.</li> </ul>
-4		-406	-12.0	-0.6%	
5		410	10.2	0.5%	
-5		-408	-11.9	-0.6%	
6		409	10.2	0.5%	
-6		-408	-12.0	-0.6%	
Determine by the procedures of ATC - 24 that $\delta_y = 14.5\text{mm}$					
7	$\delta_y$	465	14.5	0.8%	<ul style="list-style-type: none"> <li>• Weld tearing at North - top corner of infill panel = 10mm in length.</li> <li>• Whitewash flaking in webs at the bottom of both columns, and top face of beam.</li> <li>• Base of both columns: web shows signs of tension yielding.</li> </ul>
-7		-456	-14.6	-0.8%	
8		468	14.6	0.8%	
-8		-456	-14.5	-0.8%	
9		468	14.6	0.8%	
-9		-453	-14.6	-0.8%	
10	$2\delta_y$	530	28.9	1.5%	• Weld tearing at North - top corner of infill panel = 10mm in length (no growth) despite increase in out - of - plane buckling of infill panel.



Table 7-1 (continued): Test Observations

Cycle	Peak Storey Sway at Load Step	Max Load (kN)	Measured Max Stroke (mm)	Measured Drift Ratio (%)	Observations
-10	$2\delta_y$	-560	-29.26	-1.5%	• Significant whitewash flaking at top and base of columns.
11		556	29.0	1.5%	
-11		-576	-29.12	-1.5%	• Significant out - of - plane local buckling of fish plate at the North - bottom infill panel connection. • An increase in pinching of hysteresis loops is noted over repeated cycles at the same deformation (Cycles 10 - 12).
12		554	29.1	1.5%	
-12		-570	-29.1	-1.5%	
13	$3\delta_y$	560	43.6	2.3%	• Some local buckling in north - column base exterior flange • Pushover curve is clearly reaching the plateau (has entered the plastic range) • Local buckling of fish plate results in a shear tear at the south - bottom infill panel connection; welds are undamaged • Tear in the infill panel resulting from fish - plate buckling at the north - bottom corner.
-13		-620	-43.8	-2.3%	
14		575	43.6	2.3%	
-14		-610	-43.8	-2.3%	
15		557	43.5	2.3%	
-15		-590	-43.67	-2.3%	
16	$4.5\delta_y$	550	66.0	3.5%	• Operator error imparts more storey sway ( $4.5\delta_y$ ) than intended by ATC - 24 ( $4\delta_y$ ). • Tears in the infill panels at all corners due to out - of - plane fish plate buckling. Maximum tear length is roughly 15mm. Tears are roughly vertical, in line with the 5mm gap between the end of the horizontal fish plates (attached to baseplate or beams) and the end of the vertical fish plates (attached to the columns).

Table 7-1 (continued): Test Observations

Cycle	Peak Storey Sway at Load Step	Max Load (kN)	Measured Max Stroke (mm)	Measured Drift Ratio (%)	Observations
-16	4.5 $\delta_y$	-630	-66.0	-3.5%	<ul style="list-style-type: none"> <li>Obvious whitewash flaking at the outside face of columns indicates significant plastic hinging</li> </ul>
17		540	65.9	3.5%	<ul style="list-style-type: none"> <li>Some substantial out - of - plane movement of South Watt Bracing recorded.</li> <li>The southmost plastic hinge in the first storey beam is buckling east under compressive axial load.</li> </ul>
-17		-580	-65.8	-3.5%	<ul style="list-style-type: none"> <li>Hinging very clear at ends of first storey beam and at base of columns.</li> <li>The north column exterior flange tears through in line with the toe of the weld above the baseplate stiffeners (approx. 100mm above baseplate). The start of a similar tear is detected at the south column.</li> </ul>
18	3.8 $\delta_y$	434	54.8	2.9%	<ul style="list-style-type: none"> <li>An attempt to push the frame northwards to the limit of the jack stroke is stopped when the lateral instability of the south beam - to - column connection, through which jack load is applied to the frame, causes the hydraulic jacks to twist beyond acceptable limits.</li> </ul>
-18	9 $\delta_y$	-540	-131.0	-6.9%	<ul style="list-style-type: none"> <li>The frame is pulled to the limit of the jack stroke southwards.</li> <li>Column deterioration continues; cracks through flange and web at the north column base grow.</li> <li>No evidence of significant distress to infill plate welds. Aside from at corners previously discussed, there is no evidence of</li> </ul>

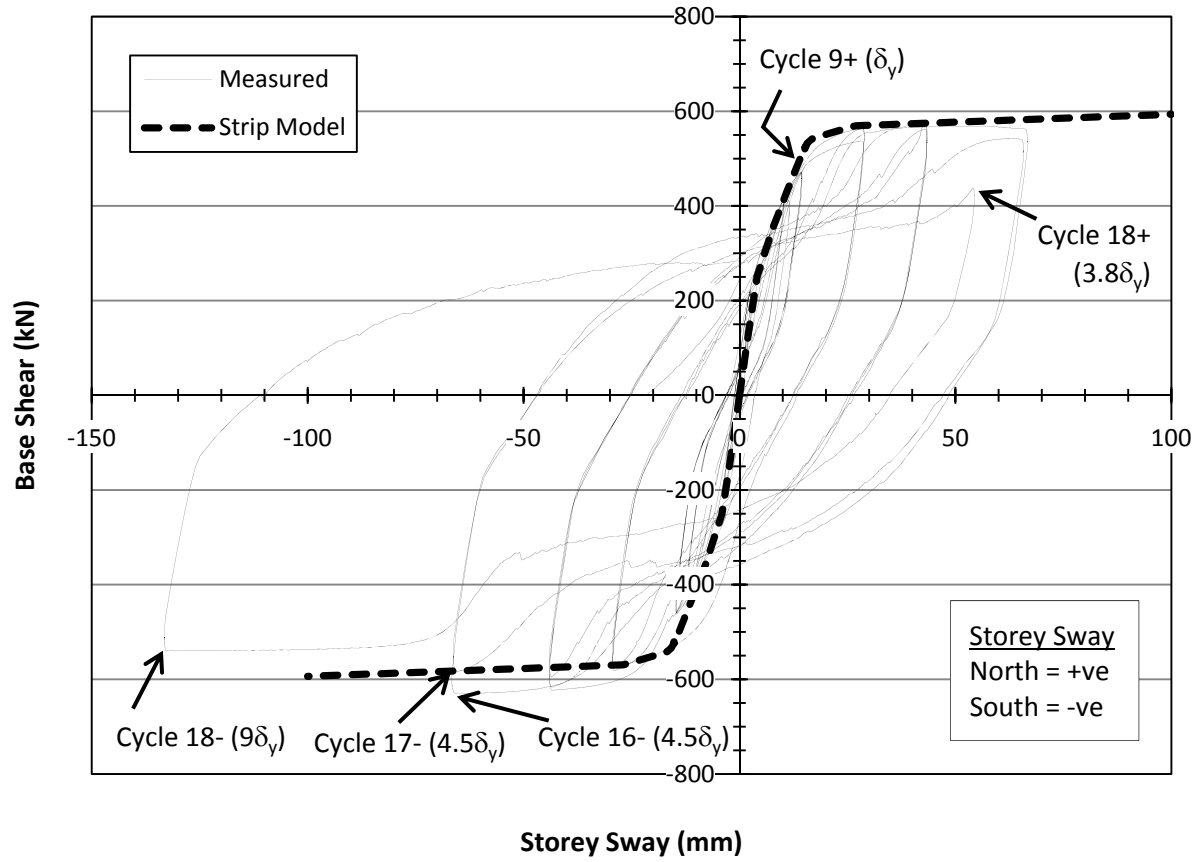


Figure 7-2: Base Shear Versus Storey Sway

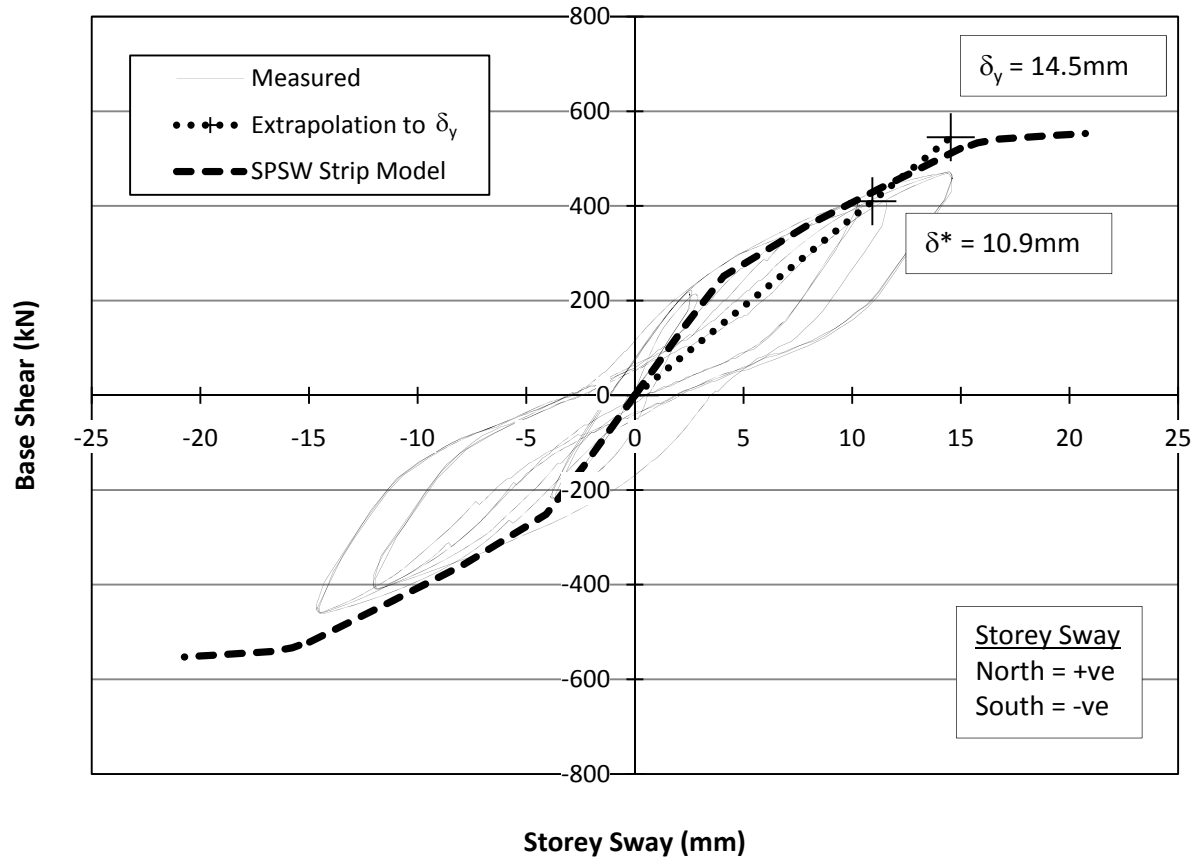


Figure 7-3: Elastic Range (Cycles 1– 9) and Illustration of  $\delta_y$

Table 7-2: Measured Strains at Cycle Peaks

Strain Gauges - Tension Field Values at Peak Load of Each Cycle						
NW Strain Rosette				NE Strain Rosette		
Cycle	Principal $\epsilon$ (mm/mm $\times 10^{-6}$ )	Principal $\sigma$ (MPa)	Angle, $\alpha$ (Degrees, $^{\circ}$ )	Principal $\epsilon$ (mm/mm $\times 10^{-6}$ )	Principal $\sigma$ (MPa)	Angle, $\alpha$ (Degrees, $^{\circ}$ )
1+	469	109.4	47.9	883	173.3	55.1
1-	947	173.4	52.2	916	173.4	46.4
2+	390	91.0	50.3	748	173.1	52.4
2-	1014	173.5	51.6	1010	173.5	36.4
3+	392	91.4	52.7	432	100.9	39.4
3-	1054	173.6	51.3	1053	173.6	36.1
4+	3541	177.4	45.2	3386	177.2	45.3
4-	4076	178.2	48.7	4049	178.2	42.6
5+	2596	176.0	45.6	2664	176.1	42.4
5-	3873	177.9	47.1	3903	178.0	40.9
6+	2739	176.2	46.0	2975	176.5	51.2
6-	3937	178.0	46.7	DATA NO LONGER RELIABLE		
7+	4415	178.8	45.1			
7-	4837	179.4	47.3			
8+	4492	178.9	48.3			
8-	4635	179.1	48.5			
9+	4235	178.5	46.5			
9-	4781	179.3	49.1			
10+	8268	184.7	45.1			
10-	10677	188.4	46.8			
11+	DATA NO LONGER RELIABLE					

**NOTE**Angle,  $\alpha$ , measured from a positive upwards vertical axis

Table 7-2 (continued): Measured Strains at Cycle Peaks

Cycle	Strain Gauges - Tension Field Values at Peak Load of Each Cycle					
	SW Strain Rosette			SE Strain Rosette		
	Principal $\epsilon$ (mm/mm $\times 10^{-6}$ )	Principal $\sigma$ (MPa)	Angle, $\alpha$ (Degrees, $^{\circ}$ )	Principal $\epsilon$ (mm/mm $\times 10^{-6}$ )	Principal $\sigma$ (MPa)	Angle, $\alpha$ (Degrees, $^{\circ}$ )
1+	720	168.1	51.3	672	156.7	36.8
1-	1228	173.8	44.4	1287	173.9	46.9
2+	665	155.0	82.3	467	108.9	34.2
2-	1300	174.0	44.9	1358	174.0	46.0
3+	813	173.2	65.1	493	115.0	33.3
3-	1357	174.0	45.2	1415	174.1	45.6
4+	3115	176.8	50.5	3012	176.6	41.4
4-	4246	178.5	43.8	4300	178.6	45.7
5+	2497	175.8	55.3	2417	175.7	31.5
5-	4399	178.7	43.8	4427	178.8	45.0
6+	2605	176.0	57.1	2546	175.9	13.5
6-	4426	178.8	43.8	4445	178.8	44.7
7+	3944	178.0	51.6	3822	177.8	39.0
7-	5364	180.2	43.4	5368	180.2	44.9
8+	4300	178.6	51.3	4197	178.4	35.6
8-	5308	180.1	44.1	5310	180.1	43.9
9+	3992	178.1	63.1	3789	177.8	33.6
9-	5372	180.2	44.1	5391	180.3	44.1
10+	8884	185.6	50.0	8928	185.7	41.7
10-	9022	185.9	38.2	9040	185.9	43.3
11+	DATA NO LONGER RELIABLE			DATA NO LONGER RELIABLE		

**NOTE**Angle,  $\alpha$ , measured from a positive upwards vertical axis

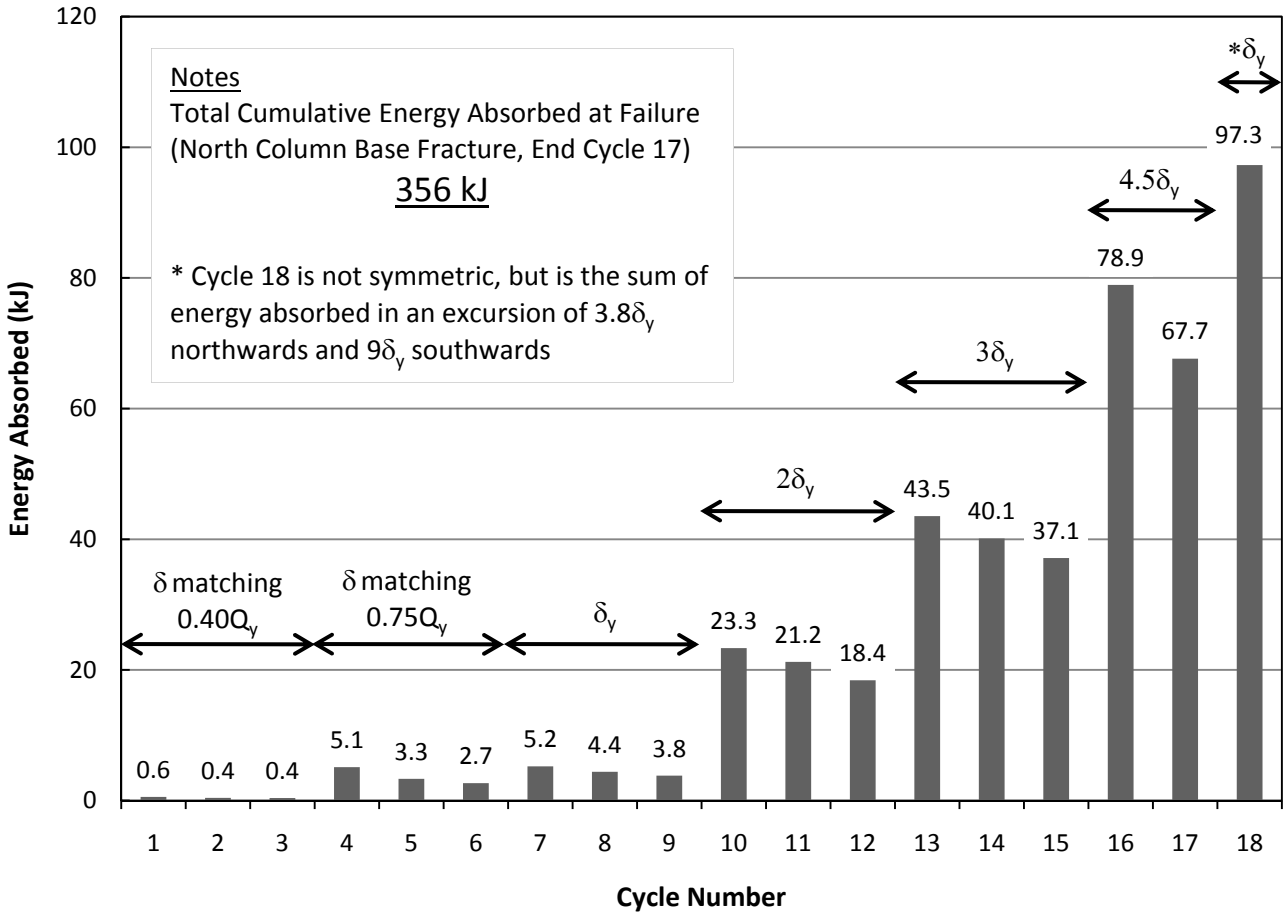


Figure 7-4: Energy Absorbed Per Cycle

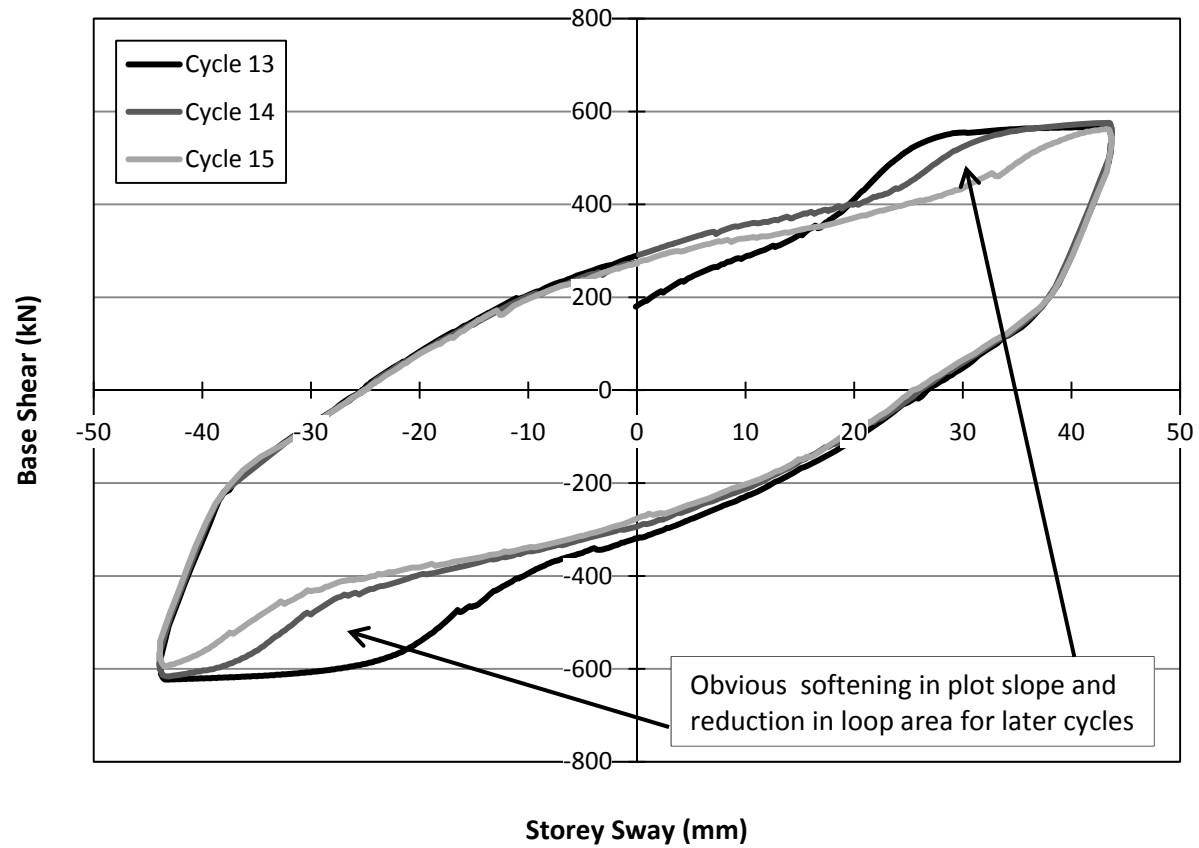
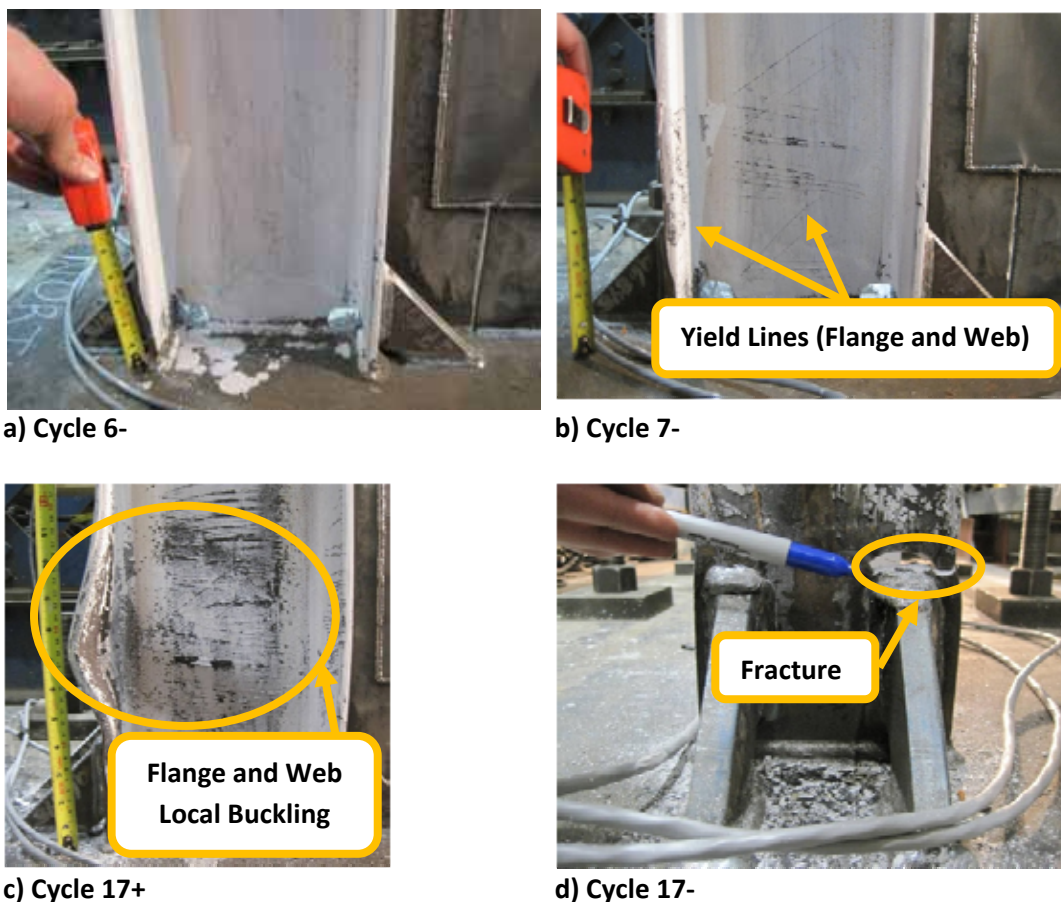


Figure 7-5: Typical Pinching Behaviour, Cycles 13 - 15 at Peak Storey Sway  $3\delta_y$



### 7.2.2 Failure Mode

The progression of damage at the base of the north column is shown in Figure 7-6. Yield lines were apparent in the web and the flange whitewash as early as at a storey sway of  $\delta_y$  at cycle 7-. Signs of local buckling became apparent at the north flange at a drift of  $3\delta_y$  (cycle 13-), and increased in magnitude with an increase in storey sway. This repeated local buckling, combined with the high level of restraint at the toe of the base stiffener weld caused high stress concentration. As a result, at a storey sway of  $4.5\delta_y$ , fracture through the column flange at the top of the base stiffener weld occurred near the peak of cycle 17-. By cycle 18+, an identical fracture had started at the south column.



**Figure 7-6: Damage Progression at the Base of the North Column**

This failure mode has been observed in previous tests and is not unexpected, however, it occurred earlier than expected. In the test conducted by Driver *et al.* (1997), gravity loads were applied at the top of the columns. The column base fractured at a storey drift of 4.0% ( $9\delta_y$ ), a drift value significantly larger than the deformation at the peak load of 2.2% ( $5\delta_y$ ). Driver *et al.* (1997) attributed the gradual reduction in capacity

following peak load to tearing of the infill panel due to cyclic formation of kinks in the infill panel, substantial damage to the corners of the infill panel-to-boundary member connection, and local buckling at the exterior flange at the base of the columns. In this test, the peak load was recorded at cycle 16- during the first southward excursion at  $4.5\delta_y$ , and the column fractured near the peak of the second cycle at this same magnitude of displacement. Strain reversals due to cycles of local buckling in the outside flange at the base of the column created a state of low-cycle fatigue. Tensile load required to initiate the fracture came from several sources. The lack of gravity loads created a particularly high tensile uplift force across the column cross-section. Additional tensile loads include the vertical component of the tension field anchorage force, the extreme fibre tensile stresses from column bending, and tensile residual stresses from welds connecting the column to the column base stiffeners.

### **7.2.3 Post-Failure Loading**

Following the initiation of column fracture, it was decided to continue the cyclic loading according to the established loading protocol in order to assess the ductility of the system as the peak load declines. However, the lateral instability of the frame when pushed north (Table 7-1, Cycle 18+) prevented further northward excursions. During northward excursions, a compressive force is applied to the south beam-to-column connection. As plastic hinges had formed both in the beam and in the column adjacent to the south beam-to-column connection (Figure 7-7), the compressive force applied at the joint caused a significant out-of-plane rotation of the panel zone and the load transfer plate, and unacceptable lateral movement of the plastic hinge in the beam was observed (Figure 7-8).

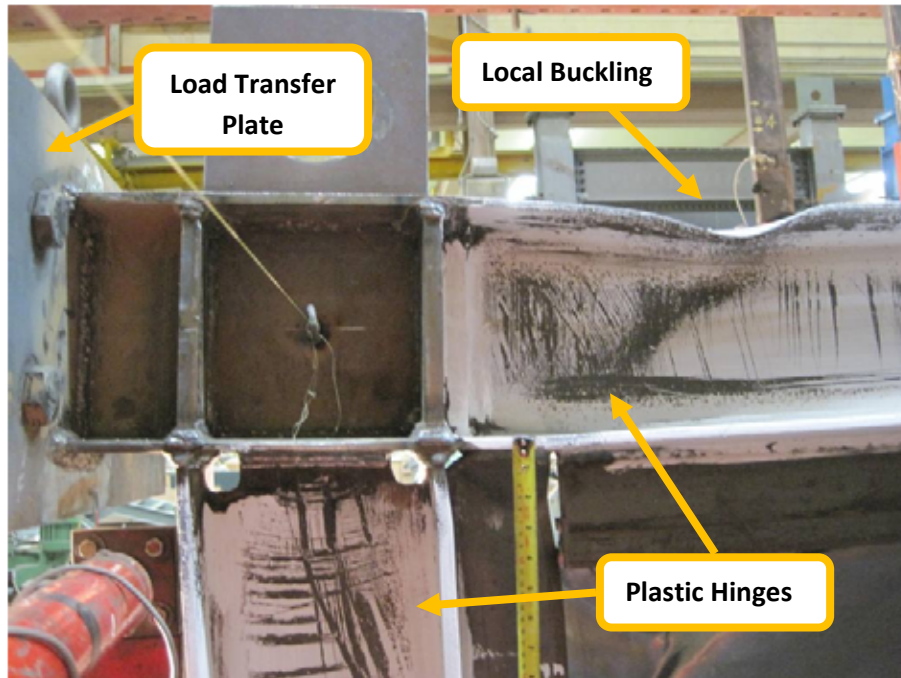
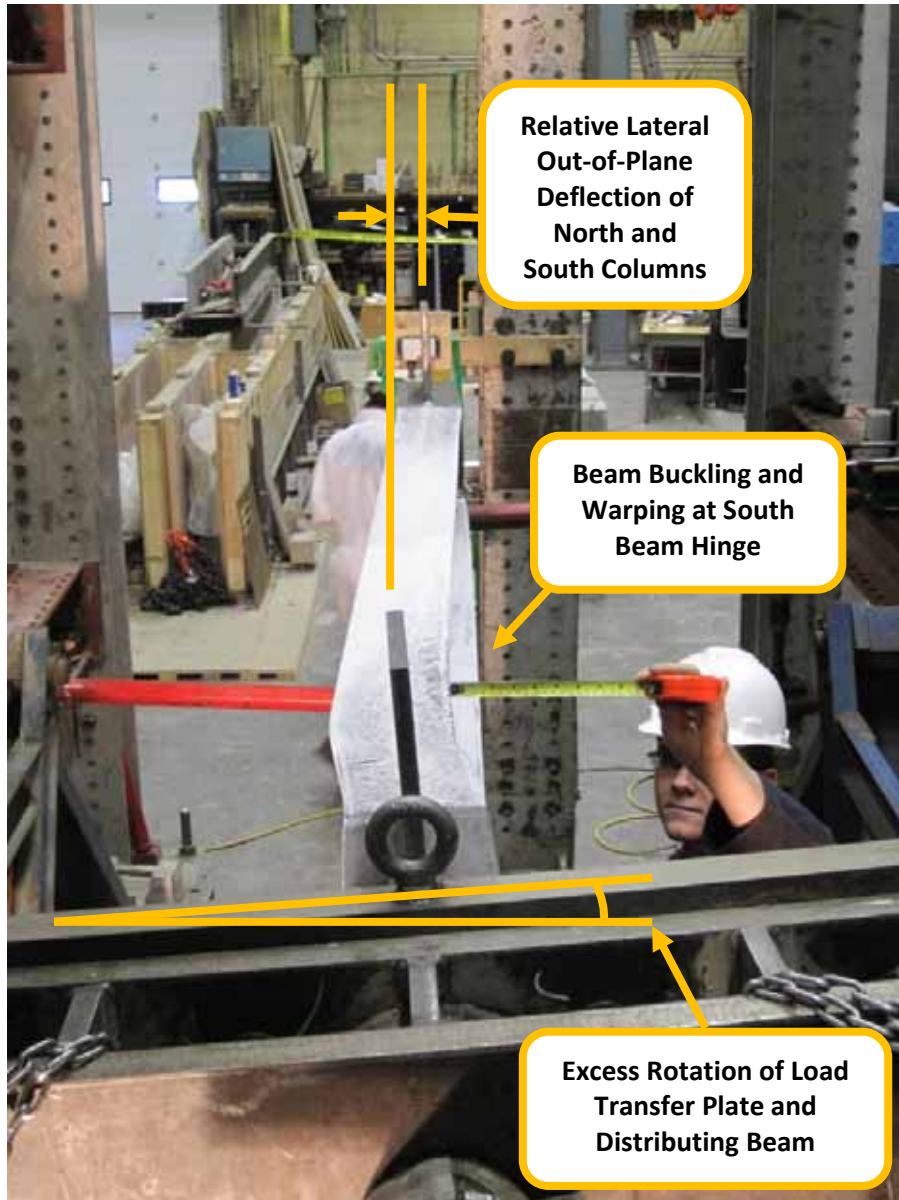


Figure 7-7: Hinges and Local Buckling at South Beam-to-Column Connection, Cycle 18+



**Figure 7-8: Excessive Out-of-Plane Deflection of Beam Hinge Adjacent to South Beam-to-Column Connection, Looking North, Cycle 18+**

It should be noted that in a SPSW installed in a steel-framed building, typically a floor slab or roof deck would provide lateral restraint at the top flange of the beam hinges, which would prevent the type of out-of-plane hinge movement that occurred in this test.

In a final effort to test the infill panel-to-fish plate joint at the highest deformation possible, the frame was deformed southward to the limit of the jack stroke, which corresponds to a storey sway of  $9\delta_y$  (cycle 18-). The axial load in the beam was tensile in this case, which enabled the hydraulic jacks to act in line with the beam as desired. A

peak cycle load of 540 kN was reached. This is 86% of the ultimate load, and represents a sufficiently significant drop in capacity to terminate the test.

#### 7.2.4 Infill Panel Performance

The infill panel performed very well throughout the test. Under 35 strain reversals (as cycles changed direction and the tension field reversed direction) and large cyclic out-of-plane deformations, the panel continued to carry high loads. Though strain gauge data is considered unreliable following cycle 10-, up to this point the infill panel strains ( $\sim 10,000 \times 10^{-6}$  mm/mm, Table 7-2) had reached only 7% of the strain required to mobilize the ultimate capacity of the infill panel steel ( $\sim 15,000 \times 10^{-6}$  mm/mm, Figure 6-4), and only 3% of the fracture strain ( $\sim 40,000 \times 10^{-6}$  mm/mm, Figure 6-4). As shown in Table 7-2, strain rosette readings taken at the maximum excursion of each cycle generally place the tension field angle,  $\alpha$ , in the range of  $38^\circ$  to  $50^\circ$  as expected by S16-01 (CSA, 2001). However, occasionally a wrinkle in the infill panel at the location of a strain gauge produced an angle well outside of this range. These outlier angles do not represent the tension field angle, since the strain gauge is detecting highly localized strains.

Other than substantial inelastic stretching due to the large strains imposed by the tension field, and the local phenomena discussed in Section 7.3, there was no damage to the infill panel. Tearing that has been observed due to kinking during out-of-plane strain reversals in specimens with infill panels about 4.8 mm thick (Driver *et al.*, 1997, and others) was not observed in this test. However, during small-scale testing (see Section 5.4), when cyclic angular displacements causing strain reversals in the infill panel material are applied, fracture of the infill panel material occasionally occurred following 60 strain reversals (30 cycles) and the application of a relatively small tensile load. Had substantially more than 35 strain reversals been applied to the infill panel, low-cycle fatigue in the infill panel where kinking was most pronounced may have resulted in the initiation of these types of tears.

#### 7.3 Infill Panel-to-Fish Plate Connection Behaviour

The infill panel-to-fish plate connection performed in a satisfactory manner since no uncontrolled tears of welds occurred at any point during testing. The connection underwent 35 load reversals and the large out-of-plane angular deformation of the infill panel at the weld, an example of which is shown in Figure 7-9.

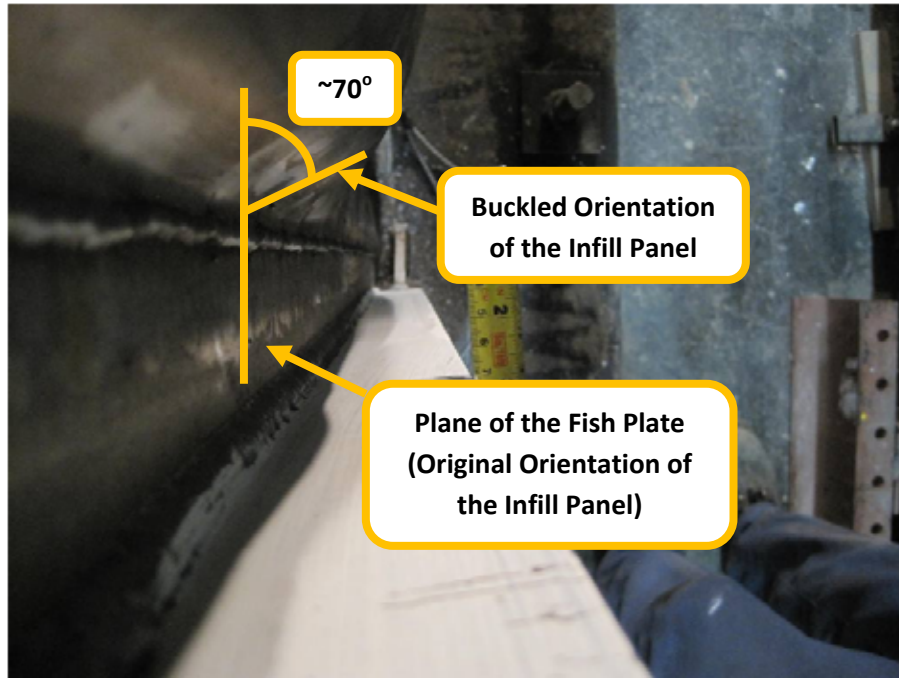


**Figure 7-9: Large Angular Deformation of Infill Panel at Fish Plate Weld, Looking Down the Infill Panel-to-Fish Plate Connection at the North Column, Cycle 18-**

Table 7-3 shows a comparison of the number of cycles and storey drift before weld failure of previously tested single storey SPSW specimens with thin infill panels, and the SPSW specimen tested in this research program, called “SPSW -1”. Only general conclusions can be drawn since so many variations in boundary element-to-fish plate connection geometry, boundary member geometry, frame aspect ratio and connection geometry, and material properties exists among the tests discussed. The infill panel-to-boundary element connection of SPSW-1 performed better than that of specimen DPSW-2, which failed. The two specimens underwent an equal number of inelastic cycles, and the specimen SPSW-1 did not fail at the infill panel-to-boundary element weld despite undergoing larger storey drifts. Unfortunately, though the infill panel-to-fish plate connection of specimen SPSW-1 showed promising behaviour, the relatively low number of cycles sustained before this test had to be stopped (for reasons unrelated to the infill panel-to-fish plate connection) make comparisons with specimen DPSW-1 and specimen F2 more difficult.

**Table 7-3: Comparison of Infill Panel-to-Boundary Element Welded Connection Performance of Past Research with Current Research**

Author	Specimen	Event	Storey Drift	Number of Inelastic Cycles (At or Beyond $\delta_y$ )
Kharrazi (2005)	DPSW-1	Weld fracture at infill panel-to-fish plate connection	5.8%	15
Kharrazi (2005)	DPSW-2	Weld fracture at infill panel-to-fish plate connection	2.0%	12
Berman and Bruneau (2005)	F2	Weld fracture at corners of infill panel-to-boundary element connection	3.65%	25
Current Research	SPSW-1	Test stopped due to lateral frame instability	3.5% (6.9%) <sup>1</sup>	12

**NOTE**

<sup>1</sup> A storey drift of 3.5% at half-cycle 17- corresponds to the last cycle of the design loading protocol where a local peak displacement is reached. The maximum storey drift of 6.9% was a departure from the loading protocol, and was only applied during the final half-cycle of the test in an attempt to stress the infill panel to the furthest extent possible. See section 7.2.3 for details.

Energy absorbed by the infill panel provides another source of comparison. However, only Berman and Bruneau (2005) have separated the contributions of the infill panel and the boundary frame. Kharrazi (2005) tested a boundary frame designated SF-1, which had identical geometry to the frames in his SPSW specimens, but did not summarize the differences in contribution of the infill panel and boundary frame. In the case of this research program, neither analytical modeling nor testing of a boundary frame have been carried out, and the infill panel's energy absorption cannot be reliably quantified.

### 7.3.1 Corner Detail

Overall, the connection of the infill panel to the fish plates at the corners performed well. Two interesting phenomena related to the corner detail were noted.

At the north-top corner, an early tear in the weld occurred at cycle 5+. This region of the weld had surface pits and was identified by the welding technician as a short length of low-quality weld at the time of welding. The tear was in the form of the weld debonding from the fish plate base material, as shown in Figure 7-10a. The tear was initiated by significant out-of-plane buckling of the portion of the infill panel bridging the gap between the fish plate against the north column and the fish plate connected to the beam. After growing to a length of 10 mm at cycle 7+, the debonding was arrested by

better-fused weld metal and propagation did not continue. Figure 7-10b shows the detail at the end of testing. The short tears in the infill panel at either side of the gap between the fish plates are the result of a different and unrelated phenomenon explained below.

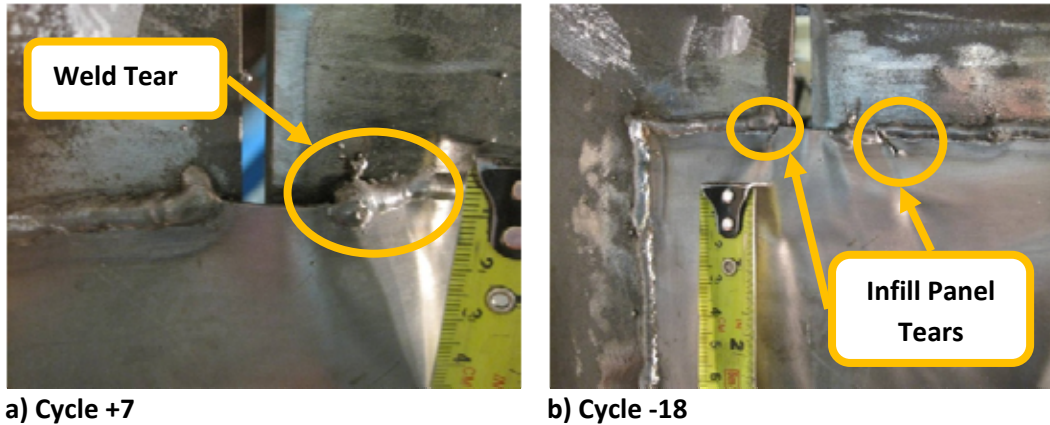


**Figure 7-10: Weld and Infill Panel Tears at North-Top Corner of Infill Plate**

The second type of behaviour in the corners was the local buckling of the column fish plates as shown in Figure 7-11. This was first noted in the fish plate at the base of the north column in cycle 11-, while the joint was closing, and soon thereafter was evident in all four corners of the infill panel.

As the angle between the column and beam, or column and baseplate, becomes smaller at increased storey drift, the column fish plate is subjected to compressive forces at the corner, which causes buckling of the fish plate. It should be noted that buckling capacity was not, and should not be, a criterion for design of the fish plates. The cross-sectional width of 100 mm was selected for weld access. The thickness of 6 mm was selected as a comfortable medium between thick enough for ease of welding with two-sided fillet welds to boundary members, and thin enough to prevent excessive rapid cooling of the infill panel-to-fish plate weld. For nominal grade 300W steel plate, these fish plates do not meet the requirement for even a Class 3 flange plate, and should be expected to buckle relatively early in compression (CSA, 2001).

Due to the out-of-plane deformation of the buckled column fish plate, the gap between the vertical fish plate and the horizontal fish plate grows substantially beyond the original dimension of 5 mm, and the infill panel material bridging this gap is subjected to high strains. Tears appear at either side of the gap between fish plates, as seen in Figure 7-11b. The tears originate at the nearest toe of the infill panel-to-fish plate welds and run into the infill panel for a maximum of 15 mm. These small tears do not reduce the ability of the corner detail to anchor the tension field, and are limited to the region of the fish plate where local buckling occurs.



Despite the alarming appearance of the fish plate local buckling and resulting small tears to the infill panel described above, they do not appear to negatively impact global performance of the system.

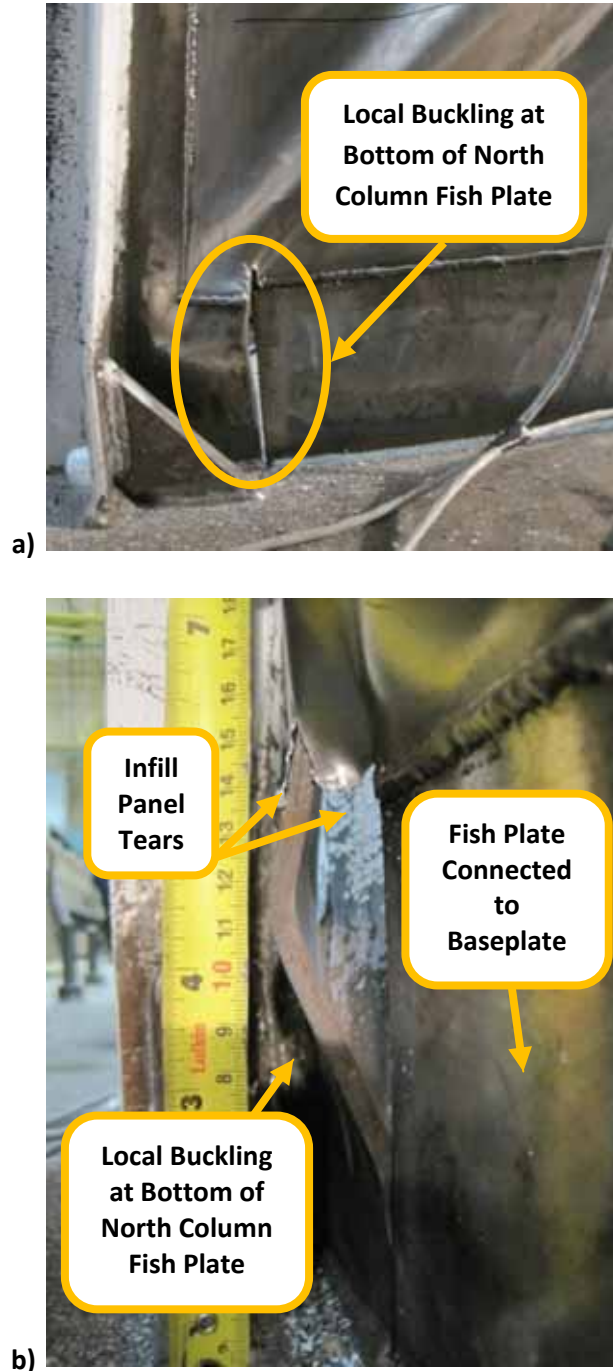


Figure 7-11: Fish Plate Buckling at Bottom of North Column, Cycle 17-  
a) Elevation View Looking East, b) Looking North at Local Buckling Location

### 7.3.2 Infill Splice at Infill Panel-to-Fish Plate Connection Detail

The configuration of the infill splice at the infill panel-to-fish plate connection is shown diagrammatically in Figure 6–2. The same detail is present at the top and bottom of the infill panel splice; a representative photo of the bottom of the infill splice before loading is shown in Figure 6–19, while a photo of the top of the infill splice during the most extreme storey sway of  $9\delta_y$  is shown in Figure 7-12. No tearing or damage to the welds or base material at any location along the infill splice was evident throughout testing. The detail at the ends of the infill splice exhibits satisfactory performance.



Figure 7-12: Infill Panel Lap Splice at the Infill Panel-to-Fish Plate Connection, Cycle 18-

## Chapter 8: Summary and Conclusions

### 8.1 Summary

Past research has shown that the unstiffened steel plate shear wall (SPSW) system employing a thin cold-rolled sheet steel infill panel can absorb large amounts of energy in a stable manner under repeated cycles of lateral loading (Cacesse *et al.*, 1993; Berman and Bruneau, 2005; Kharazzi, 2005). Though handling and welding of such thin material is not customary for steel fabricators, choosing thicker-than-required infill panel material to facilitate handling and welding may result in an overstrength problem, which is an undesirable situation for capacity design. In the context of capacity design, the forces arising from yielding of an excessively thick infill panel necessitate expensive size upgrades to the boundary members, and possibly other structural framing members that share a lateral load path with the SPSW.

A review of the literature demonstrated that a welding procedure to connect the thin infill panel to thick boundary elements has not been described in any detail previously. Since weld failure at the infill panel-to-boundary element joint has negatively impacted the performance of past SPSW test specimens (Kharazzi, 2005), the goal of this research program was to develop a welding procedure reasonably simple for steel fabricators to employ to achieve good cyclic performance.

Parameters such as joint geometry, material properties, welding process, electrode, and shielding gas were selected based on literature review and trial welds. A lap splice, which has large fit-up tolerances, was selected both for the infill panel-to-boundary element and infill panel splice joints. 6 mm thick Grade 300W fish plates were used for the thick portion of the infill panel-to-boundary element lap splice, while 20 gauge A1008 CS cold-rolled sheet steel was selected for the infill panel. Short-circuiting gas metal arc welding was selected for the weld process due primarily to its low heat input, which is required to avoid burn-through when working with thin base metal. An ER70S-6 electrode was selected due to its strength, high toughness and deoxidizer content. Two shielding gases were used, namely, 75Ar – 25CO<sub>2</sub> and pure CO<sub>2</sub>. Pure CO<sub>2</sub> was selected as it produced welds with the best arcing, wetting, and profile characteristics.

Four possible configurations for the infill panel-to-boundary element connection and two possible configurations for the infill panel splice were tested. Configurations differed depending on whether one or two welds were used in the lap joint, and whether a chill strip was placed behind the thin sheet steel during welding to reduce the probability of burn-through and magnitude of distortion. Nearly all joint configurations were subjected to three repetitions of a quasi-static tension test, and 3 repetitions of a cyclic tension-compression test. The exception was the cyclic tests for the infill panel splice, in which case excessive kinking during testing resulted in a loading condition much more severe than desired, and only one specimen of each of the two configurations was tested. Based on weld quality and ease of constructability, one configuration was chosen for each of the two joints under investigation, to be tested in a large-scale SPSW specimen.

A single-storey rigid frame SPSW meeting the requirements of CAN/CSA S16-01 (CSA, 2001) for ductile steel plate shear walls was designed using a strip model approach. The frame, 1900 mm high by 2440 mm wide, was fabricated first, then the infill panel was

installed in a manner to minimize the impact of distortion and burn-through. The installation process was described in detail in Chapter 6.

The loading protocol for the SPSW test was based on seismic testing guideline ATC-24 (ATC, 1992). The peak load of 630 kN, achieved at cycle 16-, was 1.08 times the load predicted by the strip model for this displacement. At cycle 17-, at a storey drift of 3.5%, a fracture at the base of one of the columns occurred. On the following cycle, it was found that when pushing in the northwards direction out-of-plane frame instability prevented further cycles of loading. One final excursion southwards to the limit of the hydraulic jacks reached a storey drift of 6.9% and a maximum load of 86% of the peak load.

The infill panel-to-fish plate welded connection maintained its integrity throughout the test, with the exception of two behaviours. First, a short length of poor quality weld at the north-top corner of the infill panel debonded from the fish plates during cycle 5+, but the debonding was arrested at a length of 10 mm at cycle 7+. Second, out-of-plane displacement of fish plates due to local buckling resulted in tears no longer than 15 mm at all four corners of the frame. Neither behavior had a detectable impact on the ability of the infill panel-to-fish plate connection to anchor the tension field.

The infill panel splice connection displayed no detectable loss of integrity during the SPSW test, including a region where burn-through occurred during welding and a plug-weld repair was used.

## 8.2 Conclusions

The following conclusions are valid only for the welding procedure, joint geometry, material properties, and welding procedure investigated in this research program. The welding procedure was tested only for a 20 gauge thick A1008 CS cold-rolled steel sheet and a 6 mm thick grade 300W steel plate. Attempts to extrapolate these conclusions to different parameters should be confirmed by testing to the satisfaction of relevant codes and standards and the parties responsible.

The following conclusions are drawn from the observations and analysis of the test results:

- 1) Where a weld of sufficient throat size was deposited, no measureable difference in strength was observed between lap joints between a 20 gauge thick steel sheet and a 6 mm thick steel plate welded on the edge of the 20 gauge plate (Weld #2 shown in Figure 3-4), and lap joints between the same materials welded on two edges. There appears to be no difference in performance whether out-of-plane displacement due to buckling of the flexible sheet steel works the root or the toe of the weld. In all cases where sufficient weld throat was deposited, failure took place away from the weld in the base material.
- 2) In the case of Weld #2, evidence from the small-scale tests indicates that weld axis misalignment can reduce the strength of the weld. The use of a small electrode may occasionally result in a reduced weld effective throat, since the edge of the 20 gauge sheet steel is difficult to see and small motions inherent to manual control of the welding gun may move the centerline of the deposited weld metal away from the edge of the sheet steel. Care should be taken to align the weld properly. Since the

weld metal covers the edge of the thin steel sheet, it is extremely difficult to assess visually what the size of the effective weld throat is without cutting a section from the material. Thus, despite the positive results of the SPSW test, the results of this test program cannot quantify how much weld misalignment occurred, or how much weld misalignment is permissible before the weld ceases to effectively anchor the tension field. Non-destructive testing (NDT) technology may be able to quantify the degree of weld misalignment, however, NDT was beyond the scope of this research program.

- 3) In the case of Weld #1 (edge of 6 mm plate to the thin plate) and Weld #3 (thin plate to thin plate weld) (see Figure 3–4), the use of a chill strip during welding, for the welding parameters used, resulted in reduced burn-through damage but did not result in a measureable increase in joint strength. It should be noted that the burn-through damage when a chill strip was not used may have been sufficient to warrant rejection of the welds based on visual inspection.
- 4) The use of tack welds to anchor the 20 gauge steel sheet to the 6 mm steel plate prior to fillet welding did not result in a noticeable decrease in strength when compared with a continuous weld without tack welds. In the quasi-static and cyclic tension-compression tests where sufficient weld throat was present, specimens welded with and without tack welds consistently failed in the base metal away from the weld location.
- 5) As suggested by the literature, the use of clamping, tack welds, and stitch welding were effective methods of reducing potential fit-up problems resulting from distortion. In both the so-called distortion specimens and when welding the infill panel to the boundary frame, no difficulties were encountered to ensure good fit-up.
- 6) The strip model of the SPSW specimen made an accurate prediction of the location of significant yield (see Figure 7–2), and ultimate capacity (test/predicted ratio = 1.08). This is consistent with the work of others (Thorburn *et al.*, 1983; Berman and Bruneau, 2005; and others).
- 7) The infill panel-to-fish plate joint consisting of a lap joint with a single weld at the edge of the thin plate (Weld #2) and the weld process used in the large-scale SPSW test resulted in satisfactory performance of the infill panel-to-boundary element joint. This good performance occurred despite three known weld flaws, including a lack of fusion at the north-top corner of the infill panel (see Figure 7–10), a burn-through repair in the infill panel splice (see Figure 6–11), and a pitting repair at the bottom fish plate-to-infill panel weld (see Figures 6–18 and 6–19). The satisfactory global cyclic performance of the system despite these weld flaws provides confirmation of the SPSW system's robustness.
- 8) The corner detail and infill panel-to-fish plate connection detail at the infill panel splice (see Figure 6–2) performed well. Buckling of the fish plates in the corners should be expected at large storey drifts, and short tears in the infill panel due to out-of-plane movement of fish plates do not appear to negatively impact global behaviour of the SPSW.
- 9) The use of a lap splice between two sheets of 20 gauge cold-rolled sheet steel, using the weld process described in this research program, resulted in satisfactory performance. No deterioration of any kind was evident in the lap splice joint at the conclusion of the large-scale SPSW test.

### 8.3 Recommendations for Future Work

The current research has helped to expand the knowledge base regarding the behaviour of welded connections at the infill panel-to-boundary element connection and at a lap splice in the infill panel of thin, cold-rolled infill panel steel plate shear walls. Several possible directions for future work have been identified:

- 1) Welding is not the only joining technology available for connecting thin sheet steel to thicker steel plate. Self-drilling screws are a promising alternative that are increasingly used to connect corrugated steel flooring to the top flange of supporting joists. A screwed connection would eliminate the problem of weld misalignment experienced in this test program. There may also be cost efficiencies associated with using less specialized skilled labour. A program to test the functionality of a self-drilling screw connection between the infill panel and the fish plates, including an optimization study of screw spacing, bears investigation.
- 2) This research program employed only one welding procedure, short-circuiting gas metal arc welding. This procedure was selected primarily based on its ability to weld thin sections, and because steel fabricators likely have arc welding equipment easily adaptable to this procedure. However, other welding processes may have advantages that make them a more attractive alternative. Spot welding through the thin sheet would not require tight alignment tolerances, and could overcome the weld misalignment problem discussed in point 2) of Section 8.2 above. Alternative weld processes bear investigation.
- 3) This research program has demonstrated that a methodical approach to controlling weld parameters can result in a connection between a 20 gauge A1008 CS infill panel and 6 mm 300W fish plates that performs adequately. However, a range of thicknesses of cold-rolled infill panel may be required, and a program to develop procedures for welding a wide range of thicknesses bears investigation.
- 4) This program demonstrated one option for successfully connecting the infill panel to boundary elements; however, at the time of infill panel installation the steel frame was laid in a flat position. This condition may be true for new construction, but will not be possible if a thin cold-rolled infill panel is added to an existing frame in a rehabilitation scenario. In this case, avenues for future work exist:
  - a. The thin panel, if tilted upright, will likely buckle under its own weight. It has been suggested that the thin infill panel could be assembled by joining a series of cold-rolled steel sheets on the floor in the flat position, as was done in the current research. This panel could then be connected, in the flat position, to a rigid frame consisting of fish plates or WT sections. This sub-frame could be tilted upright to fit the dimensions of the bay, and bolted or welded to the SPSW boundary members. The details of this assembly process merit investigation.
  - b. In a rehabilitation scenario where insufficient lay-down space is available to pursue a tilt-up construction option as discussed in the previous point, a solution is required for welding a series of thin cold-rolled steel sheets in the vertical position to install the infill panel. The high flexibility of the infill panel material renders fit-up and handling difficult, and if welding is used, magnets are an undesirable solution for holding the thin steel sheets in position. The details of a process for assembling and connecting the infill panel in the vertical position merits investigation.

## List of References

- AISC. 2006. AISC design guide 21: Welded connections – A primer for design engineers. American Institute of Steel Construction Inc., USA.
- AISC. 2005. AISC design guide 20: Steel plate shear walls. American Institute of Steel Construction Inc., USA.
- AISI and CSA. 2002. North american specification for the design of cold-formed steel structural members. AISI/COS/NASPEC 2001/ CSA S136-01. American Iron and Steel Institute and Canadian Standards Association, Washington, DC.
- Anon. 2010a. Welding dictionary [online]. Available from <http://www.millerwelds.com/resources/dictionary.html> [cited July 15 2010].
- Anon. 2010b. SuitCase™ X-TREME™ 12VS wire feeder improves flux cored welding, reliability for apex steel [online]. Available from <http://www.millerwelds.com/resources/articles/index?page=story133.html> [cited July 15 2010].
- ASTM. 2008. Standard specification for steel, sheet, cold-rolled, carbon, structural, high strength low-alloy, high-strength low-alloy with improved formability, solution hardened, and bake hardenable. ASTM A1008/ A1008M - 08a. ASTM International, West Conshohocken, PA.
- ASTM. 2001. Standard test methods and definitions for mechanical testing of steel products. ASTM A370 - 97a. ASTM International, West Conshohocken, PA.
- ATC. 1992. ATC-24: Guidelines for cyclic seismic testing of components of steel structures. No.24, Applied Technology Council, Redwood City, CA.
- AWS. 2008a. Structural welding code – steel. AWS D1.1/ D1.1M: 2008. American Welding Society, Miami, FL.
- AWS. 2008b. Structural welding code - sheet steel. AWS D1.3/ D1.3M: 2008. American Welding Society, Miami, FL.
- AWS. 2005a. Structural welding code - seismic supplement. AWS D1.8/ D1.8M: 2005. American Welding Society, Miami, FL.
- AWS. 2005b. Specification for carbon steel electrodes and rods for gas shielded arc welding. AWS A5.18/ A5.18M: 2005. American Welding Society, Miami, FL.
- AWS. 1976. Welding handbook. American Welding Society, Miami, FL.
- Basler, K. and Thuerlimann, A. 1961. Strength of plate girders, ASCE Proceedings of the Journal of the Structural Division, **87**: 181-197.

- Berman, J.W. and Bruneau, M. 2005. Experimental investigation of light-gauge steel plate shear walls, *ASCE Journal of Structural Engineering*, **131**: 259-267.
- Bhide, S.R., Michaleris, P., Posada, M., and DeLoach, J. 2006. Comparison of buckling distortion propensity for SAW, GMAW, and FSW, *Welding Journal*, **85**: 189-195.
- Blodgett, O.W. 2007a. Controlling distortion in design, *Welding Design and Fabrication*, **80**: 10-12.
- Blodgett, O.W. 2007b. Controlling distortion in design, part 2: Distortion control continues on the drawing board, *Welding Design and Fabrication*, **80**.
- Blodgett, O.W. 2007c. Controlling distortion in design, part 3: Distortion control moves onto the shop floor, *Welding Design and Fabrication*, **80**: 12-14.
- Brace, M. and Brook, J. 2002. Tips for successfully welding sheet metal [online]. Available from [www.aws.org/w/a/wj/2002/03/feature/index.html](http://www.aws.org/w/a/wj/2002/03/feature/index.html) [cited April 30 2009].
- Bruneau, M., Uang, C.M., and Whittaker, A. 1998. *Ductile design of steel structures*. The McGraw-Hill Companies Inc., New York, NY.
- Caccese, V., Elgaaly, M., and Chen, R. 1993. Experimental study of thin steel-plate shear walls under cyclic load, *ASCE Journal of Structural Engineering*, **119**: 573-587.
- Callister Jr., W.D. 2003. *Materials science and engineering: An introduction*. John Wiley and Sons Inc., New York, NY.
- CISC. 2008. *Moment connections for seismic applications*. Canadian Institute of Steel Construction, Markham, ON.
- Cort, A. 2008. Frame - based robotic tooling [online]. Available from [http://www.assemblymag.com/Articles/Article\\_Rotation/BNP\\_GUID\\_9-52006\\_A\\_1000000000000314541](http://www.assemblymag.com/Articles/Article_Rotation/BNP_GUID_9-52006_A_1000000000000314541) [cited April 30 2009].
- Craig, E. 1994. GMAW shielding gases: Simplifying selection, *Welding Design and Fabrication*, **September 1994**: 43-45.
- CSA. 2009. *Limit states design of steel structures*. CAN/CSA S16-09. Canadian Standards Association, Mississauga, ON.
- CSA. 2004. *General requirements for rolled or welded structural quality steel/ structural quality steel*. CSA G40.20/ G40.21. Canadian Standards Association, Mississauga, ON.



- CSA. 2003. Welded steel construction (metal arc welding). CSA W59-03. Canadian Standards Association, Mississauga, ON.
- CSA. 2001. Limit states design of steel structures. CAN/CSA S16-01. Canadian Standards Association, Mississauga, ON.
- CWB. 2005. Welding for design engineers. Canadian Welding Bureau, Mississauga, ON.
- Dastfan, M. and Driver, R.G. 2008. Flexural stiffness limits for frame members of steel plate shear wall systems. *In 2008 Annual Stability Conference, April 2, 2008 – April 5, pp. 321-334.*
- Deng, X., Dastfan, M., and Driver, R.G. 2008. Behaviour of steel plate shear walls with composite columns. *In 2008 Structures Congress - Structures Congress 2008: Crossing the Borders, April 24, 2008 - April 26, Vol. 314.*
- Driver, R.G., Kulak, G.L., Kennedy, D.J.L., and Elwi, A.E. 1997. Seismic behaviour of steel plate shear walls. Structural Engineering Report No. 215, Department of Civil Engineering, University of Alberta, Edmonton, AB.
- FEMA. 2000. FEMA 356: Prestandard and commentary for the seismic rehabilitation of steel buildings. Federal Emergency Management Agency, Washington, DC.
- Fisher, J.W., Kulak, G.L., and Smith, I.F.C. 1998. A fatigue primer for structural engineers. National Steel Bridge Alliance, American Institute of Steel Construction, Chicago, IL.
- Green, R. 2004. How to optimize mild steel GMAW, *Welding Journal*, **83**: 30-33.
- Harris, J. 2010. Understanding the common difficulties of feeding in MIG welding aluminum [online]. Available from <http://www.lincolnelectric.com/knowledge/articles/content/feedingaluminum.asp> [cited July 15 2010].
- Hitaka, T. and Matsui, C. 2003. Experimental study on steel shear wall with slits, *ASCE Journal of Structural Engineering*, **129**: 586-595.
- Houldcroft, P. 1990. Which process? : An introduction to welding and related processes and a guide to their selection. Woodhead Publishing Ltd. in association with the Welding Institute, Cambridge, England.
- Ikeagu, C.R. 2007. Evaluating the effect of different welding processes on the distortion of 4mm thick DH36 ship panels. MSc, Cranfield University, Cranfield, UK.

- Kelly, S.M., Martukanitz, R.P., Michaleris, P., Bugarewicz, M., Huang, T.D., and Kvidahl, L. 2006. Low heat input welding for thin steel fabrication, *Journal of Ship Production*, **22**: 105-109.
- Kharrazi, M.H.K. 2005. Rational method for analysis and design of steel plate walls. PhD, University of British Columbia, Vancouver, BC.
- Kou, S. 2003. *Welding metallurgy*. John Wiley and Sons Inc., Hoboken, NJ.
- Kulak, G.L. and Grondin, G.Y. 2006. *Limit states design in structural steel*. Canadian Institute of Steel Construction, Willowdale, ON.
- Lancaster, J. 1992. *Handbook of structural welding*. McGraw-Hill, New York, NY.
- Lubell, A.S., Prion, H.G.L., Ventura, C.E., and Rezai, M. 2000. Unstiffened steel plate shear wall performance under cyclic loading, *ASCE Journal of Structural Engineering*, **126**: 453-460.
- Martin, D. 2007. Mehdi Dastfan: Working towards the earthquake-proof building. Available from <http://www.uofaweb.ualberta.ca/researchandstudents/news.cfm?story=54894> [cited April 24 2009].
- Masubuchi, K. 1980. *Analysis of welded structures*. Pergamon Press, Oxford.
- Miller, D. 2001. Designing welded lap joints, *Welding Innovation*, **18**: 6-8.
- Mohler, R. 1983. *Practical welding technology*. Industrial Press Inc., New York, NY.
- Nadzam, J. 2006. *GMAW welding guide*. The Lincoln Electric Company, Cleveland, Ohio.
- Nakashima, M. 1995. Strain-hardening behaviour of shear panels made of low-yield steel, *ASCE Journal of Structural Engineering*, **121**: 1742-1749.
- NRCC. 2005. *National building code of Canada 2005*. National Research Council Canada, Ottawa, ON.
- Patchett, B.M. 2003. *CASTI metals blue book: Welding filler metals*. CASTI Publishing Inc., Edmonton, AB.
- Pekoz, T. and McGuire, W. 1981. Sheet steel welding, *ASCE Journal of the Structural Division*, **107**: 1657-1673.
- Rabinovitch, J. and Cheng, J.J.R. 1993. Cyclic behavior of steel gusset plate connections. Structural Engineering Report No. 191, Department of Civil and Environmental Engineering, University of Alberta, Edmonton, Alberta.

- Rezai, M. 1999. Seismic behaviour of steel plate shear walls by shake table testing. PhD, University of British Columbia, Vancouver, BC.
- Roberts, T.M. and Sabouri-Ghomi, S. 1992. Hysteretic characteristics of unstiffened perforated steel plate shear panels, *Thin-Walled Structures*, **14**: 139-151.
- Schumacher, A., Grondin, G.Y., and Kulak, G.L. 1999. Connection of infill panels in steel plate shear walls, *Canadian Journal of Civil Engineering*, **26**: 549-563.
- Sheng-Jin, C. and Chyuan, J. 2008. Seismic behavior of low yield point steel plate shear wall. *In Structures Congress 2008: Crossing the Borders*, April 24, 2008 - April 26, Vol. 314.
- Shiskin, J.J., Driver, R.G., and Grondin, G.Y. 2005. Analysis of steel plate shear walls using the modified strip model. Structural Engineering Report No. 261, Department of Civil and Environmental Engineering, University of Alberta, Edmonton, AB.
- Thorburn, L.J., Kulak, G.L., and Montgomery, C.J. 1983. Analysis of steel plate shear walls. Structural Engineering Report No. 107, Department of Civil and Environmental Engineering, University of Alberta, Edmonton, AB.
- Timler, P.A. 1998. Design procedures development, analytical verification, and cost evaluation of steel plate shear wall structures. Technical report no. 98-01, Earthquake Engineering Research Facility, University of British Columbia, Vancouver, BC.
- Timler, P.A. and Kulak, G.L. 1983. Experimental study of steel plate shear walls. Structural Engineering Report No.114, Department of Civil and Environmental Engineering, University of Alberta, Edmonton, AB.
- Tromposch, E.W. and Kulak, G.L. 1987. Cyclic and static behaviour of thin panel steel plate shear walls. Structural Engineering Report No. 145, Department of Civil and Environmental Engineering, University of Alberta, Edmonton, AB.
- Vian, D. and Bruneau, M. 2005. Steel plate shear walls for seismic design and retrofit of building structures. Technical Report No. MCEER-05-0010, Multidisciplinary Centre for Earthquake Engineering Research, State University of New York at Buffalo, Buffalo, NY.
- Vian, D. and Bruneau, M. 2004. Testing of special LYS steel plate shear walls. *In 13<sup>th</sup> World Conference on Earthquake Engineering*, April 1, 2004 -April 6, Vol. 978.
- Yarmuch, M. 2008. Advanced welding processes study and industry survey: Pathways to higher productivity for Alberta's fabrication industries. Alberta Research Council Inc., Edmonton, AB.

## Appendix A: Materials Data

### A1 Introduction

This appendix contains detailed material data, including a discussion of why the static values from tension coupon tests were considered unreliable and discarded (section A2), detailed tension coupon data (section A3), and scanned copies of mill certificates containing steel chemistries (section A4).

### A2 Discussion of Unreliable Static Data from Tension Coupons

Though dynamic data for tension coupons is considered reliable, static points are suspect. It was discovered following testing that the data collection system was erroneously set to halt data collection when the loading was paused. Drops in load appearing to represent static values, were in fact some value recorded between the static and dynamic value near a static point, recorded directly following the resumption of loading.

In addition, it was noted that the slope of the unloading line for the static points was not vertical, but in fact followed the elastic modulus of the material. This suggests that, as opposed to holding the displacement for the duration of the static point, some unloading occurred, which had a significant impact on the “static” value reported. So-called “static” values of yield stress and ultimate stress experienced drops much larger than expected in some cases, particularly considering the extremely slow loading rate imposed for some specimens.

Despite these issues with static points, the dynamic stress-strain curves are within an acceptable range for the materials tested. Thus, as discussed in Chapters 5 and 6, a judgment call was made to use dynamic values of the W200x31 tension coupons in the strip model, with the understanding that this might result in a slight overprediction in the contribution of the materials strength to the overall resistance of the SPSW system, but would likely prove more accurate than using the unreliable static values.

Coupons B7 through B10 were tested following the discovery of this issue. The load rates employed to determine key values were the slowest possible for the testing equipment used (0.1 mm/min). The dynamic results from these coupons were used for the A1008 CS infill panel material properties.

### A3 Tension Coupon Data

**Table A-1: Tension Coupon Labelling Scheme**

<b>Label</b>	<b>Description</b>
A	6 mm, Grade 300W steel plate used for weld procedure development. So-called “thick” portion of “thin-to-thick” specimens.
B	Grade A1008 CS Type A, 20 gauge sheet steel used for the infill panel and the “thin” portion of “thin-to-thick” and “thin-to-thin” specimens.
C	Grade 350W, W200x31 used for the SPSW test specimen moment frame. Suffix “-F” for pieces cut from the flange, and “-W” for pieces cut from the web.

Table A-2: Tension Coupon Results Including Unreliable Static Points

VARIABLE [MPa]	E	STATIC YIELD POINTS			$F_{y \text{ static}}$	$F_{y \text{ dynamic}}$	$F_{u \text{ static}}$	$F_{u \text{ dynamic}}$	
		1	2	3					
LOAD RATE [mm/s]	0.30	0.00			0.00	5.00	0.00	5.00	
COUPON	A1	200,600	281.3	288.3	N/A	284.8	334.0	N/A*	500.0
	A2	209,200	300.8	307.2	296.4	301.5	324.6	N/A*	488.7
	A3	211,200	300.3	307.1	306.2	304.5	327.8	N/A*	493.1
	A4	212,800	307.6	323.3	323.2	318.0	341.5	470.8	508.4
	A5	215,200	303.9	316.8	329.3	316.7	342.7	437.3	508.8
	A6	N/A	331.3	N/A	N/A	331.3	345.1	476.5	511.4
	CF-1	216,600	308.0	N/A	N/A	308.0	355.7	410.8	454.8
	CF-2	213,300	323.9	327.6	324.2	325.2	356.1	415.5	459.9
	CF-3	205,800	325.6	339.3	336.3	333.8	352.3	409.6	459.9
	CF-4	210,500	341.6	345.7	336.5	341.3	352.9	428.0	458.1
	CW-1	210,200	365.0	359.6	350.0	358.2	368.8	N/A*	464.5
	CW-2	205,900	360.8	361.2	360.6	360.9	375.5	N/A*	466.3
	B1	260,900	144.2	129.6	141.7	138.5	158.1	238.6	277.7
	B2	239,200	142.0	143.0	144.2	143.1	154.1	N/A*	278.2
	B3	228,800	142.6	142.7	152.0	145.8	155.3	N/A*	279.0
	B4	294,700	132.4	133.9	93.9	120.0	139.4	N/A*	278.2
B5	212,100	132.6	134.7	142.8	136.7	144.0	N/A*	283.3	
B6	229,900	123.0	117.7	116.4	119.1	142.8	247.6	278.1	

**NOTES**

- 1) " $F_{y \text{ static}}$ " = average value of the three "yield static points". **ALL STATIC POINTS ARE CONSIDERED UNRELIABLE.**
- 2) N/A\* = Either the static point was recorded at a strain beyond the yield plateau, or no point was captured by the data collection unit

Table A-3: Tension Coupon Geometry Before Testing

Coupon	Width [mm]				Thickness [mm]				AREA [mm <sup>2</sup> ]	Gauge Length [mm]			
	1	2	3	Average	1	2	3	Average		1	2	3	Average
C-1F	12.45	12.46	12.46	<b>12.46</b>	10.11	10.11	10.11	<b>10.11</b>	<b>125.94</b>	50.12	50.18	50.20	<b>50.17</b>
C-2F	12.50	12.50	12.49	<b>12.50</b>	10.04	10.05	10.03	<b>10.04</b>	<b>125.47</b>	50.36	50.33	50.34	<b>50.34</b>
C-3F	12.44	12.43	12.45	<b>12.44</b>	10.15	10.16	10.15	<b>10.15</b>	<b>126.31</b>	50.24	50.13	50.15	<b>50.17</b>
C-4F	12.47	12.46	12.48	<b>12.47</b>	9.74	9.76	9.75	<b>9.75</b>	<b>121.58</b>	50.31	50.12	50.20	<b>50.21</b>
C-5W	12.41	12.39	12.42	<b>12.41</b>	6.40	6.40	6.40	<b>6.40</b>	<b>79.40</b>	50.24	50.10	50.30	<b>50.21</b>
C-6W	12.49	12.50	12.50	<b>12.50</b>	6.39	6.39	6.39	<b>6.39</b>	<b>79.85</b>	50.55	50.63	50.40	<b>50.53</b>
<b> </b>													
A1	12.52	12.50	12.50	<b>12.51</b>	6.43	6.43	6.43	<b>6.43</b>	<b>80.42</b>	50.25	50.46	50.34	<b>50.35</b>
A2	12.49	12.49	12.47	<b>12.48</b>	6.43	6.42	6.44	<b>6.43</b>	<b>80.27</b>	50.33	50.38	50.19	<b>50.30</b>
A3	12.49	12.47	12.46	<b>12.47</b>	6.41	6.43	6.42	<b>6.42</b>	<b>80.08</b>	50.44	50.40	50.47	<b>50.44</b>
A4	12.56	12.57	12.57	<b>12.57</b>	6.41	6.40	6.42	<b>6.41</b>	<b>80.55</b>	50.06	49.89	49.96	<b>49.97</b>
A5	12.52	12.51	12.52	<b>12.52</b>	6.40	6.41	6.41	<b>6.41</b>	<b>80.19</b>	49.88	49.93	50.08	<b>49.96</b>
A6	12.50	12.49	12.49	<b>12.49</b>	6.41	6.41	6.41	<b>6.41</b>	<b>80.08</b>	50.12	50.15	50.17	<b>50.15</b>
<b> </b>													
B1	12.38	12.39	12.38	<b>12.38</b>	0.90	0.92	0.92	<b>0.91</b>	<b>11.31</b>	50.23	50.44	50.29	<b>50.32</b>
B2	12.50	12.48	12.49	<b>12.49</b>	0.92	0.91	0.92	<b>0.92</b>	<b>11.45</b>	49.89	49.92	49.82	<b>49.88</b>
B3	12.50	12.48	12.51	<b>12.50</b>	0.90	0.92	0.90	<b>0.91</b>	<b>11.33</b>	50.38	50.39	50.43	<b>50.40</b>
B4	12.52	12.52	12.52	<b>12.52</b>	0.91	0.90	0.89	<b>0.90</b>	<b>11.27</b>	50.31	50.24	50.32	<b>50.29</b>
B5	12.50	12.46	12.48	<b>12.48</b>	0.89	0.89	0.89	<b>0.89</b>	<b>11.11</b>	50.03	50.09	50.08	<b>50.07</b>
B6	12.50	12.50	12.47	<b>12.49</b>	0.89	0.90	0.90	<b>0.90</b>	<b>11.20</b>	50.09	50.25	50.14	<b>50.16</b>
B7	12.38	12.36	12.34	<b>12.36</b>	0.91	0.91	0.91	<b>0.91</b>	<b>11.20</b>	49.33	49.36	49.47	<b>49.39</b>
B8	12.38	12.36	12.35	<b>12.36</b>	0.90	0.91	0.90	<b>0.90</b>	<b>11.16</b>	49.47	49.48	49.51	<b>49.49</b>
B9	12.35	12.38	12.38	<b>12.37</b>	0.90	0.91	0.90	<b>0.90</b>	<b>11.16</b>	49.56	49.79	49.63	<b>49.66</b>
B10	12.39	12.39	12.38	<b>12.39</b>	0.90	0.90	0.90	<b>0.90</b>	<b>11.15</b>	49.40	49.36	49.42	<b>49.39</b>

Table A-4: Tension Coupon Geometry After Testing

Coupon	Width [mm]			Thickness [mm]			AREA [mm <sup>2</sup> ]	% Reduction in Area	Gauge Length [mm]			% Elongation at Fracture
	1	2	Average	1	2	Average			1	2	Average	
C-1F	7.52	7.53	7.53	5.20	5.35	5.28	39.69	68.5%	N/A*			
C-2F	7.55	7.80	7.68	5.37	5.02	5.20	39.87	68.2%	N/A*			
C-3F	7.36	7.85	7.61	5.28	5.38	5.33	40.53	67.9%	69.97	70.26	70.12	39.7%
C-4F	7.24	7.33	7.29	5.10	5.06	5.08	37.01	69.6%	70.26	70.28	70.27	40.0%
C-5W	8.20	8.23	8.22	3.00	3.05	3.03	24.85	68.7%	69.08	69.61	69.35	38.1%
C-6W	8.33	8.52	8.43	2.95	2.93	2.94	24.77	69.0%	69.96	70.16	70.06	38.7%
<b>A</b>												
A1	8.53	8.57	8.55	3.65	3.64	3.65	31.16	61.2%	65.66	65.92	65.79	30.7%
A2	8.12	8.23	8.18	3.90	3.97	3.94	32.17	59.9%	67.25	66.98	67.12	33.4%
A3	8.30	8.37	8.34	3.67	3.50	3.59	29.88	62.7%	67.53	67.47	67.50	33.8%
A4	8.90	8.91	8.91	4.14	4.16	4.15	36.96	54.1%	63.84	63.67	63.76	27.6%
A5	8.81	8.87	8.84	3.97	4.07	4.02	35.54	55.7%	62.54	62.76	62.65	25.4%
A6	8.73	8.72	8.73	3.97	3.96	3.97	34.59	56.8%	63.33	63.38	63.36	26.3%
<b>B</b>												
B1	7.65	7.80	7.73	0.64	0.65	0.65	4.98	55.9%	75.55	75.60	75.58	50.2%
B2	7.91	8.03	7.97	0.66	0.68	0.67	5.34	53.4%	72.65	72.47	72.56	45.5%
B3	7.95	8.09	8.02	0.68	0.67	0.68	5.41	52.2%	73.43	73.59	73.51	45.9%
B4	8.00	7.93	7.97	0.66	0.64	0.65	5.18	54.1%	74.45	74.49	74.47	48.1%
B5	7.70	7.61	7.66	0.63	0.65	0.64	4.90	55.9%	72.89	72.99	72.94	45.7%
B6	7.97	7.86	7.92	0.63	0.63	0.63	4.99	55.5%	72.47	72.70	72.59	44.7%
B7	7.78	8.16	7.97	0.644	0.682	0.66	5.28	52.8%	71.44	71.43	71.44	44.6%
B8	7.79	7.89	7.84	0.653	0.707	0.68	5.33	52.2%	72.91	73.23	73.07	47.7%
B9	7.98	7.94	7.96	0.639	0.691	0.67	5.29	52.6%	69.89	70.21	70.05	41.1%
B10	7.83	7.88	7.86	0.674	0.681	0.68	5.32	52.3%	70.5	70.76	70.63	43.0%



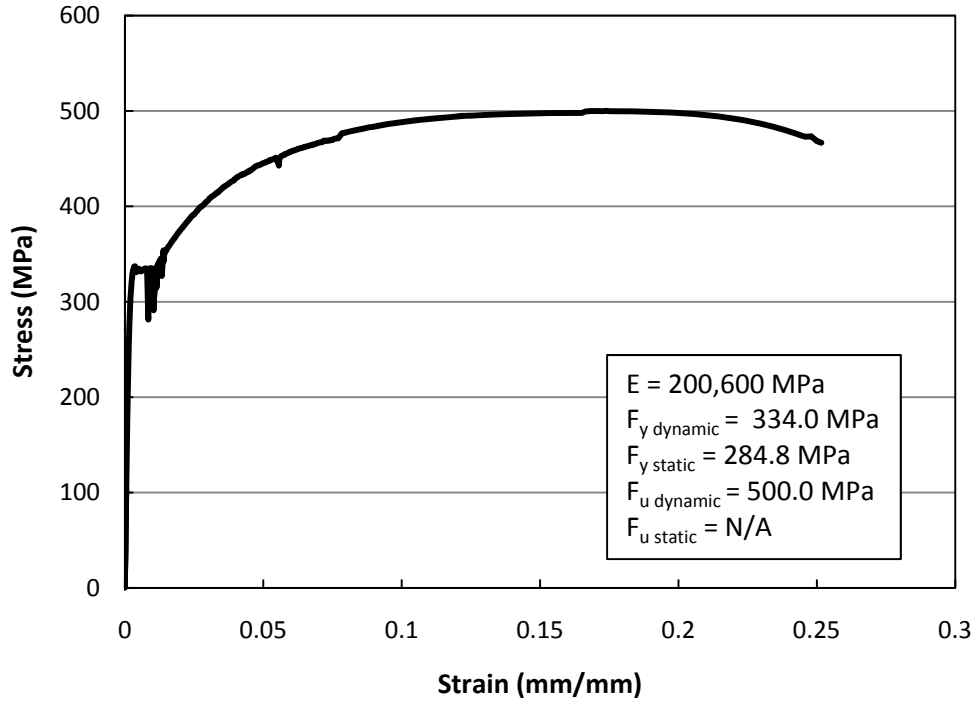


Figure A-1: Tension Coupon A1

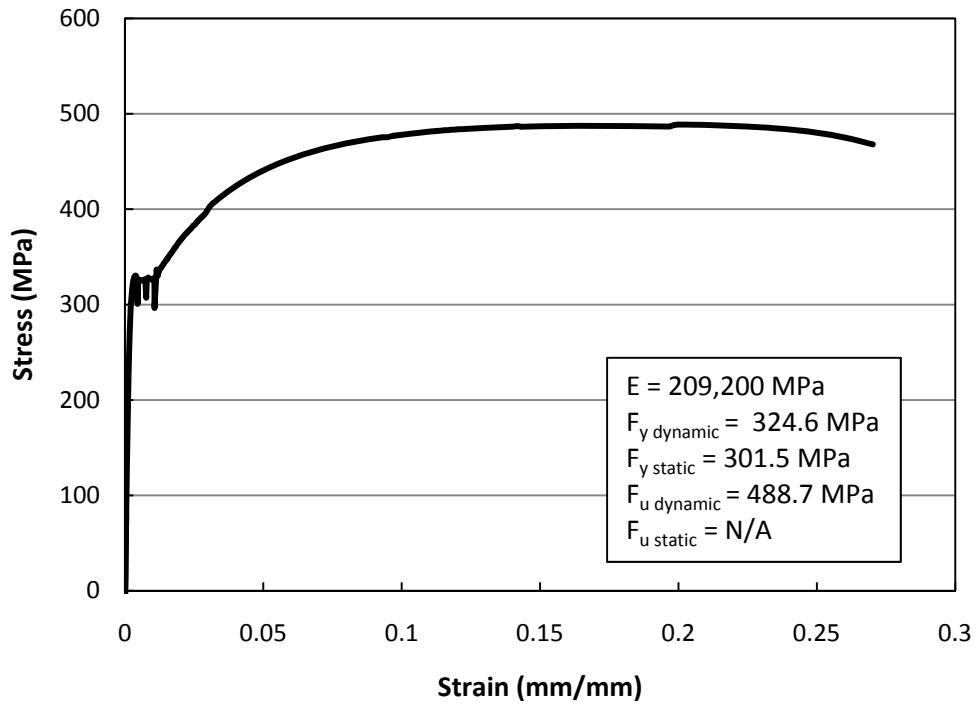


Figure A-2: Tension Coupon A2

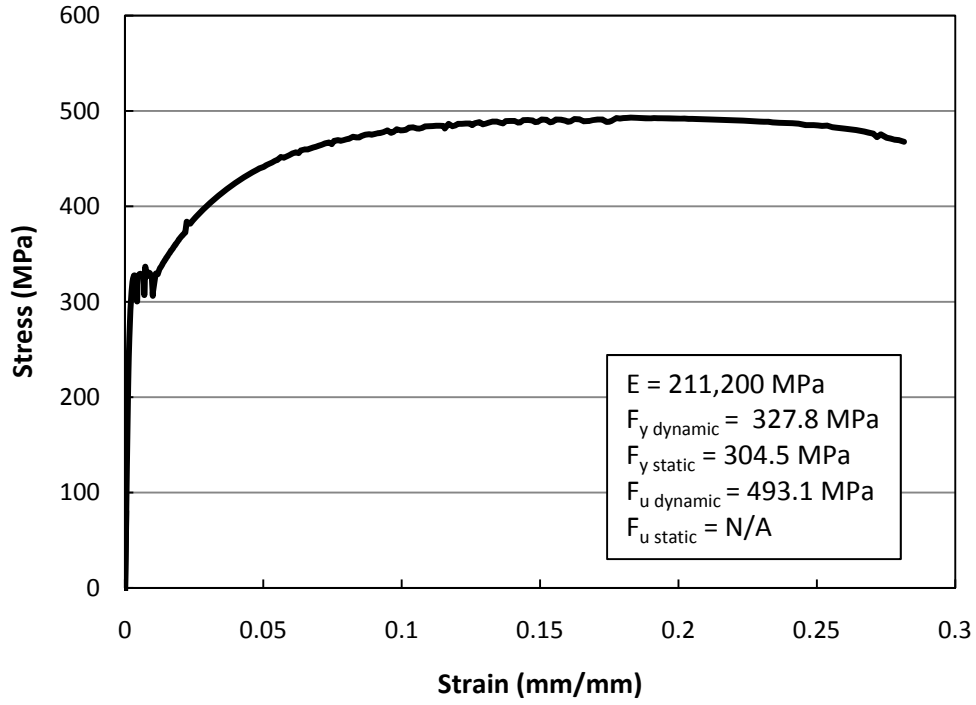


Figure A-3: Tension Coupon A3

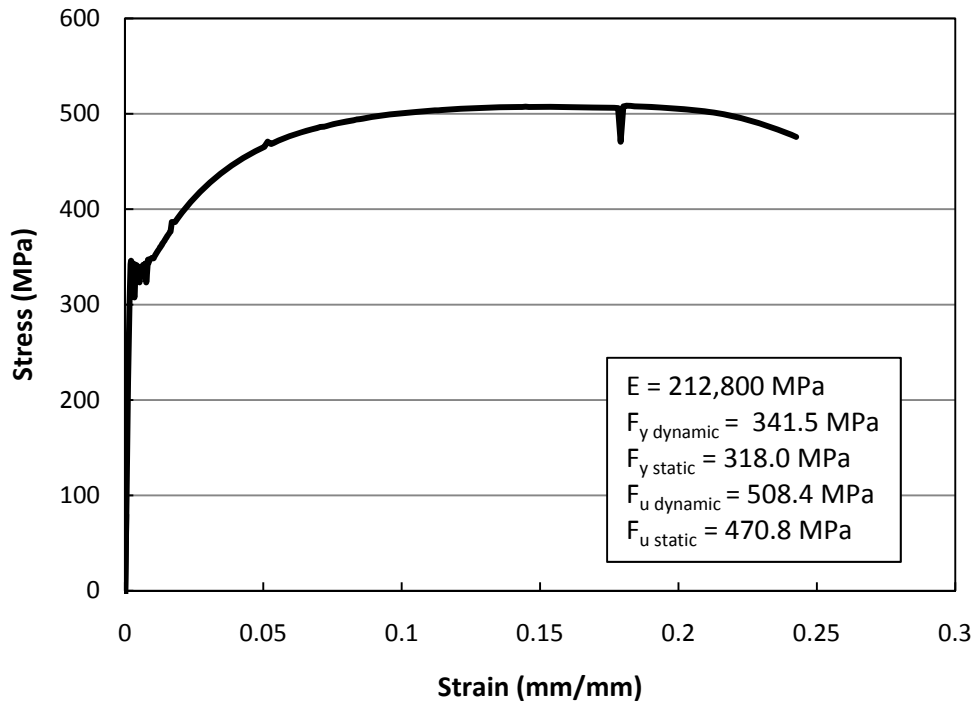


Figure A-4: Tension Coupon A4

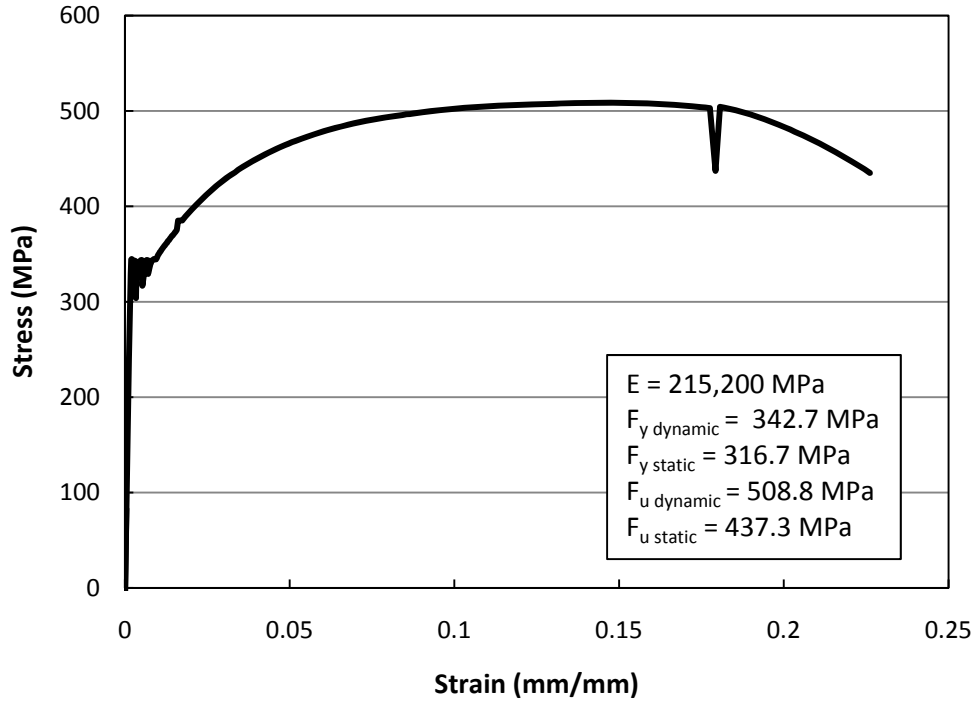


Figure A-5: Tension Coupon A5

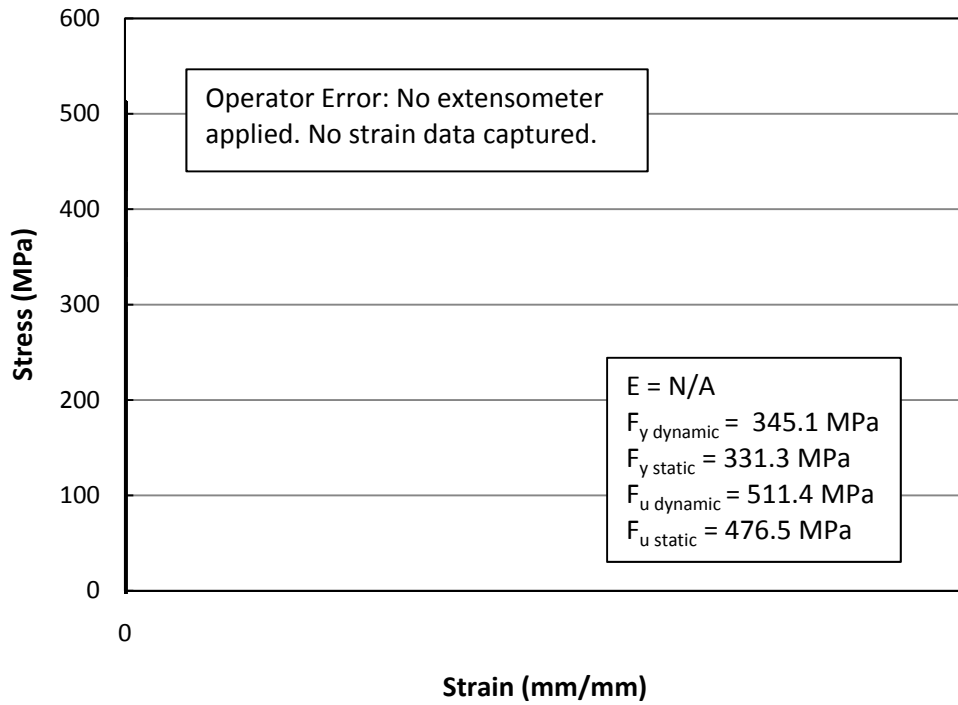


Figure A-6: Tension Coupon A6

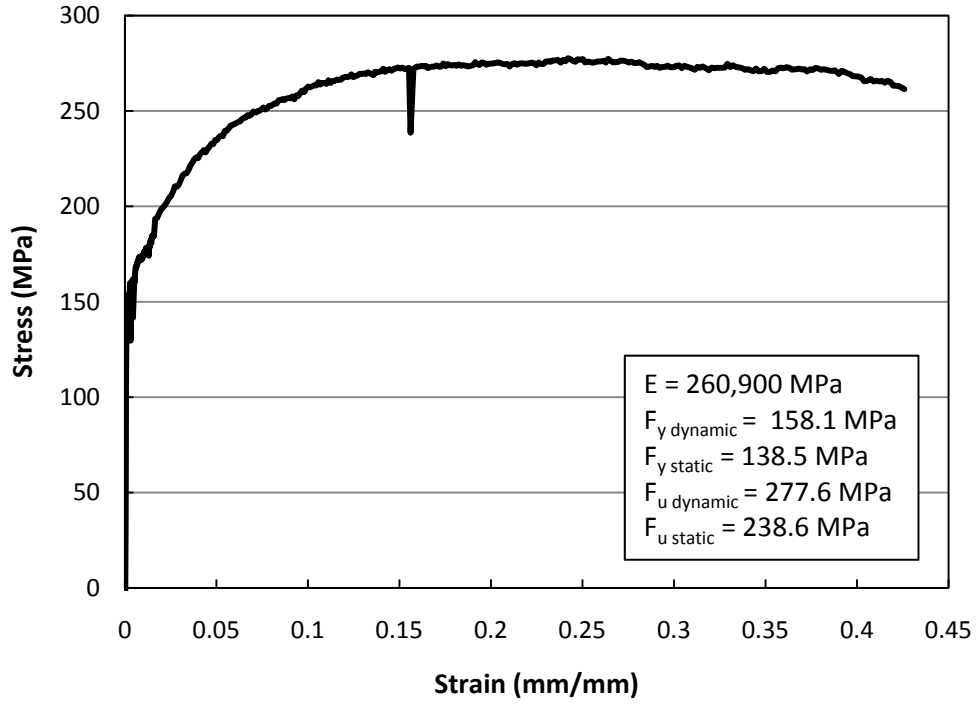


Figure A-7: Tension Coupon B1

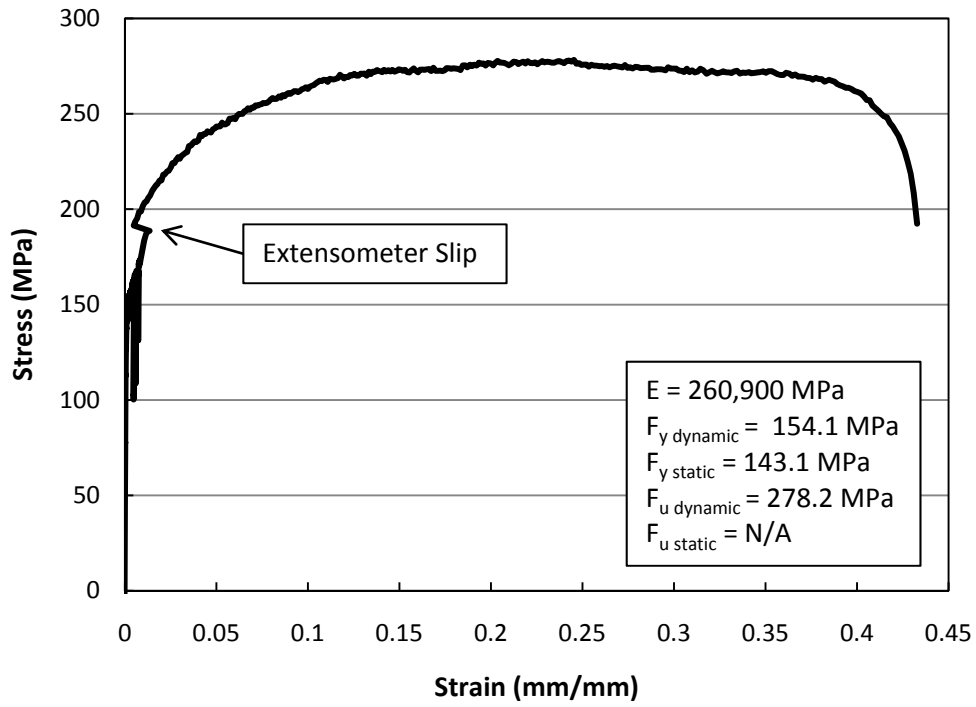


Figure A-8: Tension Coupon B2

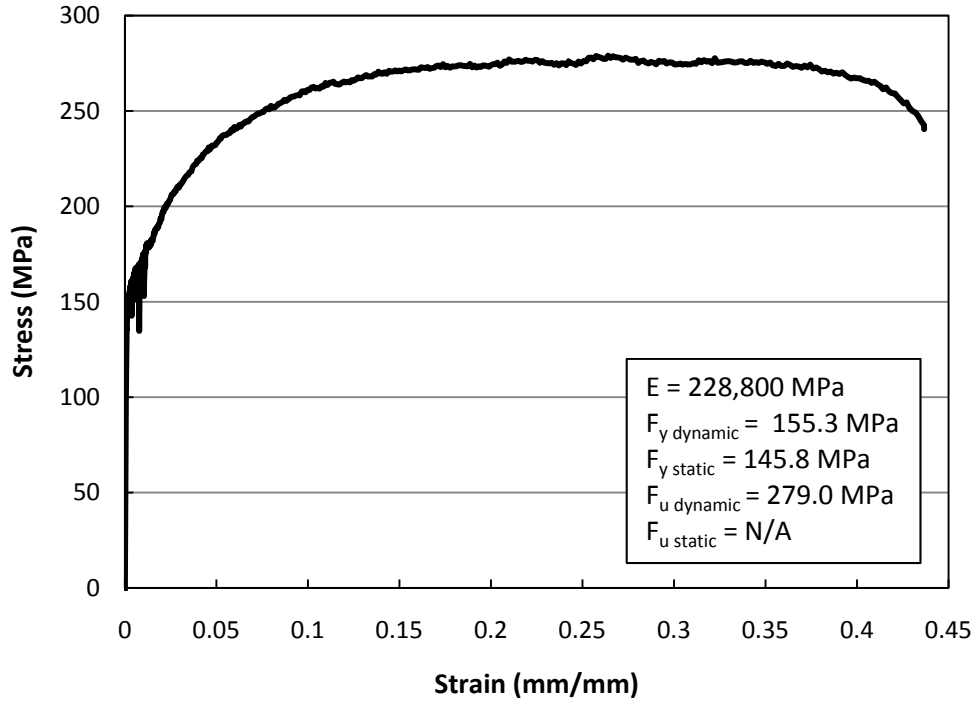


Figure A-9: Tension Coupon B3

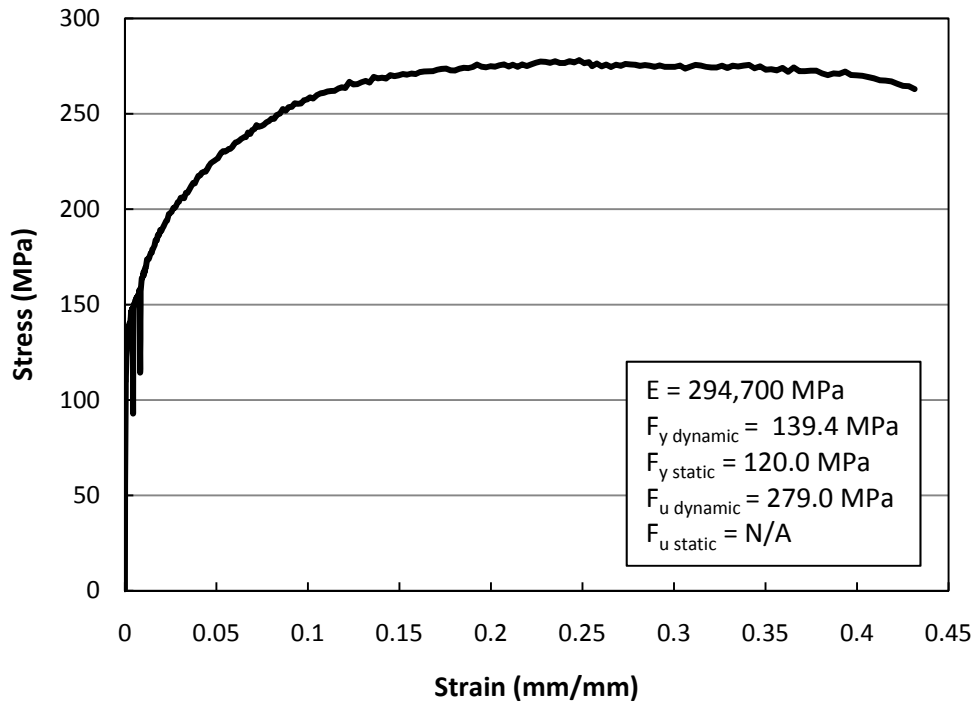


Figure A-10: Tension Coupon B4

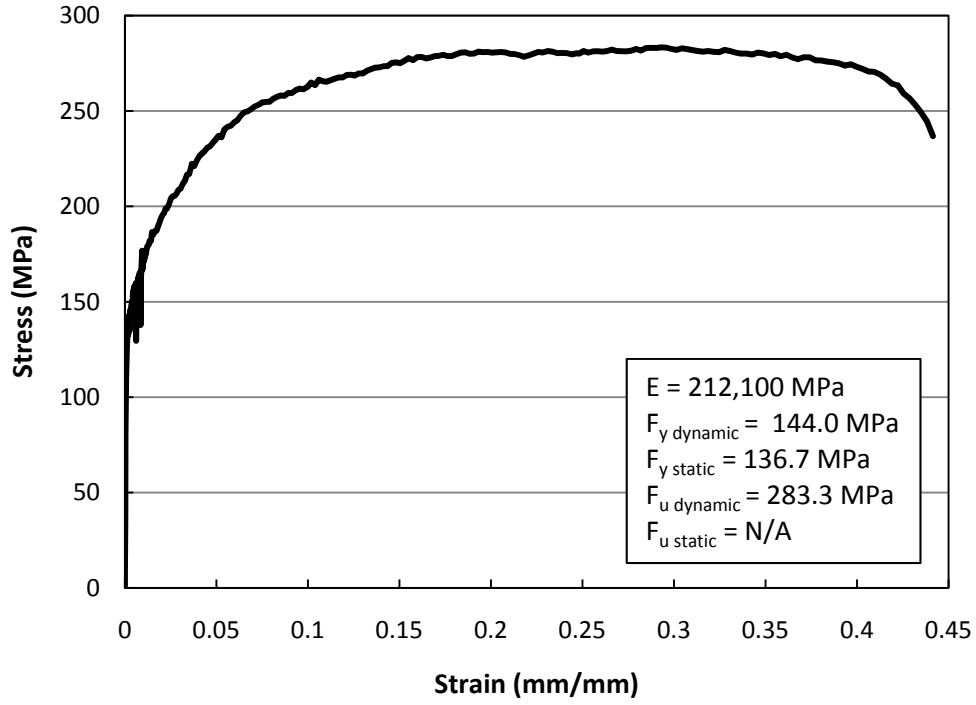


Figure A-11: Tension Coupon B5

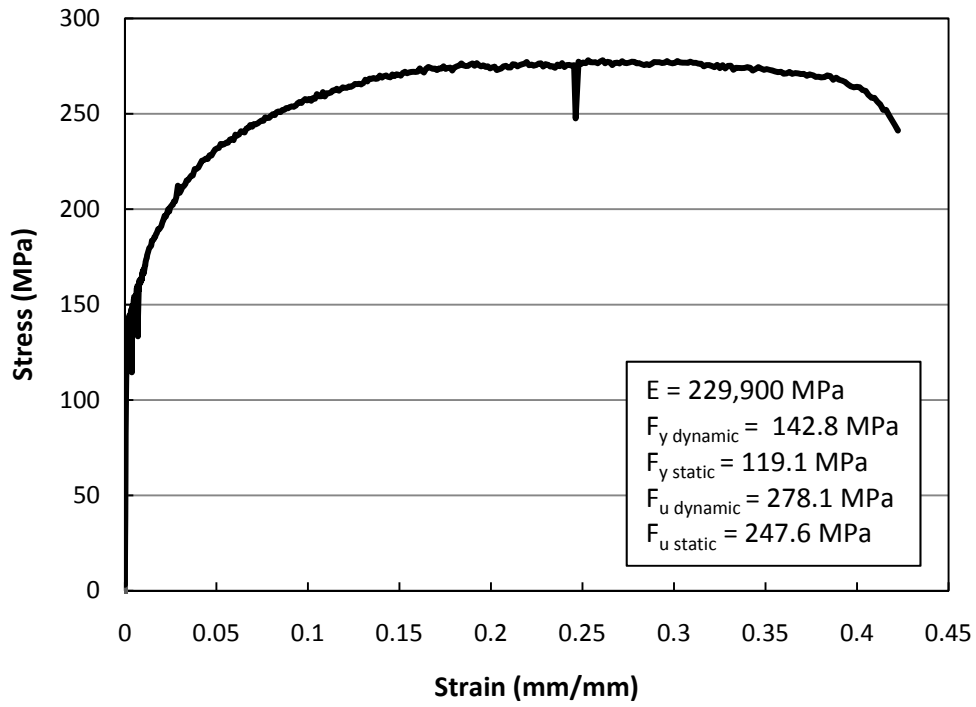


Figure A-12: Tension Coupon B6

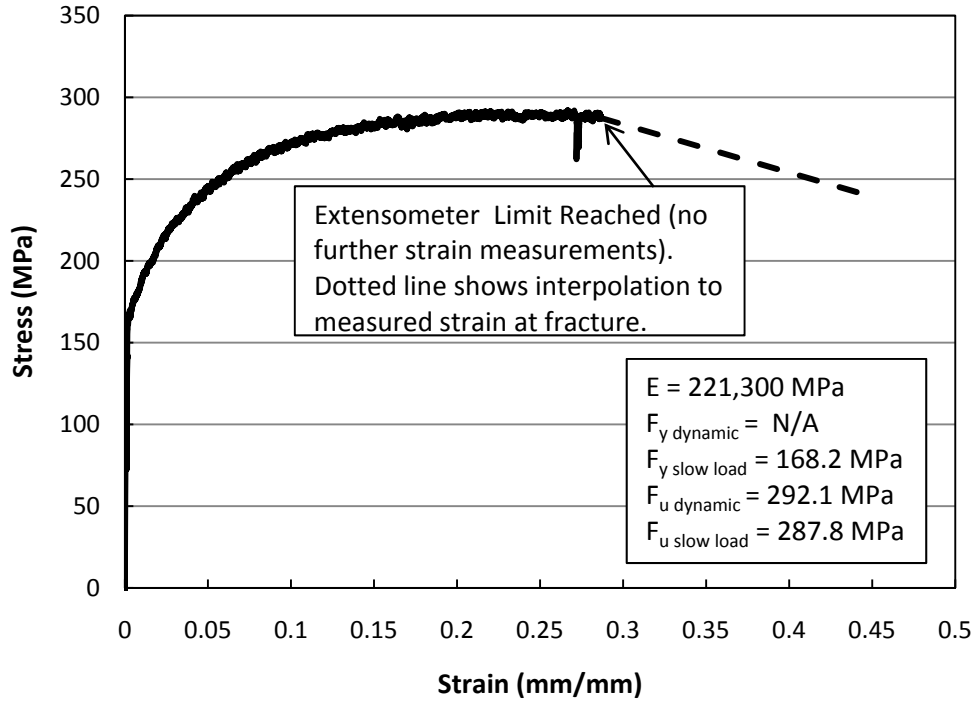


Figure A-13: Tension Coupon B7

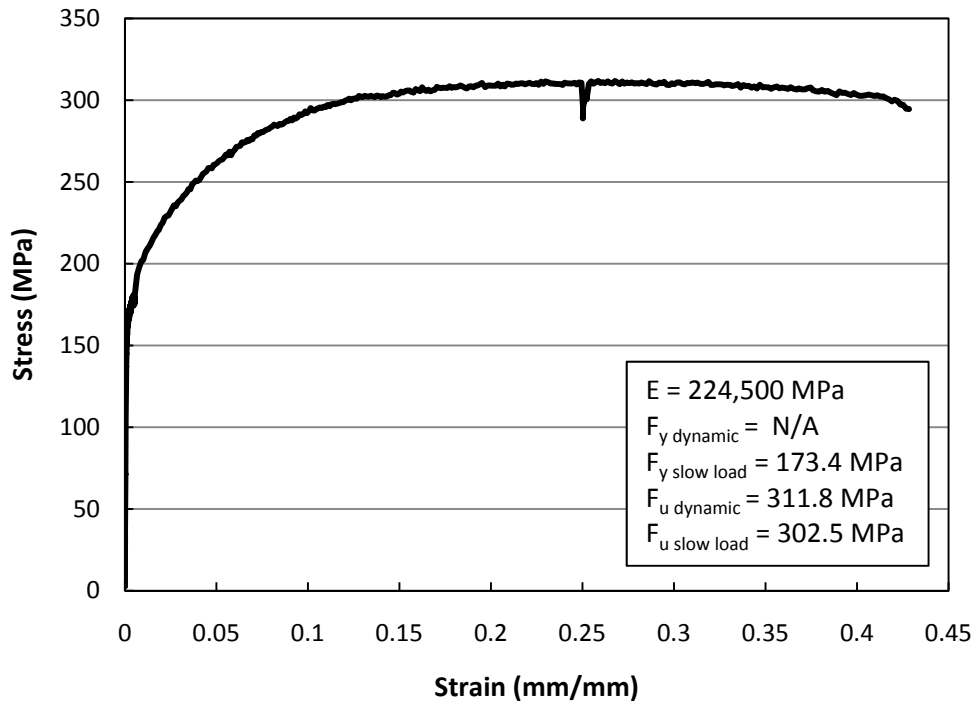


Figure A-14: Tension Coupon B8

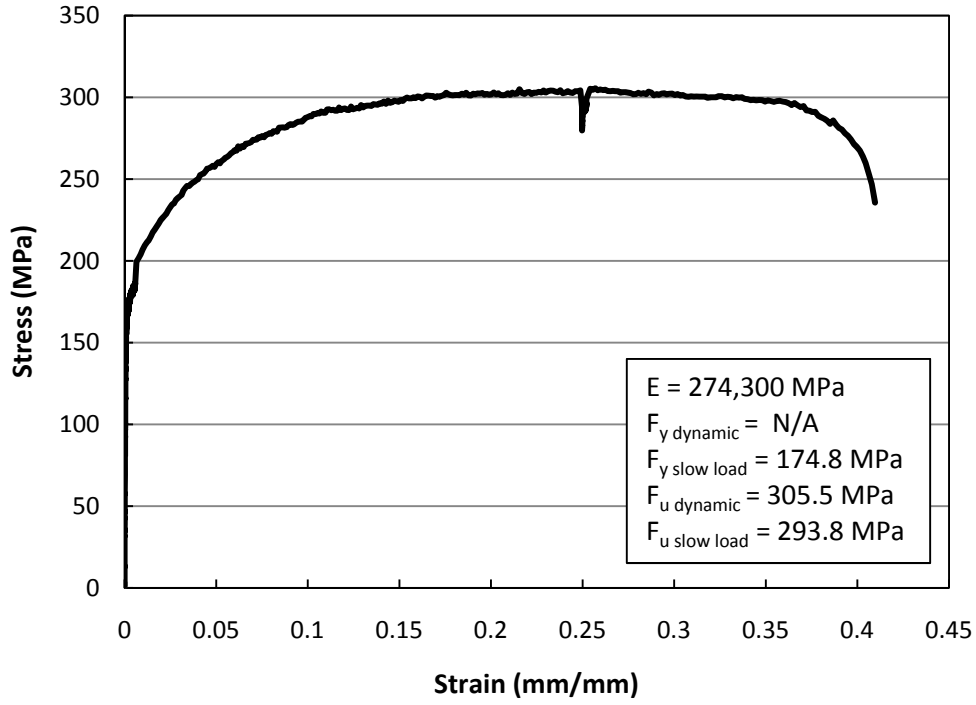


Figure A-15: Tension Coupon B9

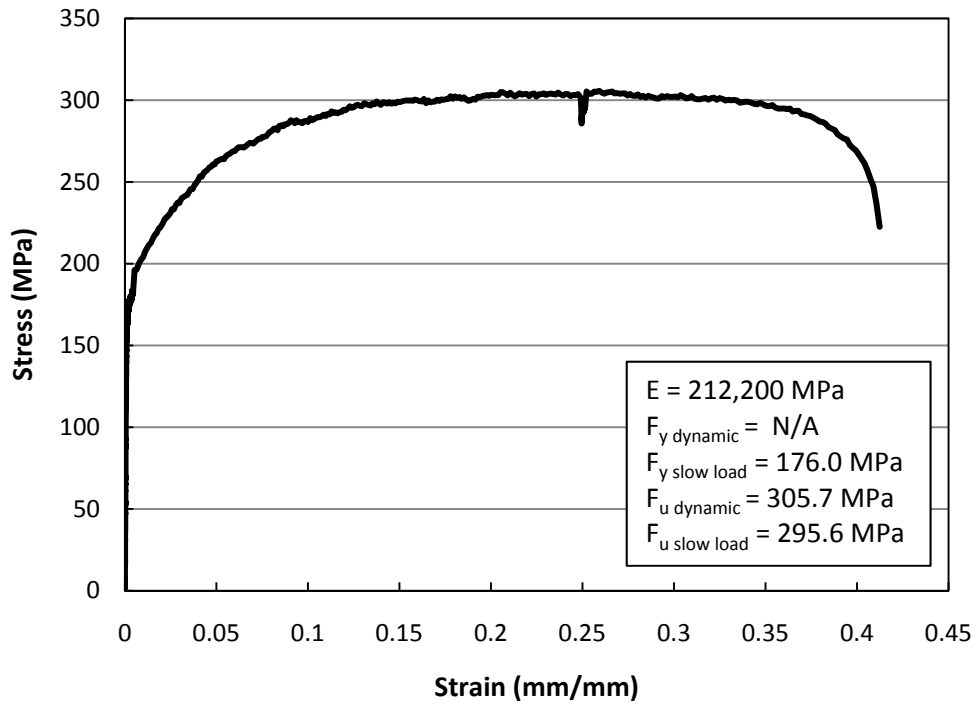


Figure A-16: Tension Coupon B10



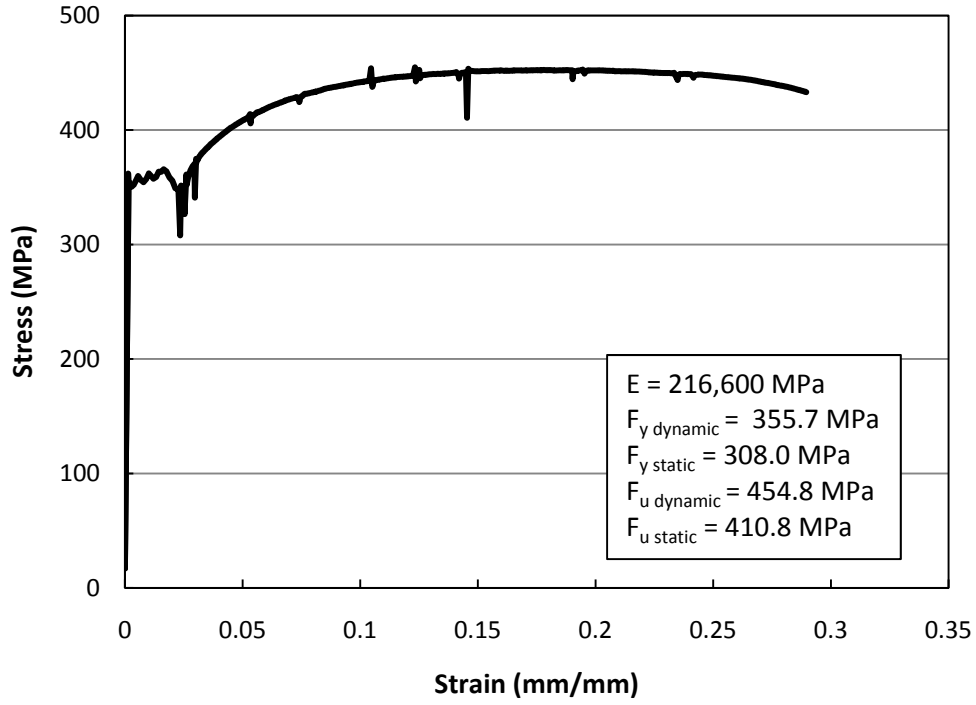


Figure A-17: Tension Coupon C1-F

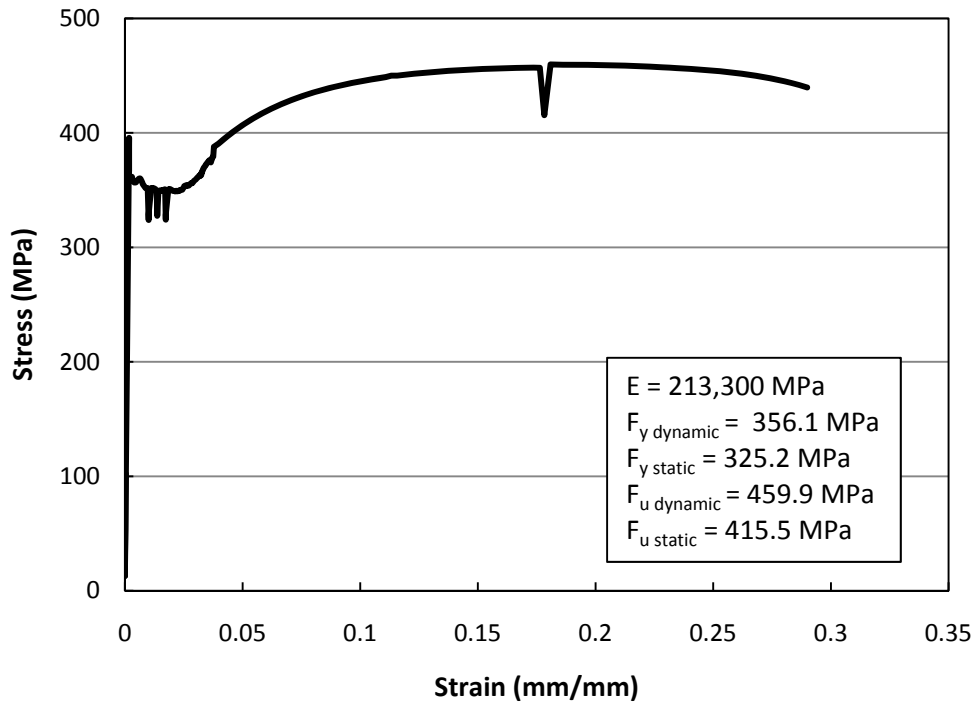


Figure A-18: Tension Coupon C2-F

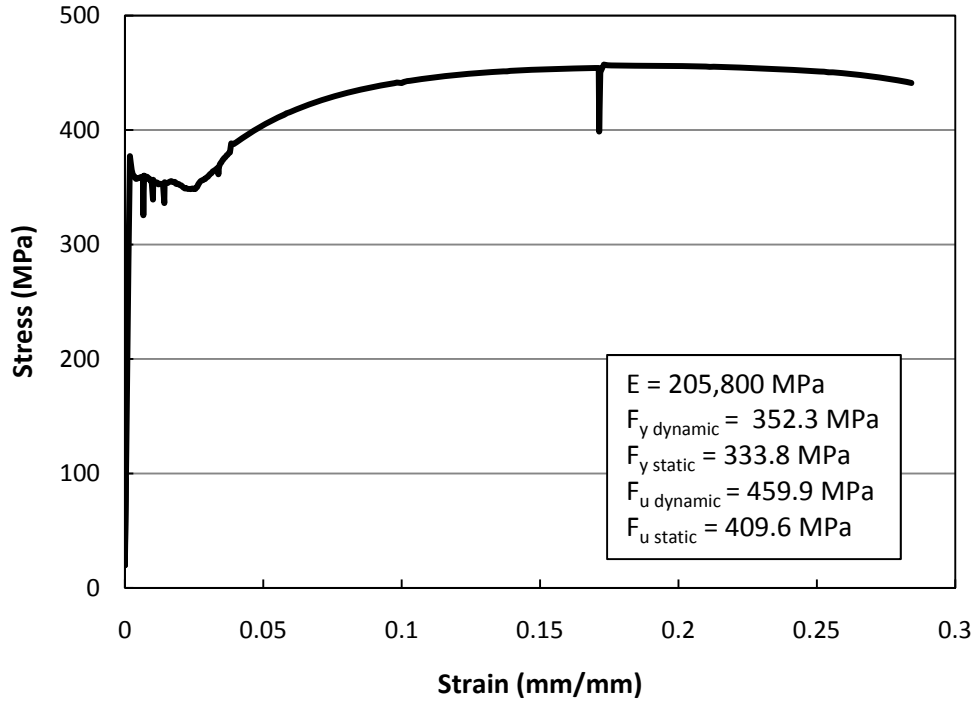


Figure A-19: Tension Coupon C3-F

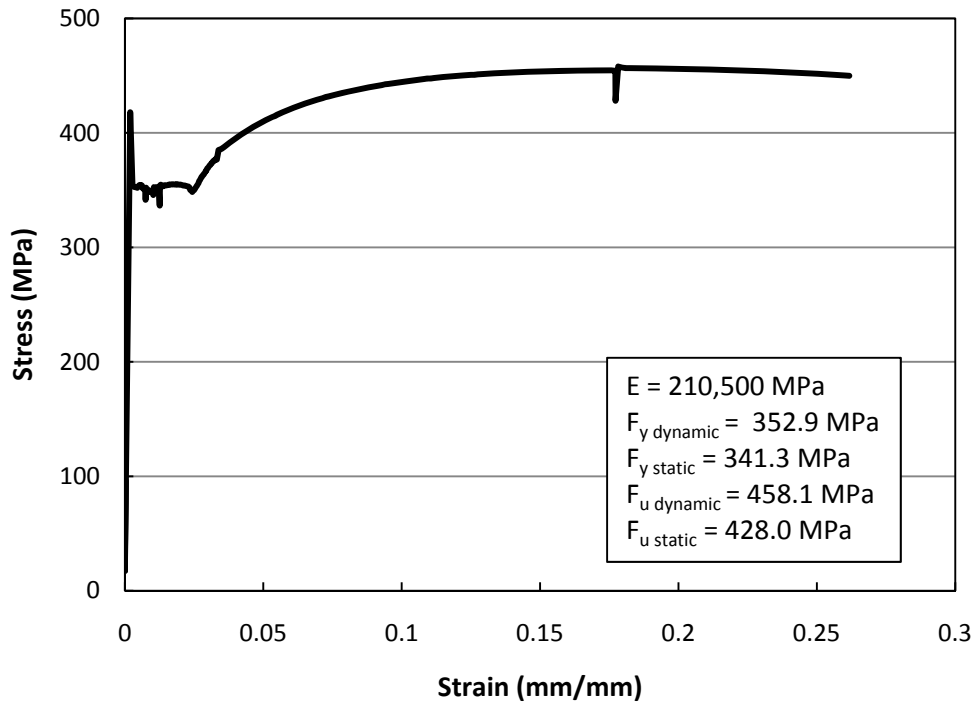


Figure A-20: Tension Coupon C4-F

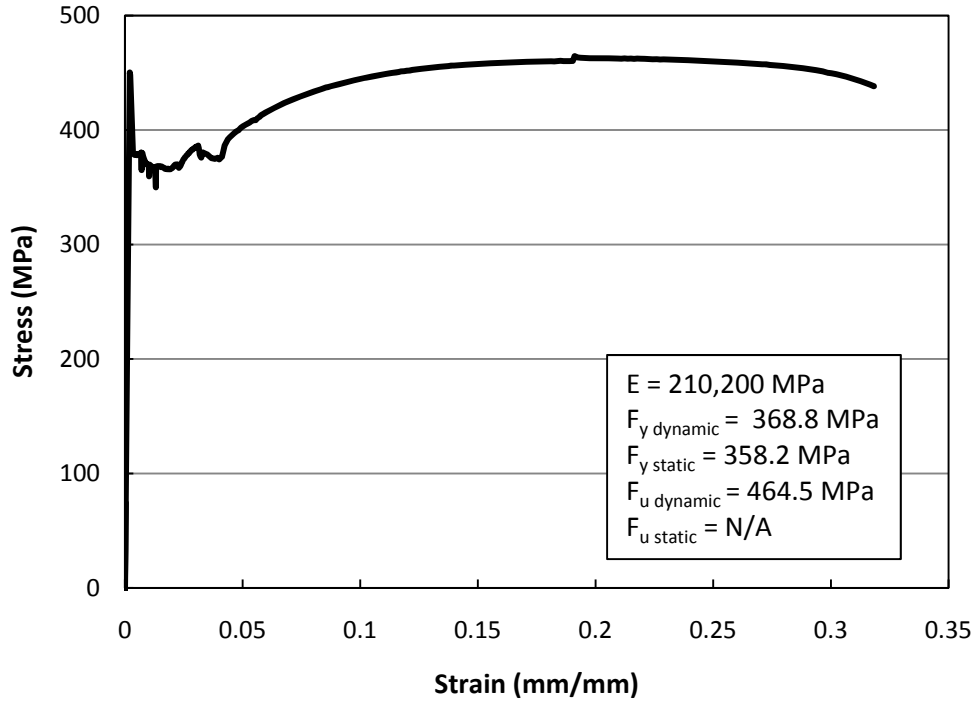


Figure A-21: Tension Coupon C5-W

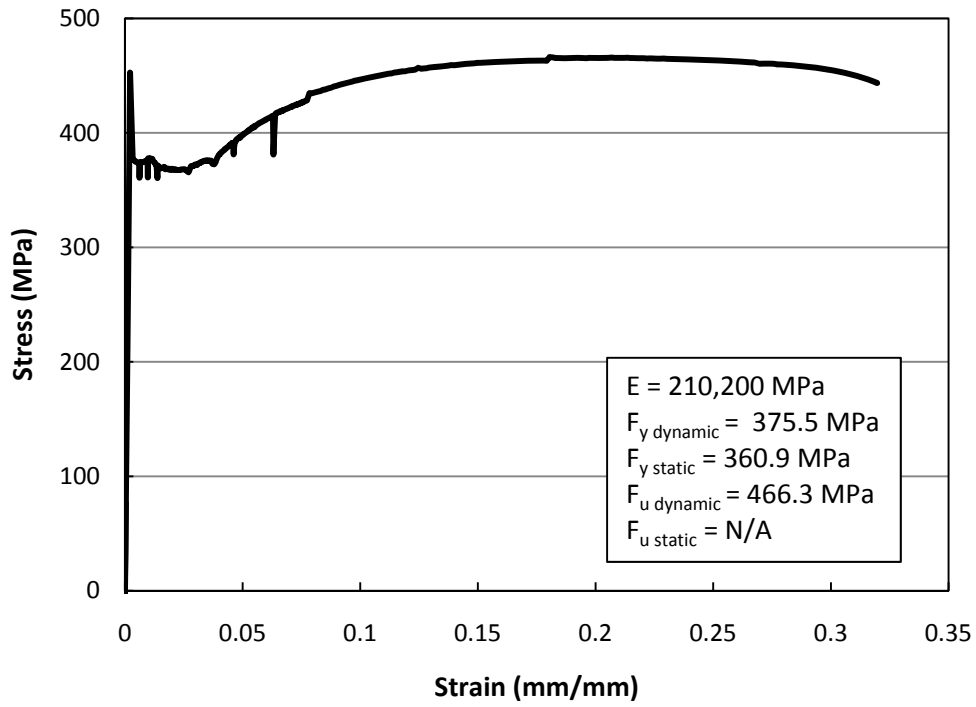


Figure A-22: Tension Coupon C6-W

#### **A4 Mill Certificates**

Photocopies of mill certificates containing chemical compositions and yield and ultimate strength results are presented in the following pages.

Mill certificates were obtained for the following materials:

- 20 gauge thick A1008 sheet steel used in the mechanical weld tests discussed in Chapter 4 and Chapter 5, and also used for the infill panel in the SPSW specimen
- 6 mm thick 300W “fish plate” portion of the infill panel-to-fish plate connection in the mechanical weld tests discussed in Chapter 4 and Chapter 5
- W200x31 used for columns and beams in the SPSW specimen
- 76mm thick 300W steel plate used as a base plate in the SPSW specimen

Mill certificates were not available for the following materials:

- 6 mm thick 300W steel plate used for fish plates in the SPSW specimen
- Miscellaneous steel plates used in the SPSW specimen, including stiffening plates at the base of columns, and continuity plates and doubler plates at the beam-to-column connection
- 51 mm thick 300W steel plate used for the load transfer plate which connected the hydraulic jack assembly to the SPSW specimen



New Zealand Steel Plant  
 31 Mission Bush Road, 2010-2011 South Auckland  
 Postal Private Bag 90721, Auckland 1142 New Zealand  
 Telephone: 09 275 8000 / 273 9111 Auckland  
 09 225 8000 / 225 2500 Waiuku  
 Fax: 09 275 8888

**TEST CERTIFICATE**

Ref: 02200493

CUSTOMER		William Steel & Mesh - Vancouver		SPECIFICATION		ASTMA1008 L5 Type A		CERTIFICATE No		TCL74914																		
CUSTOMER ON		100194		USER REF		PR01301801		PRODUCT		FLAT WIDE COIL																		
MILL ON		641197		DIMENSIONS		0.023" X 48" X (W)		DATE		12 May 2008																		
PACK NUMBER	HEAT No	CHEMICAL COMPOSITION PERCENT										MECHANICAL TESTS (TEST SPECIFICATION - ASTMA1070)																
		C	Si	Mn	P	S	Ca	Ni	Cr	Mo	V	NO	T	AL	B	CU	CEI	BEND	YIELD	T.S.	%ELONG	HARDNESS	1	LENGTH				
		x100										x1000					x1000		x100		180°					HRB	( )	(mm)
379-022017-00	666585	4	1	18	9	18	12	18	9	1	3	1	1					Pass			41				2657			
379-022018-00	666585	4	1	18	9	18	12	18	9	1	3	1	1					Pass			41				2661			
379-022019-00	666585	4	1	18	9	18	12	18	9	1	3	1	1					Pass			35				2605			
379-022020-00	666585	4	1	18	9	18	12	18	9	1	3	1	1					Pass			35				2664			

CHEM COMP % S (TR) = 0.01%	YIELD (A) 0.2% PROOF STRESS (B) LOWER YIELD STRESS	GAUGE LENGTH (G.L.)		PLASTIC STRAIN RATIO (r)		IMPACT TEST (A) 10mm x 10mm (B) 7.5mm x 10mm	(C) 5mm x 5mm (D) 2.5mm x 10mm (E) 5mm x 10mm	CARBON EQUIVALENT VALUE (CE) (A) C-MnS (B) C-MnS+(Cu+Ni)S (C) C-MnS-Si (D) C-MnS-Si
		(A) 200mm (B) 50mm	(C) 80mm (D) 5.65 * So	(A) 0 (B) 0.005	(C) 1.5 (D) 0.9 + 0.2 * S / 4			

WE HEREBY CERTIFY THAT THE MATERIAL DESCRIBED HEREIN HAS BEEN TESTED AND INSPECTED WITH SATISFACTORY RESULTS IN ACCORDANCE WITH THE REQUIREMENTS OF THE ABOVE SPECIFICATION

APPROVED *Satish Misra*  
 SENIOR METALLURGIST

Figure A-23: Mill Certificate - 20 Gauge, A1008 Sheet Steel Used in Infill Panel (Heat 666585)



New Zealand Steel Limited  
 31 Mission Bush Road, Gimblett, South Auckland  
 Postal - Private Bag 90131, Auckland 1142 New Zealand  
 Telephones: (09) 375 8888 / 375 8111 Auckland  
 (06) 335 8888 / 232 2835 Waikato  
 Fax: (09) 375 8888

**TEST CERTIFICATE**

Ref: 82550488

CUSTOMER		William Steel & Metals - Vancouver										SPECIFICATION										ASTMA1008 CS Type A										CERTIFICATE No		TC174914													
CUSTOMER ON		102154		USER REF		P021AD1001		PRODUCT		CRA WIDE COIL		PAGE		1 of 1		DATE		12 May 2008																													
MILL ON		431195		DIMENSIONS		0.033" x 48" x Coil		MECHANICAL TESTS (TEST SPECIFICATION -		ASTMA370																																					
PACK NUMBER		HEAT No		CHEMICAL COMPOSITION PERCENT										MECHANICAL TESTS (TEST SPECIFICATION -										ASTMA370																							
				C		S		Mn		P		S		Cu		Ni		Cr		Mo		V		Nb		Ti		Al		B		N		CE		DEND		YIELD		T.S		TENSILE		HARDNESS		LENGTH	
				x100																																											
R9-S23017-00		666585		4		1		18		9		18		12		18		9		1		3		1		1										Pass				41		2657					
R9-S23018-00		666585		4		1		18		9		18		12		18		9		1		3		1		1										Pass				41		2661					
R9-S23019-00		666585		4		1		18		9		18		12		18		9		1		3		1		1										Pass				35		2605					
R9-S23020-00		666585		4		1		18		9		18		12		18		9		1		3		1		1										Pass				35		2664					

CHEM. COMP % S (TR) < 0.01%	YIELD (A)=0.2% PROOF STRESS (B)=LOWER YIELD STRESS	GAUGE LENGTH (G.L.) (A)=200mm (C)=80mm (B)=50mm (D)=5.65 + 5σ	PLASTIC STRAIN RATIO (r) (A)=0 (C)=45 (B)=90 (D)=10+190+245 / 4	IMPACT TEST (A)=10mm x 10mm (B)=7.5mm x 10mm	(C)=5mm x 5mm (D)=2.5mm x 10mm (E)=5mm x 10mm	CARBON EQUIVALENT VALUE (CE) (A)=C+MnS (B)=C+MnS+(Cu+V+Mo)S+(Cu+Ni)S (C)=C+MnS+Si/24 (D)=
--------------------------------	--	---	---	--	---	---

WE HEREBY CERTIFY THAT THE MATERIAL DESCRIBED HEREIN HAS BEEN TESTED AND INSPECTED  
 WITH SATISFACTORY RESULTS IN ACCORDANCE WITH THE REQUIREMENTS OF THE ABOVE SPECIFICATION

APPROVED *Satish Misra*  
 SENIOR METALLURIST

Figure A-24: Mill Certificate - 20 Gauge, A1008 Steel Sheet Used in Infill Panel (Heat 666585)



New Zealand Steel Limited  
 111 Western Drive Road, Clarendon, South Auckland  
 Phone: (09) 375 0800 / 375 1111 Auckland  
 Telephones: (09) 375 0800 / 375 1111 Auckland  
 (09) 338 1825 / 338 3535 Waikato  
 Fax: (09) 375 1858

**TEST CERTIFICATE**

Ref: TSC350026

CUSTOMER	Wilkinson Steel & Metals - Vancouver		SPECIFICATION	CSA G40.21 44W	CERTIFICATE No	TC163863																
CUSTOMER Ord	101687	USER REF	F70921402004	PRODUCT	HOT ROLLED COIL	PAGE	1 of 1															
MILL Ord	620610	DIMENSIONS		0.25" x 48" x C68	DATE	14 November 2007																
PACK NUMBER	HEAT No	CHEMICAL COMPOSITION PERCENT											MECHANICAL TESTS (TEST SPECIFICATION - AS1151, AS1505)									
		C	Si	Mn	P	S	Cu	Ni	Cr	Mo	V	Nb	Ti	Al	B	NZ	CE (1)	BEND	YFLD	T.S.	%ELONG	HARDNESS
		x100											x10000									
III-935076-00	662923	18	1	60	14	23								51				56700	73100	32		820
III-935077-00	662923	18	1	60	14	23								51				56700	73100	32		820
III-935078-00	662923	18	1	60	14	23								51				56700	73100	32		817

YIELD (A)-0.2% PROOF STRESS (B)-LOWER YIELD STRESS	GUAGE LENGTH (G.L.) (A)-200mm (B)-50mm	PLASTIC STRAIN RATIO (S) (A)-R <sub>0.2</sub> (B)-R <sub>0.5</sub> (C)-R <sub>1.5</sub> (D)-R <sub>2.0</sub>	IMPACT TEST (A)-10mm x 10mm (B)-7.5mm x 10mm	CARBON EQUIVALENT VALUE (CE) (A)C+Mn/6 (B)C+Mn/6+(Cr+Ni)/5+(Cu)/15
(C)-90mm (D)-5.65 y 80	(E)-12"	(E)-R <sub>0.5</sub>	(C)-5mm x 5mm (D)-2.5mm x 10mm (E)-5mm x 10mm	(C)-C+Mn/6+5/100 (D)

WE HEREBY CERTIFY THAT THE MATERIAL DESCRIBED HEREIN HAS BEEN TESTED AND INSPECTED WITH SATISFACTORY RESULTS IN ACCORDANCE WITH THE REQUIREMENTS OF THE ABOVE SPECIFICATION

APPROVED *Antish Mirov*  
 ZPRAVOR METAL LIMITED

Figure A-25: Mill Certificate - 6 mm Thick 300W Fish Plate Material Used in Mechanical Tests of Chapter 4 and Chapter 5

\*\*LAND 15  
 NUCOR STEEL - BERKELEY  
 P.O. Box 2259  
 Mt. Pleasant, S.C. 29464  
 Phone: (843) 336-6000

MILL TEST REPORT

12/15/08 10:17:10  
 100% MELTED AND MANUFACTURED IN THE USA  
 All beams produced by Nucor-Berkeley are cast and rolled to a fully killed and fine grain practice.

Sold To: RUSSEL METALS, INC.  
 P.O. BOX 4128  
 EDMONTON, AB T6E 4T2

Ship To: RUSSEL METALS  
 2451 - 76TH AVE  
 EDMONTON, AB T6P 1P6

Customer #: 2914 - 2  
 Customer PO: M61031896  
 B.O.L. #: 729132  
 Invoice #: 1064462

SPECIFICATIONS: Tested in accordance with ASTM specification A6/A6M and A370.  
 AASHTO : M270-50-05  
 ASTM : A992-06a/A36-08/A572-07-50/A709-08 50/A709-345M

Description	Heat# Grade(s) Test	Yield/ Tensile Ratio	Yield (PSI) (MPa)	Tensile (PSI) (MPa)	Elong %	C Cr *****	Mn Mo *****	P Sn *****	S B *****	Si V N	Cu Nb *****	Ni ***** CI	CE1	CE2	Pcm.
													.23	.2793	.1336
W8X21 040' 00.00" W200X31.3 012.1920m	2815317 A992-06a	.82	57000 393	69300 478	25.68	.06 .03	.86 .01	.006 .0095	.024 .0004	.21 .002	.19 .026	.05	.23	.2793	.1336
10 Piece(s)															
W8X21 040' 00.00" W200X31.3 012.1920m	2816023 A992-06a	.83	57000 393	68500 472	25.03	.06 .03	.82 .00	.007 .0072	.031 .0002	.19 .003	.13 .033	.04	.22	.2673	.1275
10 Piece(s)															
W8X21 040' 00.00" W200X31.3 012.1920m	1806372 A992-06a	.83	57300 395	69100 476	27.51	.06 .02	.80 .02	.007 .0048	.024 .0000	.21 .002	.08 .025	.03	.21	.2590	.1219
10 Piece(s)															
W8X21 045' 00.00" W200X31.3 013.7160m	1806372 A992-06a	.83	57300 395	69100 476	27.51	.06 .02	.80 .02	.007 .0048	.024 .0000	.21 .002	.08 .025	.03	.21	.2590	.1219
10 Piece(s)															

Elongation based on 8" (20.32cm) gauge length. 'No Weld Repair' was performed. Hg free and no contact with Hg during manufacture.  
 CI = 26.01Cu+3.88Ni+1.20Cr+1.49Si+17.28P-(7.29Cu\*Ni)-(9.10Ni\*P)-33.39(Cu\*Cu) CE1 = C+(Mn/6)+((Cr+Mo+V)/5)+((Ni+Cu)/15)  
 Pcm = C+(Si/30)+(Mn/20)+(Cu/20)+(Ni/60)+(Cr/20)+(Mo/15)+(V/10)+5B CE2 = C+((Mn+Si)/6)+((Cr+Mo+V+Cb)/5)+((Ni+Cu)/15)

I hereby certify that the contents of this report are accurate and correct. All test results and operations performed by the material manufacturer are in compliance with material specifications, and when designated by the Purchaser, meet applicable specifications.

Bruce A. Work  
 Metallurgist

Figure A-26: Mill Certificate - Grade 350W W200x31 (Imperial Equivalent) Used in Beam and Columns of SPSW Specimen (Heat 1806372)

Appendix A: Materials Data



\*\*LAND 15  
 NUCOR STEEL - BERKELEY  
 P.O. Box 2259  
 Mt. Pleasant, S.C. 29464  
 Phone: (843) 336-6000

MILL TEST REPORT

12/15/08 10:17:10  
 100% MELTED AND MANUFACTURED IN THE USA  
 All beams produced by Nucor-Berkeley are cast and  
 rolled to a fully killed and fine grain practice.

Sold To: RUSSEL METALS, INC.  
 P.O. BOX 4128  
 EDMONTON, AB T6E 4T2

Ship To: RUSSEL METALS  
 2451 - 76TH AVE  
 EDMONTON, AB T6P 1P6

Customer #.: 2914 - 2  
 Customer PO: M61031896  
 B.O.L. #...: 729132  
 Invoice #...: 1064462

SPECIFICATIONS: Tested in accordance with ASTM specification A6/A6M and A370.  
 AASHTO : M270-50-05  
 ASTM : A992-06a:A36-08/A572-07-50/A709-08 50/A709-345M

Description	Heat# Grade(s) Test	Yield/ Tensile Ratio	Yield (PSI)	Tensile (PSI)	Elong (%)	C	Mn	P	S	Si	Cu	Ni	CE1
						Cr	Mo	Sn	B	V	Nb	CI	CE2
WBX21	2815321	.83	57900	69600	26.75	.06	.83	.008	.023	.21	.18	.05	.23
050' 00.00"	A992-06a		399	480		.03	.00	.0078	.0002	.003	.032		.2759
W200X31.3		.83	58500	70500	27.49					.0054		4.29	.1309
015.2400m			403	486		20 Piece(s)							
WBX21	2816025	.84	57800	69000	28.20	.06	.82	.006	.033	.23	.13	.04	.22
050' 00.00"	A992-06a		399	476		.02	.00	.0075	.0002	.002	.029		.2689
W200X31.3		.83	57100	68900	25.76					.0044		3.59	.1257
015.2400m			394	475		10 Piece(s)							

6 Heat(s) for this MTR.

Elongation based on 8" (20.32cm) gauge length. 'No Weld Repair' was performed.  
 CI = 26.01Cu+3.88Ni+1.20Cr+1.49Si+17.28P-(7.29Cu+Ni)-(9.10Ni\*P)-33.39(Cu\*Cu) CE1 = C+(Mn/6)+((Cr+Mo+V)/5)+((Ni+Cu)/15)  
 Pcm = C+(Si/30)+(Mn/20)+(Cu/20)+(Ni/60)+(Cr/20)+(Mo/15)+(V/10)+5B CE2 = C+((Mn+Si)/6)+((Cr+Mo+V+Cb)/5)+((Ni+Cu)/15)

I hereby certify that the contents of this report are accurate and correct. All test results and operations performed by the material manufacturer are in compliance with material specifications, and when designated by the Purchaser, meet applicable specifications.  
 \*\*END

Bruce A. Work  
 Metallurgist

Figure A-27: Mill Certificate - Grade 350W W200x31 (Imperial Equivalent) Used for Beam and Columns in SPSW Specimen (Heat 1806372)



## Appendix B: Weld Process Development, Supplementary Data

### B1 Introduction

This appendix includes three sections; section B2 presents a detailed calculation of hot cracking susceptibility based on the electrode maximum chemistry, section B3 presents the detailed calculation of hydrogen cracking likelihood based on the base metal maximum chemistry, and section B4 contains a detailed table documenting parameters and observations for each of the trial weld specimens used for weld parameter development.

### B2 Electrode Maximum Chemistry and Hot Cracking Check

As discussed in Chapter 3, Patchett (2003) presents equation 3.2 as a measure of susceptibility to hot cracking. A value of 4 or greater indicates a susceptible electrode.

$$[3.2] \quad HCS = \frac{\%C * (\%S + \%P + \frac{\%Si}{25} + \frac{\%Ni}{100})}{3 * \%Mn + \%Cr + \%Mo + \%V} * 10^3$$

The specified maximum chemical composition of the ER70S-6 electrode is shown in Table B-1.

**Table B-1: Maximum Chemical Composition of ER70S-6 Electrode**

Element	AWS A5.18 ER70S-6 Electrode
C	0.15
Mn	1.40 – 1.85
P	0.025
S	0.035
Si	0.80 – 1.15
Cu	0.050
Ni	0.15
Cr	0.15
Mo	0.15
V	0.030

When the maximum of these values are used in numerator of equation 3.2 and the minimum values are used in the denominator (i.e. Cr, Mo, and V are taken as zero, while Mn is taken at 1.40%), a value of 3.84 is obtained. Since the hot cracking index is less than 4, this electrode has a low risk of hot cracking.

### B3 Base Metal Maximum Chemistries and Hydrogen Cracking Check

For the infill panel-to-fish plate connection, since medium carbon steel is being used, it is advisable to check the risk of hydrogen cracking. The use of carbon equivalent (*CE*) as a measure of the susceptibility to hydrogen cracking is a widely accepted method. The

carbon equivalent equation from CSA W59-03 is shown in Equation 3.3, and the maximum chemical compositions of the two steels in the joint are shown in Table B-2.

$$[3.3] \quad CE = C + \left(\frac{Mn + Si}{6}\right) + \left(\frac{Cr + Mo + V}{5}\right) + \left(\frac{Ni + Cu}{15}\right)$$

**Table B-2: Maximum Chemical Composition of Base Metals Being Welded**

Element	CSA G40.21 Grade 300W Structural Steel	ASTM A1008 Grade CS Type A Sheet Steel
<b>C</b>	<b>0.22</b>	<b>0.10</b>
<b>Mn</b>	<b>0.5 – 1.5</b>	<b>0.60</b>
<b>P</b>	<b>0.04</b>	<b>0.030</b>
<b>S</b>	<b>0.05</b>	<b>0.035</b>
<b>Si</b>	<b>0.4</b>	<b>N/A</b>
<b>Cu</b>	<b>N/A</b>	<b>0.20</b>
<b>Ni</b>	<b>N/A</b>	<b>0.20</b>
<b>Cr</b>	<b>N/A</b>	<b>0.15</b>
<b>Mo</b>	<b>N/A</b>	<b>0.06</b>
<b>V</b>	<b>V + Cb &lt;= 0.10</b>	<b>0.008</b>
<b>Cb</b>		<b>0.008</b>
<b>Ti</b>	<b>N/A</b>	<b>0.025</b>

The carbon equivalent of the 300W steel is 0.56, while the maximum carbon equivalent of the A1008 steel is 0.27. It is clear that the 300W steel is the governing base metal, since it has higher carbon equivalent and is thicker (6 mm fish plate versus 0.9 mm infill panel). Table 5.3 of CSA W59-03 shows that 300W steel plates less than 20 mm thick, using clean GMAW weld process, no preheat is required to avoid cold cracking. Thus no preheat is required for the welded joint being investigated.

CSA W59-03 Appendix P: Guideline and Commentary on Alternative Methods for Determining Preheat (CSA, 2003) provides a detailed procedure to correlate the hydrogen cracking risk based on carbon equivalent, hydrogen content of the welding process, restraint of the joint, and part thickness. This procedure also indicates that no preheat is required for the joint under investigation.

**B4 Detailed Results, Visual Inspection of Trial Welds**

**Table B-3: Detailed Results, Visual Inspection of Trial Welds**

Spec. No. <sup>1</sup>	Welding Technician <sup>2</sup>	Welding Equipment <sup>3</sup>	Weld Location <sup>4</sup>	Gas Composition [%Ar] <sup>5</sup>	Gas Flow Rate [ft <sup>3</sup> /hr] <sup>6</sup>	Voltage [V] <sup>7</sup>	Current [A] <sup>8</sup>	Wire Feed Speed [ipm] <sup>9</sup>	Gauge Length of Timed Weld [mm] <sup>10</sup>	Time to Weld Gauge Length [s] <sup>11</sup>	Velocity [m/s] <sup>12</sup>	Nominal Unit Heat Input [kJ/m] <sup>13</sup>	Hand Motion <sup>14</sup>	Observations <sup>15</sup>
0	Sean	Setup #1	W #2	75Ar/25CO <sub>2</sub>	15	21.0	-----	5 or 10	N/A	N/A	N/A	N/A	straight push or pull	<ul style="list-style-type: none"> <li>Weld profile = more "bead on plate" than "triangular fillet"</li> <li>Inconsistent weld width and thickness</li> <li>Bend test = failure in sheet steel after numerous repetitions indicates a good bond</li> </ul>
1	Sean	Setup #1	W #2	75Ar/25CO <sub>2</sub>	15	16.0	43	2 -> 10	N/A	N/A	N/A	N/A	straight push or pull	<ul style="list-style-type: none"> <li>Tried settings for 20 gauge sheet from the "Millermatic Calculator" for welding two sheets of 20 gauge sheet together</li> <li>Consistent weld profile at WFS #2</li> <li>Some weld toe undercut</li> <li>Bead profile is very tall and narrow, consistent with high Ar gas mix</li> </ul>
2	Sean	Setup #1	W #2	75Ar/25CO <sub>2</sub>	15	21.0	-----	2	N/A	N/A	N/A	N/A	straight push or pull	<ul style="list-style-type: none"> <li>Varied angle of gun from horizontal (0°) to vertical (90°)</li> <li>No significant difference in weld shape</li> <li>Flat (0°) not recommended as heat is directed towards thin sheet</li> </ul>
3	Sean	Setup #1	W#2	75Ar/25CO <sub>2</sub>	15	16.0	43	2	N/A	N/A	N/A	N/A	45° angle straight push	<ul style="list-style-type: none"> <li>Cut out a cross-section of specimen to observe</li> <li>Bead is narrow and tall in shape</li> <li>Lack of fusion between weld and thick (1/4") PL; weld too cold</li> </ul>
3	Sean	Setup #1	W#1	75Ar/25CO <sub>2</sub>	15	16.0	43	2	N/A	N/A	N/A	N/A	45° angle straight push	<ul style="list-style-type: none"> <li>Bend test demonstrates good performance of weld #1</li> <li>Tall narrow bead profile</li> <li>Small void at the root of the weld results from plastic deformation of 1/4" PL during shearing</li> <li>Some undercut</li> </ul>
4	Sean	Setup #1	W #2	75Ar/25CO <sub>2</sub>	30	16.0	43	2	N/A	N/A	N/A	N/A	straight push or pull	<ul style="list-style-type: none"> <li>Compare push vs. pull weld technique</li> <li>No visually obvious difference in final weld appearance</li> <li>Welding technician indicates push or pull technique does not perceptibly alter weld difficulty</li> </ul>
5	Clerk	Setup #1	W#2	75Ar/25CO <sub>2</sub>	N/A	22.5	85	3.5	100	7.3	0.014	139	straight push or pull	<ul style="list-style-type: none"> <li>High bead profile from Ar gas - recommend switch to 100% CO<sub>2</sub></li> <li>High angular distortion opens a gap transverse to the weld, making Weld #1 difficult to install</li> <li>Some buckling distortion is also present, and could open a gap in front of the weld pool</li> <li>Heat input per unit length and weld size should be reduced</li> <li>The electrode size is the smallest available, and we already have large welds; there is no sense in using a larger electrode</li> <li>Welding tip from Clerk - aim arc towards thick plate.</li> </ul>

**Table B-3 (continued): Detailed Results, Visual Inspection of Trial Welds**

Spec. No. <sup>1</sup>	Welding Technician <sup>2</sup>	Welding Equipment <sup>3</sup>	Weld Location <sup>4</sup>	Gas Composition [%] <sup>5</sup>	Gas Flow Rate [ft <sup>3</sup> /hr] <sup>6</sup>	Voltage [V] <sup>7</sup>	Current [A] <sup>8</sup>	Wire Feed Speed [ipm] <sup>9</sup>	Gauge Length of Tined Weld [mm] <sup>10</sup>	Time to Weld Gauge Length [s] <sup>11</sup>	Velocity [m/s] <sup>12</sup>	Nominal Unit Heat Input [kJ/m] <sup>13</sup>	Hand Motion <sup>14</sup>	Observations <sup>15</sup>
5	Clark	Setup #1	W#1	75Ar/ 25CO <sub>2</sub>	N/A	22.5	85	3.5	100	9.6	0.010	183	straight: push or pull	<ul style="list-style-type: none"> <li>Heat input is too high; burn through of thin sheet is evident</li> <li>Weld bead profile is slightly concave</li> <li>Angular distortion of thin sheet from contraction of weld metal is extremely evident</li> </ul>
6	Clark	Setup #1	W#2	100CO <sub>2</sub>	22	20.5	59	2.5	100	16.1	0.006	195	straight: push or pull	<ul style="list-style-type: none"> <li>Much flatter bead profile than with 75Ar/25CO<sub>2</sub>, good tie-in, reduced undercut</li> <li>Good "bacon - frying" short - circuit sound</li> </ul>
6	Clark	Setup #1	W#1	100CO <sub>2</sub>	22	20.5	52	2.5	50	15.3	0.003	325	straight: push or pull	<ul style="list-style-type: none"> <li>Buckling distortion from Weld#2 caused a gap to open at Weld #1 filling the gap slows the welding, and increases unit heat input as more material is deposited, resulting in large burnthrough of the thin sheet. Weld terminated prematurely as a result.</li> </ul>
7	Sean	Setup #1	W#2	100CO <sub>2</sub>	22	20.5	56	2.5	95	20.2	0.005	244	straight: push or pull	<ul style="list-style-type: none"> <li>Identical settings to specimen #6, but Sean welding instead of Clark</li> <li>Note: Welding halted at 95mm - slightly erratic wire feed speed necessitates adjustments in the feeder pressure setting</li> <li>Sean's slower speed = increased metal deposition, larger weld, larger profile</li> </ul>
8	Clark	Setup #1	W#2	100CO <sub>2</sub>	22	20.0	57	2.5	100	19.1	0.005	217	straight: push or pull	<ul style="list-style-type: none"> <li>Weld profile = smaller than Sean's, but some variation in thickness of bead</li> <li>Welders complain of wandering arc as compared with 75Ar/25CO<sub>2</sub> gas</li> </ul>
9	Clark	Setup #1	W#2	100CO <sub>2</sub>	22	20.0	59	2.5	100	20.0	0.005	236	straight: push or pull	<ul style="list-style-type: none"> <li>Nice weld, uniform thickness and profile, low spatter.</li> <li>Some small angular distortion.</li> </ul>
9	Clark	Setup #1	W#1	100CO <sub>2</sub>	22	20.0	55	2.5	64	14.6	0.004	255	straight: push or pull	<ul style="list-style-type: none"> <li>A tack weld is placed at the midpoint of the specimen, and Clark attempts to carry his fillet weld around/through it.</li> <li>In order to tie-in to the tack weld, the welder slows down and heat increases. The distortion gap that opened in front of the weld bead was about 2mm large, and welding could not continue.</li> </ul>
10	Clark	Setup #1	W#2	100CO <sub>2</sub>	22	18.0	46	1.9	100	30.2	0.003	250	straight: push or pull	<ul style="list-style-type: none"> <li>Low voltage = shorter arc length, more shorting out or "stubbing" of the electrode. Frequent stops and starts.</li> <li>Lots of arc wander, and the weld line strays from the target of the thin sheet - to - thick plate contact surface</li> </ul>
10	Clark	Setup #1	W#1	100CO <sub>2</sub>	22	18.0	43	1.9	100	19.2	0.005	148	straight: push or pull	<ul style="list-style-type: none"> <li>Tack at midpoint of welded region identical to Weld #1 on specimen #9</li> <li>Same problems as #9 - high distortion at the tack</li> <li>Increased speed to reduce heat input = ugly weld; pitting, insufficient deposition, inconsistent profile</li> </ul>

**Table B-3 (continued): Detailed Results, Visual Inspection of Trial Welds**

Spec. No. <sup>1</sup>	Welding Technician <sup>2</sup>	Welding Equipment <sup>3</sup>	Weld Location <sup>4</sup>	Gas Composition [%] <sup>5</sup>	Gas Flow Rate [ft <sup>3</sup> /hr] <sup>6</sup>	Voltage [V] <sup>7</sup>	Current [A] <sup>8</sup>	Wire Feed Speed [ipm] <sup>9</sup>	Gauge Length of Tied Weld [mm] <sup>10</sup>	Time to Weld Gauge Length [s] <sup>11</sup>	Velocity [m/s] <sup>12</sup>	Nominal Unit Heat Input [kJ/m] <sup>13</sup>	Hand Motion <sup>14</sup>	Observations <sup>15</sup>
11	Clark	Setup #1	W#2	100CO <sub>2</sub>	22	19.5	62	2.3	100	19.2	0.005	232	straight push or pull	Larger specimen with several tack welds spaced at 75mm, weld continuously through tacks <ul style="list-style-type: none"> <li>Increased voltage compared with specimen #10 = enough heat to pass through tacks without slowing excessively</li> <li>Appears to work reasonably well, some slight undercut, good fusion</li> </ul>
11	Clark	Setup #1	W#1	100CO <sub>2</sub>	22	19.5	57	2.3	65	15.0	0.004	257	straight push or pull	Same settings and tack arrangement as #11, Weld #2 <ul style="list-style-type: none"> <li>Passing through second tack weld, had to slow down = increased heat, large distortion ahead of the weld bead, welding terminated prematurely</li> <li>Welding continuously over tacks does not appear ideal; we have had repeated problems</li> <li>If we stop at each tack, and start again, the tack provides a heat sink to reduce burn-through potential at arc initiation</li> </ul>
12	Clark	Setup #1	W#1	100CO <sub>2</sub>	22	19.5	55	2.3	67	13.5	0.005	216	straight push or pull	Four tack welds, three spans of roughly 3" between. Clark attempts a "leapfrog" (a.k.a "stitch welding") technique to reduce distortion <ul style="list-style-type: none"> <li>Encouraging result, good weld, fairly consistent heat input.</li> <li>Some slight buckling distortion</li> <li>It is difficult to quantify what a tolerable amount of distortion is with small, relatively unrestrained specimens</li> </ul>
13	Sean	Setup #2	W#2	100CO <sub>2</sub>	22	19.5	54	194	100	35.1	0.003	369	straight push or pull	Change from Welding Equipment Setup #1 to Welding Equipment Setup #2 <ul style="list-style-type: none"> <li>Welding Technician comments: the conventional gun is less bulky than small - spool mounted gun, bead easier to run smoothly.</li> <li>Large volume of weld metal deposited due to slow speed.</li> <li>Undercut evident on back side of weld (side furthest from thin sheet)</li> </ul>
14	Sean	Setup #2	W#2	100CO <sub>2</sub>	22	19.5	51	194	75	24.1	0.003	319	straight push or pull	Attempt same weld as #13, but with faster speed to reduce unit heat input and volume of weld metal deposited. <ul style="list-style-type: none"> <li>Feed issue with wire feeder at 3/4 of weld length; welding terminated. Wire feeder repaired.</li> </ul>
15	Sean	Setup #2	W#2	100CO <sub>2</sub>	22	19.5	55	200	100	19.6	0.005	211	straight push or pull	Similar approach to Specimen #15 <ul style="list-style-type: none"> <li>Good profile, consistency, appearance; promising weld settings.</li> </ul>
15	Sean	Setup #2	W#1	100CO <sub>2</sub>	22	19.5	55	200	100	20.7	0.005	222	straight push or pull	Three tacks, welding over two spans <ul style="list-style-type: none"> <li>Welded portion of the specimen is off the work table, i.e. no temporary heat sink behind specimen</li> <li>Middle tack slows welding; significant burn - through</li> <li>Great "bacon-fry" short-circuiting sound</li> </ul>

Table B-3 (continued): Detailed Results, Visual Inspection of Trial Welds

Spec. No. <sup>1</sup>	Welding Technician <sup>2</sup>	Welding Equipment <sup>3</sup>	Weld Location <sup>4</sup>	Gas Composition (%) <sup>5</sup>	Gas Flow Rate (ft <sup>3</sup> /hr) <sup>6</sup>	Voltage (V) <sup>7</sup>	Current (A) <sup>8</sup>	Wire Feed Speed (ipm) <sup>9</sup>	Gauge Length of Timed Weld (mm) <sup>10</sup>	Time to Weld Gauge Length (s) <sup>11</sup>	Velocity (m/s) <sup>12</sup>	Nominal Unit Heat Input (kJ/m) <sup>13</sup>	Hand Motion <sup>14</sup>	Observations <sup>15</sup>
16	Sean	Setup #2	W#1	100CO <sub>2</sub>	22	20.0	57	200	100	25.3	0.004	289	straight: push or pull	Ceramic chill strip used behind thin sheet; Clark indicates later that this is intended for the root pass of pipe welds and is actually not a very good choice for this application. Midpoint tack present in specimen <ul style="list-style-type: none"> <li>Significant burnthrough, visually unappealing weld</li> </ul>
16	Sean	Setup #2	W#2	100CO <sub>2</sub>	22	19.5	50	200	100	17.8	0.006	173	straight: push or pull	Trying for faster speed compared with Specimen #15 Weld #2; less material is deposited to reduce distortion. <ul style="list-style-type: none"> <li>Weld is visually acceptable, very similar to Specimen #15.</li> </ul>
17	Sean	Setup #2	W#2	100CO <sub>2</sub>	22	19.5	55	200	100	19.6	0.005	210	straight: push or pull	Identical settings to Specimen #15, trying to reproduce positive result <ul style="list-style-type: none"> <li>Consistent weld profile, rounded, smooth bead shape</li> <li>Visually appealing weld</li> </ul>
17	Sean	Setup #2	W#1	100CO <sub>2</sub>	22	20.0	55	200	100	33.1	0.003	354	straight: push or pull	No midpoint tack, ceramic chill strip used. <ul style="list-style-type: none"> <li>Slow speed = high heat, weld burns completely through thin sheet.</li> </ul>
18	Sean	Setup #2	W#2	100CO <sub>2</sub>	22	19.0	57	200	100	18.9	0.005	205	straight: push or pull	<ul style="list-style-type: none"> <li>Good consistency with the last few Weld #2 trials</li> <li>Nominal heat inputs are fairly close, suggesting repeatable results  Specimen #15, Weld #2 - 222 kJ/m  Specimen #16, Weld #2 - 173 kJ/m  Specimen #17, Weld #2 - 210 kJ/m  Specimen #18, Weld #2 - 205 kJ/m</li> </ul>
18	Sean	Setup #2	W#1	100CO <sub>2</sub>	22	19.5	55	200	100	24.5	0.004	263	straight: push or pull	No chill strip used <ul style="list-style-type: none"> <li>Significant burn - through of the thin sheet is visually unappealing</li> </ul>
19	Sean	Setup #2	W#3	100CO <sub>2</sub>	22	18.0	N/A	150	N/A	N/A	N/A	N/A	straight: push or pull	First of thin sheet - to - thin sheet trials. Chill strip used. <ul style="list-style-type: none"> <li>Lots of burn - through present. WFS of 150ipm is far too slow, and welder must slow down excessively to avoid stubbing, resulting in higher heat input per unit length of weld.</li> </ul>
20	Clark	Setup #2	W#3	100CO <sub>2</sub>	22	17.9	50	200	100	11.5	0.009	103	straight: push or pull	Chill strip used. Higher WFS and current than Specimen #19. <ul style="list-style-type: none"> <li>Good result. Nice profile, minimal heat input or burn - through.</li> </ul>
20	Clark	Setup #2	W#3 (other side)	100CO <sub>2</sub>	22	17.9	51	200	100	12.7	0.008	116	straight: push or pull	Same settings and positive result as previous weld. <ul style="list-style-type: none"> <li>Tip from Clark: use shears to cut the electrode tip off at a 45° angle. Arc initiation is faster and cleaner with a thin point on the electrode.</li> </ul>
21	Clark	Setup #2	W#3	100CO <sub>2</sub>	22	17.9	50	200	100	12.0	0.008	107	straight: push or pull	NO CHILL STRIP, just open air behind the weld site. <ul style="list-style-type: none"> <li>Weld can be done, but burn - through and distortion are significant, and the base metal adjacent to the weld appears significantly distressed.</li> </ul>



**Table B-3 (continued): Detailed Results, Visual Inspection of Trial Welds**

Spec. No. <sup>1</sup>	Welding Technician <sup>2</sup>	Welding Equipment <sup>3</sup>	Weld Location <sup>4</sup>	Gas Composition [%] <sup>5</sup>	Gas Flow Rate [ft <sup>3</sup> /hr] <sup>6</sup>	Voltage [V] <sup>7</sup>	Current [A] <sup>8</sup>	Wire Feed Speed [ipm] <sup>9</sup>	Gauge Length of Tied Weld [mm] <sup>10</sup>	Time to Weld Gauge Length [s] <sup>11</sup>	Velocity [m/s] <sup>12</sup>	Nominal Unit Heat Input [kJ/m] <sup>13</sup>	Hand Motion <sup>14</sup>	Observations <sup>15</sup>
21	Clark	Setup #2	W#3 (other side)	100CO <sub>2</sub>	22	17.9	51	200	100	16.5	0.006	151	straight push or pull	Identical procedure and results as previous weld.
22	Clark	Setup #2	W#3	100CO <sub>2</sub>	22	N/A	N/A	N/A	N/A	N/A	N/A	N/A	straight push or pull	Butt weld between two thin sheets as an alternate solution to the lap joint. • Fit - up is incredibly difficult. This would be totally unrealistic on a larger scale than the small 150mm x 150mm specimens in use. Do not pursue further.
23	Clark	Setup #2	W#2	100CO <sub>2</sub>	22	18.7	52	200	100	22.0	0.005	214	straight push or pull	• Good results. Confirmed weld settings for visually acceptable and weldable weld.
23	Clark	Setup #2	W#1	100CO <sub>2</sub>	22	19.0	52	200	100	25.0	0.004	247	straight push or pull	Chill strip used. • Good result. Positive that the same weld settings can be employed for both Weld #1 and Weld #2.
D1-Side 1	Clark	Setup #2	W#2	100CO <sub>2</sub>	22	19.0	N/A	200	Repeatable visually appealing welds have been obtained. Welding equipment set to those shown (Setup#2, Gas Composition and Flow, Voltage, Wire Feed Speed, Hand Motion) and held at these settings for all Distortion Specimens. No further monitoring of values contributing to nominal heat input is conducted.			straight push or pull	Tack weld every 75mm. Tack welding requires restraint provided by clamping to hold 20 gauge sheet tight against 6mm plate. After tack welding, hammer down edge of 20 gauge sheet to ensure it is flush with 6mm plate. Perform a continuous weld over all of the tacks (do not stop at each tack). • No distortion problems. • Tacks appear very large since weld metal volume at the tack location is effectively double. • Some spatter in the weld gun cup due to the short arc length; this is a classic drawback of GMAW-SC welding. • Welding technicians frequently complain that arc initiation is very slow and "stleky".	
D1-Side 2	Clark	Setup #2	W#2	100CO <sub>2</sub>	22	19.0	N/A	200				straight push or pull	Tack weld identical to D1-Side 1. Weld intervals between tacks by "backstepping"; weld one interval from left to right, then weld the interval immediately to the left of the first interval first interval, also from left to right. Continue in this manner until all welds are complete. • No distortion problems. • Tacks appear less large than in D1-Side 1 since welding stops at each tack. • Care must be taken to tie - in the weld metal to either side of tacks. The weld is terminated slightly behind the tack to ensure no burn through of the 20 gauge sheet during weld termination.	

**Table B-3 (continued): Detailed Results, Visual Inspection of Trial Welds**

Spec. No. <sup>1</sup>	Welding Technician <sup>2</sup>	Welding Equipment <sup>3</sup>	Weld Location <sup>4</sup>	Gas Composition [%] <sup>5</sup>	Gas Flow Rate [ft <sup>3</sup> /hr] <sup>6</sup>	Voltage [V] <sup>7</sup>	Current [A] <sup>8</sup>	Wire Feed Speed [ipm] <sup>9</sup>	Gauge Length of Tined Weld [mm] <sup>10</sup>	Time to Weld Gauge Length [s] <sup>11</sup>	Velocity [m/s] <sup>12</sup>	Nominal Unit Heat Input [kJ/m] <sup>13</sup>	Hand Motion <sup>14</sup>	Observations <sup>15</sup>
D1-Side 3	Clark	Setup #2	W#2	100CO <sub>2</sub>	22	19.0	N/A	200			-		straight push or pull	Tack weld identical to D1-Side 1. Weld intervals between tacks by "stitch welding"; weld one interval from left to right, then skip over the interval immediately to the right of the first interval, and weld the following interval from left to right. Continue in this manner until every second interval is welded. Then weld the remaining intervals. <ul style="list-style-type: none"> <li>Visual result is identical to D1-Side 2. There does not appear to be an appreciable difference between backstepping and stitch welding.</li> </ul>
D1-Side 4	Clark	Setup #2	W#2	100CO <sub>2</sub>	22	19.0	N/A	200			-		straight push or pull	Tack weld every 125mm. Weld intervals between tacks by "stitch welding" as described in D1-Side 3. <ul style="list-style-type: none"> <li>Distortion within 125mm lengths is excessive; a gap opens ahead of the weld pool which cannot be filled without slowing down and burning through the 20 gauge sheet. Recommend taking 75mm spacing between tack welds as the maximum.</li> </ul>
D1-Underside	Sean	Setup #2	W#1	100CO <sub>2</sub>	22	19.0	N/A	200			-		straight push or pull	Chill strip used. Tack weld every 75mm. Weld intervals between tacks by "stitch welding" as described in D1-Side 3. <ul style="list-style-type: none"> <li>Sean changes "soft start" button from "on" to "off". "soft start" is a power source regulating feature which gradually ramps up current during arc initiation. This appears to have been slowing the arc initiation, and resulting in some stubbing out. Welding technicians indicate arc initiation is much improved after this setting change.</li> <li>Overall excellent weld. Minimal burn-through, nice profile, and improved arc control.</li> </ul>
D2-Underside	Sean	Setup #2	W#1	100CO <sub>2</sub>	22	19.0	N/A	200			-		straight push or pull	Chill strip used. Tack weld every 75mm. Weld intervals between tacks by "stitch welding" as described in D1-Side 3. <ul style="list-style-type: none"> <li>Similarly satisfactory results as Specimen D1-Underside for weld #1.</li> <li>Angular distortion is significant!! Impossible to start weld #2, since 20 gauge sheet has buckled significantly and lifted away from 6mm steel plate. In future work on larger specimens, if two lines of welds are used, always tack weld both sides to restrain distortion prior to performing fillet welds.</li> </ul>

**Table B-3 (continued): Detailed Results, Visual Inspection of Trial Welds**

Spec. No. <sup>1</sup>	Welding Technician <sup>2</sup>	Welding Equipment <sup>3</sup>	Weld Location <sup>4</sup>	Gas Composition [%] <sup>5</sup>	Gas Flow Rate [ft <sup>3</sup> /min] <sup>6</sup>	Voltage [V] <sup>7</sup>	Current [A] <sup>8</sup>	Wire Feed Speed [ipm] <sup>9</sup>	Gauge Length of Tied Weld [mm] <sup>10</sup>	Time to Weld Gauge Length [s] <sup>11</sup>	Velocity [m/s] <sup>12</sup>	Nominal Unit Heat Input [kJ/m] <sup>13</sup>	Hand Motion <sup>14</sup>	Observations <sup>15</sup>
D1-Side 3	Clark	Setup #2	WR2	100CO <sub>2</sub>	22	19.0	N/A	200					straight push or pull	Tack weld identical to D1-Side 1. Weld intervals between tacks by "stitch welding"; weld one interval from left to right, then skip over the interval immediately to the right of the first interval, and weld the following interval from left to right. Continue in this manner until every second interval is welded. Then weld the remaining intervals. <ul style="list-style-type: none"> <li>Visual result is identical to D1-Side 2. There does not appear to be an appreciable difference between backstepping and stitch welding.</li> </ul>
D1-Side 4	Clark	Setup #2	WR2	100CO <sub>2</sub>	22	19.0	N/A	200					straight push or pull	Tack weld every 125mm. Weld intervals between tacks by "stitch welding" as described in D1-Side 3. <ul style="list-style-type: none"> <li>Distortion within 125mm lengths is excessive; a gap opens ahead of the weld pool which cannot be filled without slowing down and burning through the 20 gauge sheet. Recommend taking 75mm spacing between tack welds as the maximum.</li> </ul>
D1-Underside	Sean	Setup #2	WR1	100CO <sub>2</sub>	22	19.0	N/A	200					straight push or pull	Chill strip used. Tack weld every 75mm. Weld intervals between tacks by "stitch welding" as described in D1-Side 3. <ul style="list-style-type: none"> <li>Sean changes "soft start" button from "on" to "off". "soft start" is a power source regulating feature which gradually ramps up current during arc initiation. This appears to have been slowing the arc initiation, and resulting in some stubbing out. Welding technicians indicate arc initiation is much improved after this setting change.</li> <li>Overall excellent weld. Minimal burn-through, nice profile, and improved arc control.</li> </ul>
D2-Underside	Sean	Setup #2	WR1	100CO <sub>2</sub>	22	19.0	N/A	200					straight push or pull	Chill strip used. Tack weld every 75mm. Weld intervals between tacks by "stitch welding" as described in D1-Side 3. <ul style="list-style-type: none"> <li>Similarly satisfactory results as Specimen D1-Underside for weld #1.</li> <li>Angular distortion is significant!! Impossible to start weld #2, since 20 gauge sheet has buckled significantly and lifted away from 6mm steel plate. In future work on larger specimens, if two lines of welds are used, always tack weld both sides to restrain distortion prior to performing fillet welds.</li> </ul>

**Table B–3 (continued): Detailed Results, Visual Inspection of Trial Welds**

**Table Footnotes:**

- 1 Specimen numbers written on specimens in incrementing order. For distortion specimens, "D1 - Side 1" refers to one of four edges of the square plate welded on Specimen D1. Sides 2 - 4 refer to additional edges.
- 2 Clark Bicknell, CET, Journeyman Welder, 30 years experience; or, Sean Watt, CET, Apprentice Welder, 5 years experience
- 3 Setup #1: Miniature Spool Gun
- 4 Setup #2: 12VS Suitcase Welder w/t conventional gun, but diameter gas nozzle, contact tips, inlet wire guide, and drive roll specifically for a small electrode
- 5 Weld locations for Weld #1, Weld #2, and Weld #3 as shown in Chapter 4: Weld Procedure Development
- 6 Gas Composition shown in percentage by volume
- 7 Gas Flow Rate recorded from gas cylinder flow gauge
- 8 Voltage recorded manually as from welding equipment digital display
- 9 Current recorded manually from welding equipment digital display
- 10 Wire Feed Speed either 1) an arbitrary number from 1 (slowest) to 10 (fastest), which can be manually set on the base of the gun handle from Welding Equipment Setup #1, or 2) the speed in "inches per minute" set and displayed on the welding equipment power unit in Welding Equipment Setup #2
- 11 Ideally, length of timed weld is 100mm, however for welds which terminated prematurely due to weldability issues, or welds between tack welds spaced closer than 100mm, a lesser length is recorded
- 12 Time, as recorded by a manually activated stopwatch, to weld the gauge length
- 13 Velocity is an average over the gauge length of timed weld
- 14 Nominal Unit Heat input is equal to the product of Voltage and Current divided by Velocity
- 15 Hand Motion is a brief description of the Welding Technician's hand motion when directing the weld pool
- 16 Observations describe the geometric configuration of the welding, welding technician comments, and a visual appraisal of the finished weld

## Appendix C: SPSW Test Specimen Design Calculations

<p><b>C1 Introduction and Centreline Geometry Selection</b></p> <ul style="list-style-type: none"> <li>• The experiment is intended to demonstrate the performance of the infill panel-to-boundary element welded joint in a typical steel plate shear wall. Only a single storey wall is required. Established methods such as static pushover analysis and design according to the Canadian structural steel standards are used to design the test frame.</li> <li>• The specimen must meet the criteria for “ductile” plate walls, as dictated by S16 – 01 Clause 27, and other relevant clauses. These rigid-frame SPSW are detailed for use in high seismic zones.</li> <li>• The most convenient geometry matches the first storey of Deng <i>et al.</i> (2008)’s specimen, for which the test setup in the I.F. Morrison Structural Engineering Laboratory is still configured. <ul style="list-style-type: none"> <li>○ Centreline dimensions: <ul style="list-style-type: none"> <li>▪ column height = 1900mm from top of baseplate</li> <li>▪ beam length = 2440mm from CL to CL of columns</li> </ul> </li> </ul> </li> </ul>	<p>Clause of <b>S16 – 01 (default), or alternate guideline</b></p>
<p><b>C2 Boundary Element Selection (Beam and Columns)</b></p> <ul style="list-style-type: none"> <li>• <u>Philosophy:</u> Loads from a pushover analysis are based on the <i>probable</i> yield strength of the steel; those loads cannot be used to select members based on the <i>nominal</i> member strength using typical elastic member design (e.g. select a member with factored nominal strength exceeding factored applied force demand). For instance, the member stability check of S16-01 Clause 13.8.2 cannot be applied; loads from pushover analysis will always fail to satisfy this criterion. Thus, <u>accept that failure may eventually occur in the boundary members</u>, but prevent premature failure modes: <ul style="list-style-type: none"> <li>○ Members must be sufficiently stiff to anchor the tension field without buckling;</li> <li>○ Members should be as <u>small as possible</u> in order to <u>maximize</u> the contribution of the thin infill panel to the lateral resistance of the system, and <u>maximize</u> the demand placed on the infill panel-to-boundary element connection.</li> <li>○ Lateral bracing requirements to prevent member buckling must be satisfied;</li> <li>○ Members must satisfy detailing requirements of S16-01 to obtain the local ductility and stability required for a Ductile SPSW.</li> </ul> </li> <li>• Since the specimen is only a single storey in height, the so – called “strong column – weak beam” philosophy does not apply; we can</li> </ul>	<p>13.7</p> <p>27.8.2.6</p> <p>27.4.4.6</p>

<p>use the same member size for beams and columns (for cost economy).</p> <ul style="list-style-type: none"> <li>• <u>Failure Prediction</u>: Since no gravity loads are applied, and beams and columns will be the same size, large column uplift forces will be present. Assuming the infill panel-to-boundary element connection does not fail prematurely, failure will likely take the form of a tensile fracture at the plastic hinge at the base of one of the columns, similar to the test by Driver <i>et al.</i> (1997).</li> <li>• The frame must have <u>rigid</u> beam – to – column connections.</li> <li>• Columns must be I – shaped sections.</li> </ul> <p style="text-align: center;"><u>Design Member:</u>      <u>W200x31</u></p> <p style="text-align: center;">Web and Flange are Class 1 Beam Columns at all loads</p> <ul style="list-style-type: none"> <li>○ Satisfy the column flexibility parameter, <math>\omega_h</math>, by satisfying the minimum column stiffness value:</li> </ul> $I_{c \min} = 0.00307 \frac{wh^4}{L}$ $I_{c \min} = 0.00307 \frac{(0.912\text{mm})(1900\text{mm})^4}{2440\text{mm}}$ $I_{c \min} = 14.95 * 10^6\text{mm} < I_{x \text{ W200x31}} = 31.4 * 10^6\text{mm}^4, \text{OK}$ <ul style="list-style-type: none"> <li>○ Ensure a sufficiently stiff top – storey beam. Satisfy the <math>\omega_L</math> parameter of Dastfan and Driver (2008), which is expected to replace S16 – 01 Clause 20.9.1. Satisfy <math>I_{b \min}</math>:</li> </ul> $I_{b \min} = \frac{wL^4}{650L - \frac{wh^4}{I_c}}$ $I_{b \min} = \frac{(0.912\text{mm})(2440\text{mm})^4}{650(2440\text{mm}) - \frac{(0.912\text{mm})(1900\text{mm})^4}{(31.4 * 10^6\text{mm})}}$ $I_{b \min} = 20.4 * 10^6\text{mm} < I_{x \text{ W200x31}} = 31.4 * 10^6\text{mm}^4, \text{OK}$	<p>27.8.2.6 27.4.4.3</p> <p>27.8.2.2, 20.8 Table 4-3 20.4.2</p>
<p><b>C3 Plastic Analysis Requirements, including Lateral Bracing Check</b></p> <ul style="list-style-type: none"> <li>• Where a plastic analysis is used, requirements of S16 – 01 Clause 8.6 must be satisfied <ul style="list-style-type: none"> <li>○ <math>F_y \leq 0.85 * F_U, \text{OK}</math></li> </ul> </li> </ul>	<p>8.6</p>

<ul style="list-style-type: none"> <li>○ Class 1 Section, <u>OK</u></li> <li>○ Lateral bracing according to S16 – 01 Clause 13.7  <math display="block">\frac{L_{cr}}{r_y} = \frac{17250 + 15500\kappa}{F_y}</math> <math display="block">\kappa = \frac{M_p}{M_p} = +1 \text{ (double curvature)}</math> <math display="block">L_{cr} = \left( \frac{17250 + 15500(1)}{350 \text{ MPa}} \right) (32\text{mm})</math> <math display="block">L_{cr} = 2994\text{mm} &gt; 2440\text{mm} = \textit{longest unbraced span},</math> <u>OK</u></li> <li>○ Web stiffeners provided at load points where plastic hinges may form, <u>OK</u></li> <li>○ Splices in beam or column...(no splices), <u>OK</u></li> <li>○ Members are not subject to repeated heavy impact or fatigue, <u>OK</u></li> <li>○ The influence of inelastic deformation on structural strength is accounted for (second order effects, see 8.7) <ul style="list-style-type: none"> <li>▪ Since second order effects are included in the pushover analysis of the frame, <u>OK</u></li> </ul> </li> </ul>	<p>8.7</p>
<p><b>C4 Detailing: Beam-to-Column Rigid Connection</b></p> <ul style="list-style-type: none"> <li>● See Drawing S101 in Appendix D for the final configuration of the beam-to-column connection.</li> <li>● The Canadian Institute of Steel Construction document “Moment Connections for Seismic Applications” (CISC, 2008) was consulted for detailing this connection. Some provisions have been disregarded in the interest of economy, since this specimen is actually being tested quasi – statically. <ul style="list-style-type: none"> <li>○ Weld access hole dimensions for CPJ welds will conform.</li> <li>○ Backing bars and run – off tabs will be removed in conformance.</li> <li>○ Since loading of the specimen will be quasi – static, and not dynamic, fillet welds are deemed sufficient for continuity plate connections (as opposed to full penetration welds)</li> </ul> </li> <li>● Columns frame into the top beam, which is permitted for single – storey SPSW.</li> <li>● According to capacity design philosophy, the connection is designed to withstand forces arising from full plastic hinging of the beam and column (both Grade 350W, W200x31).</li> <li>● <u>Subscripts</u> <ul style="list-style-type: none"> <li>○ “p” for “plastic”</li> <li>○ “b” for “beam”</li> </ul> </li> </ul>	<p>CISC, 2008</p> <p>27.4.4.4</p> <p>27.4.4.6</p>

<ul style="list-style-type: none"> <li>○ “c” for “column”</li> <li>○ “y” for “yield”</li> <li>○ “u” for “ultimate”</li> </ul>	
<u>W200x31 Section Properties (symbols correspond to S16 – 01)</u>	
<ul style="list-style-type: none"> <li>○ <math>A = 4000 \text{ mm}^2</math></li> <li>○ <math>I_x = 31.4 * 10^6 \text{ mm}^4</math></li> <li>○ <math>r_x = 88.6 \text{ mm}</math></li> <li>○ <math>Z_x = 335 * 10^3 \text{ mm}^3</math></li> <li>○ <math>d = 210 \text{ mm}</math></li> <li>○ <math>w = 6.4 \text{ mm}</math></li> <li>○ <math>b = 134 \text{ mm}</math></li> <li>○ <math>t = 10.2 \text{ mm}</math></li> <li>○ <math>h = 190 \text{ mm}</math></li> </ul>	Property Tables W – Shapes
<u>Moment Demand Resulting from Plastic Hinge Formation</u>	
$Check R_y F_y = 1.1 * 350 \text{ MPa} = 385 \text{ MPa} \geq 385 \text{ MPa}, \underline{OK}$	27.1.7
$M_f = 1.1 * R_y * M_{pb}$	
$M_f = 1.1 * (1.1 * [Z_x * F_y])$	27.4.4.2
$M_f = 1.1 * (1.1 * [335 * 10^3 \text{ mm}^3 * 350 \text{ MPa}])$	(a)
$M_f = 141.9 \text{ kN} * \text{m}$	
$\frac{141.9 \text{ kN} * \text{m}}{\left(190 \text{ mm} * \frac{1 \text{ m}}{1000 \text{ mm}}\right)}$	
<u>Shear in the Panel Zone</u>	
<ul style="list-style-type: none"> <li>• NOTE: <u>No gravity loads (Dead load is negligible)</u></li> </ul>	27.4.4.5
$V' = \frac{M_f}{(h)}$	27.4.4.2
$V' = \frac{141.9 \text{ kN} * \text{m}}{\left(190 \text{ mm} * \frac{1 \text{ m}}{1000 \text{ mm}}\right)}$	
$V' = 746.9 \text{ kN}$	
<u>Doubler Plate Design</u>	
$V_r = 0.55 * \phi * d_b * w' * F_{yb}$ , where $w'$ is the total web width	27.8.2.5
required	27.2.4.2
	(b)



$$w' = \frac{V'}{0.55 * \phi * d_b * F_{yb}}$$

$$w' = \frac{746.9 \text{ kN} * \frac{1000 \text{ N}}{1 \text{ kN}}}{0.55 * 0.9 * 210 \text{ mm} * 350 \text{ MPa}}$$

$$w' = 20.5 \text{ mm}$$

Therefore the minimum total doubler plate thickness is

$$w_{doubler} = w' - w = 20.5 \text{ mm} - 6.4 \text{ mm}$$

$$w_{doubler} = 14.1 \text{ mm}$$

**Choose 2 x 8 mm thick doubler plates.**

Check width – to – thickness limits of panel zone:

$$\frac{a}{h} = 1$$

$$k_v = 5.34 + \frac{4}{\left(\frac{a}{h}\right)^2}$$

$$k_v = 5.34 + \frac{4}{(1)^2}$$

$$k_v = 9.34$$

$$\frac{h}{w} \leq 439 * \sqrt{\left(\frac{k_v}{F_y}\right)}$$

$$\frac{190 \text{ mm}}{8 \text{ mm}} \leq 439 * \sqrt{\left(\frac{9.34}{350 \text{ MPa}}\right)}$$

$$23.8 \leq 71.7, \text{OK}$$

For web with thickness 6.4mm

$$\frac{h}{w} = 29.7 \leq 71.7, \text{OK}$$

Doubler Plate Welding Details

- Following welding detail of CISC Moment Connections for Seismic Applications Figure 7.2 (b), bevel plate edges 30° in the K – region of the W – shape, such that the doubler plate fits snug against the web of the beam.
- Design weld size to satisfy the proportion of shear in the panel zone taken by each doubler plate:

Total width of panel zone required:

$$w' = 20.5 \text{ mm}$$

Width required for one doubler plate:

$$\frac{w' - \text{web width}}{2 \text{ doubler plates}} = \frac{20.5 \text{ mm} - 6.4 \text{ mm}}{2 \text{ doubler plates}} = 7.05 \text{ mm}$$

27.2.4.3

(b)

13.4.1.1

(a)

27.2.4.3

(c)

CISC,

2008

Figure

7.2(b)

<p>Ratio:</p> $\frac{7.05 \text{ mm}}{20.5 \text{ mm}} = 0.34$ <p>Shear force to be resisted by welds at one double plate edge:</p> $0.34 * V' = 0.34 * 746.9 \text{ KN} = 253.9 \text{ KN}$ <p>Base Metal</p> $V_r = 0.67 * \phi_w * A_m * F_u$ $253.9 * 10^3 \text{ N} = 0.67^2 * 450 \text{ MPa} * 190 \text{ mm} * l_{req'd}$ $l_{req'd} = 6.6 \text{ mm}$ <p>Weld Metal</p> $V_r = 0.67 * \phi_w * A_w * X_u * (1.00 + [\sin\theta]^{1.5})$ $253.9 * 10^3 \text{ KN}$ $= 0.67^2 * 0.707 * l_{req'd} * 190 \text{ mm} * 490 \text{ MPa}$ $l_{req'd} = 8.6 \text{ mm}, \text{ or } 9 \text{ mm fillet welds}$ <p>Note: The maximum fillet weld size against the edge of 8 mm thick doubler plates is 6 mm. Use 6mm fillets on the vertical edges (190 mm long) of doubler plates.</p> <p>Extend the horizontal length of doubler plates to 260 mm instead of 190 mm. Using a length of 260 mm instead of 190 mm in the above equations results in a minimum weld size of 6.3 mm. given the two-way action by having welds all-around the doubler plate, and possible load sharing with the continuity plates, a <b>fillet weld size of 6 mm all-around the doubler plates</b> is deemed acceptable.</p> <ul style="list-style-type: none"> <li>See Drawing S101 for doubler plate details.</li> </ul>	13.13.2.2
<p><b>C5 Continuity Plate Design</b></p> <ul style="list-style-type: none"> <li>Demand forces - design for full capacity of column flange <ul style="list-style-type: none"> <li><u>Tension</u> – assuming full yield of column flange area <math display="block">T_{f \text{ column flange}} = 1.1 * R_y * F_y * b_c * t_c</math> <math display="block">T_{f \text{ column flange}} = 1.1 * 385 \text{ MPa} * 134 \text{ mm} * 10.2 \text{ mm}</math> <math display="block">T_{f \text{ column flange}} = 578.8 \text{ kN}</math> </li> </ul> </li> </ul> <p>Tensile resistance of beam flange (taken as 0.6*T<sub>r</sub>)</p> $0.6 * T_r = 0.6 * (7 * \phi * t_b^2 * F_{yb})$	27.4.4.3

<p> <math>0.6 * T_r = 0.6 * (7 * 0.9 * [10.2 \text{ mm}]^2 * 350 \text{ MPa})</math>  <math>0.6 * T_r = 137.6 \text{ kN} &lt; 578.8 \text{ kN}</math>, <u>CONTINUITY PLATES REQ'D</u> </p> <p> <u>Compression</u> – demand is also governed by full yield of flange  <math>C_{f \text{ column flange}} = 578.8 \text{ kN}</math> </p> <p>           Bearing resistance of beam web  <math>B_r = \phi_{ci} * w_b * (t_c + 10 * t_b) * F_{yb}</math>  <math>B_r = 0.8 * 6.4 \text{ mm} * (10.2 \text{ mm} + 10 * 10.2 \text{ mm}) * 350 \text{ MPa}</math>  <math>B_r = 201.1 \text{ kN} &gt; 137.6 \text{ kN}</math>, therefore <u>tension is limiting</u> </p> <p> <math>T_r \text{ continuity plate req'd} = 578.8 \text{ kN} - 137.6 \text{ kN}</math>  <math>T_r \text{ continuity plate req'd} = 441.2 \text{ kN}</math>, <u>for each pair of continuity plate</u> </p> <ul style="list-style-type: none"> <li>• Resistance forces – stiffener sizing           <ul style="list-style-type: none"> <li>○ <math>A_{stiffener \text{ req'd}} = \frac{T_{req'd}}{\phi * F_{y \text{ stiffener}}}</math> (area for a pair of stiffeners)  <math>A_{stiffener \text{ req'd}} = \frac{441.2 \text{ kN}}{0.9 * 350 \text{ MPa}}</math>  <math>A_{stiffener \text{ req'd}} = 1401 \text{ mm}^2</math> </li> </ul> </li> </ul> <p>           Available length for stiffener to flange connection  <math>L = b - 2 * k_1 - w = 134 \text{ mm} - 2 * 13 \text{ mm} - 6.4 \text{ mm}</math>  <math>L = 101.6 \text{ mm} \sim 100 \text{ mm}</math> </p> <p>           Try <math>t_{stiffener} = 15 \text{ mm}</math> </p> <p> <math>A_{supplied} = L * t_{stiffener}</math>  <math>A_{supplied} = 100 \text{ mm} * 15 \text{ mm}</math>  <math>A_{supplied} = 1500 \text{ mm}^2 \geq 1401 \text{ mm}^2</math>, <u>OK</u> </p> <p> <u>Continuity Plate Welds</u> </p> <ul style="list-style-type: none"> <li>○ <u>Transverse Welds – Continuity Plate to Beam Flanges</u> </li> </ul> <p>           Base Metal         </p>	<p>21.3</p> <p>13.1(e)</p>
<p> <math>V_r = 0.67 * \phi_w * A_m * F_u</math>  <math>441.2 * 10^3 \text{ N} = 0.67^2 * 450 \text{ MPa} * 100 \text{ mm} * l_{req'd}</math> </p>	<p>13.13.2.2</p>

<p><math>l_{req'd} = 22 \text{ mm}</math>, or <b>double – sided 12mm fillets</b> &lt;- GOVERNS</p> <p>Weld Metal  <math>V_r = 0.67 * \phi_w * A_w * X_u * (1.00 + [\sin\theta]^{1.5})</math>  <math>441.2 \text{ KN}</math>  <math>= 0.67^2 * 0.707 * l_{req'd} * 100 \text{ mm}</math>  <math>* 490 \text{ MPa} * (1.5)</math>  <math>l_{req'd} = 19 \text{ mm}</math>, or double –sided 10 mm fillets</p> <p><u>Longitudinal Welds – Continuity Plate to Beam Web</u></p> <ul style="list-style-type: none"> <li>○ Take <b>double – sided 6 mm fillet welds</b>; shear transfer is not crucial for this member. Note that in a dynamically loaded rigid connection, CISC Moment Connections for Seismic Applications provides additional guidance for this weld.</li> </ul>	
<p><b>C6 Column-Framing-Into-Beam Weld Details</b></p> <ul style="list-style-type: none"> <li>• Conform with CISC (2008), Fig. 6</li> <li>• Neglect shear tab for erection, since this single-storey specimen will be shop fabricated in the flat position</li> <li>• See Drawing S101 for details <ul style="list-style-type: none"> <li>○ <u>Column Flanges</u> – CJP groove weld w/t 45° bevel, weld access holes conform to CISC (2008), remove backing bar, grind smooth, and seal with a 5 mm fillet weld</li> <li>○ <u>Column Web</u> - Fillet welds capable of carrying the full capacity of the web. Assume 100% longitudinal loading of weld (conservative)</li> <li>○ <math>V_f = 1.1 * R_y * F_y * ([h - \text{weld access hole}] * w)</math>  <math>V_f = 1.1 * 385 \text{ MPa} * ([190 \text{ mm} - 2 * 20 \text{ mm}] * 6.4 \text{ mm})</math>  <math>V_f = 407 \text{ kN}</math></li> </ul> </li> </ul> <p>Base Metal  <math>V_r = 0.67 * \phi_w * A_m * F_u</math>  <math>407 * 10^3 \text{ N} = 0.67^2 * 450 \text{ MPa} * 150 \text{ mm} * l_{req'd}</math>  <math>l_{req'd} = 14 \text{ mm}</math>, or double – sided 8 mm fillets</p> <p>Weld Metal  <math>V_r = 0.67 * \phi_w * A_w * X_u * (1.00 + [\sin\theta]^{1.5})</math>  <math>407 \text{ kN}</math>  <math>= 0.67^2 * 0.707 * l_{req'd} * 150 \text{ mm}</math>  <math>* 490 \text{ MPa} * (1.0)</math></p>	<p>CISC, 2008</p> <p>13.13.2.2</p>

$l_{req'd} = 17.4 \text{ mm},$ or <b>double –sided 10 mm fillets</b> <- <b>GOVERNS</b>	
<p><b>C7 Crane Lifting Detail</b></p> <ul style="list-style-type: none"> <li>• Lifting holes located in plates fillet welded to the top of the specimen as shown in Drawing S101</li> <li>• Assume, in a worst – case scenario, that 100% of the load rests on one of the two lifting holes. Neglect infill panel load.</li> <li>• Select a 15 mm thick plate, 200mm x 200mm, with a 100mm diameter opening for hooks/ clevises in the centre. <ul style="list-style-type: none"> <li>○ <u>Load - Mass of Frame</u> <math display="block">P_{f \text{ frame weight}} = 1.25</math> <p style="text-align: center;">* (full weight of frame + baseplate)</p> <math display="block">P_{f \text{ frame weight}} = 1.25</math> <math display="block">* \left( [2 * 1.9 \text{ m} + 2.44 \text{ m}] * \frac{0.308 \text{ kN}}{\text{m}} \right)</math> <math display="block">+ [3.24 \text{ m} * 0.076 \text{ m} * 0.8 \text{ m}] * 7.7 \frac{\text{kN}}{\text{m}^3}</math> <math display="block">P_{f \text{ frame weight}} = 4.3 \text{ kN} \approx 5 \text{ kN}</math> </li> <li>○ <u>Checks for vertical lift</u> <p><u>Bearing (assume contact area is 25 mm long for 2" dia clevis)</u></p> <math display="block">B_r = 1.50 * \phi * F_y * A</math> <math display="block">B_r = 1.50 * 0.9 * 350 \text{ MPa} * (25 \text{ mm} * 15 \text{ mm})</math> <math display="block">B_r = 177 \text{ kN} &gt; 5 \text{ kN}, \underline{\text{OK}}</math> <p style="text-align: right;">13.10</p> <p><u>Shear</u></p> <math display="block">V_r = \phi * A_w * F_s</math> <math display="block">V_r = 0.9 * (15 \text{ mm} * 50 \text{ mm}) * (0.66 * 350 \text{ MPa})</math> <math display="block">V_r = 156 \text{ kN} &gt; 5 \text{ kN}, \underline{\text{OK}}</math> <p style="text-align: right;">13.4.1</p> </li> <li>○ <u>Fillet Weld Design</u> <p>Base Metal</p> <math display="block">V_r = 0.67 * \phi_w * A_m * F_u</math> <math display="block">5 * 10^3 \text{ N} = 0.67^2 * 450 \text{ MPa} * 200 \text{ mm} * l_{req'd}</math> <math display="block">l_{req'd} = 1 \text{ mm}, \text{ take minimum } \underline{\text{double – sided 6 mm fillets}}</math> <p>Weld Metal</p> <p style="text-align: right;">13.13.2.2</p> </li> </ul> </li> </ul>	

$$V_r = 0.67 * \phi_w * A_w * X_u * (1.00 + [\sin\theta]^{1.5})$$

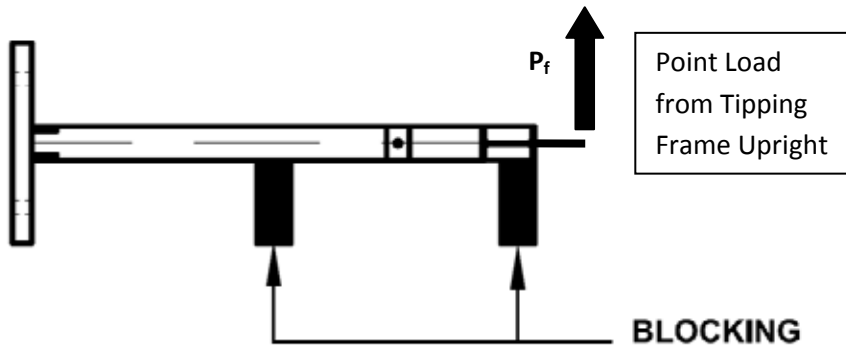
$$5 \text{ KN}$$

$$= 0.67^2 * 0.707 * l_{req'd} * 200 \text{ mm}$$

$$* 490 \text{ MPa} * (1.5)$$

$$l_{req'd} = 1 \text{ mm}$$

- The frame will be laying on its side and tipped upright by the crane at some point... consider the full weight (conservative) of the frame acting as a point load acting upwards at the end of the cantilevered frame, as shown:



- Checks for Tipping Upright  
15 mm Plate Bending at Weak Section (max diameter of hole)

$$M_f = P_f * \text{distance to section} = 5 \text{ KN} * 0.100 \text{ m}$$

$$= 0.5 \text{ kN} * \text{m}$$

$$M_r = \phi * Z_x * F_y = \phi * \left( \frac{b * d^2}{4} \right) * F_y$$

$$M_r = 0.9 * \left( \frac{[2 * 50 \text{ mm}] * [15 \text{ mm}]^2}{4} \right) * 350 \text{ MPa}$$

$$M_r = 1.78 \text{ kN} * \text{m} > 0.5 \text{ kN} * \text{m}, \underline{\text{OK}}$$

13.5

- Fillet Weld Design  
 Moment at base of 200 mm long plate, split into a force couple acting at the face of each fillet weld (each side of the 15 mm thick plate)

$$V_f = \frac{M_f}{t_{plate}} = \frac{(5 \text{ kN} * 0.2 \text{ m})}{0.015 \text{ m}} = 66.7 \text{ kN}$$

Base Metal

$$V_r = 0.67 * \phi_w * A_m * F_u$$

13.13.2.2

$66.7 * 10^3 N = 0.67^2 * 450 MPa * 200 mm * l_{req'd}$ $l_{req'd} = 2 mm, \text{ take minimum } \mathbf{double - sided 6 mm fillets}$ <p>Weld Metal</p> $V_r = 0.67 * \phi_w * A_w * X_u * (1.00 + [\sin\theta]^{1.5})$ $66.7 kN$ $= 0.67^2 * 0.707 * l_{req'd} * 200 mm$ $* 490 MPa * (1.5)$ $l_{req'd} = 2 mm$	
<p><b>C8 Fish Plate-to-Boundary Elements Connection</b></p> <ul style="list-style-type: none"> <li>• <u>Fish plate thickness will be 6 mm</u>, such that the fish plate to boundary element welds are simple, and the fish plate is sufficiently stiff to handle <ul style="list-style-type: none"> <li>○ Loading on welds – full yield of infill panel (assume tension field at 40° from the vertical)</li> </ul> </li> </ul> <p>Calculate probable yield of a unit strip of infill panel</p> $T = 1.1 * A * R_y * F_y$ $T = 1.1 * 0.912 mm * 1 mm * 385 MPa$ $T = 386 kN/m$ $T_{Longitudinal} = \frac{386 kN}{m} * \cos(40^\circ) = 295 kN/m$ <p>Base Metal</p> $V_r = 0.67 * \phi_w * A_m * F_u$ $\frac{295 kN}{m} = 0.67^2 * l_{req'd} * 1 mm * 450 MPa$ $l_{req'd} = 2 mm$ <p>Weld Metal</p> $V_r = 0.67 * \phi_w * A_w * X_u * (1.00 + [\sin\theta]^{1.5})$ $295 kN/m$ $= 0.67^2 * 0.707 * l_{req'd} * 1 mm$ $* 490 MPa * (1.0)$ $l_{req'd} = 2 mm, \text{ take } \mathbf{6 mm double - sided fillet welds}$	<p>13.2</p> <p>13.13.2.2</p>
<p><b>C9 Fish Plate Dimensions (Weld Access)</b></p>	

<ul style="list-style-type: none"> <li>• Adequate approach angles must be provided to facilitate access by the welder to make a sound weld. It has been suggested that for fillet welds an access angle of 30° is appropriate (CWB, 2005)</li> <li>• In the case of the W200x31 boundary members, the addition of large fish plates will significantly contribute to their strong – axis moment of inertia, and thus moment capacity. Relatively weak boundary elements are desired, so as to maximize the contribution of the infill panel to the system, and maximize the displacements undergone by the welds.</li> <li>• Fish plates as small as possible are required.</li> <li>• Discussion with the technicians who will be conducting the welding indicates that a shallower approach angle than 30° is acceptable for thin sheet fillet welds in the flat position.</li> <li>• <b>FINAL DIMENSIONS: Fish plates will be 6 mm thick by 100 mm wide.</b> Due to the extra width of the baseplate (800 mm wide, compared with a 134 mm wide W200x31 flange), the <b>fish plate connected to the baseplate will have a width of 200 mm to provide adequate access for welding the bottom of the infill panel</b></li> <li>• See Drawing S100 and Drawing S104 in Appendix D for fish plate dimension clarification.</li> </ul>	12.4.1 of CSA,2003
<p><b>C10 Column-to-Baseplate Connection</b></p> <ul style="list-style-type: none"> <li>• Since plastic hinges will form, the full section capacity must be carried through to the baseplate. The column will be welded to the baseplate using full penetration welds, along both the flanges and the web. Preparation will include beveling to 45°, using a backing bar with 6 mm gap between column and baseplate, removing the backing bar after welding and sealing the far side with a 5 mm fillet on the root side.</li> <li>• It is desirable for hinging to occur away from the column-to-baseplate welds, and for the uplift stress in these welds to be reduced, since this detail is vulnerable to lamellar tearing. To ensure this occurs, small triangular stiffeners will be welded to the outside faces of the column flange, as shown in Drawing S102. <ul style="list-style-type: none"> <li>○ NOTE: The provision of S16-01 27.8.2.6 calls for columns to be stiffened such that plastic hinges form at a minimum distance of 1.5 times the depth of the column above the base plate. However, the proposed release of S16 – 09 shows a more general requirement that “columns shall to be stiffened so that plastic hinging forms in the columns above the baseplate or foundation beam”. On this</li> </ul> </li> </ul>	<p>CSA, 2003</p> <p>27.8.2.6</p>



<p>specimen, only the bottom 100 mm of the columns are stiffened.</p> <ul style="list-style-type: none"> <li>○ <u>Stiffener Shear Buckling Check (meet Class 1 with Flexural Compression)</u></li> </ul> $\frac{b}{t} \leq \frac{145}{\sqrt{F_y}}$ $t \geq \frac{b * \sqrt{F_y}}{145}$ $t \geq \frac{\sqrt{([100 \text{ mm}]^2 - [50 \text{ mm}]^2) * \sqrt{300 \text{ MPa}}}{145}$ $t \geq 10.3 \text{ mm}$ <p><b>Select base stiffeners 15 mm thick, triangular, with two 100 mm edges as shown in Drawing S104. Weld 6 mm welds on all connected edges where possible. Where weld access inhibits fillet welding, use PJP groove welds. See Drawing S102 for weld details.</b></p>	Table 4-2
<p><b>C11 Load Transfer: SPSW Beam to Load Transfer Beam Connection</b></p> <ul style="list-style-type: none"> <li>• Check if axial stiffener is required on the beam web to prevent shear buckling</li> </ul> $\frac{a}{h} = \frac{75 \text{ mm}}{190 \text{ mm}} = 0.4$ $k_v = 5.34 + \frac{4}{\left(\frac{a}{h}\right)^2}$ $k_v = 5.34 + \frac{4}{(0.4)^2}$ $k_v = 30.3$ $\frac{h}{w} \leq 439 * \sqrt{\left(\frac{k_v}{F_y}\right)}$ $\frac{190 \text{ mm}}{6.4 \text{ mm}} \leq 439 * \sqrt{\left(\frac{30.3}{350 \text{ MPa}}\right)}$ $29.7 \leq 129.2, \text{OK}$ <ul style="list-style-type: none"> <li>• The load transfer plate (see Drawing S106) will be welded directly to the top beam of the specimen. Flange welds will be full penetration, backing bar removed and weld root sealed with a 5 mm fillet after welding. Fillet welds have been judged sufficiently robust for the quasi – static loading conditions to carry the web loads. <ul style="list-style-type: none"> <li>○ <u>Web Fillet Welds – Design for full yield of web</u></li> </ul> <math display="block">T_{f \text{ web}} = 1.1 * R_y * F_y * A_{\text{web}}</math> </li> </ul>	13.4.1.1 (a)

$T_{f\ web} = 1.1 * 385\ MPa * 6.4\ mm * 1\ mm$ $T_{f\ web} = 2710\ kN/m$ <p>Base Metal</p> $V_r = 0.67 * \phi_w * A_m * F_u$ $\frac{2710\ kN}{m} = 0.67^2 * l_{req'd} * 1\ mm * 450\ MPa$ $l_{req'd} = 14\ mm < \underline{\text{GOVERNS}}, \text{ take } \mathbf{8\ mm\ double\ –\ sided\ fillet\ welds}$ <p>Weld Metal</p> $V_r = 0.67 * \phi_w * A_w * X_u * (1.00 + [\sin\theta]^{1.5})$ $2710\ kN/m = 0.67^2 * 0.707 * l_{req'd} * 1\ mm * 490\ MPa * (1.5)$ $l_{req'd} = 12\ mm$	13.13.2.2
<p><b>C12 Load Transfer Plate Design</b></p> <ul style="list-style-type: none"> <li>The final configuration of the load transfer plate is shown in Drawing S106 of Appendix D.</li> <li>The flow of forces through the jack connection is linear; the load passes through the load cell which threads into the existing distributing beam, and must find its way into the end of the top storey beam of the specimen (see Drawing C101 in Appendix D). The so – called “load transfer plate” can be considered an adaptor which connects the loading jacks to the test specimen. The existing setup fits a particular loading system used in a series of SPSW tests by Deng <i>et al.</i> (2008), and it was desirable to avoid having to disassemble it for the current research.</li> <li>The plate must have sufficient shear and bending stiffness to sustain the pushover load of the specimen. Bolts connecting the load transfer plate to the existing distributing beam must be able to sustain the full pushover load in tension. Since strain hardening is not included in the pushover model, a value 25% higher than the pushover prediction is used for design:</li> </ul> $1.25 * Q_y = 1.25 * 550\ kN = 688\ kN$ <p>Dimensions of the load transfer plate match the existing distributing beam and provide sufficient space for welding the load transfer</p>	

plate to the end of the SPSW test specimen beam (see Drawing S106)

#### Plate Bending

Assume a simply-supported bending moment diagram between the two innermost boltholes ( $L = 260 \text{ mm}$ )

Applied Moment:

$$M_f = \frac{(1.25 * Q_y) * L}{4}$$

$$M_f = \frac{688 \text{ kN} * 0.26 \text{ m}}{4}$$

$$M_f = 44.7 \text{ kN} * \text{m}$$

Bending Capacity (for a 300W steel plate 51 mm tall and 320 mm wide):

$$Z_x = \frac{b * d^2}{4}$$

$$Z_x = \frac{320 \text{ mm} * 51 \text{ mm}^2}{4}$$

$$Z_x = 208080 \text{ mm}^3$$

$$M_r = \phi * Z_x * F_y$$

$$M_r = 0.9 * 208,080 \text{ mm}^3 * 300 \text{ MPa}$$

$$M_r = 56.2 \text{ kN} * \text{m} > 44.7 \text{ kN} * \text{m} = M_f, \text{ therefore OK}$$

13.5

#### Plate Shear

Maximum shear will occur along the line of boltholes when bolts are in tension (jacks are pulling the frame to the south), or through the middle of the plate when jacks are pushing the frame north and the plates are in bearing.

Option 1: Bolts in Tension:

Area to resist shear = gross section less boltholes

$$A = 51 \text{ mm} * 320 \text{ mm} - 29 \text{ mm} * 51 \text{ mm} * 2$$

$$A = 13362 \text{ mm}^2$$

Shear Resistance:

$$V_r = 0.66 * \phi * F_y * A$$

$$V_r = 0.66 * 0.9 * 300 \text{ MPa} * 13362 \text{ mm}^2$$

$$V_r = 2381 \text{ kN} > 688 \text{ kN} = 1.25 * Q_y, \text{ therefore OK}$$

13.4.2

Option 2: Load transfer plate and existing distributing beam in

<p>bearing:</p> <p>It is clear from the results of Option 1 that sufficient shear capacity exists, since even the cross section reduced for bolt holes has ample capacity for the full pushover load of the specimen.</p> <p><u>Bolt Design</u></p> <ul style="list-style-type: none"> <li>• Bolts are used to connect the custom distributing beam to the existing distributing beam. Eight bolt holes, 1 – 1/16” in diameter each, correspond to bolt hole locations on the existing distributing beam. Compression loads will be carried in bearing, tension loads through these bolts.</li> <li>• For dynamically loaded structures, bolts must be pretensioned to the minimum stated by S16 – 01 13.12.1.2. Assume all the load passes through the four bolts closest to the load path (line of action of the jacks) <ul style="list-style-type: none"> <li>○ Try A490 bolts, 1” diameter each <math display="block">T_r (1 \text{ bolt}) = 0.75 * \phi_b * A_b * F_u</math> <math display="block">T_r (1 \text{ bolt}) = 0.75 * 0.80 * \frac{\pi * (25.4 \text{ mm})^2}{4} * 1040 \text{ MPa}</math> <math display="block">T_r (1 \text{ bolt}) = 316 \text{ kN}</math> <math display="block">T_r (4 \text{ bolts}) = 316 \text{ kN per bolt} * 4 \text{ bolts}</math> <math display="block">T_r (4 \text{ bolts}) = 1265 \text{ kN} &gt; 688 \text{ kN} = 1.25 * Q_y , \text{ therefore}</math> <p><u>OK</u></p> <p><u>Pretension bolts to minimum 1/3 turn beyond the snug tight condition.</u></p> </li> </ul> </li> </ul>	<p>13.12.1.2</p> <p>23.8, Table 8</p>
---	---

## **Appendix D: SPSW Fabrication and Test Setup Drawings**

### **D1 Introduction**


This appendix consists of two drawing sets; the fabrication drawings for the frame of the SPSW test specimen, and the test setup drawings. The drawings have been shrunk from their functional size to fit the margin requirements of the Faculty of Graduate Studies and Research.

#### Large Scale Plate Wall Test Moment Resisting Frame Fabrication Drawings

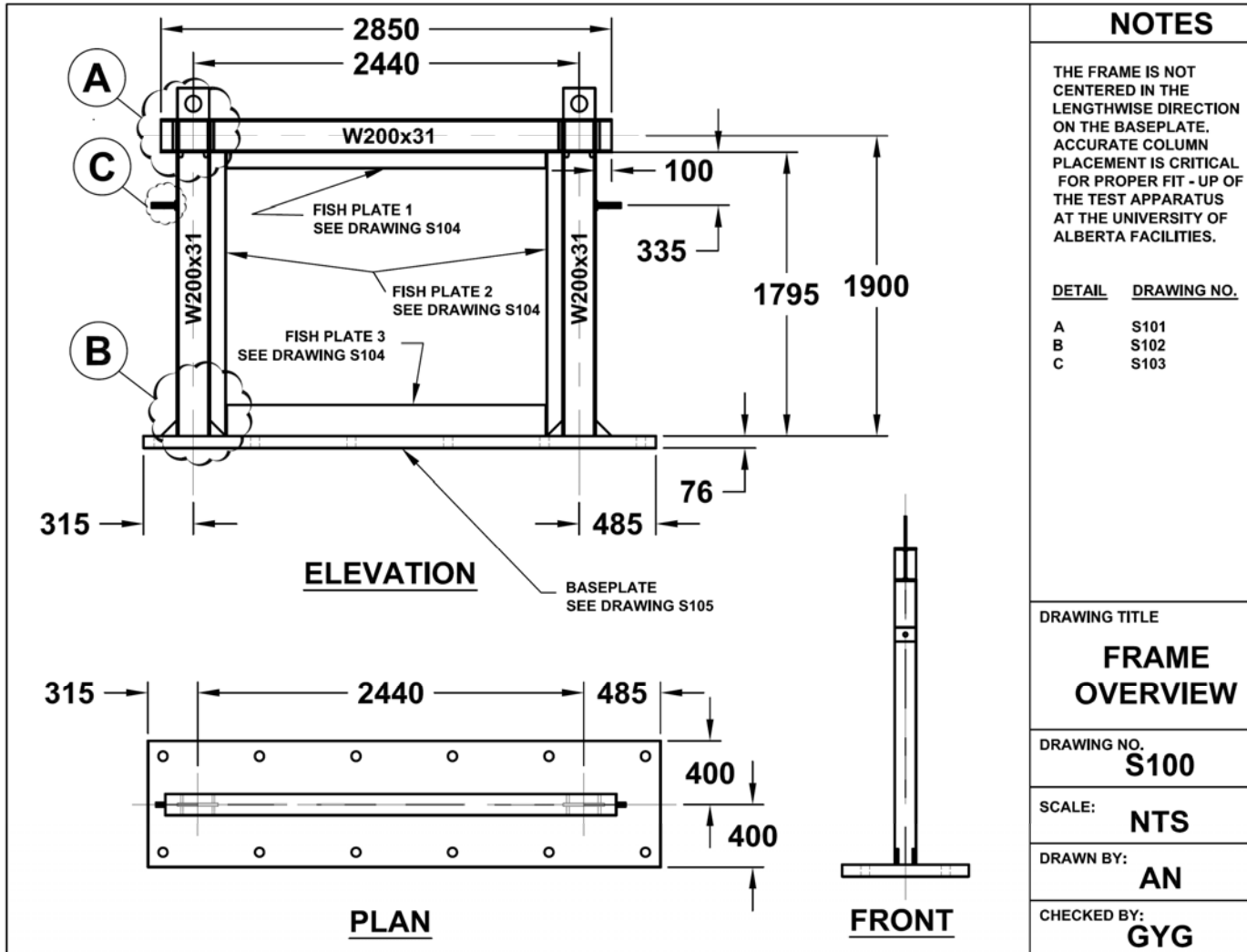
S000	Cover Page
S001	General Notes
S100	Frame Overview
S101	Detail A: Beam-Column Connection
S102	Detail B: Column Base Plate Connection
S103	Detail C: Watt Bracing Connection
S104	Misc. Steel Plates
S105	Base plate
S106	Load Transfer Plate

#### Large Scale Test – Test Setup Drawings

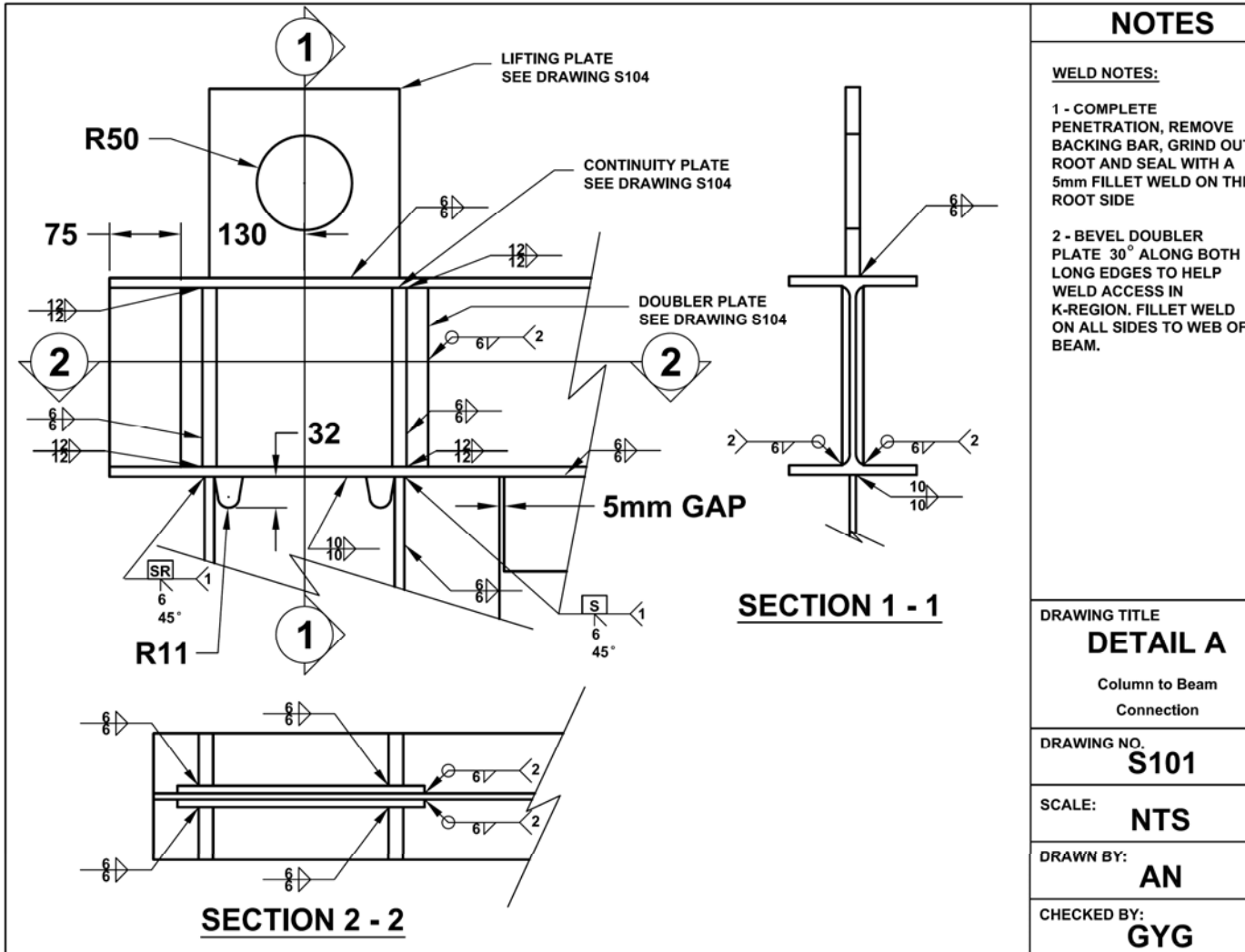
C000	Cover Page
C100	Test Setup – East Elevation
C101	Test Setup – Plan View
C102	Test Setup – Section View
C103	Detail A: Lateral Load Connection
C104	Data Collection

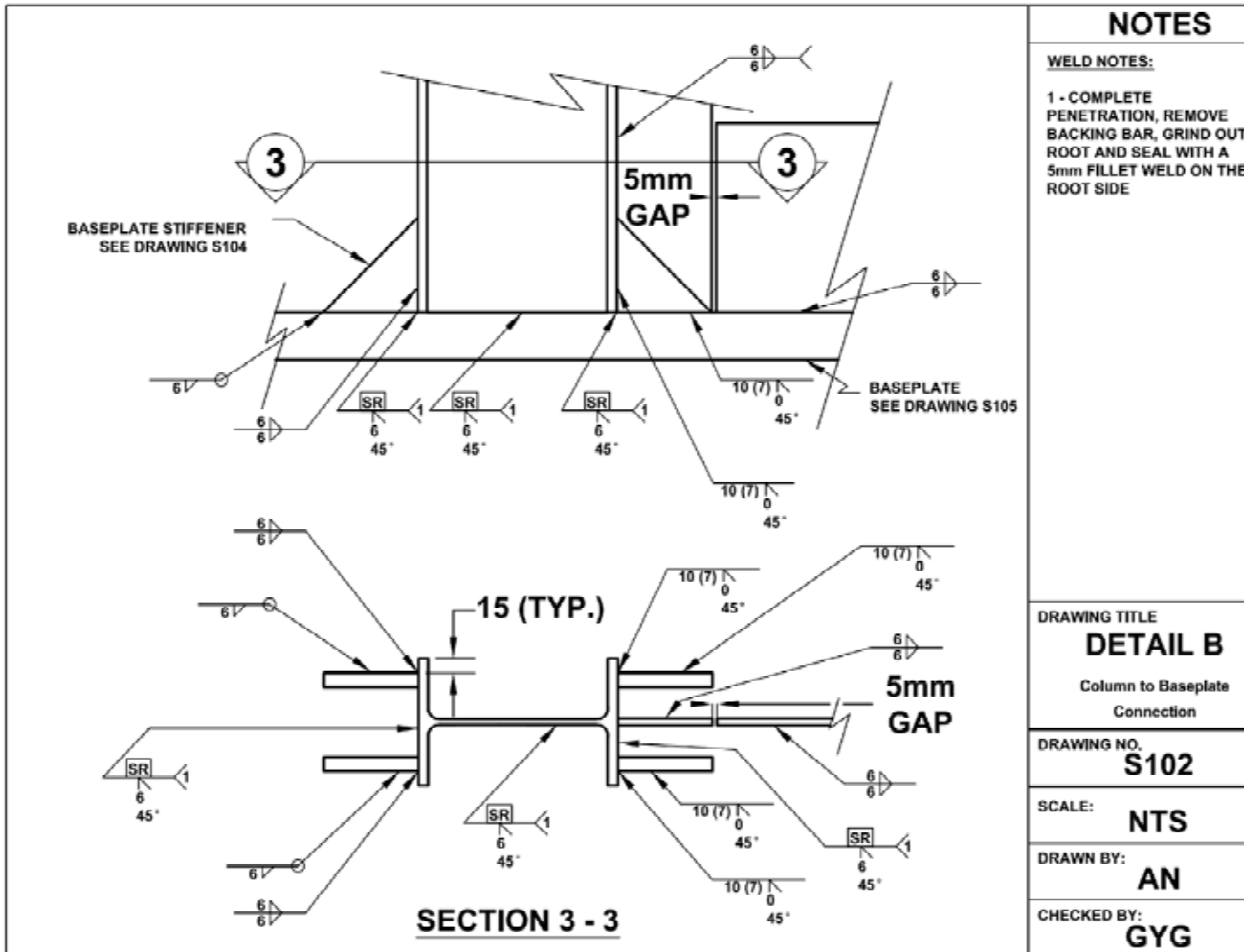
<p><b>STEEL PLATE SHEAR WALLS WITH LIGHT GAUGE INFILL PLATES</b></p> <p><b><u>LARGE SCALE PLATE WALL TEST</u></b> <b><u>MOMENT RESISTING FRAME FABRICATION DRAWINGS</u></b></p> <p><b>RESEARCHER: ANDREW NEILSON, M.Sc. CANDIDATE</b> <b>SUPERVISORS: Dr. GILBERT GRONDIN &amp; Dr. ROBERT DRIVER</b></p> <p><b><u>DWG NO. TITLE</u></b></p> <p><b>S001 GENERAL NOTES</b></p> <p><b>S100 FRAME OVERVIEW</b></p> <p><b>S101 DETAIL A: BEAM - COLUMN CONNECTION</b></p> <p><b>S102 DETAIL B: COLUMN - BASEPLATE CONNECTION</b></p> <p><b>S103 DETAIL C: WATT BRACING CONNECTION</b></p> <p><b>S104 MISC. STEEL PLATES</b></p> <p><b>S105 BASEPLATE</b></p> <p><b>S106 LOAD TRANSFER PLATE</b></p>	<b>NOTES</b>
	
	<small>DRAWING TITLE</small> <b>COVER PAGE</b>
	<small>DRAWING NO.</small> <b>S000</b>
	<small>SCALE:</small> <b>N/A</b>
	<small>DRAWN BY:</small> <b>AN</b>
	<small>CHECKED BY:</small> <b>GYG</b>

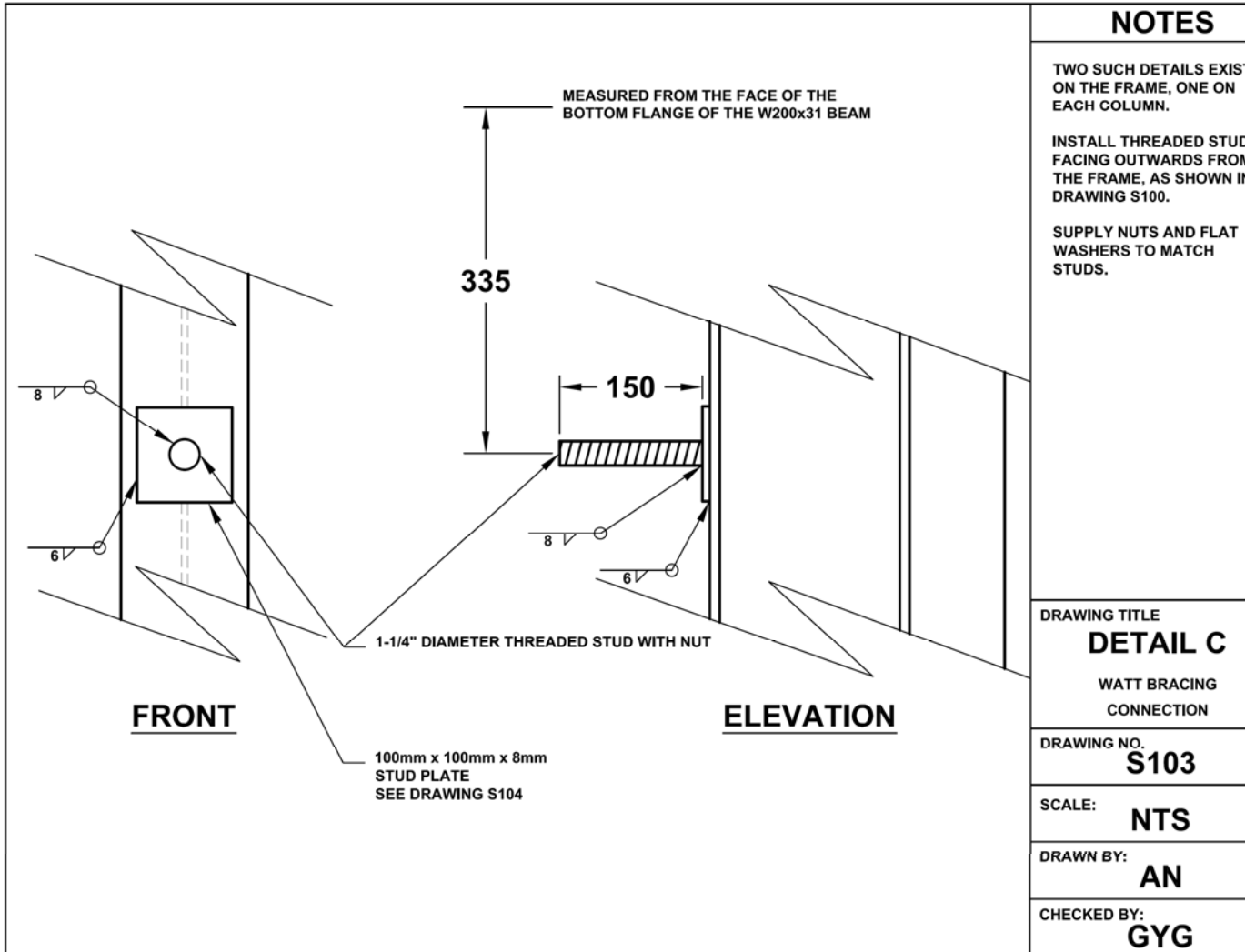
<p>1) THIS PACKAGE CONTAINS FABRICATION DRAWINGS S100 THROUGH S106.</p> <p>2) DRAWINGS SHOULD NOT BE SCALED. IF CLARIFICATION IS REQUIRED, PLEASE CONTACT ANDREW NELSON OR GILBERT GRONDIN.</p> <p>3) ALL DIMENSIONS ARE IN MILLIMETERS (mm) AND DEGREES (°) UNLESS OTHERWISE NOTED.</p> <p>4) SHOP DRAWINGS ARE REQUESTED FOR REVIEW PRIOR TO FABRICATION. WELDING PROCEDURE SPECIFICATION (WPS) SHOULD BE SUBMITTED FOR REVIEW (<math>X_u = 490 \text{ MPa}</math> HAS BEEN ASSUMED).</p> <p>5) SUBSTITUTIONS SHALL NOT BE MADE WITHOUT PRIOR APPROVAL.</p> <p>6) ALL STEEL IS CSA G40.21 GRADE 350W, WITH THE EXCEPTION OF FISH PLATE STEEL, WHICH IS 300W (SEE DRAWING S104). <u>ALL W200x31 MUST BE CUT FROM THE SAME PIECE.</u></p> <p>7) PLEASE PROVIDE 1.0m EXTRA LENGTH OF W200x31 <u>CUT FROM THE SAME PIECE AS THE FRAME MEMBERS.</u> THIS WILL BE USED FOR MATERIAL TESTING.</p> <p>8) PLEASE PROVIDE 8 x 1" DIAMETER ASTM A490 BOLTS 4-1/2" LONG WITH NUTS AND WASHERS. PLEASE PROVIDE 2 x NUTS AND WASHERS TO MATCH 1-1/4" DIAMETER THREADED ROD SHOWN IN DRAWING S104.</p> <p>9) PLEASE SUPPLY COPY OF MILL TEST REPORTS.</p> <p>10) THE SPECIMEN SHALL NOT BE PAINTED.</p>	<b>NOTES</b>
	<b>GENERAL NOTES</b>
	DRAWING NO. <b>S001</b>
	SCALE: <b>N/A</b>
	DRAWN BY: <b>AN</b>
CHECKED BY: <b>GYG</b>	

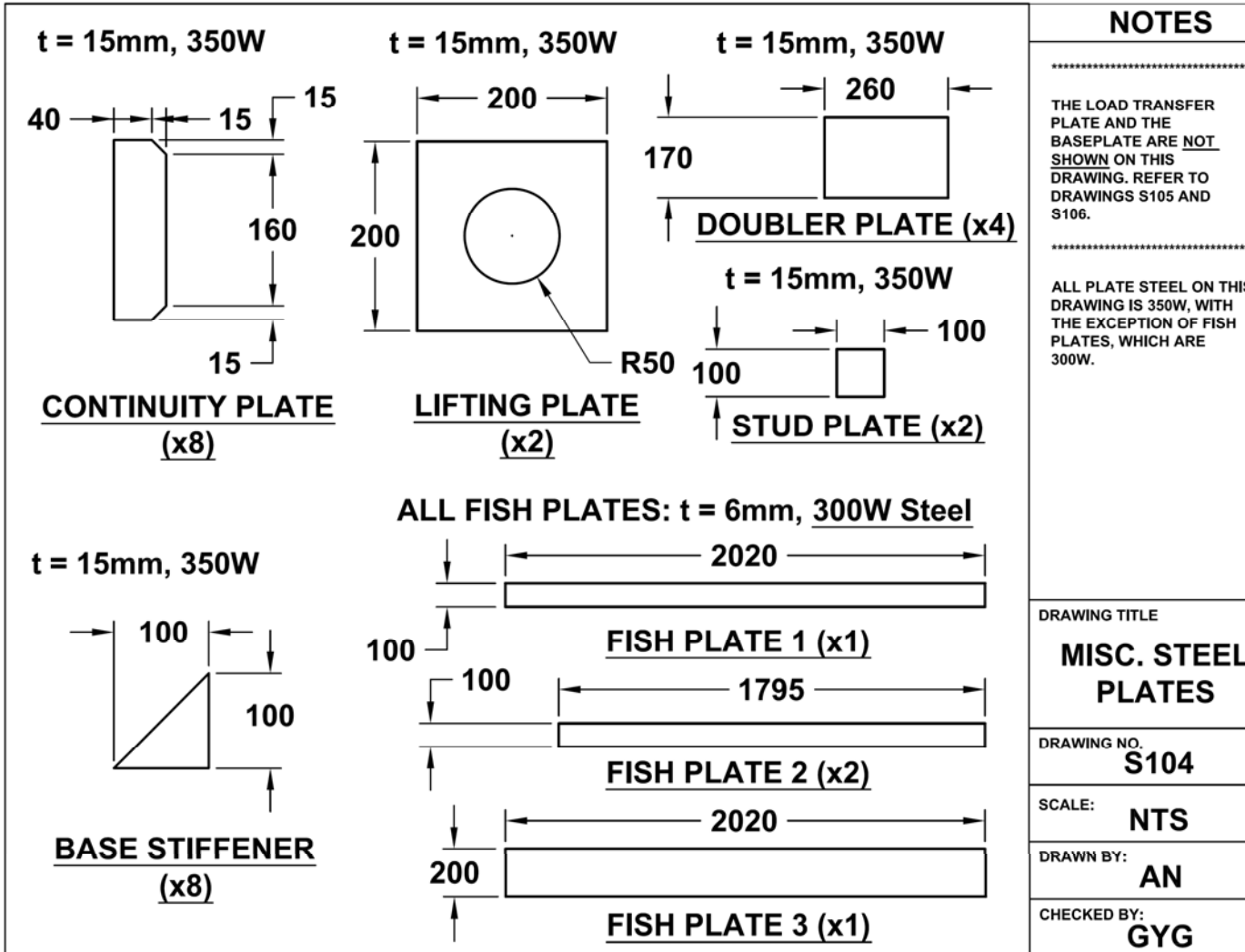












**NOTES**

THE LOAD TRANSFER PLATE AND THE BASEPLATE ARE NOT SHOWN ON THIS DRAWING. REFER TO DRAWINGS S105 AND S106.

ALL PLATE STEEL ON THIS DRAWING IS 350W, WITH THE EXCEPTION OF FISH PLATES, WHICH ARE 300W.

DRAWING TITLE

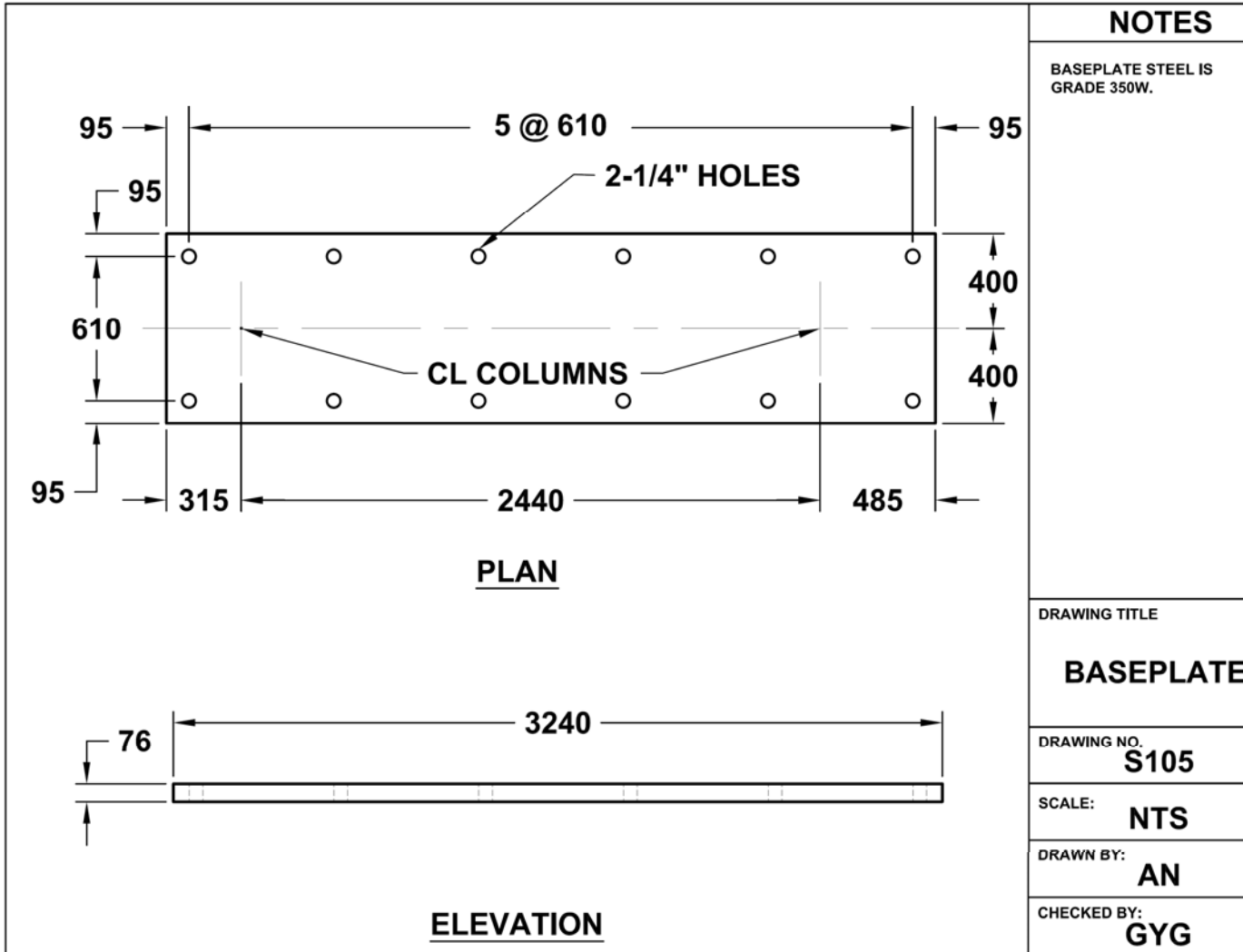
**MISC. STEEL PLATES**

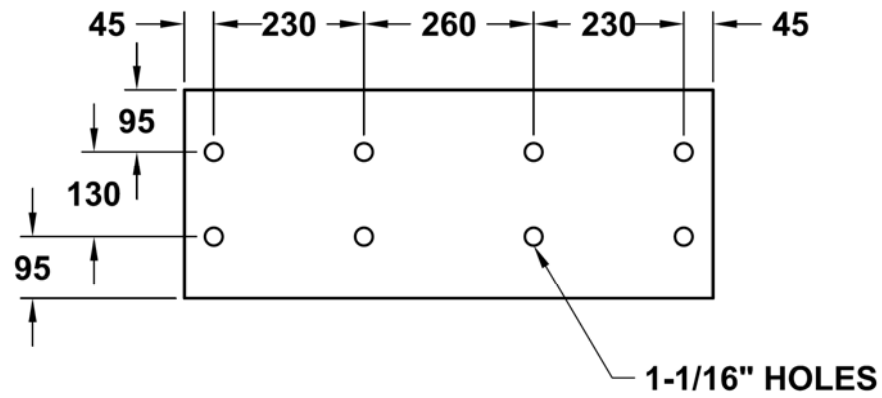
DRAWING NO. **S104**

SCALE: **NTS**

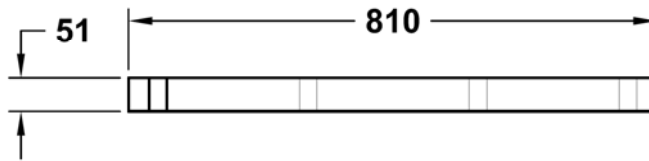
DRAWN BY: **AN**

CHECKED BY: **GYG**





**PLAN**



**ELEVATION**

**NOTES**

THIS LOAD TRANSFER PLATE IS REQUIRED FOR THE TEST SETUP, BUT IS NOT A PART OF THE SPECIMEN DISCUSSED IN DRAWINGS S100 THROUGH S105.

LOAD TRANSFER PLATE STEEL IS GRADE 300W.

HOLES ARE TO BE WATERJET CUT OR DRILLED.

DRAWING TITLE

**LOAD  
TRANSFER  
PLATE**

DRAWING NO.

**S106**

SCALE:


**NTS**

DRAWN BY:

**AN**

CHECKED BY:

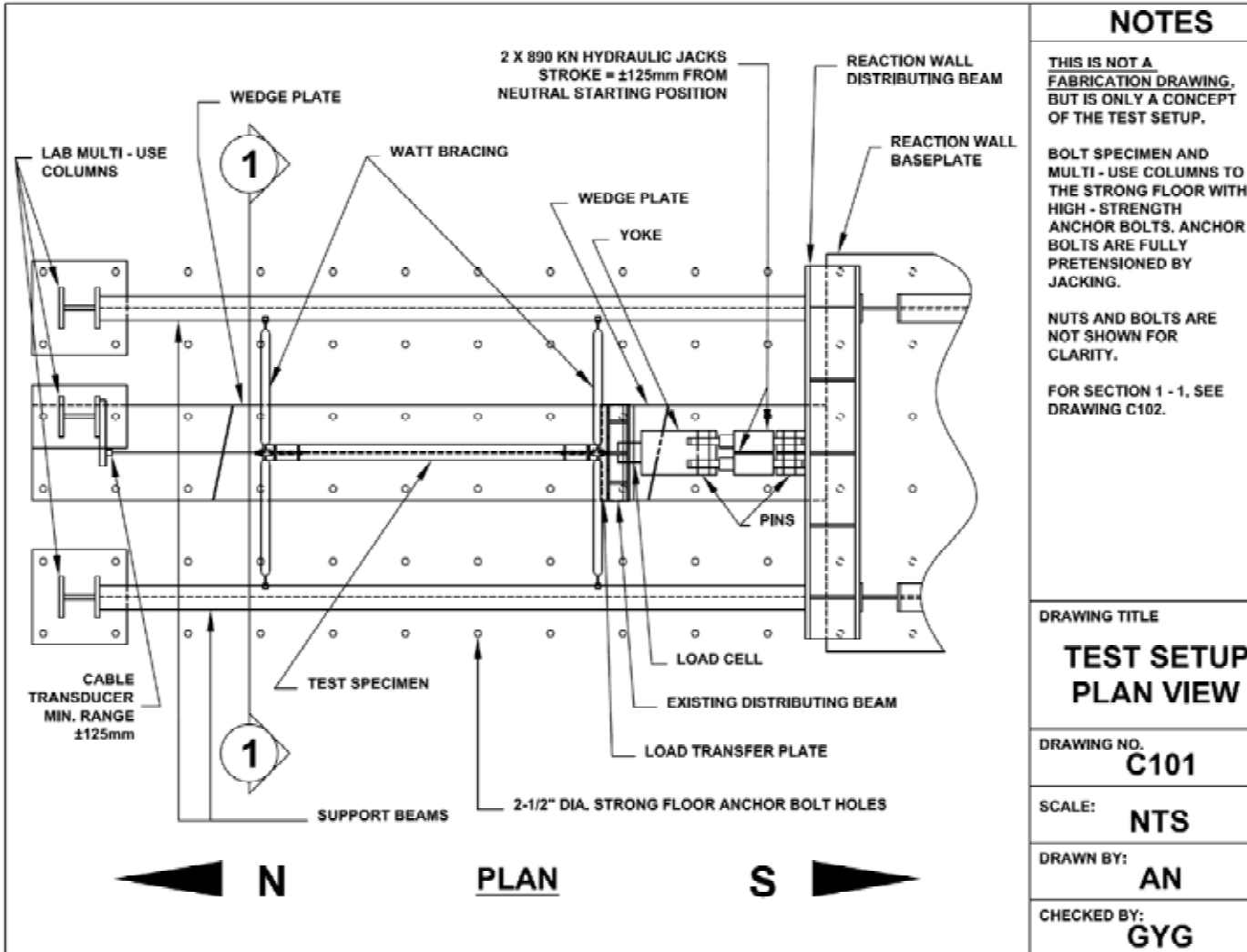
**GYG**

<p><b>STEEL PLATE SHEAR WALLS WITH LIGHT GAUGE INFILL PLATES</b></p> <p><b><u>LARGE SCALE TEST - TEST SETUP DRAWINGS</u></b></p> <p><b>RESEARCHER: ANDREW NEILSON, M.Sc. CANDIDATE</b>  <b>SUPERVISORS: Dr. GILBERT GRONDIN</b>  <b>Dr. ROBERT DRIVER</b></p> <table border="1"> <thead> <tr> <th><b>DWG NO.</b></th> <th><b>TITLE</b></th> </tr> </thead> <tbody> <tr> <td><b>C001</b></td> <td><b>GENERAL NOTES</b></td> </tr> <tr> <td><b>C100</b></td> <td><b>TEST SETUP - EAST ELEVATION</b></td> </tr> <tr> <td><b>C101</b></td> <td><b>TEST SETUP - PLAN VIEW</b></td> </tr> <tr> <td><b>C102</b></td> <td><b>TEST SETUP - SECTION VIEW</b></td> </tr> <tr> <td><b>C103</b></td> <td><b>DETAIL A: LATERAL LOAD CONNECTION</b></td> </tr> <tr> <td><b>C104</b></td> <td><b>DATA COLLECTION</b></td> </tr> </tbody> </table>	<b>DWG NO.</b>	<b>TITLE</b>	<b>C001</b>	<b>GENERAL NOTES</b>	<b>C100</b>	<b>TEST SETUP - EAST ELEVATION</b>	<b>C101</b>	<b>TEST SETUP - PLAN VIEW</b>	<b>C102</b>	<b>TEST SETUP - SECTION VIEW</b>	<b>C103</b>	<b>DETAIL A: LATERAL LOAD CONNECTION</b>	<b>C104</b>	<b>DATA COLLECTION</b>	<b>NOTES</b>
	<b>DWG NO.</b>	<b>TITLE</b>													
	<b>C001</b>	<b>GENERAL NOTES</b>													
	<b>C100</b>	<b>TEST SETUP - EAST ELEVATION</b>													
	<b>C101</b>	<b>TEST SETUP - PLAN VIEW</b>													
	<b>C102</b>	<b>TEST SETUP - SECTION VIEW</b>													
	<b>C103</b>	<b>DETAIL A: LATERAL LOAD CONNECTION</b>													
<b>C104</b>	<b>DATA COLLECTION</b>														
															
	DRAWING TITLE <b>COVER PAGE</b>														
	DRAWING NO. <b>C000</b>														
	<b>N/A</b>														
	DRAWN BY: <b>AN</b>														
	CHECKED BY: <b>GYG</b>														

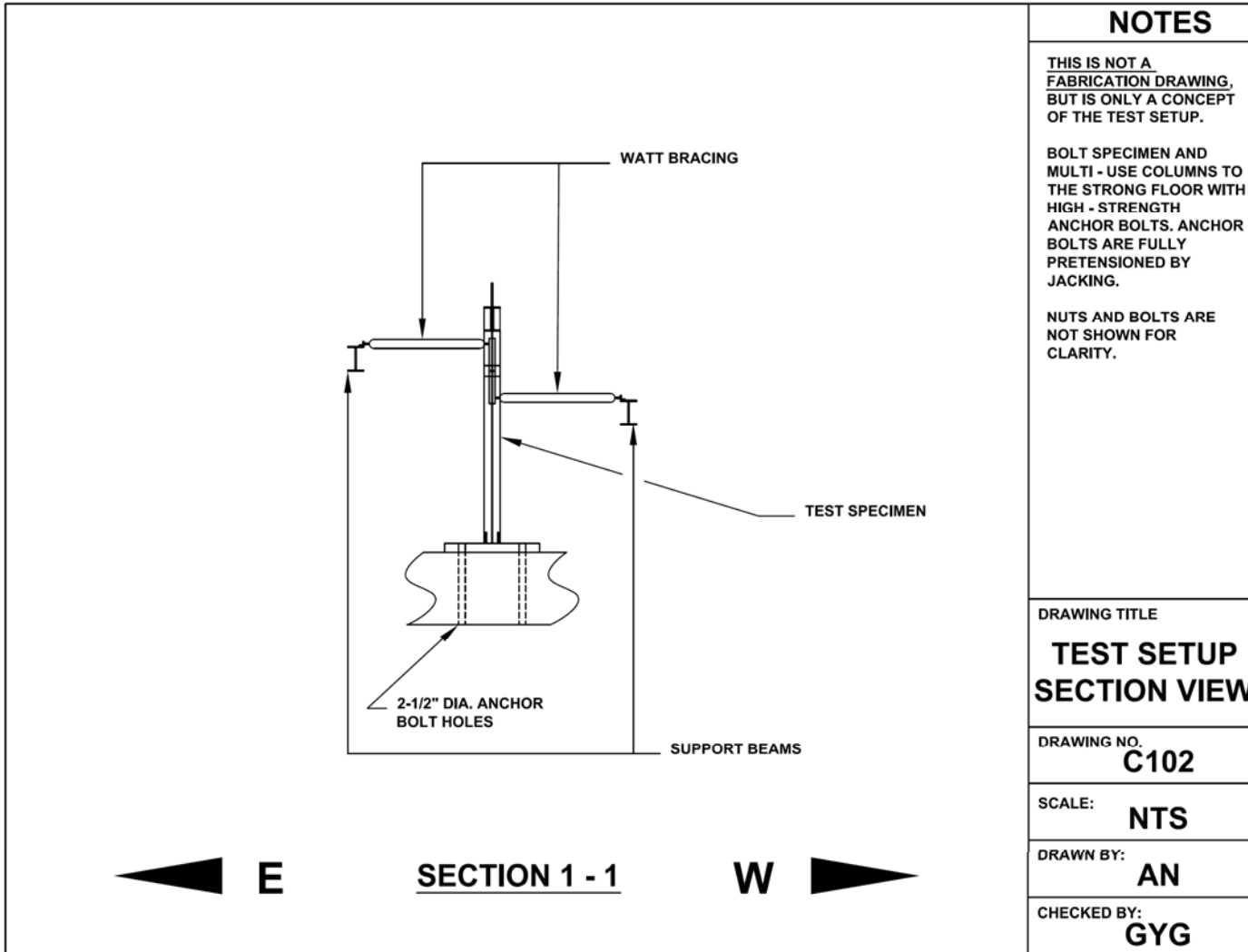
<p>1) THIS PACKAGE CONTAINS DRAWINGS C100 THROUGH C104.</p> <p>2) DO NOT SCALE DRAWINGS. IF CLARIFICATION IS REQUIRED, PLEASE CONTACT ANDREW NEILSON OR GILBERT GRONDIN.</p> <p>3) DIMENSIONS ARE IN MILLIMETERS (mm) AND DEGREES (°) UNLESS OTHERWISE NOTED.</p> <p>4) THESE DRAWINGS DESCRIBE THE KEY FEATURES OF THE TEST SETUP AND DATA COLLECTION. FOR STRUCTURAL DETAILS OF THE MOMENT RESISTING FRAME PORTION OF THE TEST SPECIMEN, REFER TO THE DRAWING SET ENTITLED "LARGE SCALE PLATE WALL TEST MOMENT RESISTING FRAME FABRICATION DRAWINGS". FOR DETAILS ON CONNECTING THE INFILL PANEL TO THE MOMENT RESISTING FRAME, SEE RELEVANT SECTIONS OF THE THESIS DOCUMENT.</p>	<b>NOTES</b>
	DRAWING TITLE <b>GENERAL NOTES</b>
	DRAWING NO. <b>C001</b>
	SCALE: <b>N/A</b>
DRAWN BY: <b>AN</b>	
CHECKED BY: <b>GYG</b>	

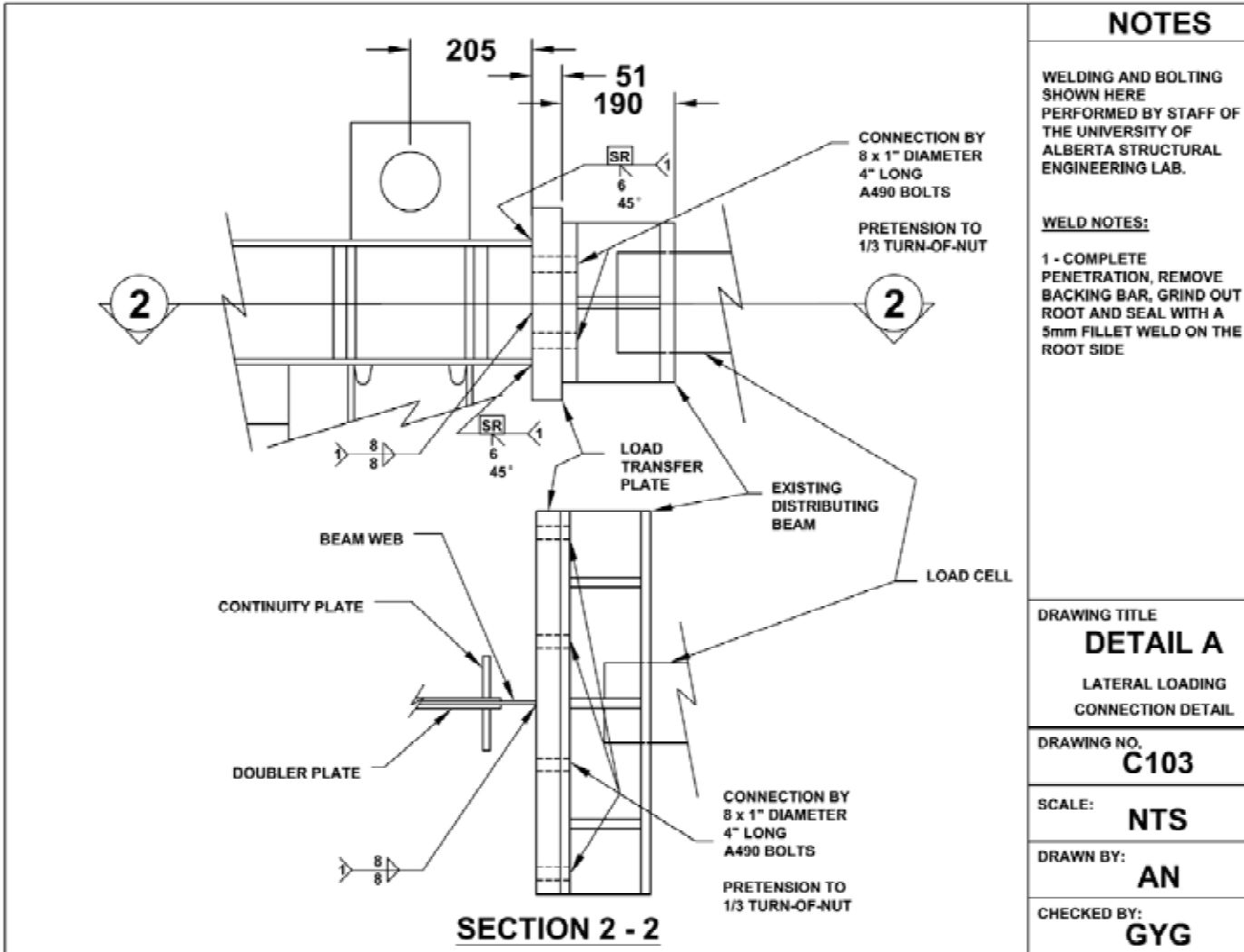


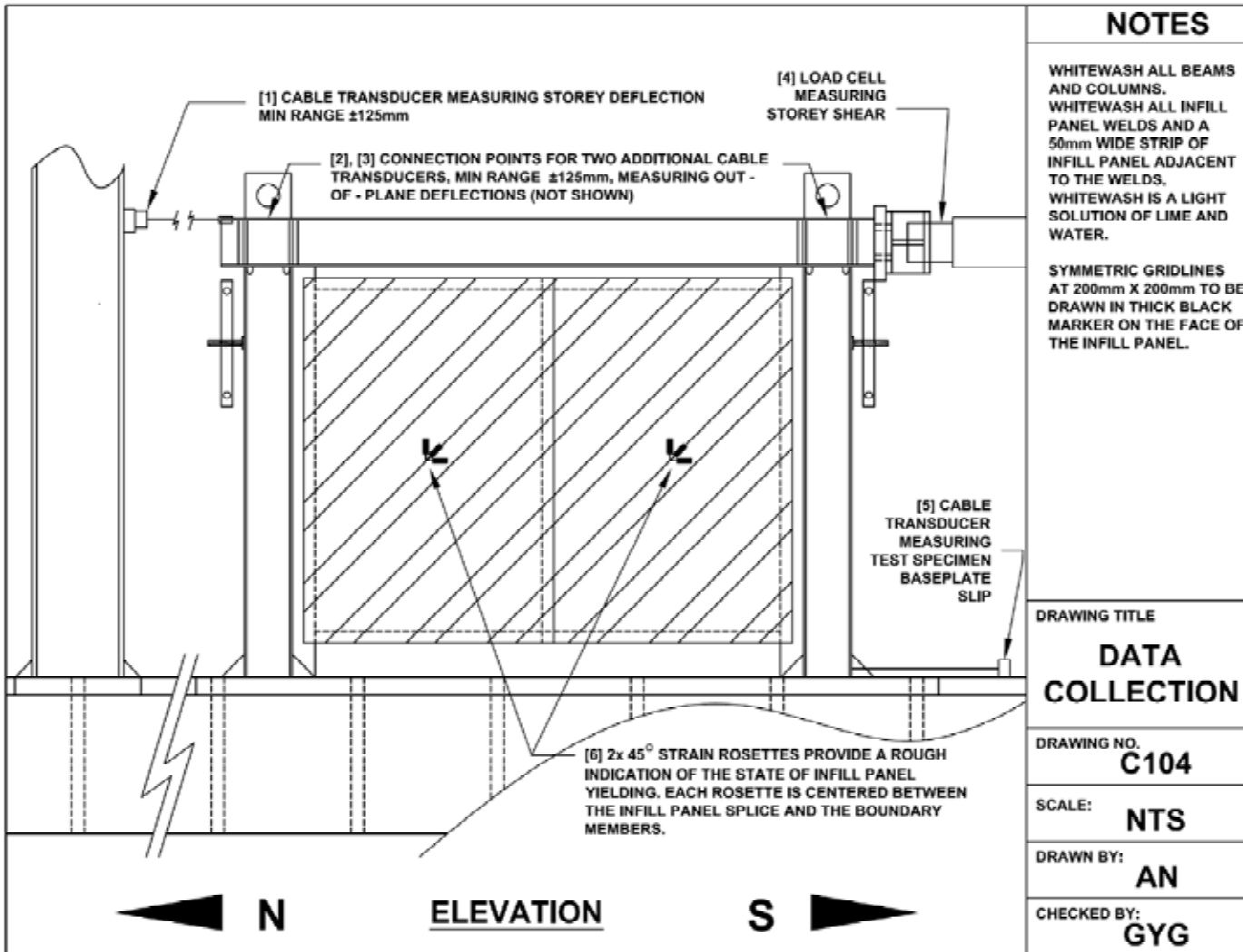




<b>NOTES</b>	
THIS IS NOT A FABRICATION DRAWING, BUT IS ONLY A CONCEPT OF THE TEST SETUP.	
BOLT SPECIMEN AND MULTI - USE COLUMNS TO THE STRONG FLOOR WITH HIGH - STRENGTH ANCHOR BOLTS. ANCHOR BOLTS ARE FULLY PRETENSIONED BY JACKING.	
NUTS AND BOLTS ARE NOT SHOWN FOR CLARITY.	
FOR SECTION 1 - 1, SEE DRAWING C102.	
DRAWING TITLE	
<b>TEST SETUP PLAN VIEW</b>	
DRAWING NO.	
<b>C101</b>	
SCALE:	
<b>NTS</b>	
DRAWN BY:	
<b>AN</b>	
CHECKED BY:	
<b>GYG</b>	







NOTES	
<p>WHITEWASH ALL BEAMS AND COLUMNS. WHITEWASH ALL INFILL PANEL WELDS AND A 50mm WIDE STRIP OF INFILL PANEL ADJACENT TO THE WELDS. WHITEWASH IS A LIGHT SOLUTION OF LIME AND WATER.</p> <p>SYMMETRIC GRIDLINES AT 200mm X 200mm TO BE DRAWN IN THICK BLACK MARKER ON THE FACE OF THE INFILL PANEL.</p>	
DRAWING TITLE	
<b>DATA COLLECTION</b>	
DRAWING NO. <b>C104</b>	
SCALE: <b>NTS</b>	
DRAWN BY: <b>AN</b>	
CHECKED BY: <b>GYG</b>	

## **Appendix E: Steel Plate Shear Wall Test, Supplementary Data**

### **E1 Introduction**

This appendix contains a single table with a summary of key values from the hysteresis results of the SPSW test. The data is the source data for several graphs and charts in Chapter 7.

Table E-1: Key Values from Hysteresis Results of SPSW Test

Cycle	Peak Storey Sway at Load Step	Max Load (kN)	Measured Max Stroke (mm)	Measured Drift Ratio (%)	Half-Cycle Energy (kJ)	Total Cycle Energy (kJ)
1+	$\delta$ matching $0.4Q_y$	214	2.8	0.1%	0.19	0.56
1-		-220	-3.6	-0.2%	0.38	
2+		218	2.5	0.1%	0.17	0.42
2-		-220	-3.7	-0.2%	0.25	
3+		221	2.6	0.1%	0.16	0.39
3-		-217	-3.8	-0.2%	0.23	
4+	$\delta$ matching $0.75Q_y$	408	11.6	0.6%	2.48	5.10
4-		-406	-12.0	-0.6%	2.62	
5+		410	10.2	0.5%	1.68	3.34
5-		-408	-11.9	-0.6%	1.65	
6+		409	10.2	0.5%	1.32	2.66
6-		-408	-12.0	-0.6%	1.34	
7+	$\delta_y$	465	14.5	0.8%	2.54	5.24
7-		-456	-14.6	-0.8%	2.70	
8+		468	14.6	0.8%	2.25	4.39
8-		-456	-14.5	-0.8%	2.14	
9+		468	14.6	0.8%	1.90	3.81
9-		-453	-14.6	-0.8%	1.91	
10+	$2\delta_y$	530	28.9	1.5%	10.09	23.33
10-		-560	-29.26	-1.5%	13.24	
11+		556	29.0	1.5%	11.01	21.22
11-		-576	-29.12	-1.5%	10.21	
12+		554	29.1	1.5%	9.36	18.41
12-		-570	-29.1	-1.5%	9.05	
13+	$3\delta_y$	560	43.6	2.3%	20.34	43.54
13-		-620	-43.8	-2.3%	23.20	
14+		575	43.6	2.3%	20.44	40.12
14-		-610	-43.8	-2.3%	19.67	
15+		557	43.5	2.3%	18.60	37.11
15-		-590	-43.7	-2.3%	18.51	
16+	$4.5\delta_y$	550	66.0	3.5%	37.80	78.92
16-		-630	-66.0	-3.5%	41.12	
17+		540	65.9	3.5%	34.73	67.65
17-		-580	-65.8	-3.5%	32.92	

**Table E–1: Key Values from Hysteresis Results of SPSW Test**

Cycle	Peak Storey Sway at Load Step	Max Load (kN)	Measured Max Stroke (mm)	Measured Drift Ratio (%)	Half-Cycle Energy (kJ)	Total Cycle Energy (kJ)
18+	$3.8\delta_y$	434	54.8	2.9%	21.57	97.27
18-	$9\delta_y$	-540	-131.0	-6.9%	75.71	

**Notes**

1) When referring to cycles of loading, the cycle number followed by a "+" indicates the half – cycle from the neutral position to the maximum northward excursion of storey sway and back to the neutral position. Conversely, the cycle number followed by a "-" indicates the half-cycle from the neutral position to the maximum southward excursion and back to the neutral position.